

**Faculty of Engineering and Science
Department of Petroleum Engineering**

**A Numerical Modelling and Optimization Approach on Sandstone
Acidizing at Elevated Temperature for Well Stimulation**

Leong Van Hong

**This thesis is presented for the Degree of
Doctor of Philosophy
of
Curtin University**

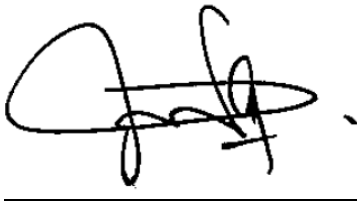
November 2018

Declaration

To the best of my knowledge and belief this thesis contains no material previously published by any other person except where due acknowledgement has been made.

This thesis contains no material which has been accepted for the award of any other degree or diploma in any university.

Signature:



Name : Leong Van Hong

Date : 06th November 2018

Acknowledgement

I would like to express my sincere gratitude toward many parties who gave me support and encouragement in any forms to complete this thesis successfully.

First and foremost, I would like to thank my thesis committee, particularly my research supervisors, Dr. Hisham Ben Mahmud, Dr. Law Ming Chiat, Dr. Henry Foo Chee Yew and Dr. Tan Inn Shi for their supervision and careful guidance throughout my years of PhD study. Their professionalism and kindness aided me in my progress of learning, comprehension and most importantly, the development of my research topic.

My deepest gratitude also extended to Mr. Mian Umer Shafiq, former faculty member of the Department of Petroleum Engineering in Curtin University, Malaysia for his useful information and advice in many technical aspects of my research area. It is also my pleasure to thank Professor Marcus Lee Man Kon, former Dean of the Curtin Malaysia Graduate School, who guided me with his expertise and suggestions.

I would like to acknowledge the Faculty of Engineering and Science (FOES), Curtin University, Malaysia and the Ministry of Higher Education (MOHE) Malaysia for awarding me the full scholarship and Fundamental Research Grant Scheme (FRGS) (*Grant No. FRGS 1044*) to conduct my research, without which this research project would not be successful. Your financial support is greatly appreciated.

I really appreciate many friends and colleagues within the Higher Degree by Research (HDR) community of Curtin Malaysia who does not only shared our knowledge and experience, but also many memorable moments together. Last but not least, special thanks to my parents and family for their unconditional love and understanding throughout the period of my study. Thank you for your endless patience and I dedicate this thesis to you.

Abstract

Sandstone matrix acidizing is a broadly developed well stimulation technique to enhance the productivity of a reservoir formation. The most popular acid used to improve the porosity and permeability of a well is the mud acid. However, there are some conventional problems associated with mud acid at high temperature conditions such as the rapid rate of reaction and early acid consumption. Therefore, various other acids had been developed to replace the conventional mud acid.

Initially, this study had conducted a preliminary screening and characterization of different acids based on literature survey to optimize the acid selection and targeting various temperatures of sandstone environment. The results obtained indicated that fluoroboric acid (HBF_4) could be useful in enhancing the sandstone acidizing process. In general, HBF_4 is a low damaging acid for sandstone acidizing due to its retardation effect and uniquely slow hydrolytic reaction to produce HF. This would allow deeper penetration of the acid into the sandstone formation at a slower rate, resulting in higher porosity and permeability enhancement. Nevertheless, there is a lack of understanding about its efficiency at elevated temperature, which was not sufficiently addressed in the literature.

Therefore, the primary purpose of this study is to develop a three-dimensional (3D) core-scale model using COMSOL® Multiphysics commercial software modules of Computational Fluid Dynamics (CFD) to simulate the acid core flooding process on sandstone core. The numerical simulations were conducted using finite element method (FEM) to examine the capability of HBF_4 in enhancing the porosity and permeability of the sandstone matrix. The simulation result had been validated against the experimental data. The results matched very well and showed good agreement with the measured plot data. Therefore, this had proven the validity of the model as a reliable basis for further parametric study and design optimization study.

The effect of temperature on the performance HBF_4 sandstone acidizing was evaluated in this study. The simulation results indicated that at low temperature of 25 °C, HBF_4 is not

very effective, as justified in its poor porosity and permeability increments of only 1.07 and 1.23 respectively. However, at elevated temperatures, the porosity and permeability enhancement also become increasingly more significant, which showed 1.26 and permeability increase of 2.06 respectively at 65 °C; and 1.67 and 7.06 respectively at 105 °C. Therefore, one can conclude that HBF₄ acid treatment performed better at elevated temperatures due to increased hydrolysis rate, which is a governing function in HBF₄ sandstone acidizing.

Then, the mechanistic model was employed to perform a parametric study to study the influences of various factors on the performance of HBF₄ during sandstone acidizing such as the formation temperature, acid concentration and acid injection rate. The simulation results indicated that an overall improvement in porosity and permeability is achieved when the formation temperature, acid concentration and acid injection rate were increased. A higher formation temperature will increase the hydrolysis rate of HBF₄ to produce HF. Meanwhile, an increased acid concentration and acid injection rate will also enhance the acid penetration into the sandstone core. However, the effect of acid concentration is remarkably more significant than that of the acid injection rate.

Finally, a response surface methodology (RSM) optimization approach was adopted to study the integrated effects of the abovementioned three main factors on the porosity, permeability and pressure drop responses. A 3³ full factorial design of experiment (DOE) had been applied to perform the simulation runs. The results showed a maximum porosity enhancement ratio, permeability enhancement ratio and pressure drop of 1.79, 8.31 and 23828.5Pa respectively at a temperature of 105 °C, 12% acid concentration and 4.46×10⁻⁵ m/s acid injection rate. In addition, this study had developed three empirical models for the prediction of porosity, permeability and pressure drop. The analysis of variance (ANOVA) had indicated and proven the reliability and robustness of these models.

Overall, the major finding and novelty of this research work is that the model developed for HBF₄ acidizing had revealed that HBF₄ could be used as an alternative stimulation fluid at elevated temperature. The optimization study formed a basis for improved sandstone acid stimulation design. Meanwhile, this study had also spotlighted on the possible research expansion for future investigation.

List of Publications

Part of this thesis have been published in the following journals and conferences.

Journal Publications

1. **Leong, V. H.** and Mahmud, H. B. (2017). A comparative study of different acids used for sandstone acid simulation: a literature review. *IOP Conference Series: Materials Science and Engineering*. 217. 012018. IOP Publishing. <https://doi.org/10.1088/1757-899X/217/1/012018>
2. **Leong, V. H.** and Mahmud, H. B. (2018). A preliminary screening and characterization of suitable acids for sandstone matrix acidizing technique: a comprehensive review. *Journal of Petroleum Exploration and Production Technology*. Springer Nature. <https://doi.org/10.1007/s13202-018-0496-6>
3. **Leong, V. H.**, Mahmud, H. B., Law, M. C., Foo, C. Y. H. and Tan, I. S. (2018). A comparison and assessment of the modelling and simulation of the sandstone matrix acidizing process: a critical methodology study. *Journal of Natural Gas Science and Engineering*. 57. 52-67. Elsevier B. V. <https://doi.org/10.1016/j.jngse.2018.06.044>
4. **Leong, V. H.**, Mahmud, H. B., Law, M. C., Foo, C. Y. H. and Tan, I. S. (2018). A numerical modelling and simulation of core-scale sandstone acidizing process: a study on the effect of temperature. *Journal of Petroleum Exploration and Production Technology*. Springer Nature. <https://doi.org/10.1007/s13202-018-0522-8>
5. **Leong, V. H.**, Mahmud, H. B., Law, M. C., Foo, C. Y. H. and Tan, I. S. (2018). A sensitivity analysis and parametric study of factors affecting sandstone acidizing using numerical simulation. *Journal of Petroleum Exploration and Production Technology*. Springer Nature. (Under review)
6. **Leong, V. H.**, Mahmud, H. B., Law, M. C., Foo, C. Y. H. and Tan, I. S. (2018). An optimization approach for sandstone acidizing process using response surface methodology (RSM) and numerical simulation. *Journal of Petroleum Science and Engineering*. Elsevier B. V. (Under review)

Conference Publications

1. **Leong, V. H.**, Mahmud, H. B. and Dol, S. S. B. (2016). Development of a new enhanced oil recovery method and model for high-temperature well stimulation using acid combinations. *In Proceeding: North Borneo Research Colloquium (NBRC) 2016*. Curtin University, Miri, Sarawak, Malaysia. 18th – 19th April 2016.
2. **Leong, V. H.** and Mahmud, H. B. (2017). A comparative study of different acids used for sandstone acid simulation: a literature review. *In Proceeding: International Conference on Materials Technology and Energy (ICMTE) 2017*. Curtin University, Miri, Sarawak, Malaysia. 20th – 21st April 2017.
3. **Leong, V. H.** and Mahmud, H. B. (2017). Sandstone acid stimulation using fluoroboric acid. *In Proceeding: 5th Postgraduate Borneo Research Colloquium 2017*. University Malaysia Sarawak (UNIMAS), Kuching, Sarawak, Malaysia. 4th – 6th July 2017.
4. **Leong, V. H.** and Mahmud, H. B. (2017). A methodological approach to model acidizing process for sandstone well stimulation: a conceptual framework. *In Proceeding: 1st One Curtin International Postgraduate Conference (OCPC) 2017*. Curtin University, Miri, Sarawak, Malaysia. 10th – 12th December 2017.
5. **Leong, V. H.**, Mahmud, H. B., Law, M. C., Foo, C. Y. H. and Tan, I. S. (2018). A study on the effect of acid concentration at various temperatures on sandstone acidizing: a numerical simulation. *In Proceeding: One Curtin International Postgraduate Conference (OCPC) 2018*. Curtin University, Miri, Sarawak, Malaysia. 26th – 28th November 2018.
6. **Leong, V. H.**, Mahmud, H. B., Law, M. C., Foo, C. Y. H. and Tan, I. S. (2018). An optimization framework for sandstone acidizing using design of experiment (DOE) and mathematical modelling. *In Proceeding: 11th Curtin University Technology, Science and Engineering (CUTSE) International Conference 2018*. Curtin University, Miri, Sarawak, Malaysia. 26th – 28th November 2018.

Awards and Recognitions

1. **First Runner-up Award - Leong, V. H.** (2016). More oil and gas? Use acid! *Competed in: Three Minute Thesis (3MT) Competition 2016.* Curtin University, Miri, Sarawak, Malaysia. 1st August 2016.
2. **Best Poster Award - Leong, V. H.** and Mahmud, H. B. (2017). Sandstone acid stimulation using fluoroboric acid. *Poster presented at: 5th Postgraduate Borneo Research Colloquium 2017.* University Malaysia Sarawak (UNIMAS), Kuching, Sarawak, Malaysia. 4th – 6th July 2017.

Table of Contents

| | |
|--|-------|
| Declaration | I |
| Acknowledgement | II |
| Abstract | III |
| List of Publications | V |
| Journal Publications..... | V |
| Conference Publications..... | VI |
| Awards and Recognitions..... | VII |
| Table of Contents | VIII |
| List of Figures | XIII |
| List of Tables | XIX |
| Nomenclature | XXII |
| List of Abbreviations..... | XXII |
| List of Units..... | XXV |
| List of Subscripts..... | XXVII |
| List of Symbols..... | XXVII |
| | |
| Chapter 1 Introduction..... | 1 |
| 1.1 Research Introduction | 1 |
| 1.2 Research Gap and Problem Statement | 3 |
| 1.3 Research Questions and Hypotheses | 4 |
| 1.4 Aims and Objectives | 5 |
| 1.5 Research Scopes..... | 6 |
| 1.6 Novelty, Research Significance and Contributions | 7 |
| 1.7 Thesis Outlines and Organization..... | 8 |
| | |
| Chapter 2 Preliminary Acid Screening and Characterization..... | 13 |
| 2.1 Introduction..... | 13 |

| | | |
|-----------|--|----|
| 2.2 | Research Background | 13 |
| 2.2.1 | Well Stimulation..... | 13 |
| 2.2.2 | Sandstone Mineralogy | 16 |
| 2.2.3 | The Practice in Sandstone Matrix Acidizing..... | 18 |
| 2.2.4 | The Treatment Design of Matrix Acidizing | 19 |
| 2.2.5 | The Use of Additives in Matrix Acidizing | 21 |
| 2.2.6 | Sandstone Channelling and Wormholing..... | 22 |
| 2.3 | Literature Review of Experimental Studies | 24 |
| 2.3.1 | Mud Acid (HF-HCl) | 24 |
| 2.3.2 | Fluoroboric Acid (HBF ₄)..... | 30 |
| 2.3.3 | Chelating Agents | 37 |
| 2.3.4 | Retarded Acids and Organic Acids | 44 |
| 2.3.5 | Overall Characterization and Comparison of Different Acids | 52 |
| 2.4 | Summary of Chapter | 58 |
| Chapter 3 | Comparison and Assessment of Modelling Approach..... | 59 |
| 3.1 | Introduction..... | 59 |
| 3.2 | Sandstone Acidizing Background..... | 59 |
| 3.2.1 | The Acid Interactions with a Sandstone Matrix | 59 |
| 3.2.2 | The Chemical Reactions during Sandstone Acidizing | 63 |
| 3.2.3 | Acid Selection and Stimulation Treatment Design | 66 |
| 3.3 | Literature Review of Numerical Modelling and Simulation Studies..... | 70 |
| 3.3.1 | Lumped-Parameter Model..... | 70 |
| 3.3.2 | Two-Parameter Model (Standard Model) | 72 |
| 3.3.3 | Four-Parameter Model..... | 74 |
| 3.3.4 | Detailed Chemistry Model | 77 |
| 3.3.5 | Comparison of Different Sandstone Acidizing Models | 78 |
| 3.3.6 | Modelling Studies of HBF ₄ Sandstone Acidizing..... | 83 |
| 3.3.7 | CFD Application in Matrix Acidizing..... | 85 |
| 3.3.8 | Multi-scale Modelling for Matrix Acidizing..... | 86 |
| 3.4 | Proposal of Modelling Methodology | 88 |

| | | |
|-----------|---|-----|
| 3.4.1 | Model Development Plan | 88 |
| 3.4.2 | Model Validation and Design Optimization..... | 90 |
| 3.5 | Summary of Chapter | 95 |
| Chapter 4 | Numerical Model Development and Validation | 96 |
| 4.1 | Introduction..... | 96 |
| 4.2 | Model Description and Governing Equations..... | 97 |
| 4.2.1 | Chemical Reaction Model | 97 |
| 4.2.2 | Hydrolysis of HBF_4 | 99 |
| 4.2.3 | Pressure Equation | 101 |
| 4.2.4 | Mass Conservation Equation of HBF_4 | 101 |
| 4.2.5 | Mass Conservation Equation of Acid Components..... | 102 |
| 4.2.6 | Mass Conservation Equation of Minerals | 103 |
| 4.2.7 | Change in Porosity | 104 |
| 4.2.8 | Change in Permeability | 105 |
| 4.2.9 | Initial Conditions | 106 |
| 4.2.10 | Boundary Conditions..... | 106 |
| 4.2.11 | Summary of Governing Equations | 108 |
| 4.3 | Numerical Solution and Model Implementation..... | 109 |
| 4.3.1 | Geometry Creation | 109 |
| 4.3.2 | Grid Blocks Creation and Mesh Independence Analysis | 110 |
| 4.3.3 | Model Input and Settings..... | 112 |
| 4.4 | Model Validation | 116 |
| 4.5 | Summary of Chapter | 118 |
| Chapter 5 | Parametric Study and Sensitivity Analysis | 119 |
| 5.1 | Introduction..... | 119 |
| 5.2 | Design for Parametric Study..... | 120 |
| 5.3 | Numerical Visualization of the Effect of Temperature..... | 123 |
| 5.3.1 | Porosity and Permeability Distribution | 123 |
| 5.3.2 | Pressure and Acids Concentration Distribution | 129 |

| | | |
|-----------|---|-----|
| 5.3.3 | Minerals Volume Fraction Distribution | 138 |
| 5.4 | Effect of Acid Concentration at different Temperatures | 144 |
| 5.4.1 | Porosity and Permeability Enhancement Ratio | 144 |
| 5.4.2 | Pressure Drop | 150 |
| 5.5 | Effect of Acid Injection Rate at different Temperatures..... | 154 |
| 5.5.1 | Porosity and Permeability Enhancement Ratio | 154 |
| 5.5.2 | Pressure Drop | 160 |
| 5.6 | Summary of Chapter | 164 |
| Chapter 6 | Optimization Study using Response Surface Methodology (RSM) | 165 |
| 6.1 | Introduction..... | 165 |
| 6.2 | Optimization Methodology for Process Analysis and Modelling..... | 166 |
| 6.2.1 | Response Surface Methodology (RSM)..... | 166 |
| 6.2.2 | Design of Experiment (DOE)..... | 171 |
| 6.2.3 | Empirical Modelling and Determination of Optimal Conditions... | 173 |
| 6.3 | Results and Discussion | 173 |
| 6.3.1 | ANOVA of Response and Empirical Model Development | 176 |
| 6.3.2 | Empirical Model Development | 184 |
| 6.3.3 | Residuals Analysis of Response Data | 188 |
| 6.3.4 | Empirical Model Fitting and Validation..... | 200 |
| 6.3.5 | Optimization of Response Data..... | 204 |
| 6.4 | Summary of Chapter | 217 |
| Chapter 7 | Conclusions and Recommendations | 218 |
| 7.1 | Conclusion | 218 |
| 7.1.1 | Numerical Study | 218 |
| 7.1.2 | Parametric Study | 219 |
| 7.1.3 | Optimization Study..... | 220 |
| 7.1.4 | Overall Remarks | 220 |
| 7.2 | Recommendations..... | 221 |

| | |
|---|-----|
| References..... | 222 |
| Appendix..... | 245 |
| Appendix A. Derivation of Governing Equations | 245 |
| A.1 Pressure Equation | 245 |
| A.2 General Material Balance Equation..... | 248 |
| A.3 Mass Conservation Equation of Acid Components..... | 249 |
| A.4 Mass Conservation Equation of HF | 252 |
| A.5 Mass Conservation Equation of H_2SiF_6 | 254 |
| A.6 Mass Conservation Equation of Minerals | 256 |
| A.7 Mass Conservation Equation of Fast-Reacting Minerals | 256 |
| A.8 Mass Conservation Equation of Slow-Reacting Minerals..... | 258 |
| A.9 Mass Conservation Equation of Silica Gel..... | 259 |
| A.10 Change in Porosity | 260 |
| A.11 Initial Conditions | 261 |
| A.12 Boundary Conditions..... | 261 |

List of Figures

| | | |
|------------|---|----|
| Figure 1.1 | Overview of the steps taken in this research study | 12 |
| Figure 2.1 | Pore scale figure of matrix acidizing process when the acid is being injected and acid passes through the pore space illustrated by Veldkam and Boxem (2015) | 14 |
| Figure 2.2 | Oil Well Stimulations Illustration (Conservancy 2016) | 16 |
| Figure 2.3 | Constituents of sandstone, all of which are soluble in HCl-HF mud acid system as described by Crowe et al. (1992) | 17 |
| Figure 2.4 | Wormholes in Bandera Sandstone by Lamb (1998) | 22 |
| Figure 2.5 | Wormholes in Berea Sandstone by Lamb (1998) | 23 |
| Figure 2.6 | Wormholes in South America Sandstone by Kalfayan and Metcalf (2000) | 23 |
| Figure 2.7 | Optimum HF concentration based on mineral content determined by Abdelmoneim and Nasr-El-Din (2015) | 26 |
| Figure 2.8 | The production improvement in the Nigerian oil well (Ayorinde et al. 1992) | 31 |
| Figure 2.9 | Comparison of SEM results showing pore filling clay (kaolinite) before and after treatment with mud acid and fluoroboric acid (Crowe et al. 1992) | 32 |
| Figure 3.1 | Different minerals and clays in sandstone with different morphologies such as (A) pore-filling kaolinite books, (B) fibrous illite, (C) carbonate overgrowth, (D) feldspar overgrowth and (E) quartz cement (Ali et al. 2004) | 60 |
| Figure 3.2 | The Typical Acid Response Curves (Smith and Hendrickson 1965) | 62 |
| Figure 3.3 | Scanning electron microscope (SEM) photograph of different clay minerals content such as (a) kaolinite (b) illite (c) chlorite and (d) smectite presented in sandstone rock as illustrated by McLeod (1984) | 64 |

| | | |
|-------------|---|-----|
| Figure 3.4 | Primary, secondary and tertiary reactions between HF and minerals in terms of distance from the wellbore described by Al-Harthy et al. (2009) | 65 |
| Figure 3.5 | A radially symmetry model of the formation and the analysis of the main controlling factors in sandstone matrix acidizing as described by Crowe et al. (1992) | 71 |
| Figure 3.6 | The modelling system and the interaction of acid and rock (Zakaria 2003) | 75 |
| Figure 3.7 | Normalized Effluent HF Concentration at high injection rate (Al-Shaalan and Nasr-El-Din 2000) | 79 |
| Figure 3.8 | Normalized Effluent HF Concentration at moderate injection rate (Al-Shaalan and Nasr-El-Din 2000) | 80 |
| Figure 3.9 | Normalized Effluent HF Concentration at low injection rate (Al-Shaalan and Nasr-El-Din 2000) | 80 |
| Figure 3.10 | The permeability m^2 distributions of the sandstone core after being simulated with mud acid (upper) and with HF_4 (lower) at 65 °F (Zhou et al. 2016) | 84 |
| Figure 3.11 | The permeability profile along the sandstone core length after being simulated with mud acid and HF_4 at 65 °F (Zhou et al. 2016) | 84 |
| Figure 3.12 | A field scale model in COMSOL (Ameri et al. 2016) | 86 |
| Figure 3.13 | Different Scales in the Modelling of Matrix Acidizing (Golfier et al. 2004) | 87 |
| Figure 3.14 | Flow chart of research methodology (part 1) | 91 |
| Figure 3.15 | Flow chart of research methodology (part 2) | 92 |
| Figure 3.16 | Flow chart of research methodology (part 3) | 93 |
| Figure 3.17 | Flow chart of research methodology (part 4) | 94 |
| Figure 4.1 | The meshing of the geometry using extra-fine element size (unit = inch) | 111 |
| Figure 4.2 | Plot of comparison between fluoroboric acidizing simulation result and experimental data at 25 °C | 117 |

| | | |
|-------------|--|-----|
| Figure 4.3 | Plot of comparison between fluoroboric acidizing simulation result and experimental data at 65 °C | 117 |
| Figure 5.1 | Porosity distribution after 25 mins (left) and after 35 mins (right) of fluoroboric acid injection at (a) 25 °C, (b) 65 °C and (c) 105 °C | 125 |
| Figure 5.2 | The effect of temperatures on sandstone porosity after fluoroboric acidizing | 126 |
| Figure 5.3 | Permeability distribution after 25 mins (left) and after 35 mins (right) of fluoroboric acid injection at (a) 25 °C, (b) 65 °C and (c) 105 °C | 127 |
| Figure 5.4 | The effect of temperatures on sandstone permeability after fluoroboric acidizing | 128 |
| Figure 5.5 | Initial pressure distribution at the beginning of acid injection | 130 |
| Figure 5.6 | Initial HBF ₄ acid distribution at the beginning of acid injection | 130 |
| Figure 5.7 | Pressure distribution after 25 mins (left) and after 35 mins (right) of fluoroboric acid injection at (a) 25 °C, (b) 65 °C and (c) 105 °C | 131 |
| Figure 5.8 | The effect of temperatures on sandstone pressure drop after fluoroboric acidizing | 132 |
| Figure 5.9 | HBF ₄ acid distribution after 25 mins (left) and after 35 mins (right) of fluoroboric acid injection at (a) 25 °C, (b) 65 °C and (c) 105 °C | 133 |
| Figure 5.10 | The effect of temperatures on HBF ₄ concentration along acid injection time | 135 |
| Figure 5.11 | The effect of temperatures on HF concentration along acid injection time | 136 |
| Figure 5.12 | The effect of temperatures on H ₂ SiF ₆ concentration along acid injection time | 137 |
| Figure 5.13 | Initial fast-reacting mineral distribution at the beginning of acid injection | 139 |
| Figure 5.14 | Initial silica gel precipitate distribution at the beginning of acid injection | 139 |

| | | |
|-------------|---|-----|
| Figure 5.15 | Fast-reacting mineral (left) and silica gel (right) distribution after 35 mins of fluoroboric acid injection at (a) 25 °C, (b) 65 °C and (c) 105 °C | 140 |
| Figure 5.16 | The effect of temperatures on fast-reacting mineral composition over injection time | 142 |
| Figure 5.17 | The effect of temperatures on silica gel precipitate composition over injection time | 143 |
| Figure 5.18 | The effect of acid concentration on sandstone porosity after acidizing at 25 °C | 145 |
| Figure 5.19 | The effect of acid concentration on sandstone porosity after acidizing at 65 °C | 147 |
| Figure 5.20 | The effect of acid concentration on sandstone porosity after acidizing at 105 °C | 147 |
| Figure 5.21 | The effect of acid concentration on sandstone permeability after acidizing at 25 °C | 149 |
| Figure 5.22 | The effect of acid concentration on sandstone permeability after acidizing at 65 °C | 149 |
| Figure 5.23 | The effect of acid concentration on sandstone permeability after acidizing at 105 °C | 150 |
| Figure 5.24 | The effect of acid concentration on pressure drop after acidizing at 25 °C | 151 |
| Figure 5.25 | The effect of acid concentration on pressure drop after acidizing at 65 °C | 153 |
| Figure 5.26 | The effect of acid concentration on pressure drop after acidizing at 105 °C | 153 |
| Figure 5.27 | The effect of acid injection rate on sandstone porosity after acidizing at 25 °C | 155 |
| Figure 5.28 | The effect of acid injection rate on sandstone porosity after acidizing at 65 °C | 157 |
| Figure 5.29 | The effect of acid injection rate on sandstone porosity after acidizing at 105 °C | 157 |

| | | |
|-------------|--|-----|
| Figure 5.30 | The effect of acid injection rate on sandstone permeability after acidizing at 25 °C | 159 |
| Figure 5.31 | The effect of acid injection rate on sandstone permeability after acidizing at 65 °C | 159 |
| Figure 5.32 | The effect of acid injection rate on sandstone permeability after acidizing at 105 °C | 160 |
| Figure 5.33 | The effect of acid injection rate on pressure drop after acidizing at 25 °C | 161 |
| Figure 5.34 | The effect of acid injection rate on pressure drop after acidizing at 65 °C | 163 |
| Figure 5.35 | The effect of acid injection rate on pressure drop after acidizing at 105 °C | 163 |
| Figure 6.1 | A flow chart for optimization process | 167 |
| Figure 6.2 | A 3 ³ full factorial design of experiment | 169 |
| Figure 6.3 | Normal probability plot of residuals (upper) and predicted vs. actual plot (bottom) for porosity enhancement ratio response | 189 |
| Figure 6.4 | Normal probability plot of residuals (upper) and predicted vs. actual plot (bottom) for permeability enhancement ratio response | 190 |
| Figure 6.5 | Normal probability plot of residuals (upper) and predicted vs. actual plot (bottom) for pressure drop response | 191 |
| Figure 6.6 | Residuals vs. predicted plot (upper) and leverage plot (bottom) for porosity enhancement ratio response | 193 |
| Figure 6.7 | Residuals vs. predicted plot (upper) and leverage plot (bottom) for permeability enhancement ratio response | 194 |
| Figure 6.8 | Residuals vs. predicted plot (upper) and leverage plot (bottom) for pressure drop response | 195 |
| Figure 6.9 | Box-cox plot before (upper) and after (bottom) an inverse power transformation for porosity enhancement ratio response | 197 |
| Figure 6.10 | Box-cox plot before (upper) and after (bottom) an inverse square root power transformation for permeability enhancement ratio response | 198 |

| | | |
|-------------|--|-----|
| Figure 6.11 | Box-cox plot before (upper) and after (bottom) a natural log power transformation for pressure drop response | 199 |
| Figure 6.12 | 2D contour plot (upper) and 3D surface plot (bottom) for porosity enhancement ratio response of Factors AB | 206 |
| Figure 6.13 | 2D contour plot (upper) and 3D surface plot (bottom) for permeability enhancement ratio response of Factors AB | 207 |
| Figure 6.14 | 2D contour plot (upper) and 3D surface plot (bottom) for pressure drop response of Factors AB | 208 |
| Figure 6.15 | 2D contour plot (upper) and 3D surface plot (bottom) for porosity enhancement ratio response of Factors AC | 210 |
| Figure 6.16 | 2D contour plot (upper) and 3D surface plot (bottom) for permeability enhancement ratio response of Factors AC | 211 |
| Figure 6.17 | 2D contour plot (upper) and 3D surface plot (bottom) for pressure drop response of Factors AC | 212 |
| Figure 6.18 | 2D contour plot (upper) and 3D surface plot (bottom) for porosity enhancement ratio response of Factors BC | 214 |
| Figure 6.19 | 2D contour plot (upper) and 3D surface plot (bottom) for permeability enhancement ratio response of Factors BC | 215 |
| Figure 6.20 | 2D contour plot (upper) and 3D surface plot (bottom) for pressure drop response of Factors BC | 216 |
| Figure A.1 | The control volume of the acidizing model | 245 |

List of Tables

| | | |
|------------|---|----|
| Table 2.1 | Mineralogy of a typical Berea sandstone (Al-Shaalan and Nasr-El-Din 2000) | 17 |
| Table 2.2 | Solubility of sandstone minerals (Portier et al. 2007) | 18 |
| Table 2.3 | Guideline for treatment fluid selection (Crowe et al. 1992) | 20 |
| Table 2.4 | Alternate sandstone acid procedures established by Portier et al. (2007) | 20 |
| Table 2.5 | Summary of the additives used in matrix acidizing and their functions | 21 |
| Table 2.6 | Summary of core flow test results in Jauf and Berea cores (Thomas et al. 2002b) | 24 |
| Table 2.7 | Summarized interpretation of reviewed papers on mud acid used in matrix acidizing | 28 |
| Table 2.8 | Summarized interpretation of reviewed papers on fluoroboric acid used in matrix acidizing | 34 |
| Table 2.9 | Summarized interpretation of reviewed papers on chelating agents used in matrix acidizing | 40 |
| Table 2.10 | Summarized interpretation of reviewed papers on retarded and organic acids used in matrix acidizing | 48 |
| Table 2.11 | Alternatives acids for high and low quartz content sandstone | 53 |
| Table 2.12 | Interpretive characterization and comparison of different acids used in matrix acidizing | 54 |
| Table 3.1 | Chemical composition of typical sandstone minerals (Economides and Nolte 2000) | 60 |
| Table 3.2 | The primary chemical reactions in acid treatments (Guo et al. 2007) | 63 |
| Table 3.3 | Recommended Acid Type and Strength for Sandstone Acidizing (Guo et al. 2007) | 67 |

| | | |
|------------|---|-----|
| Table 3.4 | Typical stage sequence for a sandstone acidizing treatment (Economides and Nolte 2000) | 68 |
| Table 3.5 | Summary of the Parameters included in the Modelling of Sandstone Acidization (Al-Shaalan and Nasr-El-Din 2000) | 78 |
| Table 3.6 | Comparison of Different Models Developed for Sandstone Acidizing | 81 |
| Table 4.1 | Required input parameter in the model | 113 |
| Table 5.1 | Summary of all the simulation cases in the parametric study for the effect of acid concentration | 121 |
| Table 5.2 | Summary of all the simulation cases in the parametric study for the effect of acid injection rate | 122 |
| Table 5.3 | Effect of temperature on porosity enhancement ratio | 126 |
| Table 5.4 | Effect of temperature on permeability enhancement ratio | 128 |
| Table 5.5 | Effect of temperature on pressure drop | 132 |
| Table 5.6 | Effect of temperature on HBF ₄ concentration | 135 |
| Table 5.7 | Effect of temperature on HF concentration | 136 |
| Table 5.8 | Effect of temperature on H ₂ SiF ₆ concentration | 137 |
| Table 5.9 | Effect of temperature on fast-reacting mineral volume fraction | 142 |
| Table 5.10 | Effect of temperature on silica gel volume fraction | 143 |
| Table 5.11 | Effect of acid concentration on porosity enhancement ratio | 146 |
| Table 5.12 | Effect of acid concentration on permeability enhancement ratio | 148 |
| Table 5.13 | Effect of acid concentration on pressure drop | 152 |
| Table 5.14 | Effect of acid injection rate on porosity enhancement ratio | 156 |
| Table 5.15 | Effect of acid injection rate on permeability enhancement ratio | 158 |
| Table 5.16 | Effect of acid injection rate on pressure drop | 162 |
| Table 6.1 | Summary of factors | 168 |
| Table 6.2 | Summary of build information | 169 |
| Table 6.3 | Simulation design layout | 172 |
| Table 6.4 | Summary of responses | 174 |
| Table 6.5 | Tabulation of simulation results | 175 |
| Table 6.6 | Fit summary of responses | 177 |

| | | |
|------------|--|-----|
| Table 6.7 | Sequential Model Sum of Squares of responses | 177 |
| Table 6.8 | Model summary statistics of responses | 179 |
| Table 6.9 | ANOVA for quadratic model of porosity enhancement ratio response | 181 |
| Table 6.10 | ANOVA for quadratic model of permeability enhancement ratio response | 181 |
| Table 6.11 | ANOVA for quadratic model of pressure drop response | 182 |
| Table 6.12 | Fit statistics of response | 184 |
| Table 6.13 | Coefficients in terms of coded factors of porosity enhancement ratio response | 185 |
| Table 6.14 | Coefficients in terms of coded factors of permeability enhancement ratio response | 186 |
| Table 6.15 | Coefficients in terms of coded factors of pressure drop response | 186 |
| Table 6.16 | Comparison of predicted data and actual data for porosity enhancement ratio response | 200 |
| Table 6.17 | Comparison of predicted data and actual data for permeability enhancement ratio response | 202 |
| Table 6.18 | Comparison of predicted data and actual data for pressure drop response | 203 |

Nomenclature

List of Abbreviations

| | |
|---|----------------------------|
| 1D | One-Dimensional |
| 2D | Two-Dimensional |
| 3D | Three-Dimensional |
| M | Mineral |
| K | Potassium |
| F | Fluorine |
| Na | Sodium |
| Ca | Calcium |
| Al | Aluminium |
| Fe | Iron |
| Mg | Magnesium |
| ¹¹ B | Boron-11 |
| ¹⁹ F | Fluorine-19 |
| Si | Silicon |
| SiO ₂ | Quartz |
| SO ₄ | Sulphate |
| SiF ₄ | Silicon Tetra fluoride |
| Si(OH) ₄ | Silicic Acid or Silica Gel |
| Na ₂ SiF ₆ | Sodium Fluorosilicate |
| K ₂ SiF ₆ | Potassium Fluorosilicate |
| K _{0.5} Na _{0.5} AlSi ₃ O ₈ | Feldspar |
| CaMg(CO ₃) ₂ | Dolomite |
| FeCO ₃ | Siderite |
| Mg ₆ Si ₄ O ₁₀ (OH) ₈ | Chlorite |
| KAl ₃ Si ₃ O ₁₀ (OH) ₂ | Mica / Illite |

| | |
|----------------------------------|----------------------------|
| Fe(OH)_2 | Iron Hydroxide |
| AlCl_3 | Aluminium Chloride |
| AlF_3 | Aluminium fluoride |
| Al_2SiO_5 | Aluminosilicates |
| CaF_2 | Calcium Fluoride |
| CaCO_3 | Calcium Carbonate |
| CH_3COOH | Acetic Acid |
| $\text{C}_6\text{H}_8\text{O}_7$ | Citric Acid |
| CH_3OH | Methanol |
| BF_4^- | Fluoroborate ion |
| H^+ | Hydrogen Ion |
| H_2 | Hydrogen Gas |
| H_2O | Water |
| HF | Hydrofluoric Acid |
| HCl | Hydrochloric Acid |
| H_3PO_4 | Phosphoric Acid |
| HCOOH | Formic Acid |
| HCOOCH_3 | Methyl Formate, |
| HCO_3^- | Bicarbonate |
| HCOO^- | Formate Anion |
| HBF_4 | Fluoroboric Acid |
| HBF_3OH | Borofluoric Acid |
| $\text{HBF}_2(\text{OH})_2$ | Dihydroxyfluoroboric Acid |
| $\text{HBF}(\text{OH})_3$ | Trihydroxyfluoroboric Acid |
| H_3BO_3 | Boric Acid |
| HSiF_5 | Fluorosilicic Acid |
| H_2SiF_6 | Fluorosilicic Acid |
| N_2 | Nitrogen Gas |
| NH_4Cl | Ammonium Chloride |
| NH_4F | Ammonium Fluoride |
| NH_4^+ | Ammonium Cation |

| | |
|-----------------------|--|
| APC | Aminopolycarboxylic Acid |
| EDG | Ethanol diglycine |
| NTA | Nitrilotriacetic Acid |
| APCA | Aminopolycarboxylic Acid |
| HACA | Hydroxyethylaminocarboxylic acid |
| GLDA | Glutamic Acid N,N-Diacetic Acid |
| Na-GLDA | Sodium Glutamic Acid N,N-Diacetic Acid |
| EDTA | Ethylenediaminetetraacetic Acid |
| HEIDA | Hydroxyethyliminodiacetic Acid |
| HEDTA | Hydroxyethylethylenediaminetriacetic Acid |
| Na ₃ HEDTA | Sodium Hydroxyethylethylenediaminetriacetic Acid |
| EOR | Enhanced Oil Recovery |
| HSE | Health, Safety and Environment |
| HTHP | High Temperature High Pressure |
| HTDP | High Temperature Deep Penetrating |
| BOPD | Barrel Oil per Day |
| BLPD | Barrel Liquid per Day |
| BHST | Bottomhole Static Temperature |
| Porosity-Perm | Porosity-Permeability |
| SEM | Scanning Electron Microscope |
| FESEM | Field Emission Scanning Electron Microscope |
| CT scan | Computerized Tomography Scan |
| ICP | Induced Coupled Plasma |
| NMR | Nuclear Magnetic Resonance |
| XRD | X-Ray Diffraction |
| OES | Optical Emission Spectrographic |
| EDS | Energy Dispersive X-Ray Spectroscopy |
| TSP | Thin Section Petrographic |
| FAAS | Flame Atomic Absorption Spectroscopy |
| PVTB | Pore Volume to Breakthrough |
| CFD | Computational Fluid Dynamics |

| | |
|-----------|---|
| FEM | Finite Element Method |
| FDM | Finite Difference Method |
| 2FI | Two-factor interaction |
| ANOVA | Analysis of variance |
| CI | Confidence interval |
| CCD | Central composite design |
| Df | Degree of freedom |
| DOE | Design of experiment |
| Ln | Natural logarithm |
| exp | Exponential |
| p-value | Probability value |
| PERM | Permeability enhancement ratio |
| PORO | Porosity enhancement ratio |
| Prob. | Probability |
| PRDR | Pressure drop |
| PRESS | Predicted residual error sum of squares |
| RSM | Response surface methodology |
| Sqrt | Square root |
| Std. Dev. | Standard Deviation |
| VIF | Variance inflation factor |
| Vs. | Versus |
| vol | Volume |
| MOHE | Ministry of Higher Education |
| FRGS | Fundamental Research Grant Scheme |
| FOES | Faculty of Engineering and Science |

List of Units

| | |
|-----|----------------|
| 1 | dimensionless |
| % | percentage |
| wt% | weight percent |

| | |
|------------------------|--------------------------------|
| °C | degree Celsius |
| K | degree Kelvin |
| °F | degree Fahrenheit |
| pH | potential of Hydrogen |
| psi | pounds per square inch |
| Pa | Pascal |
| Pa.s | Pascal second |
| s | second |
| min | minute |
| ft | feet |
| in | inch |
| m | meter |
| md / mD | milli Darcy |
| m ² | meter square |
| ml | millilitre |
| m/s | meter per second |
| m ² /s | meter square per second |
| g | gram |
| 1/m or m ⁻¹ | per meter |
| barrel/min | barrel per minute |
| gal/ft | gallon per feet |
| cm/s | centimetre per second |
| g/m ³ | gram per meter cube |
| kg/m ³ | kilogram per meter cube |
| g/m ³ s | gram per meter cube second |
| g/mol | gram per mol |
| mol/m ³ | mol per meter cube |
| mol/m ² s | mol per meter square second |
| mol/m ³ s | mol per meter cube second |
| cal/mol.K | calories per mol degree kelvin |

List of Subscripts

| Subscript | Description |
|-----------|---|
| x | x -direction / x -axis |
| y | y -direction / y -axis |
| z | z -direction / z -axis |
| i | Type of acids (1 = HF, 2 = H ₂ SiF ₆) |
| j | Type of minerals (1 = fast-reacting mineral, 2 = slow-reacting mineral, 3 = silica gel) |
| x_1 | Temperature (x -axis) |
| x_2 | Acid concentration (y -axis) |
| x_3 | Acid injection rate (z -axis) |
| i | Type of variables |
| j | Type of variables |

List of Symbols

| Symbol | Description | Unit |
|----------------|---|-----------|
| x | Average F/Al Ratio | 1 |
| y | Fluoride number coordinated with Al after tertiary reaction | 1 |
| n | Coefficient related to the formation condition | 1 |
| s | Specific surface area | 1/m |
| e | Exponential function | - |
| ∂ | Partial differential function | - |
| $\bar{\nabla}$ | Divergence function | - |
| Σ | Summation function | - |
| R | Universal gas constant | cal/mol.K |
| γ | Ratio of gravity | 1 |
| t | Time | s or min |

| | | |
|-----------------|---|-------------------|
| T | Temperature | °C or K |
| P | Pressure | Pa |
| P_0 | Initial pressure | Pa |
| P_f | Final pressure | Pa |
| P_{out} | Back pressure at the outlet of the core | Pa |
| P_{ref} | Reference pressure level | Pa |
| ΔP | Pressure drop | Pa |
| Δx | x distance of control volume | m |
| Δy | y distance of control volume | m |
| Δz | z distance of control volume | m |
| Δt | change in time | s or min |
| μ | Viscosity of acid | Pa.s |
| ∞ | Viscosity of acid | Pa.s |
| D_c | Diffusion coefficient of acid | m ² /s |
| ν_i | Stoichiometry coefficient of reactions | 1 |
| $\nu_1 - \nu_8$ | Stoichiometry coefficient of reactions | 1 |
| u | Velocity of injected acid | m/s |
| \vec{u} | Vector velocity | m/s |
| u_x | Average Darcy velocity in y - z plane | m/s |
| u_y | Average Darcy velocity in x - z plane | m/s |
| u_z | Average Darcy velocity in x - y plane | m/s |
| ν | Injection rate of acid | m/s |
| Q | Injection rate of acid | m/s |
| ϕ | Porosity | 1 |
| ϕ_1 | Porosity at time step 1 | 1 |
| ϕ_2 | Porosity at time step 2 | 1 |
| ϕ^0 | Initial porosity | 1 |
| ϕ_f | Final porosity | 1 |
| k | Permeability | m ² |
| k_1 | Permeability at time step 1 | m ² |
| k_2 | Permeability at time step 2 | m ² |

| | | |
|---------------------|--|------------|
| k_0 | Initial permeability | m^2 |
| k_f | Final permeability | m^2 |
| r_h | Hydrolysis rate of HBF_4 | mol/m^3s |
| k_h | Equilibrium rate constant | $1/s$ |
| M_1 | Lumped group of fast-reacting minerals | 1 |
| M_2 | Lumped group of slow-reacting minerals | 1 |
| M_3 | Silica gel | 1 |
| $K_{Si(OH)_4}^{SP}$ | Solubility product of silica gel | 1 |
| C_i | Concentration of acid | mol/m^3 |
| C_i^0 | Initial Concentration of acid | mol/m^3 |
| C_{acid} | Concentration of acid | mol/m^3 |
| C_3 | Concentration of HBF_4 | mol/m^3 |
| C_{HBF_4} | Concentration of HBF_4 | mol/m^3 |
| C_{HF} | Concentration of HF | mol/m^3 |
| $C_{H_2SiF_6}$ | Concentration of H_2SiF_6 | mol/m^3 |
| C_{H^+} | Concentration of hydrogen ion | mol/m^3 |
| $C_{BF_4^-}$ | Concentration of fluoroborate ion | mol/m^3 |
| v_{acid} | Volume of acid | m^3 |
| $v_{mineral}$ | Volume of mineral | m^3 |
| V_j | Volume fraction of mineral | 1 |
| V_1 | Volume fraction of fast-reacting mineral | 1 |
| V_2 | Volume fraction of slow-reacting mineral | 1 |
| V_3 | Volume fraction of silica gel | 1 |
| V_1^0 | Original volume fraction of fast-reacting mineral | 1 |
| V_2^0 | Original volume fraction of slow-reacting mineral | 1 |
| V_3^0 | Original volume fraction of silica gel | 1 |
| $V_{a,j}$ | Number of acids reacting with minerals $j=2$ | 1 |
| N_m | Total number of minerals reacting with acids $i=3$ | 1 |
| $E_{f,i,j}$ | Reaction rate between the acid and mineral | m/s |
| S_j^* | Reaction surface of mineral | $1/m$ |
| MW_i | Molecular weight of acid i | g/mol |

| | | |
|----------------|--|----------------------|
| MW_{acid} | Molecular weight of acid | g/mol |
| $MW_{mineral}$ | Molecular weight of mineral | g/mol |
| ρ | Density of acid | kg/m ³ |
| ρ_{acid} | Density of acid | kg/m ³ |
| ρ_j | Density of mineral j | kg/m ³ |
| ρ_s | Density of solid | kg/m ³ |
| $\beta_{i,j}$ | Dissolving power of mineral j by acid i | 1 |
| n | Coefficient of sandstone condition = 3 | 1 |
| l or L | Length of core sample | in |
| r | Radius | in |
| r_c | Radius of core sample | in |
| D | Diameter of core sample | in |
| W_i | Overall mass of component i in the control volume | g/m ³ |
| $\omega_{i,j}$ | Mass fraction of component i in phase j | 1 |
| $\omega_{i,s}$ | Mass fraction of component i in solid phase | 1 |
| g_i | Mass of component i | g |
| $g_{phase j}$ | Mass phase j | g |
| g_{solid} | Mass solid phase | g |
| St_j | Saturation of phase j | 1 |
| N_i | Flux of component i | m/s |
| u_j | Darcy velocity of phase j | m/s |
| $K_{i,j}$ | Dispersion coefficient of component i in phase j | 1 |
| R_i | Source of component i | g/m ³ s |
| r_i | Surface area – specific reaction rate of i | mol/m ² s |
| S_j | Surface area of mineral j in a unit of bulk volume | 1/m |
| N_{DA} | Damkohler number | 1 |
| Λ | Dimensionless composition of mineral | 1 |
| N_{AC} | Dimensionless acid capacity number | 1 |
| A | Temperature | °C |
| B | Acid concentration | % |
| C | Acid injection rate | m/s |

| | | |
|---------------|--------------------------------|---------|
| ε | Statistical error term | 1 |
| f | Function | 1 |
| k | Number of factors | 1 |
| β_0 | Constant coefficient | 1 |
| β_i | Linear coefficient | 1 |
| β_1 | Linear coefficient | 1 |
| β_2 | Linear coefficient | 1 |
| β_3 | Linear coefficient | 1 |
| β_{11} | Quadratic coefficient | 1 |
| β_{22} | Quadratic coefficient | 1 |
| β_{33} | Quadratic coefficient | 1 |
| β_{ij} | Interaction coefficient | 1 |
| β_{12} | Interaction coefficient | 1 |
| β_{13} | Interaction coefficient | 1 |
| β_{23} | Interaction coefficient | 1 |
| x_i | Independent variables | 1 |
| x_j | Independent variables | 1 |
| R1 | Porosity enhancement ratio | 1 |
| R2 | Permeability enhancement ratio | 1 |
| R3 | Pressure drop | Pa |
| Y | Predicted response | 1 or Pa |

Chapter 1 Introduction

1.1 Research Introduction

In the recent years, the energy demand around the globe has continued to grow. According to a prediction, the aggregate requirement of energy would be 40% more in 2020 than in the present (Aboud et al. 2007). The industry aims to ensure a higher economical production and cutting production cost at the same time. Therefore, an innovative and feasible technology development in well stimulation and enhanced oil recovery (EOR) become one of the primary focuses in the oilfield (Leong and Mahmud 2017). Well operations like drilling, completion, workover and production often result in formation damage (McLeod 1984). This would eventually cause a significant and rapid decline in oil and gas productivity especially after many years of production (William et al. 1979). In order to solve this problem, matrix acidizing has been employed to recover the production profile of a well and preventing economical loss of a well (Schechter 1992, Kalfayan and Metcalf 2000, Economides et al. 2013). Acid can prominently improve the porosity and permeability of a reservoir formation as well as enhancing the well productivity (Kalfayan 2008). It can also mitigate the formation damage issue such as fines migration and mud invasion (Ebrahim et al. 2014).

In the past, the most popular acid used in sandstone stimulation treatment is the mud acid (Kalfayan and Metcalf 2000). It had been extensively applied and had achieved great success since it was developed in the early days (Smith and Hendrickson 1965). HF can effectively react and dissolve the quartz, feldspar and clay minerals, which are the main constituents of a sandstone matrix. Whereas HCl is well known in precipitation control (Leong and Ben Mahmud 2018). However, there are some significant problems of using conventional mud acid at high temperature condition (Al-Harthy et al. 2009). At temperature above 200 °F, it causes rapid reduction in well productivity and in some case, it even resulted in total production loss, which is an undesirable drawback to an enhanced oil recovery (EOR) operation (Shafiq and Ben Mahmud 2017). Such a situation was

mainly due to the early and rapid rate of reaction between the mud acid and the sandstone minerals (Shuchart and Gdanski 1996, Al-Dahlan et al. 2001).

According to the literature, there are a variety of acids that have been developed apart from the conventionally used mud acid such as the chelating agents (Legemah et al. 2015, Garcia et al. 2016, Shafiq et al. 2017, Shafiq et al. 2018), retarded acids (Aneto 2012, Ji et al. 2014, Ji et al. 2016), organic acids (Andotra 2014, Zhou and Nasr-El-Din 2016) as well as Fluoroboric Acid (HBF_4) (Pituckchon 2014, Zhou et al. 2016). Different kinds of acids have their own suitability in stimulating formations that have different minerals components. However, considering unconsolidated sandstone core that is high in silicates minerals, fluoroboric acid (HBF_4) is the most suitable alternatives due to its unique retardation effect to penetrate slow and deep in acidizing (Leong and Ben Mahmud 2018).

However, the understanding on the use of HBF_4 for sandstone acidizing is still limited in the literature. There are many other practical and crucial yet remained unknown questions related to the efficient use of HBF_4 in sandstone acidizing (Pituckchon 2014). For example, the effect of temperatures, acid concentration and acid injection rate in enhancing the porosity and permeability of a sandstone formation are not studied extensively. In term of numerical and modelling study, it is also found that less effort had been made in the development of model for HBF_4 acidizing (Leong et al. 2018b).

Furthermore, an optimization approach for sandstone acid stimulation design is very important. The reservoir condition must be carefully studied before the acid is being applied into a targeted reservoir (Zakaria 2013). Numerous approaches have been employed to develop different methodologies to understand the effect of various parameters affecting the performance of sandstone acidizing process in well stimulation, but these approaches had mainly focused on the use of mud acid (Li et al. 2004, Xie et al. 2005). However, less emphasis had been given to the optimization of various parameters that may significantly affect the fluoroboric acidizing performance.

Therefore, the aim of this thesis is to solve the abovementioned problems associated to sandstone acidizing using fluoroboric acid by adopting both the numerical modelling and optimization approach. This research would also widen the knowledge of well stimulation by throwing some insights into the use of fluoroboric acid at elevated temperature.

1.2 Research Gap and Problem Statement

Most of previous studies covered the use of mud acid in sandstone matrix acidizing. However, there are numerous disadvantages of mud acid at high temperature conditions, which lead to the urge for researchers to seek for alternative solution. In recent years, there are many acids, which have been developed and experimentally investigated to identify their suitability to become an alternative to mud acid. However, there is no clear classification of the parameters and conditions that affect performance of the acids on the sandstone matrix acidizing results.

From the literature survey, HBF_4 is one of the developed acids to replace the mud acid. However, there is no detail modelling investigation into the use of HBF_4 acid for sandstone acidizing as well as benchmarking against the experimental data. Although there are some benefits of HBF_4 in sandstone acidizing, there is no proper guidelines on how to make its application in sandstone acid stimulation a successful one. Furthermore, the understanding of how various key factors such as the temperature, acid concentration and acid injection rate affect the performance of HBF_4 acidizing remains unanswered. The effect of temperature had only been investigated up to 65 °C, which is not high enough to represent the deep field condition with temperature higher than 100 °C.

In addition, the optimum conditions at which the acid can be applied into sandstone matrix acidizing remain blurry and unclear. It was found that no systematic optimization study had been conducted on sandstone acidizing using fluoroboric acid. Moreover, it was found that there is insufficient information about the empirical relationships that correlate the porosity, permeability and pressure drop with the sandstone acidizing conditions such as the temperature, acid concentration and injection rate.

Therefore, these research problems leave some gaps to be filled in this area of study. Hence, this leads to the conceptual formulation and development of this research topic and has motivated this research to be carried out. In the following section, some of the research questions and their corresponding hypotheses had been formulated. This research would to bridge the mentioned research gap by solving these research questions.

1.3 Research Questions and Hypotheses

The research questions to be answered in this work are listed as follow.

- 1) How much does HBF_4 improve the rock properties, such as porosity and permeability quantitatively at elevated temperature condition?
- 2) To what degree does HBF_4 acid concentration and acid injection rate affect the performance of sandstone acidizing?
- 3) How to determine the optimal condition for the application of HBF_4 in sandstone acid stimulation?

The hypotheses of this research are then formulated.

- 1) The hydrolysis rate and reaction between HBF_4 with the sandstone minerals at high operating temperature condition might have increased, hence becoming more effective in porosity and permeability enhancement.
- 2) The variation in acid concentration and acid injection rate during sandstone acidizing is expected to affect the level of improvement in the pore spaces and the permeability of the core plug, thus the overall stimulation performance.
- 3) A systematic optimization methodology could be helpful to determine the optimum solution for sandstone acidizing using HBF_4 by considering all the concerned factors and obtaining suitable responses data.

To address or answer the derived research question and also proving the hypotheses, a new mechanistic model will be developed for HBF_4 acidizing process using COMSOL® Multiphysics commercial software. Furthermore, a new optimization approach will be used for describing the relationship between the factors of temperature, acid concentration and injection rate with the responses of porosity, permeability and pressure. This would optimize the benefits of HBF_4 while preventing undesired drawbacks.

1.4 Aims and Objectives

The ultimate aim of current research is to determine the optimum design of the sandstone matrix acidizing core flooding process. The main focal point of this research is to evaluate the efficiency of the fluoroboric acid (HBF_4) in well stimulation. The research scopes and detailed objectives to be achieved are listed below:

1. To thoroughly evaluate and characterize different acids developed and used for sandstone acidizing by performing a preliminary screening and survey of the literature against the criteria of feasibility, reaction mechanism as well as cost, health, safety and environment (HSE).
2. To propose a feasible numerical and modelling approach for sandstone acid core flooding process through a comparison and assessment of the modelling techniques in the literature by considering the reactions and mechanisms between the acids and the sandstone minerals.
3. To utilize and implement the proposed approach by developing a core-scale three-dimensional (3D) mechanistic model in COMSOL® Multiphysics commercial software modules of Computational Fluid Dynamics (CFD) using a finite element method (FEM).
4. To analytically evaluate the effects of temperature, acid concentration and acid injection rate on the core flooding model by performing a parametric study and sensitivity analysis after validating the simulation results by benchmarking against the experimental data.
5. To perform a design optimization study in Design-Expert® software using a response surface methodology (RSM) approach for sandstone acidizing process and developing empirical models for the relationships between the factors and responses of porosity, permeability and pressure.

1.5 Research Scopes

In obtaining the optimum design of sandstone acidizing core flooding process, this research examines and look into the parameters that have significant effects, in association with the acid performance. These parameters include the temperature, acid concentration, and acid injection rate. The scope of present study undertaken to investigate these parameters involves the extensive literature survey, a 3D numerical finite element modelling, parametric study and sensitivity analysis as well as design optimization and empirical modelling. The following is a general overview of the work within the scope to achieve the aim and objectives set for this research study.

Firstly, the literature survey conducted in this study covers two main areas of research. The first part focuses on screening through different acids that are suitable for sandstone acidizing. The acids are classified based on different criteria to achieve research objective 1. Meanwhile, the second part specifies on the comparison and assessment of the numerical approach that had been conducted on mud acid. A proposal of modelling methodology for HBF_4 modelling is aimed to accomplish research objective 2.

The finite element numerical modelling investigation is performed using COMSOL® Multiphysics version 5.2a. The model is developed to be verified against the results obtained from the experimental work available in the literature to ensure the accuracy, reliability and predictability of the model developed. This stage of study is performed to fulfil objective 3. In addition, this calibrated model is then being adopted to perform parametric sensitivity analysis to investigate the individual effect of the temperature, acid concentration, acid choice and acid injection rate on the performance of matrix acidizing outcomes. This stage of study is carried out to achieve research objective 4.

Next, the design optimization of the sandstone matrix acidizing core flooding process is achieved by using the Design-Expert® version 11. A response surface methodology (RSM) is proposed to conduct the design of experiment (DOE) in order to satisfy research objective 5. Last but not least, the scope of study also includes the constructive future work recommendation in this research area. This is to ensure a continuous improvement and enhancement in current technology of sandstone acid stimulation.

1.6 Novelty, Research Significance and Contributions

This research study carried out is unique and novel in different aspects and areas of petroleum engineering, specifically in the well stimulation topics of enhanced oil recovery (EOR). This research will generate a new knowledge on reservoir stimulation technique, in the aspect of sandstone matrix acidizing using HBF_4 acid in particular. Some of the major research achievements over the course of work are outlined as follow.

First and foremost, current work will provide a detailed screening and characterization of different acids that have been applied for sandstone acidizing. The evaluation against the criteria of feasibility, reaction mechanism as well as cost, health, safety and environment (HSE) would provide an insight on the suitability of each acids in different scenarios and conditions. Besides, this study would extensively compare and assess all the modelling technique for sandstone acidizing process. This is very useful in providing clear classification of the advantages and shortcomings of each modelling approach. This would also contribute to ensure the feasibility of the model developed for HBF_4 acid stimulation.

The newly developed HBF_4 acidizing model that had been validated with the experimental data can be further applied to investigate the effect of elevated temperatures, different acid concentration and injection rate on the change in porosity and permeability of a sandstone matrix. The parametric study and sensitivity analyses provided in this research could determine if each of the factors are significant in sandstone acidizing. This is crucial to ensure that the benefits of HBF_4 could be maximized.

Moreover, this research is intended to determine the optimum conditions for HBF_4 to show a significant improvement in enhancing the porosity and permeability of a low permeable sandstone formation reservoir at high temperatures. Therefore, this research would be able to make a significant breakthrough in the oil and gas industry by diversifying the acid choice, concentration and injection rate, in order to optimize the sandstone matrix acidizing process at elevated temperatures. The empirical models formulated from this research would contribute to predict and forecast the sandstone matrix acidizing process in the future.

1.7 Thesis Outlines and Organization

This thesis comprised of a research study on the numerical modelling and optimization approach of sandstone matrix acidizing process, which is documented into 7 chapters. At the end of this chapter, Figure 1.1 shows a clear overview of this thesis layout.

Chapter 1 presents an introduction to the research study and thesis organization. An overview of the research idea is drawn to attention, providing a fundamental insight into the next chapter. The research gap and problems are highlighted and the main aim and objectives to be achieved from this research study are formulated. It also includes the novelty, research question and hypotheses as well as the research significance and major contributions of this thesis.

Chapter 2 covers some of the major background theories that is crucial to provide a basic understanding towards many relevant aspects of the research topic. Most of the technical terms used in this thesis are explained in detail in this chapter, prior to an in-depth look into the following chapters. This chapter also includes a preliminary screening and characterization of all suitable acids for sandstone acidizing through a comprehensive literature survey of the experimental works. This literature review is essential as it does not only understand the state-of-art of the current technologies developed, but also helps to highlight the technical research gaps. The materials in Chapter 2 is based on:

Journal Paper

1. **Leong, V. H.** and Mahmud, H. B. (2018). A preliminary screening and characterization of suitable acids for sandstone matrix acidizing technique: a comprehensive review. *Journal of Petroleum Exploration and Production Technology*. Springer Nature. <https://doi.org/10.1007/s13202-018-0496-6>

Conference Paper

2. **Leong, V. H.** and Mahmud, H. B. (2017). A comparative study of different acids used for sandstone acid simulation: a literature review. *In Proceeding: International Conference on Materials Technology and Energy (ICMTE) 2017*. Curtin University, Miri, Sarawak, Malaysia. 20th – 21st April 2017.

Chapter 3 provides some of the background study on the interaction, chemical reactions and mechanisms between the acids and rock minerals during sandstone acidizing. It also reviews the literature from the main aspects of this research topic, which is the numerical modelling works that have been done by previous researchers. The modelling techniques used for mud acid previously are also sorted out and summarized. This literature review proposes the most suitable mechanistic modelling design for sandstone acidizing using HBF_4 . The modelling methodology outlined serves as an important guideline for this research study, which is explained clearly in the next chapter. The materials in Chapter 3 is based on:

Journal Paper

1. **Leong, V. H.**, Mahmud, H. B., Law, M. C., Foo, C. Y. H. and Tan, I. S. (2018). A comparison and assessment of the modelling and simulation of the sandstone matrix acidizing process: a critical methodology study. *Journal of Natural Gas Science and Engineering*. 57. 52-67. Elsevier B. V. <https://doi.org/10.1016/j.jngse.2018.06.044>

Conference Paper

2. **Leong, V. H.** and Mahmud, H. B. (2017). A methodological approach to model acidizing process for sandstone well stimulation: a conceptual framework. *In Proceeding: 1st One Curtin International Postgraduate Conference (OCPC) 2017*. Curtin University, Miri, Sarawak, Malaysia. 10th – 12th December 2017.

Chapter 4 describes the development of the numerical model for HBF_4 acidizing process by implementing the four-parameter modelling technique. The model includes the modules in COMSOL® Multiphysics, version 5.2a such as the chemical species transport module, fluid flow module and mathematics module, based on kinetic approach. All the governing equations are presented, along with the initial and boundary condition set for each module of the model. The numerical solution and implementation of the module is also demonstrated clearly. The validation of the model against the experimental data are also demonstrated in this chapter before conducting further detailed study. The materials in Chapter 4 is based on:

Journal Paper

1. **Leong, V. H.**, Mahmud, H. B., Law, M. C., Foo, C. Y. H. and Tan, I. S. (2018). A numerical modelling and simulation of core-scale sandstone acidizing process: a study on the effect of temperature. *Journal of Petroleum Exploration and Production Technology*. Springer Nature. <https://doi.org/10.1007/s13202-018-0522-8>

Conference Paper

2. **Leong, V. H.** and Mahmud, H. B. (2017). Sandstone acid stimulation using fluoroboric acid. *In Proceeding: 5th Postgraduate Borneo Research Colloquium 2017*. University Malaysia Sarawak (UNIMAS), Kuching, Sarawak, Malaysia. 4th – 6th July 2017.

Chapter 5 discusses the results of the parametric study and sensitivity analyses. This chapter is comprised of the study on the individual effects of the formation temperature, acid concentration and injection rate on the performance of sandstone acidizing. The results of simulation are demonstrated using the numerical visualization and graphical representation. The results presented include the change in porosity, permeability, acid concentration and mineral concentration during the core flooding process. Hence, the efficiency of the acid at different acidizing conditions are compared and analysed. This would show the significance of each factor in affecting sandstone acidizing. The materials in Chapter 5 is based on:

Journal Paper

1. **Leong, V. H.**, Mahmud, H. B., Law, M. C., Foo, C. Y. H. and Tan, I. S. (2018). A sensitivity analysis and parametric study of factors affecting sandstone acidizing using numerical simulation. *Journal of Petroleum Exploration and Production Technology*. Springer Nature. (Under review)

Conference Paper

2. **Leong, V. H.**, Mahmud, H. B., Law, M. C., Foo, C. Y. H. and Tan, I. S. (2018). A study on the effect of acid concentration at various temperatures on sandstone

acidizing: a numerical simulation. *In Proceeding: One Curtin International Postgraduate Conference (OCPC) 2018*. Curtin University, Miri, Sarawak, Malaysia. 26th – 28th November 2018.

Chapter 6 describes the response surface methodology (RSM) applied for the optimization study of this research. It consists of the techniques on how the design of experiment (DOE) is carried out for the empirical modelling and determination of the optimal conditions. The results and discussions presented in this chapter include the analysis of variance (ANOVA) of the responses, residual analysis of response data as well as empirical model fitting and optimization. This chapter had provided an optimized solution for sandstone acidizing. The materials in Chapter 6 is based on:

Journal Paper

1. **Leong, V. H.**, Mahmud, H. B., Law, M. C., Foo, C. Y. H. and Tan, I. S. (2018). An optimization approach for sandstone acidizing process using response surface methodology (RSM) and numerical simulation. *Journal of Petroleum Science and Engineering*. Elsevier B. V. (Under review)

Conference Paper

2. **Leong, V. H.**, Mahmud, H. B., Law, M. C., Foo, C. Y. H. and Tan, I. S. (2018). An optimization framework for sandstone acidizing using design of experiment (DOE) and mathematical modelling. *In Proceeding: 11th Curtin University Technology, Science and Engineering (CUTSE) International Conference 2018*. Curtin University, Miri, Sarawak, Malaysia. 26th – 28th November 2018.

Chapter 7 concludes and summarizes the major findings of this research study. It also proposed some recommendations of future study that can be done in this area of research to ensure continuous improvement and enhancement of current technologies.

At the end of this thesis, substantial amount of references used in this research study are listed to give accreditation and recognition to the work conducted by previous researchers.

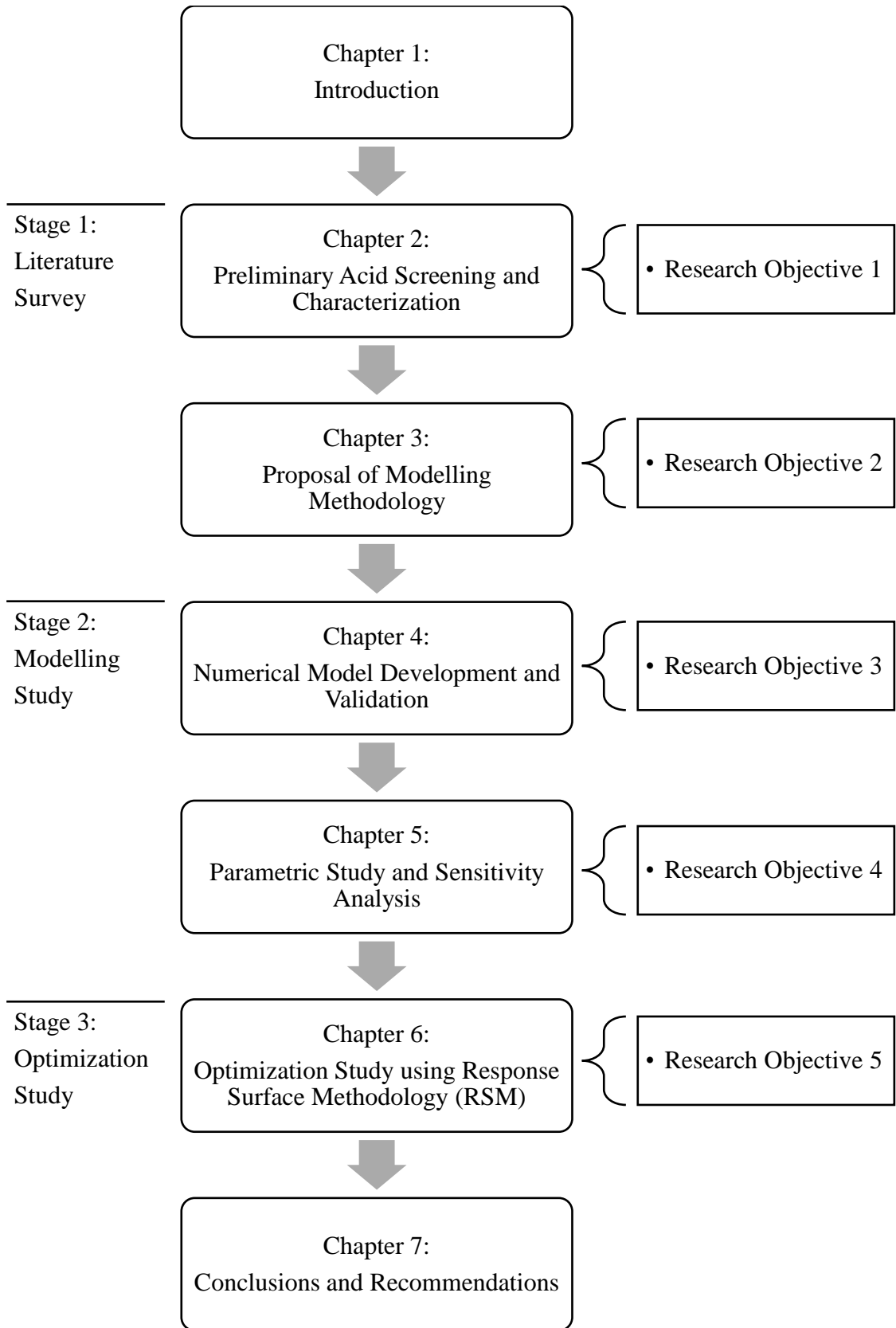


Figure 1.1 Overview of the steps taken in this research study

Chapter 2 Preliminary Acid Screening and Characterization

2.1 Introduction

In chapter 1, only a brief introduction about the research study is presented, giving a surface understanding of the research idea. There is no discussion on the underlying knowledge about the research such as the relevant theories, principles and technicalities. Therefore, chapter 2 would be focusing on discussing the detailed background information about many technical aspects of the research topic, which includes the well stimulation, sandstone mineralogy, the practice in sandstone matrix acidizing, the treatment design, the use of additives and sandstone channelling and wormholing.

The primary aim of this chapter is to comprehensively and critically review all the experimentations that were performed using different types of acid. In this chapter, a preliminary screening and comparison of different acids based on literature studies was conducted to optimize the selection of acid, targeting various temperatures of sandstone condition. Synchronously, an evaluation of the pros and cons of the acids used in association with sandstone formation were clearly addressed and highlighted. At the end of chapter 2, an outlook or insight into the research significance of further studies had been proposed.

2.2 Research Background

2.2.1 Well Stimulation

The operations in oil and gas field such as drilling, completion, workover, production and other long time operations result in the deposition of minerals near wellbore over time. Consequently, this results in production depletion due to formation damage occurring

around the wellbore (William et al. 1979). Therefore, field engineers must determine the solution to perform well treatment in order to bring up the productivity of the wells to ensure economic returns. One such solutions is known as well stimulation (Schechter 1992, Economides et al. 2013).

Well stimulation is a technique applied to enhance the production of oil or gas from the reservoir to the wellbore. It has played an important role in the development of oil and gas wells, ensuring good economic returns (Cipolla 2003). In recent years, many creative and innovative approaches are used to treat the wells (Coulter 2011). Hydraulic fracturing enhances the oil and gas production by creating fracture in the reservoir well through injection of hydraulic fluid at a pressure higher than that of the formation pressure (Economides et al. 2013). In the industry, hydraulic fracturing still represents the higher interest than other well stimulation methods. However, acidizing also plays a major role in different case studies. The use of acids like hydrochloric acid, hydrofluoric acid, formic acid and acetic acid are all important (Coulter 2012).

The most common stimulation techniques include hydraulic fracturing, matrix acidizing and fracture acidizing. Each of these techniques has different advantages and limitations in stimulating a well. Figure 2.1 shows the penetration of acid being injected into a sandstone matrix during acidizing.

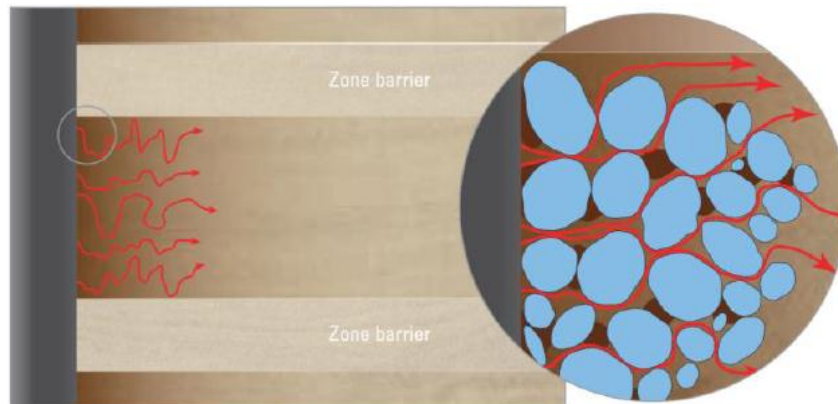


Figure 2.1 Pore scale figure of matrix acidizing process when the acid is being injected and acid passes through the pore space illustrated by Veldkam and Boxem (2015)

Chapter 2 Preliminary Acid Screening and Characterization

Often, questions have been raised up on the choice of fracturing or acidizing. In fact, the decision whether to fracture a well or acidize it depends on various factors which include the formation geology, production history and well intervention objectives (Al-Harthy et al. 2009).

The loose formations with relatively better porosity and permeability require less intensive hydraulic fracturing, whereas tight formations with relatively lower porosity and permeability require highly intensive hydraulic fracturing. The formation permeability is a very important parameter to be considered before performing hydraulic fracturing (Holman 1982). However, for loosely bound formations, hydraulic fracturing has high tendency to cause formation collapse due to the overburden pressure. Furthermore, the formation with damage due to drilling and production is not recommended to be stimulated with hydraulic fracturing. This is because it might cause further damage to the wellbore such as collapse. Instead, matrix acidizing is more suitable for such formation (Houseworth 2014).

In common practice acid fracturing is applied to carbonate formations, which are rich in limestones and dolomites (King 1986, Milligan 1994). The acid is channelled into the fracture surface to prevent it from being closed by overburden stress. Acid fracturing is more successful to be applied in carbonate formations with high natural fractures and high permeability (Houseworth 2014).

For sandstone formations, matrix acidizing tends to have limited penetration depth. Typically, matrix acidizing has a shorter penetration depth of about 0.3m in comparison to hydraulic fracturing and fracture acidizing. Usually, matrix acidizing is not recommended for formations with extremely low permeability. This is because such formations would require a deeper penetration depth in order to be successfully stimulated. As such, hydraulic fracturing is more suitable in this case. However, matrix acidizing is viable and effective when the well is naturally fractured and is normally used to remove the formation damage near the well, which prevents flow into the well. Hence, the acid can dissolve the plugging minerals in the production flow path (Economides et al. 2013). Therefore, different well stimulation methods as shown in Figure 2.2, have different practicality and suitability for different formations.

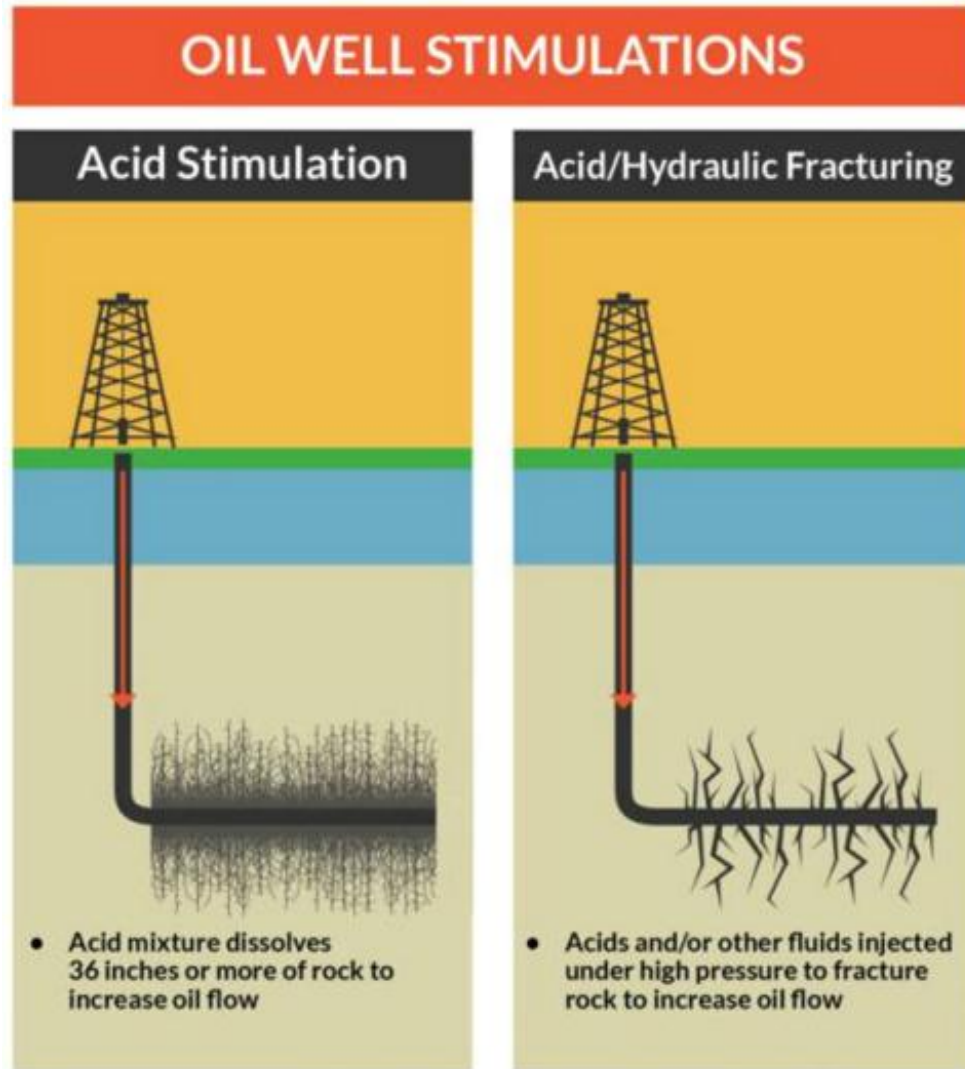


Figure 2.2 Oil Well Stimulations Illustration (Conservancy 2016)

2.2.2 Sandstone Mineralogy

Sandstone is a clastic sedimentary rock. Sometimes, it is also called arenite. Sandstone is made up of silica, SiO_2 and many silicate minerals. The main compositions of a sandstone matrix include quartz, feldspar and different forms of clay. Zeolite may also present in a sandstone although it is rare (Muecke 1982). Table 2.1 shows the concentration of different minerals present in a typical Berea Sandstone core sample used in the industry for core flooding test. Figure 2.3 shows the mineral components of a sandstone rock.

Chapter 2 Preliminary Acid Screening and Characterization

When reacting with HF acid, clays and feldspar have higher dissolution rate than quartz. This is due to the characteristic of quartz, having a more stable structure and relatively lower specific surface area.

Table 2.1 Mineralogy of a typical Berea sandstone (Al-Shaalan and Nasr-El-Din 2000)

| Mineral | Concentration (wt.%) | Chemical Formulae |
|---------------|----------------------|---|
| Quartz | 75 | SiO ₂ |
| Feldspar | 5 | K _{0.5} Na _{0.5} AlSi ₃ O ₈ |
| Dolomite | 5 | CaMg(CO ₃) ₂ |
| Siderite | 5 | FeCO ₃ |
| Chlorite | 5 | Mg ₆ Si ₄ O ₁₀ (OH) ₈ |
| Mica / Illite | 5 | KAl ₃ Si ₃ O ₁₀ (OH) ₂ |

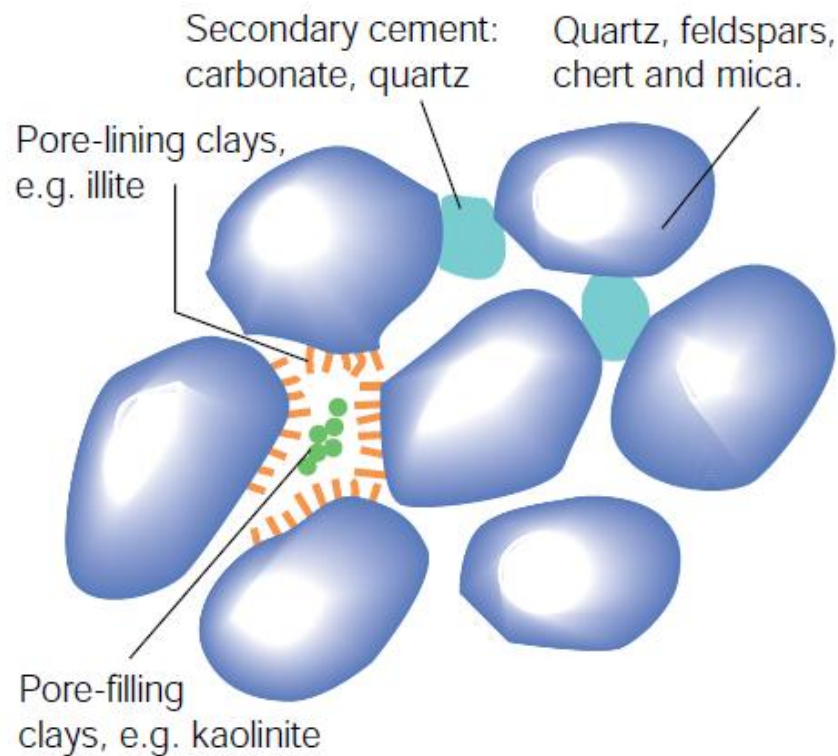


Figure 2.3 Constituents of sandstone, all of which are soluble in HCl-HF mud acid system as described by Crowe et al. (1992)

2.2.3 The Practice in Sandstone Matrix Acidizing

The main purpose of matrix acidizing is to enhance the production of a sandstone well and to reduce its skin. This technique has been used in many years to stimulate reservoir formations by changing the rock properties, which are the porosity and permeability (Crowe et al. 1992). During operation, the injection pressure of the acid is lower than the formation fracture pressure. When the acid is injected, it dissolves all the minerals within the soluble reservoir rock. This creates more pore spaces, thus increasing the flow rate of fluid from the reservoir formation layers to the wellbore (Ali et al. 2004). In the early stage, the use of mud acid in sandstone acidizing is a major breakthrough in the area of well stimulation technique (Kalfayan 2008). The commonly practiced acid composition during operation is 3% HF and 12% HCl (Smith and Hendrickson 1965, Gidley 1985). Table 2.2 shows the chemical compositions of minerals that are present in a sandstone and their solubility in HCl and HCL-HF mud acid.

Table 2.2 Solubility of sandstone minerals (Portier et al. 2007)

| Minerals | Solubility | |
|-----------|-----------------|--|
| | HCl | HCL - HF |
| Quartz | No | Very low |
| Feldspar | No | Low to moderate |
| Mica | No | Low to moderate |
| Kaolinite | No | High |
| Illite | No | High |
| Smectite | No | High |
| Chlorite | Low to moderate | High |
| Calcite | High | High, but CaF ₂ precipitation |
| Dolomite | High | High |
| Ankerite | High | High |
| Siderite | High | High |

In a typical operation, sandstone matrix acidizing is divided into three main phases (Hill et al. 1981, Hill et al. 1994, Zeit 2005, Nasr-El-Din et al. 2005), which are discussed as follow:

1. A pre flush phase using HCl to dissolve Sodium (Na), Potassium (K) and Calcium (Ca) ions that will have reactions with the silica, forming insoluble silicates.
2. A main flush phase to dissolve the silicates, quartz, feldspar, clay as well as undissolved carbonates after pre-flush.
3. An after flush phase using NH_4Cl to remove the spent acid in order to keep the wettability in its original state and clean the formation.

2.2.4 The Treatment Design of Matrix Acidizing

Kalfayan and Metcalf (2000) emphasized that the development of acid treatment design is of paramount importance to a successful sandstone acidizing treatment. Generally, the design procedure should be based on the conventional treatment steps. Technical analyses and statistical survey were conducted extensively over 650 cases of matrix stimulation treatments in 9 countries. The studies revealed that incorrect field procedure was the main reason causing the acidizing failure (Paccaloni and Tambini 1993). However, the specific design procedure should remain open and could be reduced to include only necessary steps, depending on case by case basis. A few successful applications of field case study had been demonstrated in the Netherland (van Domelen et al. 1997), Saudi Arabia (Hashem et al. 1999), North America, South America and Far East (Kalfayan and Metcalf 2000).

During a matrix acidizing operation, all information such as well history, laboratory test data as well as previous operation experience are important for an engineer to decide the acidizing treatment fluid. To ensure the success of a matrix acidizing treatment, a comprehensive reservoir characterization workflow approach is essential (Schmid et al. 2016). Every detail from treatment design until execution must be considered carefully. McLeod (1984) recommended the treatment fluid selection guideline for sandstone acidizing, aiming to enhance the permeability. This guideline provided the choices for acid concentration and was formed based on different level of rock permeability, clay and

Chapter 2 Preliminary Acid Screening and Characterization

silt content. Table 2.3 shows the guideline for treatment fluid selection. [Portier et al. \(2007\)](#) later also suggested an alternative sandstone acid procedure for specific formation conditions as shown in Table 2.4.

Table 2.3 Guideline for treatment fluid selection ([Crowe et al. 1992](#))

| Condition | Main Acid | Pre-Flush |
|-----------------------------------|--------------------|-----------------------------|
| HCl Solubility (> 20%) | Use HCl only | |
| High Permeability (> 100md) | | |
| High quartz (80%), low clay (<5%) | 12% HCl, 3% HF | 15% HCl |
| High feldspar (>20%) | 13.5% HCl, 1.5% HF | 15% HCl |
| High clay (>10%) | 6.5% HCl, 1% HF | Sequestered 5% HCl |
| High iron chloride clay | 3% HCl, 0.5% HF | Sequestered 5% HCl |
| Low Permeability (<10 md) | | |
| Low clay (<5%) | 6% HCl, 1.5% HF | 7.5% HCl or 10% acetic acid |
| High chlorite | 3% HCl, 0.5% HF | 5% acetic acid |

Table 2.4 Alternate sandstone acid procedures established by [Portier et al. \(2007\)](#)

| Well and formation conditions | Treatment fluid recommendation |
|---|-------------------------------------|
| Bottom hole treating temperatures > 100°C | 1.5% HF + 13.5% HCl |
| Permeability < 5 md | 1.5% HF + 13.5% HCl |
| Quartz content: | |
| Over 90% | 3% HF + 12% HCl |
| 50 to 90% | 3% HF + 12% HCl or retarded HF |
| Feldspar, 15 – 30% | 1.5% HF + 13.5% HCl |
| Chlorite clay: | |
| 1 to 5% | 3% HF + 10% acetic acid |
| < 5% | 1.5% HF + 10% acetic or formic acid |

2.2.5 The Use of Additives in Matrix Acidizing

Matrix acidizing can cause a number of well problems such as the release of fine particles, the generation of precipitants, the formation of emulsions, the generation of sludge and also the corrosion of steel (O'Driscoll et al. 2005, Dehghani 2010, Rabie and Nasr-El-Din 2015). For instance, Hanafy et al. (2015) and Hanafy and Nasr-El-Din (2016) deduced that fines migration that was induced by clay caused porosity reduction of 40%. At high temperatures of 150°F and 250°F, fines migration became more sensitive to hydrochloric acid, causing more severe porosity reduction, especially at the outlet part of the sandstone core. There is a list of acid additives that have been used during matrix acidizing in order to solve some of the common problems that exist (Bybee 2003). Table 2.5 shows the summary of additives used in matrix acidizing and their functions.

Table 2.5 Summary of the additives used in matrix acidizing and their functions

| Acid Additives | Functions |
|----------------------|---|
| Corrosion Inhibitors | <ul style="list-style-type: none"> - To reduce or retard the rate of corrosion of steel by acid. - To create an inhibitory film on the metal surface. - To protect the acid pumping and handling equipment. - To protect the equipment and tool such as casing, pump and valve. |
| Clay Stabilizers | <ul style="list-style-type: none"> - To keep clay and fines in suspension. - To prevent migration and swelling of clays. |
| Diverting Agents | <ul style="list-style-type: none"> - To place the reactive fluid evenly. - To bracket the interval exposed to the acidizing fluid. |
| Iron Control Agents | <ul style="list-style-type: none"> - To dissolve the corrosion products in the casing or tubing. - To dissolve the iron minerals in the well. |
| Surfactants | <ul style="list-style-type: none"> - To lower the surface and interfacial tensions. - To change or maintain the wettability of the wells. - To break and weaken the emulsions. |

2.2.6 Sandstone Channelling and Wormholing

Wormholing pattern is common in carbonate acidizing. Whereas for sandstone acidizing, a uniform face dissolution pattern is observed, and no preferential flow path is being generated. It is uncommon to generate wormholes especially in homogeneous sandstone formation. This due to low rate of reaction between the acid HF and the quartz, which is the major minerals presented in the sandstone (Xie 2005).

Nevertheless, several literature researches indicated that a channelling pattern, which is similar to carbonate wormholing could occur during sandstone acidizing process. If the sandstone is highly heterogeneous, then a high permeability fine-scale channelling pattern would exist (Wehunt et al. 1993). Figure 2.4 and 2.5 shows the wormholes generated in Bandera and Berea sandstone core flooding experiment conducted by Lamb (1998) respectively.

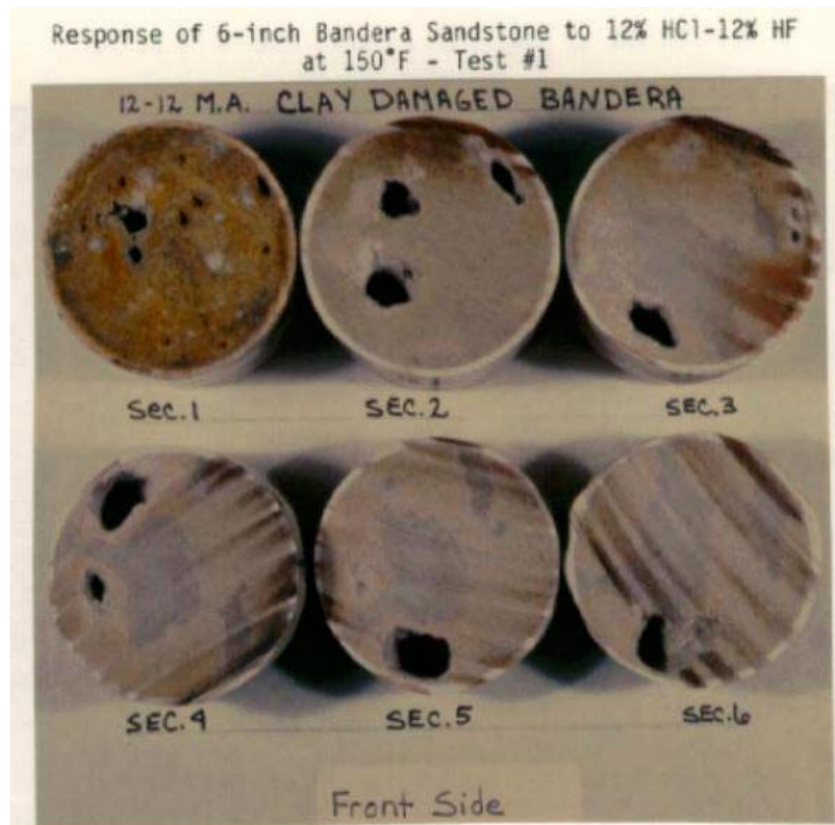


Figure 2.4 Wormholes in Bandera Sandstone by Lamb (1998)



Figure 2.5 Wormholes in Berea Sandstone by [Lamb \(1998\)](#)

According to the sandstone core flooding experiment conducted by [Kalfayan and Metcalf \(2000\)](#), it is also indicated that some sandstone channels or wormholes were created after being treated with 6 wt% and 9 wt% HF, as shown in Figure 2.6. The results of laboratory investigation indicated that lower rate of acid injection is a positive factor to generate wormholes in sandstone.

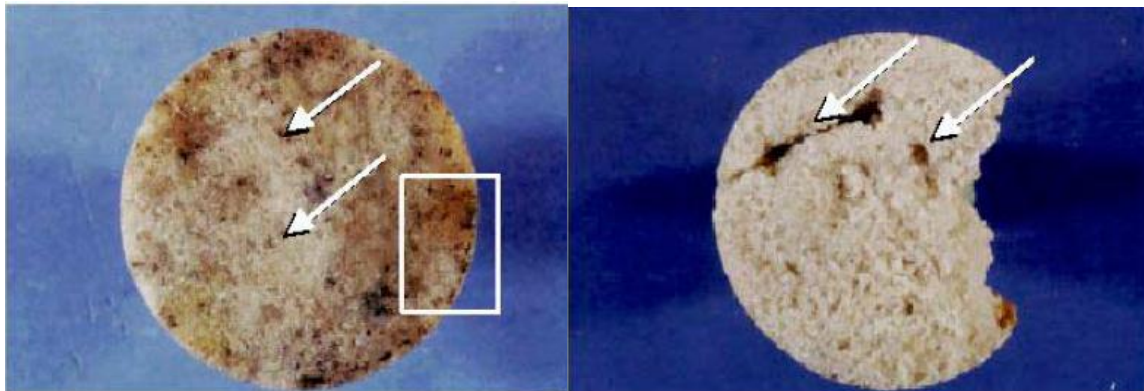


Figure 2.6 Wormholes in South America Sandstone by [Kalfayan and Metcalf \(2000\)](#)

2.3 Literature Review of Experimental Studies

The choices of acid and additives selection are made based on the characteristics of reservoir rock as well as the main purpose of the stimulation (McLeod 1984). There are many reported experimentations that carry out investigations on the efficiency of various kinds of acid used in sandstone acidizing. A critical review on these significant studies has been reported. Therefore, the outcomes of this study have basically provided a conceptual framework for the setup and planning of experimental and numerical works that are recommended in the future.

2.3.1 Mud Acid (HF-HCl)

Thomas et al. (2001) performed core flooding on Jauf core samples using HCl and acetic acid in the pre-flush at 150 °C. The results reflected the importance of the pre-flush acid used before the mud acid due to the channels created. Channelling effects had significantly enhanced the permeability during the main acid application. Then, Thomas et al. (2002a) also investigated the effect of concentration ratio of mud acid on the change in permeability of both Jauf and Berea core samples. The results are shown in Table 2.6.

Table 2.6 Summary of core flow test results in Jauf and Berea cores (Thomas et al. 2002b)

| Type of Core | Core No. | Treatment: 1) Preflush 2) Main Fluid 3) Overflush | Initial Permeability (mD) | Final Permeability (mD) | Final/Original Permeability Ratio |
|--------------|----------|---|---------------------------|-------------------------|-----------------------------------|
| Jauf | 774 | 1. 10 wt% Acetic Acid 2. 4 wt% HCl – 1 wt% HF 3. 6 wt% NH ₄ Cl | 22.7 | 43.4 | 1.9 |

Chapter 2 Preliminary Acid Screening and Characterization

| | | | | | | | |
|-------|-----|----|--------|--------------------|------|-----|------|
| Jauf | 777 | 1. | 10 wt% | Acetic Acid | 18.7 | 180 | 9.6 |
| | | 2. | 9 wt% | HCl – 1 wt% HF | | | |
| | | 3. | 6 wt% | NH ₄ Cl | | | |
| Jauf | 778 | 1. | 10 wt% | Acetic Acid | 8.5 | 195 | 22.9 |
| | | 2. | 12 wt% | HCl – 3 wt% HF | | | |
| | | 3. | 6 wt% | NH ₄ Cl | | | |
| Berea | 1 | 1. | 10 wt% | Acetic Acid | 73 | 105 | 1.4 |
| | | 2. | 9 wt% | HCl – 1 wt% HF | | | |
| | | 3. | 6 wt% | NH ₄ Cl | | | |
| Berea | 2 | 1. | 10 wt% | Acetic Acid | 87 | 264 | 3.0 |
| | | 2. | 12 wt% | HCl – 3 wt% HF | | | |
| | | 3. | 6 wt% | NH ₄ Cl | | | |
| Berea | 7 | 1. | 10 wt% | Acetic Acid | 81 | 129 | 1.6 |
| | | 2. | 4 wt% | HCl – 1 wt% HF | | | |
| | | 3. | 6 wt% | NH ₄ Cl | | | |

[Nevito Gomez \(2006\)](#) had designed, set-up and tested matrix acidizing apparatus on conventional mud acid. The experiment was conducted on Berea sandstone core at both room temperature and at high temperature of 100 °F. At room temperature, higher flow rate resulted in higher permeability enhancement. Whereas at 100 °F, the optimum flow rate was determined to be 30ml/ml.

Gomaa et al. (2013) and Wang et al. (2013) had investigated the effect of mud acid concentration ratio on the change in permeability of the sandstone core matrix at a temperature of 180°F. There are four different mixture of mud acid concentration ratio, which include 1.9% HF+15% HCl, 2.3% HF+10% HCl, 2.6% HF+5% HCl and 2.8% HF+3% HCl, respectively. All of these were tested using the core sample by applying the core flooding method. The experimental results indicated that all four acid mixing ratios can positively increase the permeability of the core sample. Nevertheless, it was observed that the result of permeability increases when the HF-HCl ratio increases. At the same time, there was also a reduction in the acid injection volume required.

Abdelmoneim and Nasr-El-Din (2015) determined the optimum HF concentration for high temperature sandstone formations. High temperatures of 280 °F and 325 °F were used to conduct the core flooding tests on both Bandera core and Grey Berea core. Based on the result, the correlation between the optimum HF concentration and mineralogy was formed as an inverse relationship as shown in Figure 2.7. Retarded acid was suggested for temperatures higher than 300 °F.

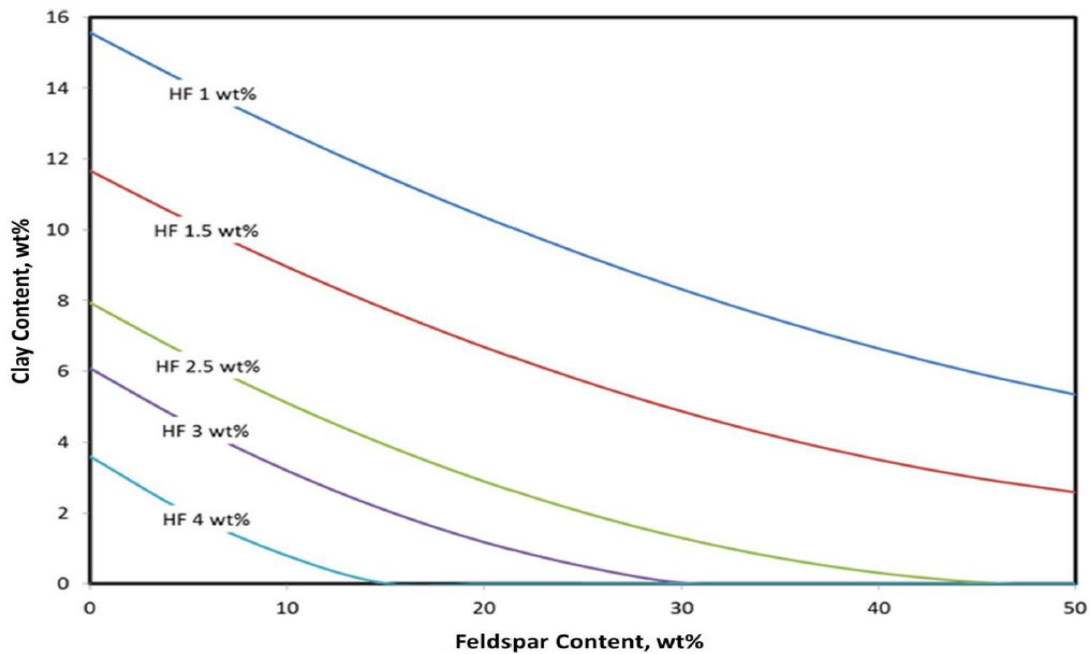


Figure 2.7 Optimum HF concentration based on mineral content determined by Abdelmoneim and Nasr-El-Din (2015)

Chapter 2 Preliminary Acid Screening and Characterization

Al-Harthy et al. (2009) stated that mud acid had proven its performance and effectiveness in sandstone acidizing, thus gaining popularity. However, it was reported to result in rapid rate of reaction when the temperature was increased to 200 °F. This is because of the rapid kinetics of secondary and tertiary precipitation reactions at such high temperature. This reduced the inefficiency of sandstone acidizing because of undesirably early consumption of the acids. This was also the main reason causing acid treatment to fail in many cases. Furthermore, significant reduction of compressive strength of the formation with high clay content after being treated with HF caused the formation to disintegrate (Thomas and Crowe 1981).

HCl played an important role in mud acid as it leaves no insoluble products from the reactions with the minerals. In addition to its cost effective advantage, HCl had been widely applied in sandstone stimulation. However, HCl is also highly corrosive and hazardous to the well, especially in high temperature, high pressure (HTHP) formation environment (Van Domelen and Jennings 1995). Therefore, in the future research, the disadvantages of mud acid must be carefully included in considerations. A summarized classification of the reviewed experimental works using mud acid is presented in Table 2.7.

Table 2.7 Summarized interpretation of reviewed papers on mud acid used in matrix acidizing

| Reference | Methodology | Approach | Analysis | Rock Type | Acid System | Condition | Remarks |
|--|--------------|---------------|----------------------------|---|-------------|-----------------|---|
| Thomas et al. (2001, 2002a, 2002b) | Experimental | Core Flooding | XRD SEM Thin Section | Berea Sandstone Jauf Sandstone | Mud acid | 300 °F | Mud acid ratio of 12-3, 9-1 and 4-1 yield different reaction products. |
| Nevito Gomez (2006) | Experimental | Core Flooding | CT Scan | Berea Sandstone Cream chalk Carbonate Indiana Limestone | Mud acid | 72 °F 100 °F | The higher the flow rate, the higher the permeability change at room temperature. Optimum flow rate is determined at 30 ml/min for Berea sandstone at 100 °F. |
| Gomaa et al. (2013) & Wang et al. (2013) | Experimental | Core Flooding | XRD | Berea Sandstone Bandera Sandstone | Mud acid | 180 °F | Single stage mud acid ratio of 15-1.9, 10-2.3, 5-2.6 and 3-2.8 improved the permeability of Bandera sandstone. A pre-flush using HCl is needed. |

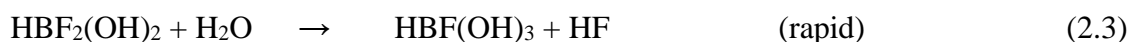
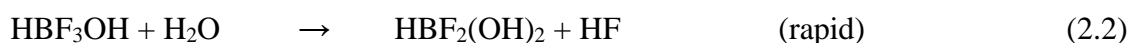
Chapter 2 Preliminary Acid Screening and Characterization

| | | | | | | | |
|------------------------------------|--------------|---------------|-----|-----------------------------------|----------|----------------|--|
| Abdelmoneim and Nasr-El-Din (2015) | Experimental | Core Flooding | ICP | Berea Sandstone Bandera Sandstone | Mud acid | 280 ℉ 325 ℉ | The best HF concentration are 1 wt% for Bandera sandstone and 1.5 wt% for Berea sandstone. Retarded acids are recommended for high temperature sandstone condition at 300 ℉. |
| Al-Harthy et al. (2009) | Review | N/A | N/A | N/A | Mud acid | 200 ℉ | The use of mud acid at high temperature of 200 ℉ leads to rapid reaction rate and early acid consumption. |

2.3.2 Fluoroboric Acid (HBF₄)

Fluoroboric acid (HBF₄) has a unique slow hydrolysis reaction to produce hydrofluoric acid (HF). Its hydrolysis process is however a function of temperature and concentration (Ryss 1956). Wamser (1948, 1951) carried out investigation on the hydrolysis of HBF₄ at room temperature condition to produce HF. Based on the result, the equilibrium constant of HBF₄ is determined to be 2.3×10^{-3} [1] at room temperature.

Mcbride et al. (1979) and Thomas and Crowe (1981) demonstrated the application of Fluoroboric acid in different case studies. HBF₄ generates HF at a slower rate, therefore allowing more time for the acid to penetrate into the sandstone. Fluoroboric acid will hydrolyse in aqueous solution to form hydrofluoric acid until it reaches a limit extent, as shown in Equations (2.1) – (2.4).



HBF₄ is applied to stimulate the sandstone reservoirs. It is found to be useful in removing formation damage as well as stabilizing the clays and other fines. It had also demonstrated its efficiency in enhancing the penetration of live acid (Thomas and Crowe 1978, 1981, Svendsen et al. 1992). However, the retardation of HBF₄ becomes less significant when the temperature increases to 150 °F.

Kunze and Shaughnessy (1983) showed that hydrolysis of HBF₄ in water to form HF accelerated when the temperature increased. Meanwhile, Bertaux (1989) tested on the use of 8% HBF₄ on sandstone that contained K-feldspar. It was indicated that the precipitate, KBF₄ formed did not damage the sandstone. So, HBF₄ had demonstrated enhanced sandstone permeability. On the other side, the precipitate, K₂SiF₆ formed resulted in reduced sandstone permeability significantly.

Ayorinde et al. (1992) showed the advantage of HBF_4 in treating a Nigerian oil well that faced severe fines migration related issues created by conventional mud acid. HBF_4 had proven its compatibility in stabilizing fines migration. After being acidized with mud acid, the production of the oil well is 850 barrels liquid per day (BLPD). However due to fines migration, the production declined to nearly zero. After successful HBF_4 treatment, the production increased to 2500 BLPD and maintain a 220 barrel oil per day (BOPD) oil production even after one year. Figure 2.8 shows the production improvement in the Nigerian oil well.

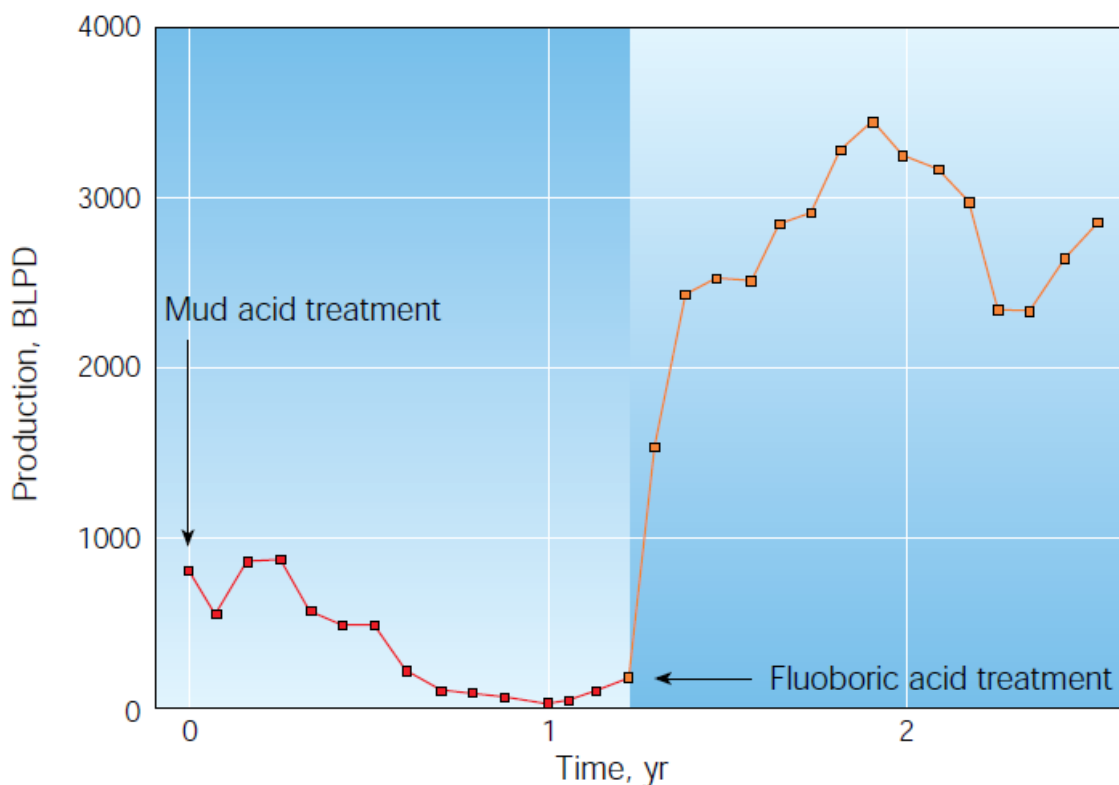


Figure 2.8 The production improvement in the Nigerian oil well (Ayorinde et al. 1992).

Figure 2.9 demonstrates the scanning electron microscope (SEM) results of pore filling clay before and after treatment with conventional mud acid and fluoroboric acid, respectively. It was clear in the figure on the lower left, that clays were dissolved; while on the lower right, showing partially fused kaolinite platelets. This had prevented the issue of fine migration (Ayorinde et al. 1992).

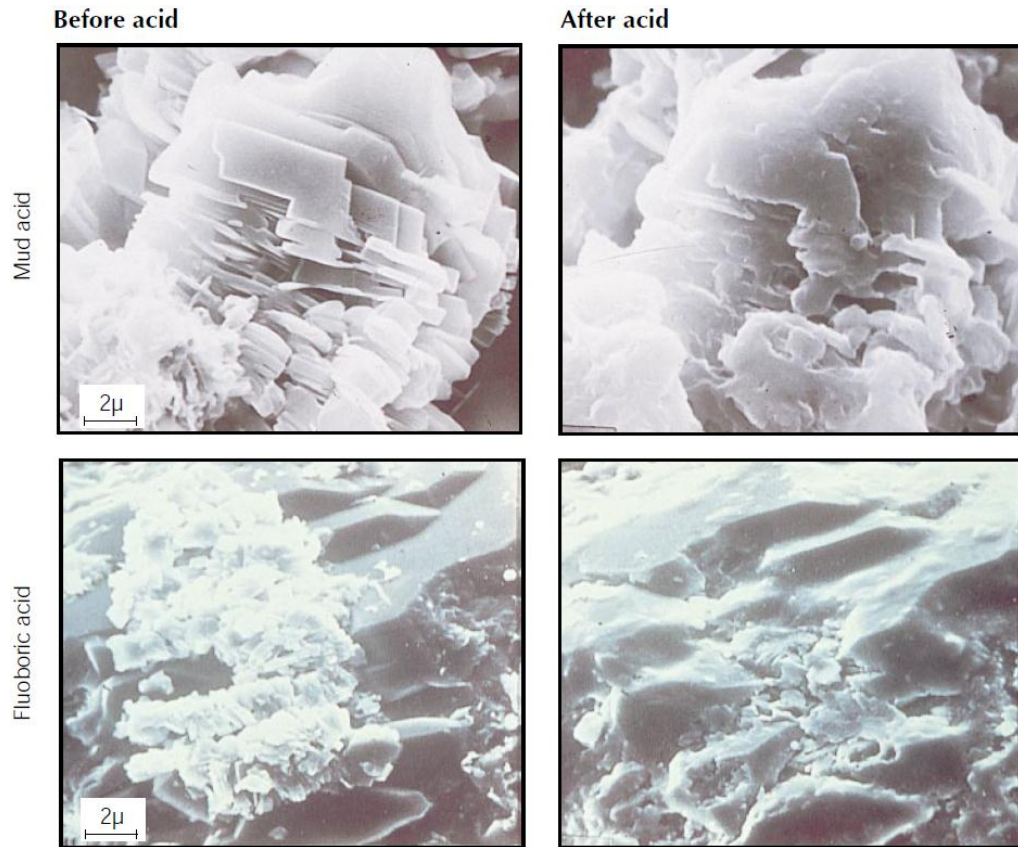


Figure 2.9 Comparison of SEM results showing pore filling clay (kaolinite) before and after treatment with mud acid and fluoroboric acid (Crowe et al. 1992).

Moreover, after being treated with HBF_4 , Paccaloni and Tambini (1993) reported a successful 5 years production of a silt and clay damaged well caused by mud acid previously. Meanwhile, Kume et al. (1999) showed that the adoption of HBF_4 in treating the Niger Delta wells caused a mixture of both positive and negative results. Some wells permeability was not only unimproved but also reported to be reduced.

Jaramillo et al. (2010) further improved the use of HBF_4 acid in sandstone acidizing. A new acid system named as Organic Clay Acid (OCA) was developed by mixing organic acid and HBF_4 . Many wells had been stimulated using OCA and treated in low temperature reservoirs at below 140 °F. The real field results proved the effectiveness of OCA in fines control and clay stabilization. In comparison with the initial production increase of the wells treated with an organic mud acid, it had been observed that higher

Chapter 2 Preliminary Acid Screening and Characterization

initial production increase happened on the wells stimulated with OCA. This indicated that OCA had successfully mitigated the issue of fine migration caused by organic mud acid.

In addition, [Feng et al. \(2011\)](#) carried out an investigation on a high temperature deep penetrating (HTDP) acid. In this research, a mixture of complex organo-phosphate hydrolysed fluoride salts was developed as a new corrosion inhibitor. It could generate HF and therefore making HTDP acid compatible at high temperature formations. The HTDP acid was determined to have a much higher solubility for quartz mineral than mud acid and it will also cut back the precipitation. HTDP acid is also better than HBF_4 in terms of permeability enhancement.

[Restrepo et al. \(2012\)](#) combined the use of HBF_4 with the organic acids. Based on the result, a deep live acid penetration is obtained while minimizing the secondary and tertiary precipitation reaction. [Pituckchon \(2014\)](#) studied the chemistry of HBF_4 to better understand its potential application in real field stimulation. After conducting core flooding tests, ^{11}B and ^{19}F Solution State High Field Nuclear Magnetic Resonance (NMR) are used to analyse the spent acid over a period of time interval. The core flooding experiments were conducted at 75 °F and 200 °F to determine the effect of temperature on the compatibility of HBF_4 . The results showed a reduction in core permeability at 200 °F due to the precipitation of amorphous silica.

[Zhou et al. \(2016\)](#) also performed core flooding experiments using 12% HBF_4 combined with 12% HCl at 25 °C and 65 °C. The results were compared to conventional 3% HF and 12% HCl. The results indicated that the permeability enhancement reflected by the fluoroboric acid combination is 40% higher than the conventional mud acid. Also, permeability enhancement is greater at 65 °C than 25 °C. The work done by [Zhou et al. \(2016\)](#) only compared two temperatures, which are 25 °C and 65 °C. There is no optimization work being conducted and therefore the optimum temperature range for the recommended use of HBF_4 remains undetermined. In addition, the core sample used is a heterogeneous sandstone, with 9% being clay and calcite. An evaluation of the homogeneous clean sandstone is also recommended in the future. A summary of classification on the reviewed experimental works using HBF_4 is interpreted in Table 2.8.

Chapter 2 Preliminary Acid Screening and Characterization

Table 2.8 Summarized interpretation of reviewed papers on fluoroboric acid used in matrix acidizing

| Reference | Methodology | Approach | Analysis | Rock Type | Acid System Applied | Condition | Remarks |
|---|--------------|--------------------------------|-------------------|--|---------------------|----------------|---|
| Mcbride et al. (1979) | Experimental | Field Result Core Flow Test | SEM | Sandstone | HBF ₄ | N/A | HBF ₄ stabilizes migratory formation fines. HBF ₄ removes damage effectively. |
| Thomas and Crowe (1978) | Experimental | Core Flow Test | SEM XRD | Berea Sandstone Sadlerochit Sandstone Miocene Sand | Clay Acid | 150 ℉ 200 ℉ | Clay acid prevents clay migration and swelling. Clay acid is less damaging than mud acid. |
| Thomas and Crowe (1981) | Experimental | Core Flow Test | SEM XRD OES | Berea Sandstone Sadlerochit Sandstone Miocene Sand Unconsolidated Frio Sand | HBF ₄ | 150 ℉ 200 ℉ | HBF ₄ generates HF at a slower rate, allowing deep acid penetration. HBF ₄ is normally used with mud acid. |

Chapter 2 Preliminary Acid Screening and Characterization

| | | | | | | | |
|------------------------------------|--------------|--------------------------------------|----------------------------------|-------------------------------------|---|---------------------------|--|
| Svendsen et al. 1992 | Experimental | Field Result Core Flow Test | XRD SEM TSP | Poorly Consolidated Sandstone | Clay Acid (8% HBF ₄) | 70 °C | A combination of clay acid and mud acid can successfully stimulate the high permeable but unconsolidated sandstone. |
| Kunze and Shaughnessy (1983) | Experimental | Core Flooding | Effluent Chemical Analysis | Berea Sandstone | HBF ₄ | 72 °F 150 °F 200 °F | Retardation effect of HBF ₄ is demonstrated at room temperature but not at elevated temperatures. Hydrolysis of HBF ₄ increases with temperature increase. |
| Ayorinde et al. (1992) | Case Study | Field Result | N/A | N/A | HBF ₄ | N/A | HBF ₄ resulted in production enhancement of Nigerian Oil field well. |
| Jaramillo et al. (2010) | Experimental | Core Flow Test | SEM XRD ICP | Shaly Sandstone | Organic Clay Acid (OCA) HBF ₄ | 120 °F 140 °F | OCA is efficient in clay stabilization and fine control. |

Chapter 2 Preliminary Acid Screening and Characterization

| | | | | | | | |
|-----------------------|--------------|--------------------------------------|---|---|--------------------------|---------------|--|
| Feng et al. (2011) | Experimental | Case History Core Flow Test | N/A | Sandstone (China offshore Oilfield) | HTDP HBF ₄ | 293 ℉ | HTDP has slow reaction and can penetrate deeper. HTDP results in significant well production improvement in more than 20 field in Chinese Offshore Oilfield. |
| Pituckchon (2014) | Experimental | Core Flooding | ICP ¹¹ B NMR ¹⁹ F NMR | Berea Sandstone | HBF ₄ | 75 ℉ 200 ℉ | The retardation effect of HBF ₄ is sensitive to temperature. It is suitable at 75 ℉ but not at 200 ℉. |
| Zhou et al. (2016) | Experimental | Core Flooding | SEM XRD | Tahe Sandstone | HBF ₄ | 25 ℃ 65 ℃ | At 25 ℃, the permeability change is not much due to slow hydrolysis. At 65 ℃, the permeability change is 2.39 times the initial value. |

2.3.3 Chelating Agents

[Frenier et al. \(2004\)](#) developed chelant based on hydroxyethylaminocarboxylic acid (HACA) and tested it on Berea sandstone. The results revealed that this HACA chelant can be used for high temperature sandstone reservoir. The benefits of this chelant included reduced corrosion rate, reaction rate and close to neutral pH value. HACA acts as a corrosion inhibitor to form insoluble surface chelates. It also features a low reaction rate with dolomite. Also, the near-neutral pH value of HACA would eliminate the need for fluid treatment before disposal. Therefore, this chelant had advantages considering aspects of health, safety and environment (HSE) due to lower HSE footprint. [Tuedor et al. \(2006\)](#) also used a newly developed sandstone stimulating system, which was a Chelant based system, resulting in not only effective acidizing at 200 °F – 300 °F, but also less corrosive, safer to handle and lower HSE footprint.

In addition, [Ali et al. \(2008\)](#) had studied the effect of Sodium Hydroxy-ethylethylenediaminetriacetic Acid (Na₃HEDTA), which is a low pH solution to stimulate a high temperature formation in West Africa using experimental approach. The result indicated that the chelating fluid is efficient in increasing the permeability of the high temperature well. Moreover, [Parkinson et al. \(2010\)](#) also applied an alternative approach to stimulate the production zone of Pinda formation that is located in West Africa. The Pinda formation was having multilayers of carbonates. The bottomhole static temperature (BHST) of this formation was 300 °F. The six production wells from the formation zone were being stimulated with a pH 4 HEDTA chelant during the main flush stage. The result showed that all the six wells are then producing at a doubled rate after the stimulation, indicating a high economical return resulted from the stimulation acid at a high temperature.

[LePage et al. \(2009\)](#) had investigated the reaction between Glutamic Acid N, N-Diacetic Acid (GLDA) and calcites in carbonate rock. In their study, GLDA had been compared to many other chelating agents such as the Ethylenediaminetetraacetic Acid (EDTA), Hydroxyethylethylenediaminetriacetic Acid (HEDTA), Nitrilotriacetic Acid (NTA) and Ethanediglycine Acid (EDG). In the discussion, the efficiency of GLDA is the same as HEDTA although it is not as corrosive as HCl. Aside from that, GLDA was also used by [Mahmoud et al. \(2011\)](#) to study its effect on stimulating sandstone formations. The

Chapter 2 Preliminary Acid Screening and Characterization

research focused on multiple parameters, including temperature, rate of injection, volume and initial pH value of GLDA. The results clearly revealed the powerful capability of GLDA to chelate calcium, iron and magnesium. Besides, GLDA was found to chelate even small amounts of aluminium ions in the sandstone cores (Mahmoud 2011). Moreover, the concentration of GLDA was found to be almost the same prior to and after core flooding test. GLDA also demonstrated a high thermal stability at 300°F and potentially lower corrosion properties. This was further proven by Nasr-El-Din (2013). According to the result, GLDA increased the core permeability of 21% at 200 °F and 84% at 300 °F respectively. Whereas on the opposite side, HCl resulted in the precipitation of iron hydroxide, $\text{Fe}(\text{OH})_2$, causing a 42% permeability reduction.

Furthermore, Reyes et al. (2015) used a low 2.5 pH GLDA chelant to investigate its stimulation on high quartz clean sandstone matrix and high clay heterogeneous sandstone matrix. The results reflected a 20% permeability decrease for the clean sandstone, but a 30% permeability increase for the heterogeneous sandstone. This indicated that this GLDA/HF chelant is more suitable for sandstone with clay content, but not clean sandstone.

Another chelant based fluid system was tested by Rignol et al. (2015) to stimulate sandstone core at 375 °F, which is an ultra-high temperature environment. This acid system was a combination of low pH chelant and fluoroboric acid, HBF_4 . The core plugs were experimented with flow test and some chemical analyses. Based on the sequential dissolution analyses, the results showed that the chelant-based fluid did not cause silica precipitation as HCl is absent. Furthermore, it had increased the permeability of the core effectively. Garcia et al. (2016) had revealed the advantages of Aminopolycarboxylic Acid (APCA) fluid that contained 1 – 1.5% of HF. This fluid system is better than the conventional mud acid that is inefficient to stimulate high temperature sandstone condition above 300 °F due to the precipitation of sodium and potassium iron. The application of APCA/HF* blend fluid system in offshore reservoirs was a success, resulting in 30 to 50% barrel oil per day production improvement for more than a period of 12 months.

Chapter 2 Preliminary Acid Screening and Characterization

Legemah et al. (2015) proposed a two-step injection process using chelating agents to treat high temperature wells. Firstly, the author suggested injection of less volume but high concentration APC, then followed by injection of high volume but low concentration APC such as GLDA. Mahmoud et al. (2015) examined the carbonates removal compatibility of GLDA, HEDTA and 15wt% HCl using illitic sandstone core at high temperature of 300 °F. The outcomes of the core flooding experiment revealed that HCl is not compatible to remove carbonates in illitic sandstone, but resulting in reduced porosity and permeability, which damaged sandstone matrix. On the other hand, both GLDA and HEDTA demonstrated high efficiency in carbonates minerals removal.

Based on the earlier literature review, many experimentations using chelating agents were conducted and reported by past researchers. These chelants could be applied to stimulate high temperature well. The efforts of these past studies, focusing on the effectiveness of chelants at high temperature condition were highly appreciated. It was proven that these acid systems were suitable and reliable to gain extensively wide application in real field practice. However, it should also be alerted that chelating agents are generally less suitable for clean homogeneous sandstones because of the silica precipitation during acidizing. Therefore, they are more suitable for heterogeneous carbonates and clay-rich sandstones. Another point of view that should be noticed is that chelants are very costly products as compared to mud acid, retarded acid and organic acids. Although chelating agents can reduce the cost of corrosion inhibitor used, it is still important to optimize the budget between the costly chelants and corrosion inhibitor. A summary of classification on the reviewed experimental works using chelating agents is presented in Table 2.9.

Chapter 2 Preliminary Acid Screening and Characterization

Table 2.9 Summarized interpretation of reviewed papers on chelating agents used in matrix acidizing

| Reference | Methodology | Approach | Analysis | Rock Type | Acid System | Condition | Remarks |
|-----------------------|--------------|-------------------------------------|-------------------------------|--|---|----------------------------------|--|
| Frenier et al. (2004) | Experimental | Field Result Core Flooding | XRD ICP- OES CT-Scan | Berea Sandstone Carbonate (Limestone) | HACA | 370 ℉ 400 ℉ | HACA can successfully stimulate both sandstone and carbonate core at high temperature. HACA had low corrosion rate. |
| Tuedor et al. (2006) | Experimental | Core Flooding | SEM XRD ICP | Berea Sandstone (Medium to High carbonate content – 12% and 30%) | Not revealed (Only mentioned chelant-based new system) | 210 ℉ 250 ℉ 300 ℉ 375 ℉ | This new chelant system is suitable for sandstone formation with 200 ℉ to 300 ℉. More effective for medium to high carbonate content sandstone. |
| Ali et al. (2008) | Experimental | Core Flooding | SEM ICP XRD | Offshore West Africa Sandstone (Low, Medium and High | Na ₃ HEDTA (Low pH 4) | 149 °C | pH 4 Na ₃ HEDTA is effective in stimulating medium carbonate content sandstone. |

Chapter 2 Preliminary Acid Screening and Characterization

| | | | | | | | |
|---|--------------|-----------------|----------------|--|-------------------------------------|----------------|--|
| | | | | carbonate content) | | | Less corrosive and cause no damage to well tubular. |
| Parkinson et al. (2010) | Experimental | Core Flow Test | ICP | Pinda Core (Multilayer sandstone and 2% to 100% carbonate) | pH 4 HEDTA HEDTA+0.4% HF | 300 F | pH 4 HEDTA proves it capability to stimulate different carbonates level formation. Require less corrosion inhibitor due to low corrosion rate than HCl. |
| LePage et al. (2009) | Experimental | Solubility Test | NMR FAAS | N/A | GLDA EDTA HEDTA NTA EDG | 300 F 350 F | GLDA is highly soluble in HCL. GLDA is as effective as HEDTA to prevent Iron Oxide precipitation. GLDA is biodegradable as compared to other chelants. |
| Mahmoud et al. (2011, 2015) | Experimental | Core Flooding | ICP CT-Scan | Berea Sandstone | GLDA HEDTA | 300 F | The pH of GLDA can significantly affect the stimulation result. |

Chapter 2 Preliminary Acid Screening and Characterization

| | | | | | | | |
|-------------------------------------|--------------|-------------------|--------------------|--|--------------------|----------------|--|
| | | | | | | | Low injection rate is better than high injection rate. GLDA is better than HEDTA at 300 Ƒ. |
| Nasr-El-Din (2013) | Review | N/A | N/A | N/A | GLDA | 200 Ƒ 300 Ƒ | GLDA can improve the well productivity in carbonate formation. GLDA is environmentally friendly and not hazardous. |
| Reyes et al. (2015) | Experimental | Core Flow Test | XRD ICP- OES | Leopard Sandstone (Clean, 95% Quartz) Bandera Sandstone (Heterogeneous, 65% Quartz) | pH 2.5 GLDA/HF* | 360 Ƒ | GLDA/HF* is not suitable for clean sandstone, due to 20% permeability decrease. It is suitable for heterogeneous and clay-rich sandstone, showing 30% increase in permeability. |

Chapter 2 Preliminary Acid Screening and Characterization

| | | | | | | | |
|-----------------------|--------------|----------------|--------------------------|--|--|-------|--|
| Rignol et al. (2015) | Experimental | Core Flow Test | XRD SEM EDS ICP | Gulf of Thailand Sandstone (9% Clay) | Low pH chelant+HBF ₄ Organic Acid+HBF ₄ | 375 F | New chelant system effectively removes clay and prevents fine migration. Low corrosion rate. |
| Garcia et al. (2016) | Experimental | Core Flow Test | XRD ICP OES | Leopard Sandstone (Clean, 95% Quartz) Bandera Sandstone (Heterogeneous, 65% Quartz) | APCA/HF* APCA HCOOH | 360 F | APCA/HF* is suitable for clean sandstone. It is highly effective for heterogeneous and clay-rich sandstone. |
| Legemah et al. (2015) | Experimental | Core Flooding | ICP- OES CT-Scan | Indiana Limestone | APC | 350 F | Proposed a two steps injection process using APC. |

2.3.4 Retarded Acids and Organic Acids

Addition of retarding agent into conventional mud acid formed another study to solve the problem associated with the reaction of acids and the clay minerals. According to the investigation by [Ji et al. \(2014\)](#) and [Ji et al. \(2016\)](#), Aluminium Chloride, AlCl_3 was added into conventional mud acid to form retarded mud acid. It was also known as fines control acid, which is comprised of 15% HCl, 1.5% HF and 5% $\text{AlCl}_3 \cdot 6\text{H}_2\text{O}$. The experiment was carried out on Berea core samples at both 75 °F and 200 °F. Based on the solubility test result, no AlF_3 precipitate was detected at both temperatures. [Aneto \(2012\)](#) also conducted core flooding tests and compared the use of retarded mud acid using AlCl_3 . The result showed a reduction in rate of reaction by the retarded acid, allowing deeper acid penetration and better damage removal.

In the earlier years, organic acids such as acetic and formic acid; and powdered acid such as sulfamic and chloroacetic acid were developed by researchers ([Farley et al. 1970](#), [Wehunt et al. 1993](#), [Shuchart and Gdanski 1996](#), [Shuchart 1997](#)). For instance, [Templeton et al. \(1975\)](#) discovered a new approach to retard the consumption rate of HF acid by using methyl formate to generate formic acid, CH_3COOH . Then, HF is generated at a controllable rate by adding Ammonium Fluoride, NH_4F . In general, methyl formate hydrolyses slowly to produce HF. The chemical reactions to form HF was described in Equations (2.5) – (2.6).



Furthermore, [Van Domelen and Jennings \(1995\)](#) applied the use of two organic acids, which are Acetic acid (CH_3COOH) and Formic acid (HCOOH) in stimulating HTHP wells. Both of these organic acids have the favourable properties in sandstone acidizing, included weak ionization and slow reaction. Therefore, these acids cause less corrosion to the well equipment and allow longer reaction period. The acid blend had been applied on Arun Limestone formation in Indonesia with high temperature of 350 °F. The well response and

Chapter 2 Preliminary Acid Screening and Characterization

corrosion response reflected positively in both technical and economic efficiency of the acid blend used.

Roger et al. (1998) conducted core flooding on the sandstone core using different formulations of the acid, other than the typical 10% HCl and 1.5% HF. It had been proven that this conventional acid combination caused the formation damage as indicated by 74% permeability reduction. Based on the results, 10% Citric acid blended with 1.5% HF was determined to be the optimum acid combination. The production enhancement of 7400 to 16000 BOPD were observed in five producing wells stimulated using the optimum acid combination.

These organic acids are being further developed as shown in many recent publications. For instance, experimental investigation was conducted by Al-harbi et al. (2012) using various mixtures of organic-HF acid system in stimulating sandstone cores. The acid combinations included Acetic (CH_3COOH)-HF, Formic (HCOOH)-HF and Citric ($\text{C}_6\text{H}_8\text{O}_7$)-HF. The authors study the precipitations that occurred during the acid and rock reactions as well as the factors affecting those precipitations. Based on the results, the precipitate type and amount mainly depend on the pH of solution, type of organic-HF combination, and initial concentration of free fluoride (Al-harbi et al. 2011). Apart from that, F/Al ratio was found to be the main parameter that is associated with the precipitation of aluminium-fluoride. The precipitation of aluminium fluoride occurred at a certain point over the critical ratio.

Andotra (2014) evaluated the use of citric acid as a chelating agent and compared the result with conventional mud acid of ratio 9:1. The optimum result was obtained when 1 wt% citric acid was added into the mud acid. However, the author also mentioned the issue of much higher cost induced by adding citric acid as compared to HCl and HF. Furthermore, L-Glutamic acid N,N-Diacetic Acid, Na-GLDA was combined with HF and tested using Bandera and Berea cores. The results reflected positively on the chelation of Iron (Fe), Calcium (Ca) and Magnesium (Mg) but not aluminosilicates (Al_2SiO_5). Nevertheless, the advantages of these chelating agents over HCl were provided such as lower corrosion, not being sensitive to minerals, being stable at high temperature greater than 200 °F and also being biodegradable.

Chapter 2 Preliminary Acid Screening and Characterization

Yang et al. (2012a) conducted another experiment using a blend of HF-organic acids instead of mud acid to mitigate the problems associated with mud acid. The authors analysed the kinetic and products of reactions. The findings of research showed that the type of minerals present in the core plugs have an effect on the reactions (Yang et al. 2012b, Yang 2012). Moreover, Zhou and Nasr-El-Din (2013) studied the efficiency of a single stage sandstone acid combination, which is a blend of HF and phosphonic acid during sandstone acid stimulation at 300 °F high temperature formation. The authors also evaluated the performance of multiple acid system to remove carbonate minerals from a sandstone core plug that included a low pH 3.8 GLDA, HEDTA and Formic acid, HCOOH. All the acid systems were observed to increase the permeability of Berea sandstone core sample. However, HCOOH is still more efficient than GLDA and HEDTA in dissolving the carbonate minerals in Bandera sandstone core samples.

Experiments performed by Shafiq et al. (2013a) to analyse the combination of Acetic acid and Hydrochloric acid in pre-flush stage. The author then compares the result with the conventional use of only Hydrochloric acid in that stage. The use of acid combination 7.5% HCl + 2.5% CH₃COOH resulted in 18.5% porosity enhancement. This proved that the usability of this acid combination is much better to be used as a pre-flush acid than the conventional 10% HCl, which resulted in only 10.9% porosity change. At the same time, this research also highlighted the importance of pre-flush stage in matrix acidizing to dissolve the carbonates in order to prevent precipitation during the main acid stage.

The research group in recent years led by Shafiq et al. presented multiple experimentations using various acid combinations (Shafiq et al. 2013b, Shafiq et al. 2014, Shafiq and Shuker 2013, Shafiq et al. 2015, Shafiq and Ben Mahmud 2016). The acid combinations tested by the authors included a mixture of Orthophosphoric (H₃PO₄) acid and HF; Fluoroboric (HBF₄) acid and HCOOH; and HCOOH and HF. The methodology applied were core saturation method, whereby the sandstone core plugs are saturated with the mentioned acid combinations. Multiple analyses were carried out to discuss the change in porosity, permeability, mineralogy and strength before and after the experiment. According to their findings, the best acid combination is 3% HF: 9% H₃PO₄. However, all these acid combinations are suitable to be applied as the main acid during sandstone acid stimulation. With 135.32% increase in permeability, this acid combination is even more superior to

Chapter 2 Preliminary Acid Screening and Characterization

the standard mud acid (3% HF: 12% HCl), showing lower increase in permeability, which is 101.76%. Therefore, it was proven that varying the acid combination would result in different outcomes, either in major or minor disparity. However, it should be noted that most of the experimentations were conducted only at ambient or room temperature conditions, which could not represent the real field environment. Hence, this left a research gap that can be bridged in the future studies.

In addition, a study on the phosphonic-based HF acid system was reported by [Zhou and Nasr-El-Din \(2016\)](#) as an alternate solution to mud acid. The author investigated several parameters affecting the interactions between the new acid systems with the clay minerals such as the concentration of acid, the reaction time and temperature. As shown in the result, phosphonic-based HF acid system resulted in significantly higher enhancement of permeability than mud acid and that was 177.86% at 300 °F. A summarized classification of the reviewed experimental works using retarded and organic acids is interpreted in Table 2.10.

Chapter 2 Preliminary Acid Screening and Characterization

Table 2.10 Summarized interpretation of reviewed papers on retarded and organic acids used in matrix acidizing

| Reference | Methodology | Approach | Analysis | Rock Type | Acid System | Condition | Remarks |
|---------------------------|--------------|-------------|---------------------|-----------|-------------------------|-----------|---|
| Ji et al. (2014, 2016) | Experimental | Core | ¹⁹ F NMR | Berea | 5 wt% AlCl ₃ | 75 ℉ | AlCl ₃ is recommended to be added into mud acid at both temperatures as a retard agent. AlCl ₃ results in better retardation when its concentration increases. No AlF ₃ precipitates are observed for both temperatures. |
| | | Flooding | SEM | Sandstone | + Mud Acid | 200 ℉ | |
| | | Solubility | EDS | | | | |
| | | Test | ICP-OES CT-Scan | | | | |
| Aneto (2012) | Experimental | Core | ICP | Berea | 5 wt% AlCl ₃ | 150 ℉ | AlCl ₃ reduces the rate of reaction, allowing deeper rate of penetration and more damage removal. |
| | | Flooding | | Sandstone | + Mud Acid | 300 ℉ | |
| Templeton et al. (1975) | Experimental | Field Test | XRD | Clayey | Methyl | 104 ℉ | Methyl Formate, HCOOCH ₃ generated formic acid, HCOOH plus NH ₄ F will |
| | | Gravimetric | | Sandstone | Formate | 122 ℉ | |
| | | Method | | East Bay | generated | 140 ℉ | |
| | | | | Sandstone | | 158 ℉ | |

Chapter 2 Preliminary Acid Screening and Characterization

| | | | | | | | |
|---------------------------------|--------------|----------------------------------|-------------------|---|---|----------------|--|
| | | Silica Analysis Method | | | formic acid + NH ₄ F | | produce in-situ HF over a period. This can dissolve suspended clay in the sandstone formation. |
| Van Domelen and Jennings (1995) | Field Result | Chemical Analysis Corrosion Test | N/A | Arun Limestone | CH ₃ COOH + HCOOH | 350 °F (HPHT) | A blend of acetic and formic acid can replace HCl-based acid. Significantly less corrosion than HCl while retaining similar dissolving power. |
| Roger et al. (1998) | Experimental | Core Flooding | SEM XRD | Turbidite Sandstone + Zeolite Cement (Gulf of Mexico) | 10% Citric Acid, C ₆ H ₈ O ₇ + 1.5% HF | N/A | The organic acid blend significantly dissolves the Zeolite. The citric acid mixture also prevents precipitation of silica gel. |
| Al-harbi et al. (2011, 2012) | Experimental | Solubility Test | ICP SEM XRD | Clean Sandstone | Acetic – HF Formic – HF Citric - HF | 50 °C 75 °C | All organic-HF acids mixture shows positive retardation |

Chapter 2 Preliminary Acid Screening and Characterization

| | | | | | | | |
|---|--------------|---------------|----------------------------|--------------------------------------|---|---------------------------------|---|
| | | | | Illitic Clayey Sandstone | | | effect in comparison with HCl. These organic acid systems are suitable for clean sandstone and illite clay. However, they are not suitable for chlorite clay due to AlF_3 precipitation. |
| Andotra (2014) | Experimental | Core Flooding | SEM-EDS ICP | Berea Sandstone Bandera Sandstone | 1 wt% Citric Acid + 9:1 Mud Acid | 300 Ƒ | Adding 1 wt% Citric Acid into 9:1 mud acid is recommended as it provides optimum result for maximum clay dissolution but minimum precipitation effect. |
| Yang et al. (2012a, 2012b) Yang (2012) | Experimental | Core Flooding | SEM ICP ^{19}F NMR | Berea Sandstone Bandera Sandstone | 9 wt% Formic acid + HF 13 wt% Acetic acid + HF | 75 Ƒ 150 Ƒ 250 Ƒ 350 Ƒ | The performance of both the organic acids are similar The effectiveness of formic acid to remove clay increases with temperature. |

Chapter 2 Preliminary Acid Screening and Characterization

| | | | | | | | |
|---|--------------|------------------------|---|---|--|--------|--|
| | | | | | | | The organic acid did not cause AlF_3 precipitation. |
| Zhou and Nasr-El-Din (2013, 2016) | Experimental | Core Flooding | ICP-OES | Berea Sandstone (5 wt% clay) Bandera Sandstone (11 wt% clay) | 9 wt% Formic acid | 300 °F | Formic acid is compatible and highly effective to remove the carbonates from Bandera sandstone at low pH value. |
| Shafiq et al. (2013a, 2013b, 2014, 2015) Shafiq and Shuker (2013), Shafiq and Ben Mahmud (2016) | Experimental | Core Saturation Method | Porosity-Perm FESEM pH Value and colour change Test | Sandstone Core | Acetic Acid Formic Acid HF HCl H_3PO_4 | 75 °F | Acetic acid and HCl can be combined to be used in the preflush stage to remove carbonates. HF + P_3PO_4 and HBF_4 + $HCOOH$ can be combined to be used in the main acid stage |

2.3.5 Overall Characterization and Comparison of Different Acids

To sum up the whole literature review, there are numerous acids that have been developed in the past years, aiming to continuously improve the permeability enhancement result, while preventing precipitation. Generally, four groups of acids are identified, which include the mud acid, fluoroboric acid, chelating agents, retarded and organic acid.

Mud acid is very suitable to stimulate unconsolidated sandstone at low to moderate temperature of 25 °C to 50 °C. It had been commonly applied in sandstone acidizing and had successfully enhance the porosity and permeability of sandstone formation with quartz mineral content. However, mud acid is not recommended to be used at high temperature conditions due to rapid rate of reaction with the sandstone mineral, resulting in early acid consumption. Mud acid is also very hazardous and corrosive to the well equipment.

On the other hand, HBF_4 is an alternative acid to mud acid at moderate temperature condition of 65 °C. It is also suitable for unconsolidated sandstone with quartz mineral. However, due to its slow hydrolysis reaction to produce HF, HBF_4 acidizing would result in deeper penetration rate into the sandstone formation. HBF_4 is also reported to be effective in fine control, clay stabilization and damage removal. Nevertheless, the literature lacks study on application of HBF_4 at elevated temperature conditions, which worth further investigation.

Furthermore, chelating agents are effective for heterogeneous carbonate or clay-rich sandstone at very high temperatures. Chelating agents can prevent iron oxide precipitation and is less corrosive. However, it is not recommended for homogeneous clean sandstone because of silica precipitation, which would lower the porosity and permeability. Therefore, the suitability of chelating agents would significantly depend on the mineral contents of the sandstone or carbonates.

Finally, the retarded and organic acids are suitable for carbonates or sandstone with high clay content. It is not effective for dissolving quartz content because it lacks fluoride ions. It also causes some precipitation at high temperature conditions. Table 2.11 provides a

clear view on the suitable acids for sandstone with high and low quartz content. In this study, a detailed evaluation of all these acids were presented as shown in Table 2.12.

Table 2.11 Alternatives acids for high and low quartz content sandstone.

| Mineral Content | Suitable Acid |
|--|---|
| High quartz content | Mud acid |
| | HF: HCl |
| | Fluoroboric acid HBF ₄ |
| Low quartz content | Chelating Agents |
| | HACA |
| | GLDA |
| | EDTA |
| | HEDTA |
| | NTA |
| | EGD / HEIDA |
| | HTDP |
| | APCA |
| | APC |
| | Organic Acids |
| | HCOOH |
| | CH ₃ COOH |
| C ₆ H ₈ O ₇ | |
| Retarded Acids | |
| H ₃ PO ₄ | |

Chapter 2 Preliminary Acid Screening and Characterization

Table 2.12 Interpretive characterization and comparison of different acids used in matrix acidizing

| Acid Formulae | Authors and Years | Aspects | Positive Indication | Cautionary Indication |
|---|------------------------------------|--|---|---|
| Conventional Mud Acid HF: HCl | Thomas et al. (2001, 2002a, 2002b) | Feasibility | - Suitable for Berea and Bandera sandstone. | - Becomes a drawback for high temperature wells. |
| | Nevito Gomez (2006) | | - Effective for low temperature wells. | - Require the use of retarded acids for high temperature sandstone condition at 300 °F. |
| | Gomaa et al. (2013) | | - Permeability improvement is observed using different HF: HCl concentrations | |
| | Wang et al. (2013) | | | |
| | Abdelmoneim and Nasr-El-Din (2015) | Reaction | - HF dissolves minerals in sandstone, targeting quartz minerals. | - Cause rapid reaction rates at high temperature of 200 °F. |
| | Al-Harthy et al. (2009) | Mechanism | - HCl mainly controls precipitation. | - Inefficiency of acidizing process as the acids are consumed too early. |
| | | Cost, Health, Safety and Environmental | - Popular and wide field application in past years. - Resulted in many successful well stimulations. | - Hazardous, difficult for safety control and corrosive to wellbore equipment. |

Chapter 2 Preliminary Acid Screening and Characterization

| | | | | |
|---|--|---|---|--|
| Fluoroboric Acid HBF ₄ | Ryss (1956) | Feasibility | - Suitable for stimulating highly permeable unconsolidated sandstone. - Permeability enhancement is observed at 65 °C. - Retardation effect is shown at room temperature, 75 °F. | - Suitability at high temperature condition above 200 °F remain unclear. - Optimum hydrolysis rate is not identified. - Permeability enhancement at 25 °C is not much due to too low hydrolysis rate. |
| | Wamser (1948, 1951) | | | |
| | Mcbride et al. (1979) | | | |
| | Thomas and Crowe (1978, 1981) | | | |
| | Svendsen et al. (1992) | Reaction Mechanism | - Slow hydrolysis reaction rate to form HF. - Allow deeper penetration rate into the formation. - Effective in controlling fine migration and swelling. - Effective for clay stabilization. - Effectively removes damage. | - Reaction mechanism with sandstone minerals at high temperatures is not investigated up to date. - Suitable temperature range is not identified and optimized. - Less investigation shown at elevated temperatures. |
| | Kunze and Shaughnessy (1983) | | | |
| | Bertaux (1989) | | | |
| | Ayorinde et al. (1992) | | | |
| | Paccaloni and Tambini (1993) | | | |
| | Kume et al. (1999) | | | |
| Jaramillo et al. (2010) | Cost, Health, Safety and Environmental | - Less corrosion and damaging compared to mud acid. | - Less practical results in field. | |
| Feng et al. (2011) | | | | |
| Restrepo et al. (2012) | | | | |
| Pituckchon (2014) | | | | |
| Zhou et al. (2016) | | | | |

Chapter 2 Preliminary Acid Screening and Characterization

| | | | | |
|-------------------------|---|--|---|---|
| Chelating Agents | Frenier et al. (2004) | Feasibility | - Highly effective for heterogeneous carbonate and clay-rich sandstone. | - Less suitable for clean sandstone due to the precipitation of silica. |
| HACA | Ali et al. (2008) | | | |
| GLDA | Parkinson et al. (2010) | | - High thermal stability up to 300 °F. | - More preferable over usage on carbonates formation. |
| EDTA | LePage et al. (2009) | | | |
| HEDTA | Mahmoud et al. (2011, 2015) | | - Suitable for medium to high carbonate content sandstone formation with 200 °F to 300 °F. | |
| EGD / HEIDA | Nasr-El-Din (2013) | | | |
| HTDP | Reyes et al. (2015) | Reaction | - Prevent Iron Oxide, Fe ₂ O ₃ precipitation | - Lack of fluoride ions limit their efficiency in dissolving quartz mineral. |
| APCA | Rignol et al. (2015) | Mechanism | - Successful application in offshore wells, with improved production of 30% - 50% BOPD. | - Chemical reaction and mechanism with minerals not clear. |
| APC | Garcia et al. (2016) Legemah et al. (2015) | | | |
| | | Cost, Health, Safety and Environmental | - Less corrosive than HCl. and not hazardous. - Cause no damage to well tubular - Biodegradable and environmentally friendly. | - Induced high cost in comparison to other acids. - Require optimization between the high chelating agent cost and reduced corrosion inhibitor cost. |

Chapter 2 Preliminary Acid Screening and Characterization

| | | | | |
|--|--|---------------|---|---|
| Retarded and Organic Acids | Ji et al. (2014, 2016) | Feasibility | - Suitable for clean sandstone and illite clay. | - More suitable for carbonate or sandstone with high clay content due to their sensitivity to clay. |
| | Aneto (2012) | | | |
| HCOOH | Templeton et al. (1975) | | - Resulted in higher permeability increase in comparison with the mud acid. | |
| CH ₃ COOH | Van Domelen and Jennings (1995) | | | - Not favorable for chlorite clay due to AlF ₃ precipitation. |
| C ₆ H ₈ O ₇ | Roger et al. (1998) | | | |
| H ₃ PO ₄ | Al-harbi et al. (2011, 2012) | Reaction | - Act as a buffer acid. | - Absence of fluoride ions restricts their effectiveness in dissolving quartz mineral. |
| | Andotra (2014) | Mechanism | - Able to penetrate deeper formation before spending. | |
| | Yang et al. (2012a, 2012b) | | - Not sensitive to undissolved fines and minerals. | - Chemical reaction and mechanism with sandstone is not clear up to date. |
| | Yang (2012) | | - Can dissolve suspended clay in the sandstone formation | |
| | Zhou and Nasr-El-Din (2013, 2016) | | - Similar dissolving power as HCl. | - Formation of some precipitates at high temperatures. |
| | Shafiq et al. (2013a, 2013b, 2014, 2015) | Cost, Health, | - Lower corrosion rate. | - Expensive cost. |
| | Shafiq and Shuker (2013) | Safety and | - Less potential risk. | - Need to optimize cost of expensive organic acid and lower corrosion inhibitor cost. |
| | Shafiq and Ben Mahmud (2016) | Environmental | - Stable and biodegradable. | - Less practical results in field. |

2.4 Summary of Chapter

From a large perspective, it is clear that there are many different acids that can be technically used in sandstone stimulation besides the mud acid, which is a conventional option and has already been widely tested. In view of the shortcoming of the mud acid at high temperatures, HBF_4 is foreseen as a better selection in contrast. In the past, many researchers had proven various advantages that were offered by fluoroboric Acid (HBF_4) when compared to the mud acid. It is expected to not only improve the porosity and permeability, but also eliminating the previously existing problems as it is relatively less corrosive, stable and allowing deeper penetration due to slow hydrolysis rate. It also results in lower strength reduction of the core plug.

Despite this, there are few studies indicating the precise temperature range, in which HBF_4 can be suitably applied, resulting in successful sandstone acid treatment. The limitation of retardation effect of HBF_4 still remains unknown without detailed optimization approach. More studies are deserved to consolidate the claimed advantages of HBF_4 . The key and major parameter affecting the acid stimulation results of HBF_4 must be optimized, along with other parameters like acid concentration and injection rate. The literature survey provided in chapter 2 had accomplished research objective 1, which is to screen through, characterize and compare all the acids for sandstone acidizing.

Relevant publications that had been arisen from chapter 2 are:

1. **Leong, V. H.** and Mahmud, H. B. (2018). A preliminary screening and characterization of suitable acids for sandstone matrix acidizing technique: a comprehensive review. *Journal of Petroleum Exploration and Production Technology*. Springer Nature. <https://doi.org/10.1007/s13202-018-0496-6>
2. **Leong, V. H.** and Mahmud, H. B. (2017). A comparative study of different acids used for sandstone acid simulation: a literature review. *In Proceeding: International Conference on Materials Technology and Energy (ICMTE) 2017*. Curtin University, Miri, Sarawak, Malaysia. 20th – 21st April 2017.

Chapter 3 Comparison and Assessment of Modelling Approach

3.1 Introduction

Initially, chapter 3 presented an introductory remark on some of the sandstone acidizing background, specifically the acid interactions with sandstone matrix, the chemical reactions and mechanisms during sandstone acidizing, as well as the acid selection and stimulation treatment design. This would not only enlighten the research purpose, but also inspiring the following literature survey which is of paramount importance.

The main purpose of this chapter is to extensively review all the numerical studies which were conducted on sandstone acidizing process. In this chapter, a detail comparison and assessment of all the models developed through literature survey helped to select a suitable model that closely matched the experimental results. An evaluation of the advantages and shortcomings of the models for core flooding process were thoroughly emphasized. Furthermore, this chapter also looks into the computational fluid dynamics (CFD) application and multi-scale modelling of matrix acidizing to select a feasible software for simulation purpose. At the end of chapter 3, the most representative modelling approach is proposed to be implemented in this study to perform the simulation of HBF_4 acidizing process. An overview of the research methodology in this study is also demonstrated.

3.2 Sandstone Acidizing Background

3.2.1 The Acid Interactions with a Sandstone Matrix

Typically, the sandstone mineralogy consists of two major groups of minerals, known as the silicate minerals and carbonate minerals. The silicates include quartz, bentonite, kaolinite, albite and orthoclase. Whereas the carbonates include calcite, dolomite,

anhydrite and siderite (Muecke 1982). In a sandstone matrix, some minerals and clays can decrease the permeability of sandstone, which are known as the pore-filling and pre-lining minerals and clays as shown in Figure 3.1. Other minerals present in a sandstone matrix are summarized in Table 3.1.

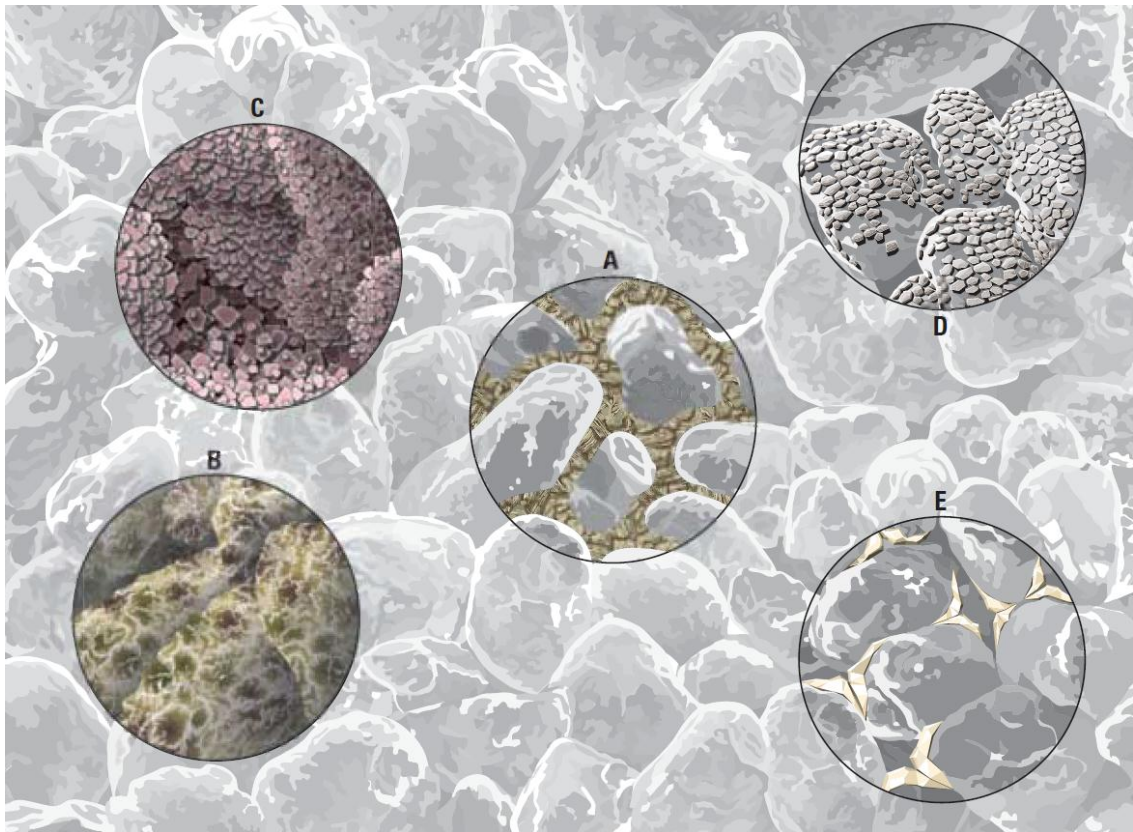


Figure 3.1 Different minerals and clays in sandstone with different morphologies such as (A) pore-filling kaolinite books, (B) fibrous illite, (C) carbonate overgrowth, (D) feldspar overgrowth and (E) quartz cement (Ali et al. 2004)

Table 3.1 Chemical composition of typical sandstone minerals (Economides and Nolte 2000)

| Classification | Mineral | Chemical Composition |
|----------------|---------|----------------------|
| Quartz | Silica | SiO ₂ |

Chapter 3 Comparison and Assessment of Modelling Approach

| | | |
|----------------|-------------|--|
| Feldspar | Microcline | KAlSi_3O_8 |
| | Orthoclase | KAlSi_3O_8 |
| | Albite | $\text{NaAlSi}_3\text{O}_8$ |
| | Plagioclase | $(\text{Na,Ca})\text{Al}(\text{Si,Al})\text{Si}_2\text{O}_8$ |
| Mica | Biotite | $\text{K}(\text{Mg,Fe}^{2+})_3(\text{Al,Fe}^{3+})\text{Si}_3\text{O}_{10}(\text{OH})_2$ |
| | Muscovite | $\text{KAl}_2(\text{AlSi}_3)\text{O}_{10}(\text{OH})_2$ |
| | Chlorite | $(\text{Mg,Fe}^{2+},\text{Fe}^{3+})\text{AlSi}_3\text{O}_{10}(\text{OH})_8$ |
| Clay | Kaolinite | $\text{Al}_2\text{Si}_2\text{O}_5(\text{OH})_4$ |
| | Illite | $(\text{H}_3,\text{O,K})_y(\text{Al}_4 \cdot \text{Fe}_4 \cdot \text{Mg}_4 \cdot \text{Mg}_6)(\text{Si}_{8-y} \cdot$ |
| | Smectite | $\text{Al}_y\text{O}_{20}(\text{OH})_4$ |
| | Chlorite | $(\text{Ca}_{0.5}\text{Na})_{0.7}(\text{Al,Mg,Fe})_4(\text{Si,Al})_8\text{O}_{20}(\text{OH})_4 \cdot n\text{H}_2\text{O}$ $(\text{Mg,Fe}^{2+},\text{Fe}^{3+})\text{AlSi}_3\text{O}_{10}(\text{OH})_8$ |
| Carbonate | Calcite | CaCO_3 |
| | Dolomite | $\text{CaMg}(\text{CO}_3)_2$ |
| | Ankerite | $\text{Ca}(\text{Fe,Mg,Mn})(\text{CO}_3)_2$ |
| | Siderite | FeCO_3 |
| Sulfate | Gypsum | $\text{CaSO}_4 \cdot 2\text{H}_2\text{O}$ |
| | Anhydrite | CaSO_4 |
| Chloride | Halite | NaCl |
| Metallic Oxide | Iron oxides | $\text{FeO}, \text{Fe}_2\text{O}_3, \text{Fe}_3\text{O}_4$ |

The most common acid used to dissolve these minerals is the mud acid, which includes the hydrofluoric acid (HF) and the hydrochloric acid (HCl) (Smith and Hendrickson 1965). HF in mud acid used to stimulate sandstone formations contains Fluoride Ion (F^-), which is a very reactive ion and is the only ion that reacts with the sand and clay significantly (Flood 1933). The reactivity of HF acid with silica, SiO_2 makes it unique in sandstone acidizing applications. Other acids such as hydrochloric, nitric and sulphuric acid are unreactive with silica (Ponce da Motta et al. 1992).

Chapter 3 Comparison and Assessment of Modelling Approach

In normal practice, mud acid with a composition of 3% HF – 12% HCl was injected into the well (Smith and Hendrickson 1965, Gidley 1985). However, other mud acid combinations (1.9% HF:15% HCl, 2.3% HF:10% HCl, 2.6% HF:5% HCl and 2.8% HF:3% HCl) were also suitable to be applied in different well conditions (Gomaa et al. 2013, Wang et al. 2013). Figure 3.2 shows the typical acid response curves when 8wt%, 4wt% and 2wt% HF were being used at Berea sandstone at 80 °F and 100psi.

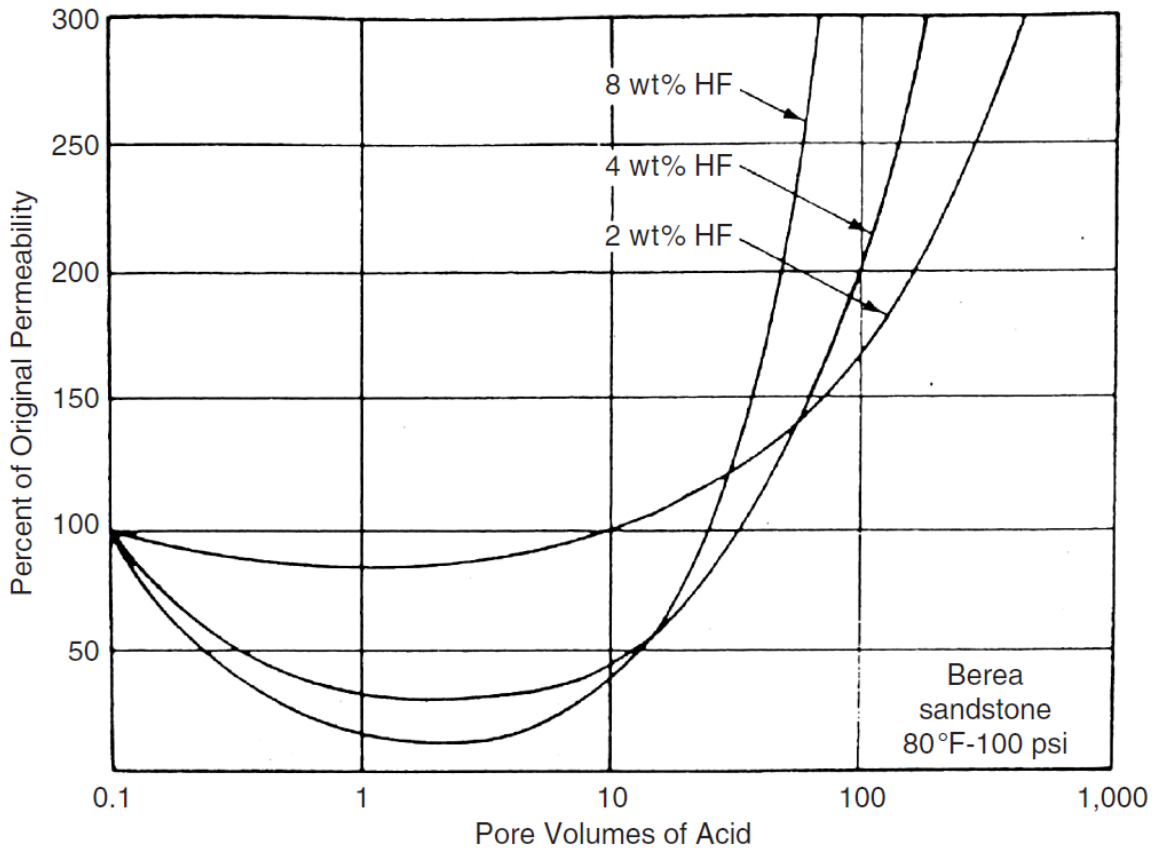


Figure 3.2 The Typical Acid Response Curves (Smith and Hendrickson 1965)

HCl in mud acid is responsible to prevent the precipitation of the reaction products. HCl is unreactive with the quartz and silicates. Hence, the reaction of HCl and sandstone formation can be neglected if the concentration of calcium carbonate, CaCO_3 is relatively low (Al-Shaalan and Nasr-El-Din 2000). Table 3.2 shows the primary chemical reactions in acid treatments.

Table 3.2 The primary chemical reactions in acid treatments (Guo et al. 2007)

| Sandstone Minerals | Acids | Chemical Reactions |
|-----------------------------|--------|---|
| Quartz | HF/HCl | $\text{SiO}_2 + 4\text{HF} \leftrightarrow \text{SiF}_4 + 2\text{H}_2\text{O}$ $\text{SiF}_4 + 2\text{HF} \leftrightarrow \text{H}_2\text{SiF}_6$ |
| Montmorillonite (Bentonite) | HF/HCl | $\text{Al}_4\text{Si}_8\text{O}_{20}(\text{OH})_4 + 40\text{HF} + 4\text{H}^+ \leftrightarrow 4\text{AlF}_2^+ + 8\text{SiF}_4 + 24\text{H}_2\text{O}$ |
| Kaolinite | HF/HCl | $\text{Al}_4\text{Si}_8\text{O}_{10}(\text{OH})_8 + 40\text{HF} + 4\text{H}^+ \leftrightarrow 4\text{AlF}_2^+ + 8\text{SiF}_4 + 18\text{H}_2\text{O}$ |
| Albite | HF/HCl | $\text{NaAlSi}_3\text{O}_8 + 14\text{HF} + 2\text{H}^+ \leftrightarrow \text{Na}^+ + \text{AlF}_2^+ + 3\text{SiF}_4 + 8\text{H}_2\text{O}$ |
| Orthoclase | HF/HCl | $\text{KAlSi}_3\text{O}_8 + 14\text{HF} + 2\text{H}^+ \leftrightarrow \text{K}^+ + \text{AlF}_2^+ + 3\text{SiF}_4 + 8\text{H}_2\text{O}$ |
| Calcite | HCl | $\text{CaCO}_3 + 2\text{HCl} \rightarrow \text{CaCl}_2 + \text{CO}_2 + \text{H}_2\text{O}$ |
| Dolomite | HCl | $\text{CaMg}(\text{CO}_3)_2 + 4\text{HCl} \rightarrow \text{CaCl}_2 + \text{MgCl}_2 + 2\text{CO}_2 + 2\text{H}_2\text{O}$ |
| Siderite | HCl | $\text{FeCO}_3 + 2\text{HCl} \rightarrow \text{FeCl}_2 + \text{CO}_2 + \text{H}_2\text{O}$ |

3.2.2 The Chemical Reactions during Sandstone Acidizing

There are two kinds of reactions occurring during sandstone acidizing, which include the homogeneous reaction in aqueous phase and heterogeneous reaction between the mineral surface and the aqueous phase (Al-Shaalan and Nasr-El-Din 2000). As HF enters sandstone core, almost all the minerals begin to dissolve, but at different rates depending on the intrinsic rates of heterogeneous reactions and the exposed surface areas. The reacting minerals can be divided into two distinct categories: slow and fast reacting. Quartz tends to act at a slower rate whereas feldspar and clay tend to react at a faster rate (Martin 2004). Figure 3.3 shows the clay minerals such as (a) kaolinite (b) illite (c) chlorite and (d) smectite presented in sandstone.

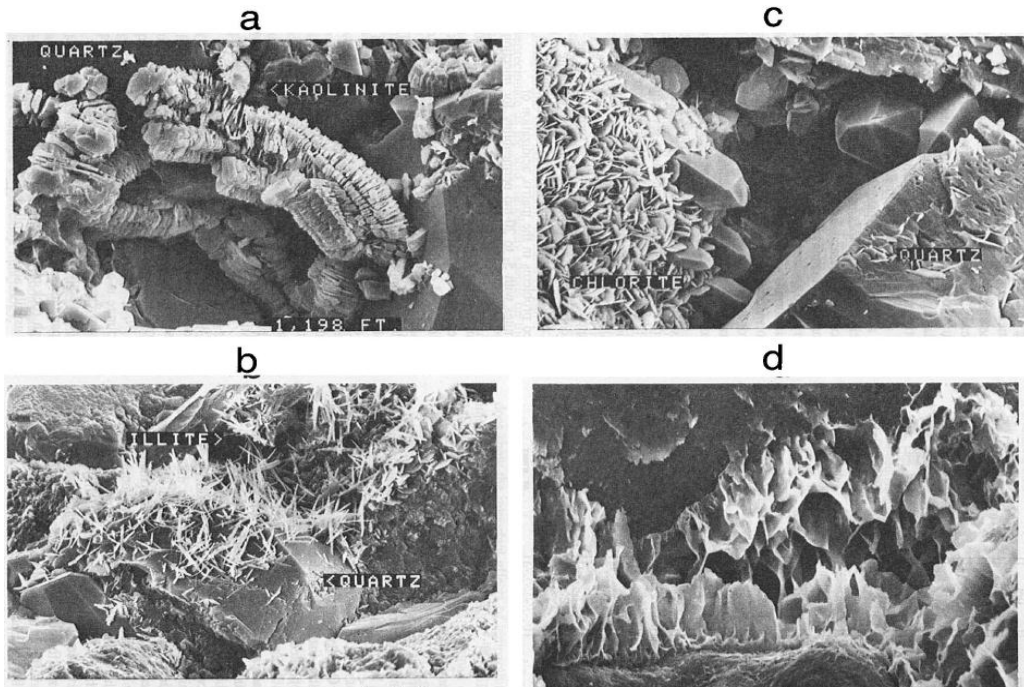
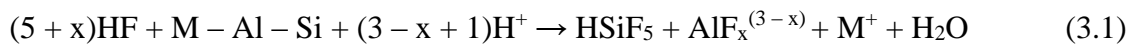


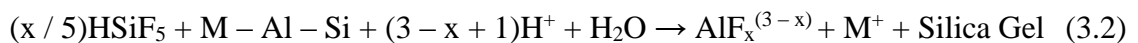
Figure 3.3 Scanning electron microscope (SEM) photograph of different clay minerals content such as (a) kaolinite (b) illite (c) chlorite and (d) smectite presented in sandstone rock as illustrated by [McLeod \(1984\)](#)

HF can dissolve aluminosilicates and silica. When HF reacts with feldspar, three reactions take place, namely the primary, secondary and tertiary reaction ([Li et al, 1998](#), [Gdanski 1998, 1999, 2000](#)). The reactions can be described in Equations (3.1) – (3.3) (x = average F/Al Ratio; y = fluoride number coordinated with Al after tertiary reaction, $y < x$):

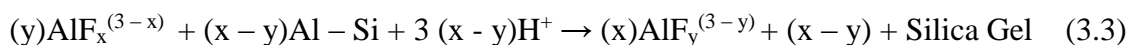
(i) Primary reaction ([Gdanski 1998](#), [Shucchart and Buster 1995](#)):



(ii) Secondary reaction ([Thomas and Crowe 1981](#), [Crowe 1986](#), [Gdanski 1999](#)):



(iii) Tertiary reaction ([Nasr-El-Din et al. 1998](#), [Gdanski 2000](#), [Thomas et al 2002](#)):



Chapter 3 Comparison and Assessment of Modelling Approach

The reactions between HF and minerals in sandstone matrix can also be described with respect to the distance from the wellbore (Al-Harthy et al. 2009, Rignol et al. 2015). From the distance closest to the wellbore, primary reaction takes place whereby rapid reaction between acids and the minerals occur to form aluminium and silica fluorides, without the formation of any precipitates. After that, when the acidizing process occur at farther distance, products resulted from primary reaction will proceed with secondary reaction. The secondary reactions occur at a slower rate. Silica gel and precipitations are formed during the reactions. Then, tertiary reactions occur at farther distance for precipitate more silica gel (Al-Harthy et al. 2009). Figure 3.4 shows the demonstration of these three reactions occurring at different distances from the wellbore.

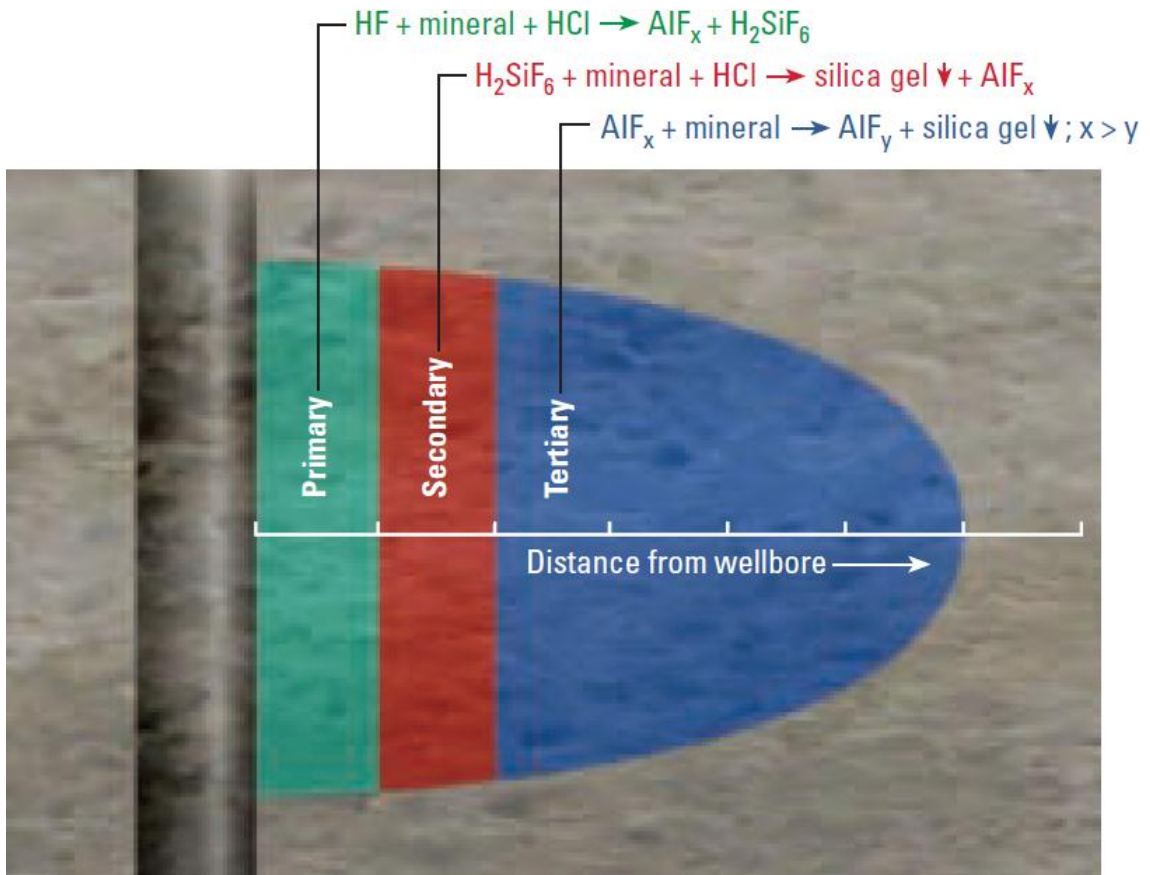


Figure 3.4 Primary, secondary and tertiary reactions between HF and minerals in terms of distance from the wellbore described by Al-Harthy et al. (2009)

During sandstone acidizing, the following precipitation reactions as shown in Equations (3.4) – (3.9) take place and may lead to formation damage and reduction in the porosity and permeability (Shaughnessy and Kunze 1981, Ayotte et al. 2005):

(i) Precipitation of hydrated silica:



(ii) Precipitation of sodium, Na silicates, potassium, K silicates, and calcium, Ca fluoride:



3.2.3 Acid Selection and Stimulation Treatment Design

Sandstone acidizing is a challenging task due to multiple stages of fluids and reaction of these fluids with the minerals in porous media (McLeod 1984). At high temperatures, these reactions cause precipitation reactions, which are dangerous as the formation can be damaged. To avoid reactions (4), (5) and (6), HCl or organic acid is used in the main acid stage. To avoid reactions (7), (8) and (9), ammonium chloride or hydrochloric acid is used as a pre-flush ahead of the main acid, which usually contains HF acid (Muecke 1982). Nitrogen gas, N₂, 15% HCl or 2% to 4% Ammonium Chloride, NH₄Cl can be used in the afterflush stage to clean the core (Gidley 1985).

Typically, sandstone matrix acidizing consists of three stages (Hill et al. 1981, Hill et al. 1994, Zeit 2005, Nasr-El-Din et al. 2005), which are:

1. Pre-flush to dissolve Na, K and Ca ions that will react with the silica to form insoluble silicates due to their reactions with silica.

2. Main-flush to dissolve the silicates, quartz, feldspar, clay as well as undissolved carbonates after pre-flush.
3. After-flush to remove the spent acid in order to keep the wettability in its original state and clean the formation.

In many cases, the consideration of acid concentrations during this stage is highly dependent to the formation mineralogy. The recommendation of the acid type and concentration, including the pre-flush acid selection were summarized in Table 3.3. Each acidizing step have its specific function and it is critical for engineers to take each step carefully during the design of acid stimulation especially the main stage number 5, which is the hydrofluoric acid selection. Table 3.4 shows the typical stage sequence for a sandstone acidizing treatment in a more detailed view.

Table 3.3 Recommended Acid Type and Strength for Sandstone Acidizing (Guo et al. 2007)

| Condition | Main Acid |
|---------------------------------------|---------------------------------|
| HCl Solubility (> 20%) | Use HCl only |
| High Permeability (> 100md) | |
| High quartz (80%), low clay (<5%) | 12% HCl, 3% HF ^a |
| High feldspar (>20%) | 13.5% HCl, 1.5% HF ^a |
| High clay (>10%) | 6.5% HCl, 1% HF ^b |
| High iron chloride clay | 3% HCl, 0.5% HF ^b |
| Low Permeability (<10 md) | |
| Low clay (<5%) | 6% HCl, 1.5% HF ^c |
| High chlorite | 3% HCl, 0.5% HF ^d |

^aPreflush with 15% HCl.

^bPreflush with sequestered 5% HCl.

^cPreflush with 7.5% HCl or 10% acetic acid.

^dPreflush with 5% acetic acid.

Table 3.4 Typical stage sequence for a sandstone acidizing treatment (Economides and Nolte 2000)

| No. | Stage | Reason for Stage | Information Source | Stage Composition | Stage Volume | |
|-----|------------------------------|--|---|--|---|-----------------------|
| 1 | Crude oil displacement | To prevent oil sludge formation by the acid | Acid-crude oil sludge test | Aromatic solvent | To achieve 3-ft radial displacement | |
| 2 | Formation water displacement | To prevent scale deposition | HCO ₃ and SO ₄ contents from formation water analysis | Ammonium chloride (NH ₄ Cl) at 3%-8% depending on the salinity of the formation water | To achieve 3-ft radial displacement | |
| 3 | Acetic acid | Iron compounds in formation (pyrite, siderite, hematite), chlorite, clay, zeolites | X-ray-Diffraction (XRD) analysis | 3%-10% acetic acid | CaCO ₃ (%) | Volume (gal/ft) |
| | | | | | 0-5 | 25 |
| | | | | | 5-10 | 50 |
| | | | | | 10-15 | 75 |
| | | | | | 15-20 | 100 |
| 4 | Hydrochloric acid | CaCO ₃ or other HCl-soluble minerals | HCl solubility test and/or XRD analysis | According to core mineralogy: 3%-15% HCl | Calculated based on HCl solubility and porosity or this schedule: | |
| | | | | | HCl Solubility of HF (%) | Stage Volume (gal/ft) |

Chapter 3 Comparison and Assessment of Modelling Approach

| | | | | | <5 | 50 |
|---|---|---|---|---|---|-----|
| | | | | | 5-10 | 100 |
| | | | | | 10-20 | 200 |
| 5 | Hydrofluoric acid (not used for carbonates and sandstones where HCl solubility > 20%) | To remove clay, other formation fines and mud damage | XRD analysis, SEM analysis, HF: HCl solubilities | According to formation mineralogy: 3%-15% HCl with 0.5%-3% HF | 75-100 gal/ft | |
| 6 | Overflush | To spend acid and flush spent acid away from the near-wellbore area | Always used | 3%-8% NH ₄ Cl or 3%-5% HCl in all wells followed by nitrogen (gas wells), kerosene (oil wells) or 5% HCl (water injection wells) | One to two volumes of the HF: HCl volume or to achieve 5-ft radial displacement | |
| 7 | Diversion | To improve injection throughout the interval | Used as required for heterogeneous formation permeability | OSR for oil or low gas/oil ratio wells, foam for either oil or gas wells and water-soluble resins for water injection wells | | |

3.3 Literature Review of Numerical Modelling and Simulation Studies

Numerical models in sandstone acidizing had been developed since 1960s. Generally, the chemical reactions and mechanisms between the sandstone minerals and the mud acid had been modelled mathematically (Al-Shaalan and Nasr-El-Din 2000) and most of the model developed are based on the kinetics of HF and sandstone minerals (Li et al. 2016). There are basically four main models developed, which include the lump-parameter model, two-parameter model, four-parameter model and detailed chemistry model. The advantages and limitations of each of the models are clearly addressed.

Figure 3.5 shows an illustration of the matrix acidizing simulation using a radially symmetric model of a formation (Crowe et al. 1992). The time dependent computational of the acid stimulation job should include the analysis of pressure and flow rate using Darcy's law, transportation of acid, mineral dissolution, transportation of minerals and the change in porosity and permeability. The simulation of sandstone matrix acidizing generally involved the division of the total time taken into the smaller time steps. Then, an evaluation of all the chain reactions is accounted for each time step. The result or output of each time step serve as the input of the next time step. The computational will be progressed for all the blocks or meshes simultaneously for each time step. Hence, the change in porosity and permeability of the formation will be observed at the end of the simulation.

3.3.1 Lumped-Parameter Model

The lumped-parameter model makes a simplification over all the chemical reactions between the acids and the sandstone minerals into single generalized chemical reaction: $\text{HF} + \text{Minerals} \rightarrow \text{Products}$. Schechter and Gidley (1969) developed a lumped-parameter model to investigate the effect of surface reactions in a porous media in order to enhance the understanding in sandstone matrix acidizing. The pore size distribution of the matrix and their changes after surface reactions were modelled. The comparison with the

experimental results showed that the experimental porosity increase was two or three times greater than that predicted by the diffusion model developed.

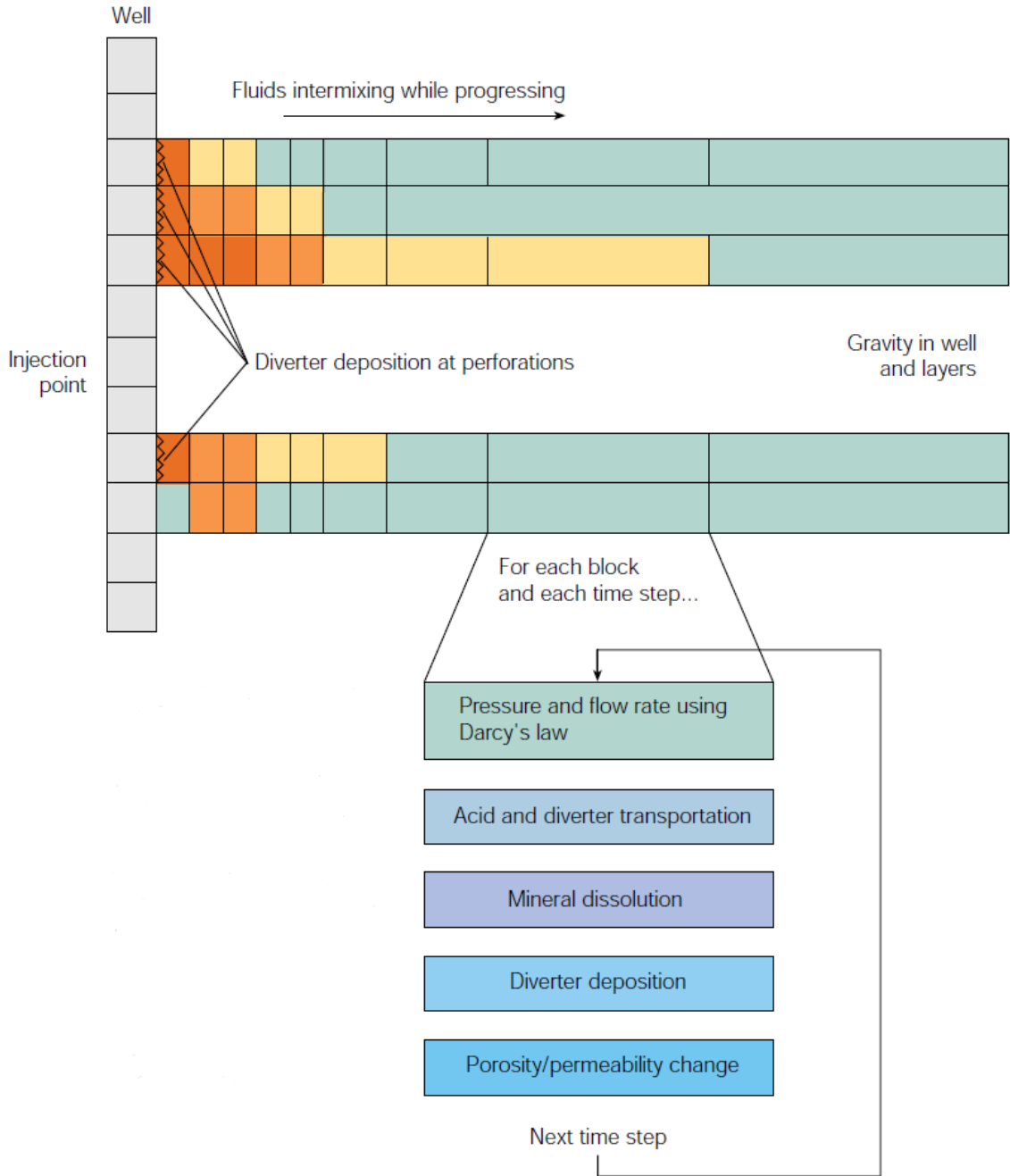


Figure 3.5 A radially symmetry model of the formation and the analysis of the main controlling factors in sandstone matrix acidizing as described by Crowe et al. (1992)

Williams and Whiteley (1971) developed a theory for the change in porosity in a clean homogeneous sandstone based on the reaction with HF. This was used to determine the reaction rate constant. The result found that the reaction rate constant is first order in terms of the concentration of the acid. Lund et al. (1973) also studied the reaction kinetics between the sandstone matrix with the HF acid, which included the kinetic rate equation, diffusion rate and dissolution mechanism. This study was taking into account of consideration only a few minerals, included the calcite, dolomite, microcline and albite.

Mccune et al. (1975) modelled the chemical and physical changes during sandstone matrix acidizing. A new mathematical model was developed to investigate the acid penetration in the sandstone core. The linear model was then extended to a radial geometry around the wellbore. The result from the radial model demonstrated that the radius of the acid reaction zone is smaller than that filled by acid injected from the wellbore.

Labrid (1975) provided a thermodynamic study of the process of mineral dissolution by HF. In this model, it was assumed that the acid reaction rate depends on the concentration of HF. Fogler et al. (1976) developed a model to predict the acid penetration and change in the permeability in sandstone core as a function of acid concentration and flow rate. However, the model was criticized as being not accurate to represent sandstone acidizing process because the reactivity of quartz, feldspar and clays are not the same. At the same time, the secondary and tertiary reactions as well as precipitations were not considered. Thus, a two-parameter model is developed to address the shortcomings of lump-parameter model.

3.3.2 Two-Parameter Model (Standard Model)

Hekim et al. (1982) developed a distributed parameter (two-parameter) model that considered different minerals dissolve at different rate. Therefore, the model classified the minerals into two major groups, namely the fast reacting types (feldspar and clays) and the slow reacting types (quartz). This model is known as a standard model as it had been widely used in the industry. The model was used to investigate the effects of high temperatures and longer injection time on the change in permeability of sandstone core.

Chapter 3 Comparison and Assessment of Modelling Approach

The experimental results correlated well with the model. This model gained popularity as it can predict the variation in permeability.

This model was further applied by [Taha et al. \(1986, 1989\)](#) and [Perthuis et al. \(1989\)](#) to investigate other sandstone mineral dissolution parameters, which include the temperature, mineral concentration, surface area and acid concentration. [Bartko et al. \(1997\)](#) highlighted the importance of field validation of the models developed previously in order for the field engineer to perform well treatment design optimization successfully. Therefore, they applied the numerical model developed by [Perthuis et al. \(1989\)](#) to work on a number of case study to perform field validation of the model. Five wells, which had been stimulated by matrix acidizing were involved in the case studies. The simulation results indicated a 5% skin value from the real field well testing results.

By considering only two pseudo-chemical minerals dissolving at different rates, [Lea et al. \(1993\)](#) derived a 2D model, demonstrating single phase acid flow in a perforated sandstone. Numerical case studies revealed the effectiveness of sandstone matrix acidizing in removing damage caused by drilling fluid as well as perforation. [Da Motta et al. \(1993\)](#) presented the experimental results that revealed the significance of silicon fluoride in dissolving feldspar at high temperature due to the high concentration of silicon fluoride. This reaction is known as the secondary reaction, which is the reaction between silicon fluoride and aluminosilicates to form silica gels and aluminium fluoride.

[Rahman \(2000\)](#) conducted 3D two-parameter numerical studies to predict the effect of acid concentration on the porosity and permeability sandstone. After validating the numerical results with the experimental results, it is concluded that moderate acid concentration and rate of injection are recommended for matrix acidizing. This can allow deeper acid penetration rate as well as preventing formation collapse due to excessive sandstone dissolution.

[Guimarães et al. \(2017\)](#) studied the prediction of volume and the injection rate during sandstone matrix acidizing by applying a two-parameter model that considered only fast dissolution and slow dissolution minerals. Nevertheless, the reactivity of fluorosilicic acid, H_2SiF_6 , which is a by-product formed in-situ was neglected. The secondary reaction between H_2SiF_6 and the fast-reacting minerals would result in silica gel precipitation. This

had been overlooked and was not considered in the two-parameter model. So, the problem of oversimplifying the acid reaction with sandstone minerals still persist in this model. Hence, an improved four-parameter model is introduced.

3.3.3 Four-Parameter Model

Hereafter, [Bryant \(1991\)](#) developed the first model that takes the secondary reaction and the precipitation of silica gel into consideration. This improved model is commonly known as the four-parameter model. In this model, the reaction between H_2SiF_6 and aluminosilicates was included. This model was proven to be better than the previous standard model in terms of porosity change. Therefore, this had provided a reliable and useful basis for the prediction of permeability change after mud acidizing in the sandstone matrix over many years.

[Hsi et al. \(1993\)](#) further validated the improved model developed by [Bryant \(1991\)](#) by calibrating the model with more core flooding tests with different sandstone cores under different acid concentration and injection rate. This had improved the reliability of the model. Meanwhile, [Sumotarto et al. \(1995\)](#) further applied the four-parameter model in his development of a new sandstone acidizing expert system, the UTACID simulator. This is a powerful software used as an optimization tool for sandstone acidizing treatment design.

Moreover, a 2-acid, 3-mineral sandstone acidizing model based on the permeability response was developed by [Rodoplu et al. \(2003\)](#) in order to study the effect influence of rock morphology change and formation permeability distribution on the sandstone permeability prediction. This implemented model was validated against the experimental results and had shown good agreement. Then, the application of the model in a field well treatment was also tested by history matching.

[Li et al. \(2004\)](#) developed a fine-scale model based on [Bryant \(1991\)](#)'s work to study the effect of heterogeneity in sandstone acidizing. The simulation results show that the depth of acid penetration into heterogeneous sandstone formation is significantly greater than that of homogeneous. The rate of penetration is also doubled ([Li 2004](#)). This model can

Chapter 3 Comparison and Assessment of Modelling Approach

be further developed into a field-scale model. Xie et al. (2005) further applied the fine-scale model developed by Li et al. (2004) to investigate the conditions that enhance the wormhole channelling in sandstone acidizing. Based on the results, sandstone heterogeneity and low rate of acid injection is better for wormhole channelling (Xie 2004).

Morgenthaler et al. (2006) also used Li's fine-scale model to investigate the effect of heterogeneity during sandstone acidizing. It was found that the influence of small-scale heterogeneity on acid penetration was higher than that of sandstone mineralogy. Therefore, careful characterization of the permeability distribution in the sandstone formation is very essential to ensure proper design of acid treatment, especially for laminated formations.

Zakaria (2013) reviewed the modelling and simulation of sandstone acidizing. In this paper, the finite difference equations of the four-parameter model (2-acids 3-minerals model) are described. It is the most common model used in sandstone acidizing. Then, investigation was carried out using simulation software to analyse the effects of sandstone damage radius, damage severity, injection flow rate and acid concentration on sandstone acidizing. An illustration of the modelling process was shown in Figure 3.6.

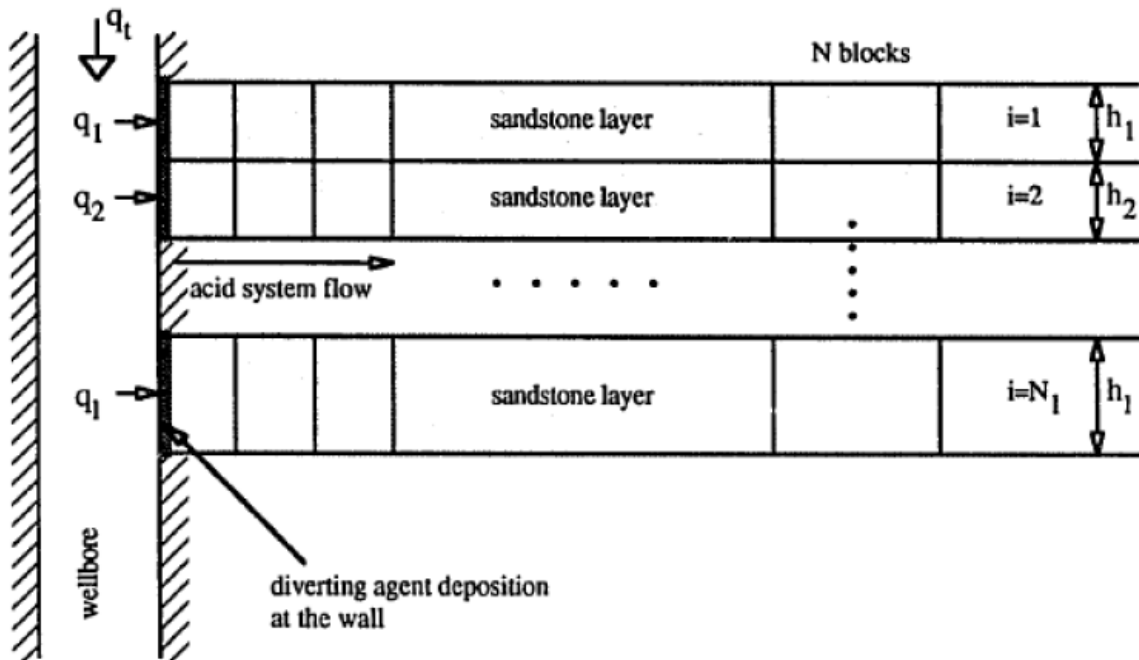


Figure 3.6 The modelling system and the interaction of acid and rock (Zakaria 2003).

Yang and Zheng (2014) also simulated a lab scale cylindrical sandstone core acidizing process by incorporating the transport equation and chemical reaction equation between the acid reactants and the minerals. Similar to most of other recent literature, the two-acid, three-mineral model was being developed. The model was implemented to investigate the most accurate equation to estimate the permeability from the porosity. Three permeability-porosity correlations that had been reviewed by Bernabe et al. (2003) were used to estimate the final permeability, which were shown in Equations (3.10) – (3.12):

1. the Labrid Equation (Labrid 1975),

$$\frac{k_2}{k_1} = \left(\frac{\phi_2}{\phi_1} \right)^n \quad (3.10)$$

2. Lund and Fogler Equation (Lund et al. 1975),

$$\frac{k_2}{k_1} = \exp[n(\phi_2 - \phi_1)] \quad (3.11)$$

3. Walsh and Brace Equation (Walsh and Brace 1984)

$$\frac{k_2}{k_1} = \frac{s_1^2 \phi_2^2}{s_2^2 \phi_1^2} \quad (3.12)$$

Where n is the coefficient related to the formation condition and s is the specific surface area. The calculation results based on the three equations are determined to be 56.4 mD, 124.2 mD and 117.4 mD respectively. After being compared to the experimentally measured result, which was 65.0 mD, the Labrid equation was the most accurate equation to simulate Liaohe sandstone (Yang and Zheng 2014).

When compared to the previous model, this four-parameter model demonstrated a higher accuracy in predicting the change in porosity and permeability after HF acidizing in sandstone matrix. Nonetheless, the limitation of this model is that the tertiary reaction and

other precipitation reactions are not considered. Thus, a detailed chemistry model is developed later.

3.3.4 Detailed Chemistry Model

[Sevougian et al. \(1995\)](#) and [Ying-Hsiao et al. \(1998\)](#) tried to develop a detailed chemistry model based on similar approach, whereby the mineral dissolution rates are controlled by the reaction kinetics. However, these models considered different kinds of minerals individually. The difference between these two models is that [Sevougian et al. \(1995\)](#) considered seven elements, thirteen minerals and thirteen species in their model whereas [Ying-Hsiao et al. \(1998\)](#) considered eleven elements, eight minerals and 74 species in their model. Both the models had good validation against the experimental results only at high acid injection rate. However, at low acid injection rate, the models failed to validate.

[Murtaza et al. \(1999\)](#) also presented an improved model for sandstone acidizing that considered eight minerals. This model had provided reliable estimation of porosity evolution and acid consumption in sandstone acidizing. Furthermore, [Quinn et al. \(1997\)](#) applied a KGEOFLOW model previously developed by [Walsh et al. \(1982\)](#) that accounted for an arbitrary number of kinetic and equilibrium reactions with an arbitrary number of minerals. Unexpectedly, the detailed chemistry model, which considered more chemical reactions did not improve the prediction of experimental results. Overall, this model that treated the chemical reactions in a much complex way failed to bring advancement in the sandstone acidizing prediction. This is mainly due to over complication of the model reactions. On the other hand, the four parameter model can predict experimental results at all acid injection rates. Therefore, it can be concluded that four-parameter model is still more reliable than the other models.

3.3.5 Comparison of Different Sandstone Acidizing Models

Al-Shaalan and Nasr-El-Din (2000) made a comparison of the agreement between two-parameter model, four-parameter model and detailed chemistry model with the experimental data from Lindsay (1976) as shown in Table 3.5.

Table 3.5 Summary of the Parameters included in the Modelling of Sandstone Acidization (Al-Shaalan and Nasr-El-Din 2000)

| Chemical Reactions | Lumped-Parameter Model | Two-Parameter Model | Four-Parameter Model | Detailed Chemistry Model |
|---------------------------|-------------------------------|--|--|-------------------------------------|
| Mineral Dissolution | Lumped Together | 1- Lumped Slow Reactions 2- Lumped Fast Reactions | 1- Lumped Slow Reactions 2- Lumped Fast Reactions | Each Minerals Treated Independently |
| Secondary Reactions | No | No | Yes | Yes |
| Tertiary Reactions | No | No | No | Yes |
| Precipitation | No | No | Only Silica Gel | Yes |
| Homogeneous Reactions | No | No | No | Yes |

The results of comparison by Al-Shaalan and Nasr-El-Din (2000) reflected that at high acid injection rate of 0.04894 cm/s, all models validated Lindsay’s experimental result except the detailed chemistry model by Ying-Hsiao et al. (1998). However, at moderate acid injection rate of 0.02526 cm/s, only the four-parameter model and detailed chemistry model by Ying-Hsiao et al. (1998) showed good matching with Lindsay’s experimental data. Whereas at low acid injection rate of 0.01243 cm/s, only the four-parameter model validated Lindsay’s experimental result successfully and the others failed to be validated. The results can be seen in Figure 3.7 – 3.9. Considering different injection rates, it had been clear that the four-parameter model is the most suitable model to be used to accurately simulate the sandstone acid stimulation process. Table 3.6 shows the detailed comparison of different models developed for sandstone acidizing with an evaluation of their pros and cons.

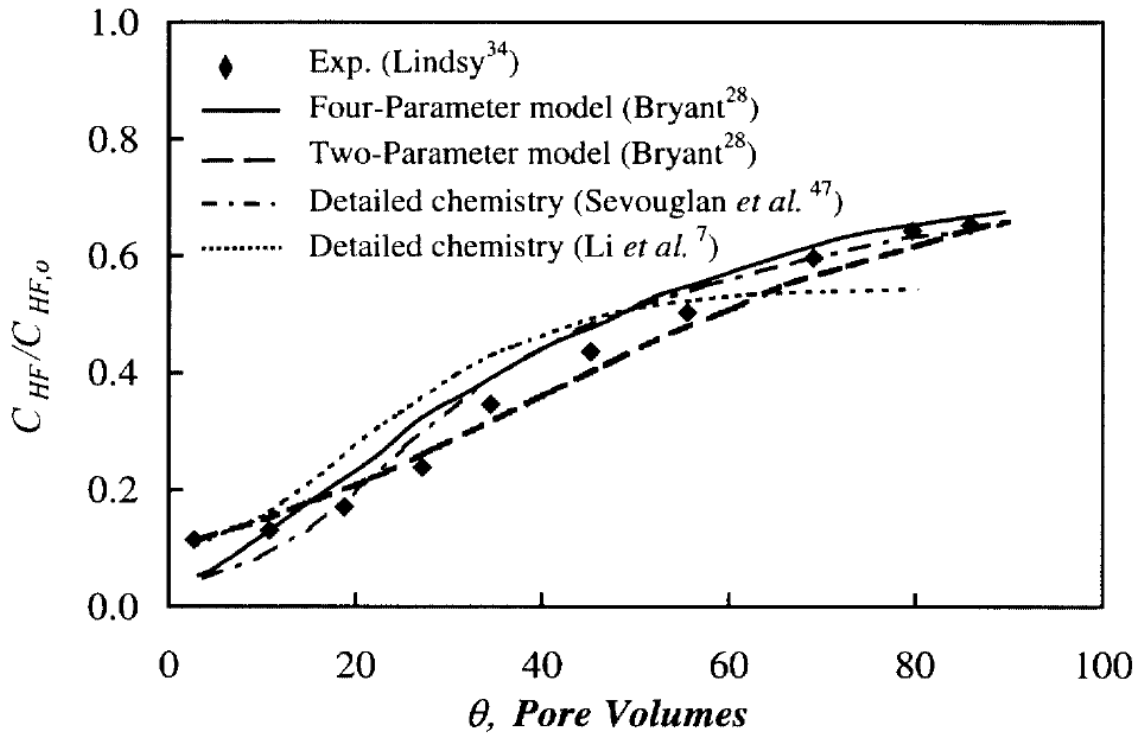


Figure 3.7 Normalized Effluent HF Concentration at high injection rate (Al-Shaalan and Nasr-El-Din 2000).

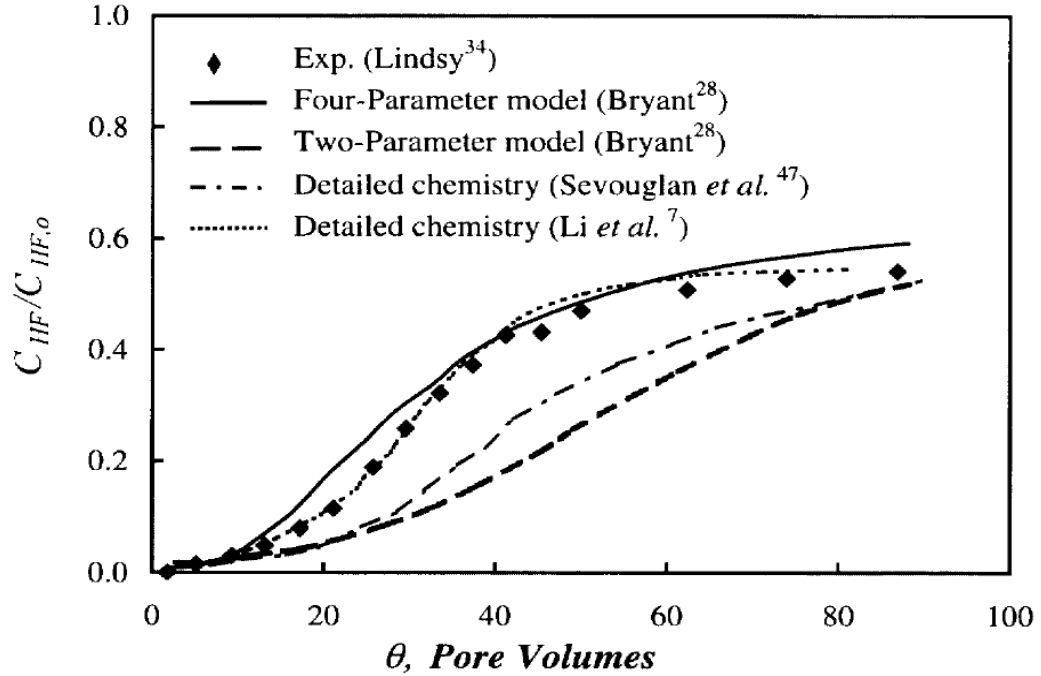


Figure 3.8 Normalized Effluent HF Concentration at moderate injection rate (Al-Shaalan and Nasr-El-Din 2000).

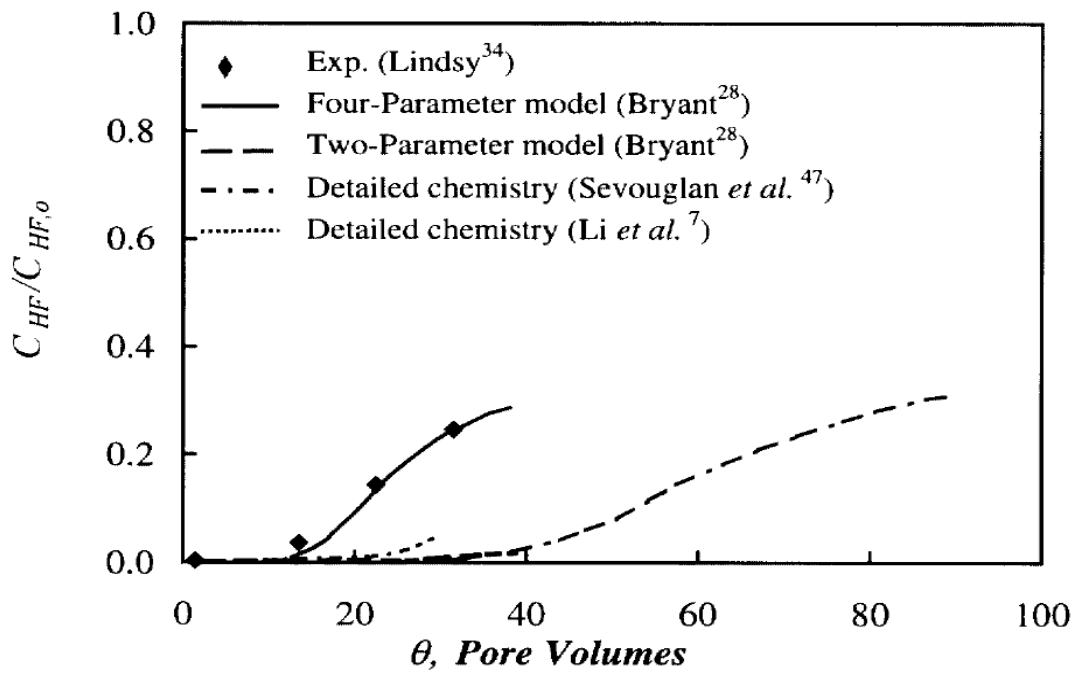


Figure 3.9 Normalized Effluent HF Concentration at low injection rate (Al-Shaalan and Nasr-El-Din 2000).

Table 3.6 Comparison of Different Models Developed for Sandstone Acidizing

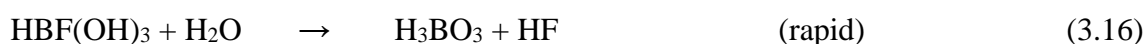
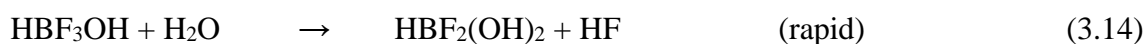
| Models | Authors and Years | Advantages | Shortcomings |
|------------------------|---|---|---|
| Lumped-Parameter Model | <p>Schechter and Gidley (1969)</p> <p>Williams and Whiteley (1971)</p> <p>Lund et al. (1973)</p> <p>Mccune et al. (1975)</p> <p>Labrid (1975)</p> <p>Fogler et al. (1976)</p> | <ul style="list-style-type: none"> - Able to simplify the complex reaction of mud acid with sandstone minerals. - All the sandstone minerals are being lumped together. | <ul style="list-style-type: none"> - This model is oversimplifying the reactions. - Not accurate because the reactivity of quartz, feldspar and clays are not the same. - The secondary, tertiary and precipitation reactions were not considered. |
| Two-Parameter Model | <p>Hekim et al. (1982)</p> <p>Taha et al. (1986, 1989)</p> <p>Perthuis et al. (1989)</p> <p>Bartko et al. (1997)</p> <p>Lea et al. (1993)</p> <p>Da Motta et al. (1993)</p> <p>Rahman (2000)</p> <p>Guimarães et al. (2017)</p> | <ul style="list-style-type: none"> - Considered different minerals dissolve at different rate. - Classified the minerals into two major groups: <ul style="list-style-type: none"> - The fast reacting types (feldspar and clays) and - The slow reacting types (quartz) | <ul style="list-style-type: none"> - The secondary reaction was not considered. - The problem of oversimplifying the acid reaction with sandstone minerals persist. |

Chapter 3 Comparison and Assessment of Modelling Approach

| | | | |
|--------------------------|---|---|--|
| Four-Parameter Model | <p>Bryant (1991)</p> <p>Hsi et al. (1993)</p> <p>Sumotarto et al. (1995)</p> <p>Rodoplu et al. (2003)</p> <p>Li et al. (2004)</p> <p>Xie et al. (2005)</p> <p>Morgenthaler et al. (2006)</p> <p>Zakaria (2013)</p> <p>Yang and Zheng (2014)</p> <p>Zhou et al. (2016)</p> | <p>- The secondary reaction is taken into consideration.</p> <p>- The precipitation reaction, forming the silica gel is included.</p> <p>- Accurately validated the sandstone acid stimulation process at different injection rates.</p> <p>- More reliable and had been widely applied till today.</p> | <p>- The tertiary reaction is not considered.</p> <p>- The precipitation reaction considers only the silica gel.</p> |
| Detailed Chemistry Model | <p>Walsh et al. (1982)</p> <p>Sevougian et al. (1995)</p> <p>Quinn et al. (1997)</p> <p>Ying-Hsiao et al. (1998)</p> <p>Murtaza et al. (1999)</p> | <p>- Accounted for an arbitrary number of kinetic and equilibrium reactions.</p> <p>- Considered an arbitrary number of minerals independently.</p> <p>- Had good validation against the experimental results at high acid injection rate.</p> | <p>- Failed to be validated at low acid injection rate.</p> <p>- Failed to improve the prediction of experimental results.</p> <p>- Less reliable.</p> |

3.3.6 Modelling Studies of HBF₄ Sandstone Acidizing

Up to date, all the models developed for sandstone acidizing are based on the mud acid (HF-HCl), its chemical reactions and mechanism only. In this review, there is no literature showing the model developed based on other acid combination. Just recently, [Zhou et al. \(2016\)](#) has made a breakthrough by introducing a new model developed for Fluoroboric Acid (HBF₄) acidizing. The reaction mechanism of HBF₄ were clearly discussed. Furthermore, the hydrolysis of HBF₄ to form HF was being modelled. The hydrolysis of HBF₄ allowed deeper acid penetration into sandstone core, hence improving its permeability. Fluoroboric acid will hydrolyse in aqueous solution to form hydrofluoric acid until it reaches a limit extent, as shown in the following Equations (3.13) – (3.16):



This model has been well correlated with the experimental results at 25 °C and 65 °C. Thus, the reliability of this model has been demonstrated. Figure 3.10 shows the permeability distributions of the sandstone core after being simulated with mud acid (upper) and with HBF₄ (lower) at 65 °F. Such comparison in the form of graph can also be seen in Figure 3.11. Clearly, the simulation showed that HBF₄ penetrates much deeper into the core than mud acid.

Nonetheless, this is a newly developed model and it has not been verified against the experimental results at elevated temperatures higher than 65 °C. This model is still not representative for the real field condition, which is having very high temperature of 200 °F. Hence, there is a huge research gap in term of HBF₄ acidizing model, which leads to the research motivation for further detailed investigation. It is imperative for these few research gaps to be bridged. Therefore, HBF₄ modelling at elevated temperatures is proposed in the future by adopting the approach developed by [Zhou et al. \(2016\)](#).

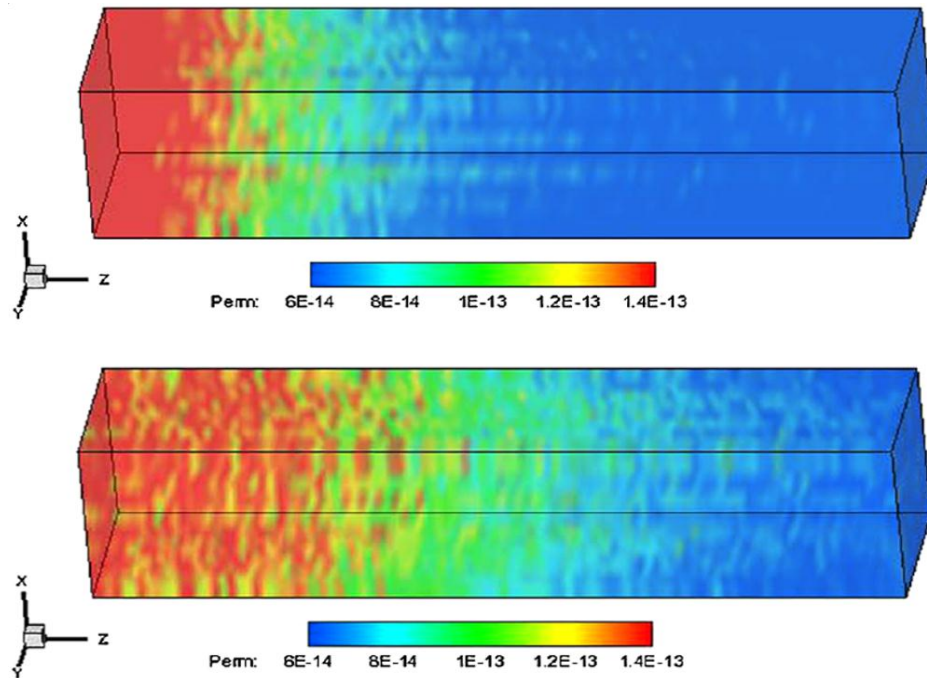


Figure 3.10 The permeability m^2 distributions of the sandstone core after being simulated with mud acid (upper) and with HBF_4 (lower) at 65 °F (Zhou et al. 2016).

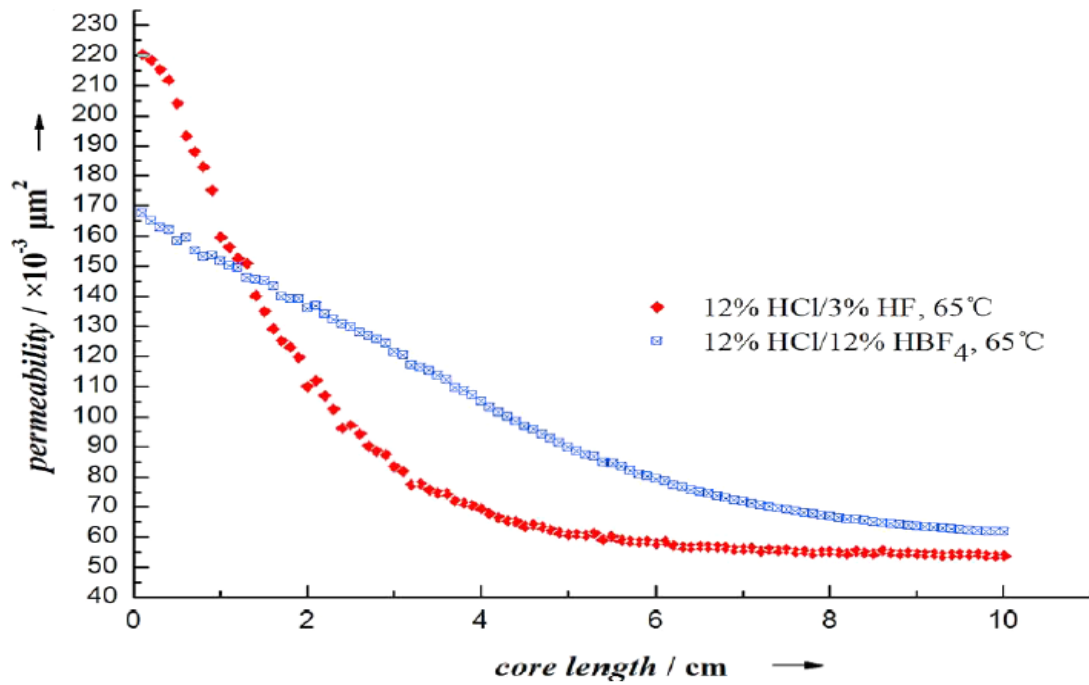


Figure 3.11 The permeability profile along the sandstone core length after being simulated with mud acid and HBF_4 at 65 °F (Zhou et al. 2016).

3.3.7 CFD Application in Matrix Acidizing

Computational Fluid Dynamics (CFD) is a powerful software, which can be used to simulate matrix acidizing process. Many literatures revealed the application of CFD commercial software such as ANSYS Fluent and COMSOL Multiphysics in core flooding process. [De Oliveira et al. \(2012\)](#) developed a methodology to study the effect matrix acidizing on the porosity, permeability, carbonate dissolution patterns, pore volumes to breakthrough (PVTB) and mineralogy heterogeneity using numerical simulation. The model was simulated in the commercial package of Computational Fluid Dynamics (CFD) software using ANSYS Fluent. The 3D simulation results showed good validation with the experimental results. In addition, [Melo and Oliveira \(2013\)](#) also used CFD to solve near wellbore problem. The wormhole propagation of the acidizing process in a carbonates core was modelled and simulated. This demonstrated that CFD is a powerful tool in evaluating matrix acidizing issue. The optimization of the acid injection was also completed using this commercial software.

[Tan et al. \(2016\)](#) developed an improved 1-D averaged model and an empirical correlation to predict wormhole propagation by considering the acid spending and leak off velocity profile. The simulation was done using a CFD software. A 6-inch core length is a critical length for matrix acidizing core flooding experiment ([Dong et al. 2014](#)). Based on the study for long wormhole longer than 6 in, acid spending and leak off had significant effect on the wormhole propagation at low injection rate of lower than 1 bbl/min. The effect of acid spending was not significant at high injection rate of greater than 3 bbl/min.

[Ameri et al. \(2016\)](#) presented a comparative study on carbonates matrix simulation using GLDA and HEDTA. Both core scale and field scale 3D acid transport were simulated using COMSOL Multiphysics software by implementing Finite Element Model (FEM). After validating the core scale model using the results from core flooding experiment, the model is further extended to develop the field scale model. According to the field scale simulation results, the radial flow characteristic of the acid had significantly affected the acid penetration depth and wormhole propagation in the carbonate matrix. However, these simulations were performed on carbonates acidizing process. The mentioned CFD codes

and software, use different governing equations and are for different scales. Figure 3.12 shows the meshing of a field scale model in COMSOL (Ameri et al. 2016).

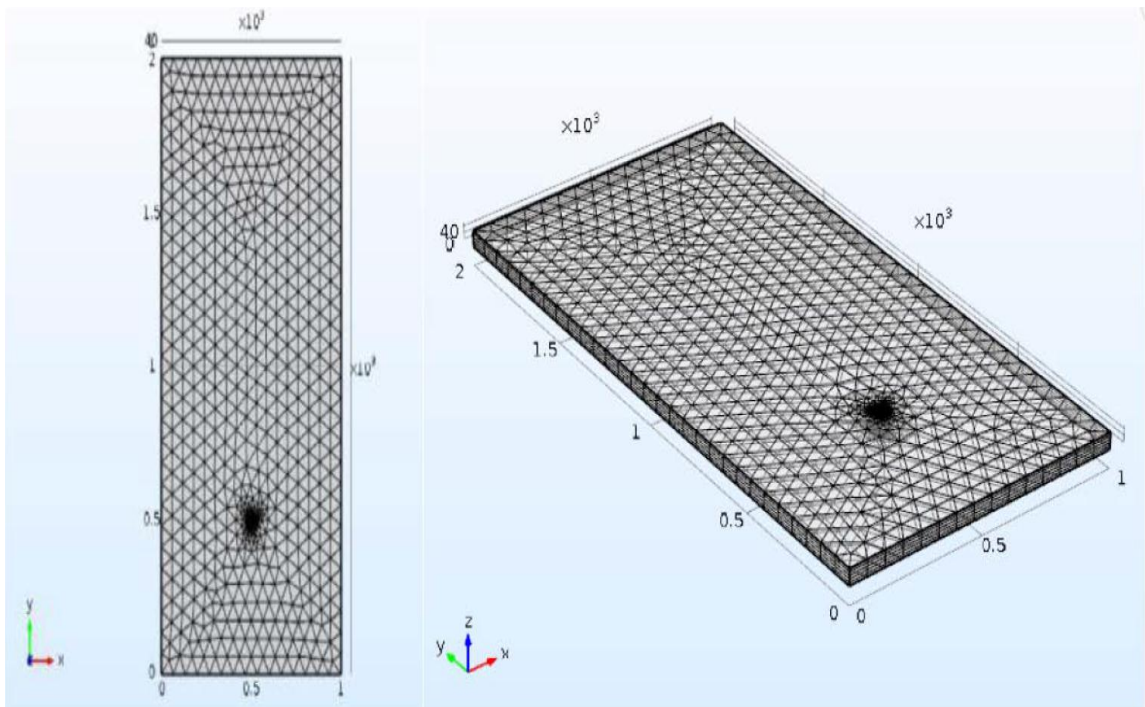


Figure 3.12 A field scale model in COMSOL (Ameri et al. 2016)

3.3.8 Multi-scale Modelling for Matrix Acidizing

Golfier et al. (2004, 2006) developed two core scale transport reaction models based on the average behaviour of Darcy scale dissolution models. In order to extend the current dissolution models at the Darcy scale to field scale, it is very important to understand and study the upscaling of core scale (Golfier et al. 2004). However, in these studies, the dissolution mechanisms are considered in a general way and not only focusing on well stimulation by acidizing technique. Therefore, only single phase flow (interaction of acid with rock) is modelled, neglecting the effect of oil phase, which is very important in real field phenomena (Golfier et al. 2006). Figure 3.13 shows an illustration of different scales in the modelling of matrix acidizing. In real field situation, it is crucial to model the field scale situation for accurate prediction of the matrix acidizing. The bridge of pore-scale and Darcy-scale analyses was developed by Okabe (2005).

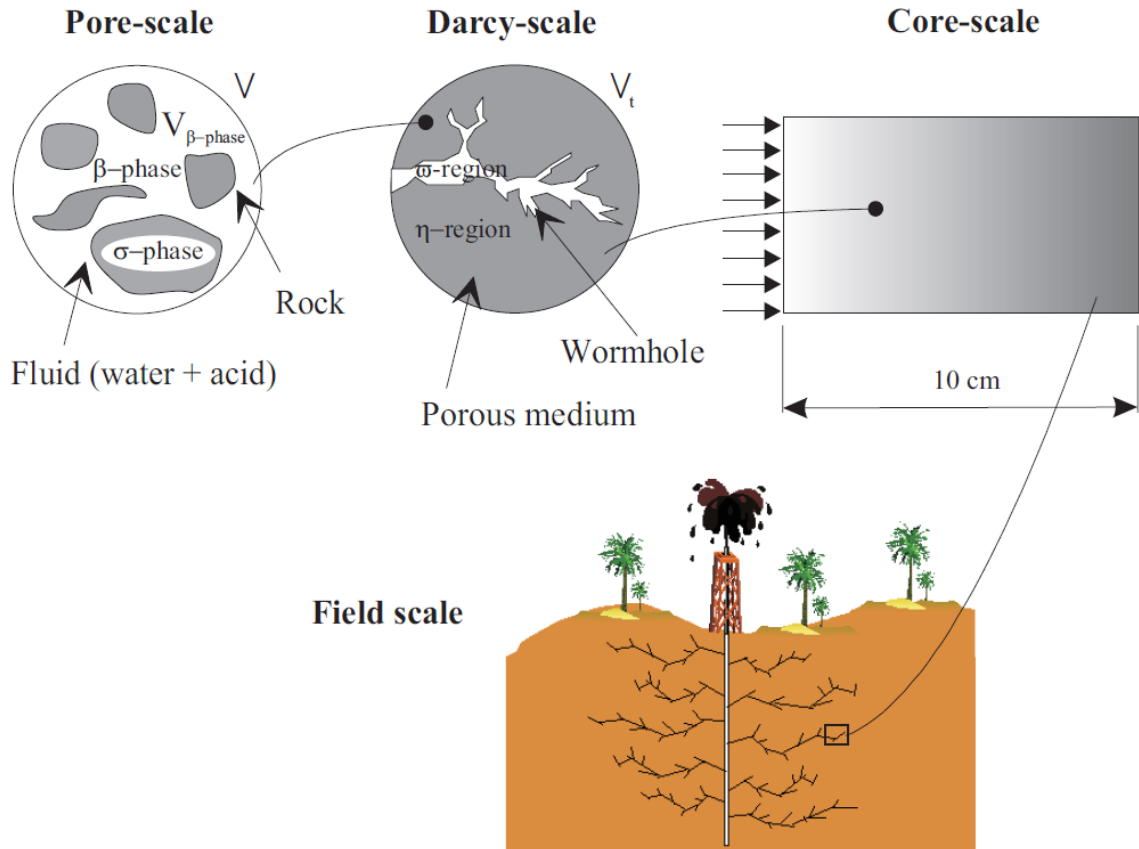


Figure 3.13 Different Scales in the Modelling of Matrix Acidizing (Golfier et al. 2004)

Dong et al. (2017) developed a model to determine the optimum carbonate acidizing conditions. Although this model is based on the optimal acid flux of the tip of the wormhole, it was scaled up to a linear flow core flooding experiment and also field applications. The results indicated that the acid injection rate should be increased during field application due to acid consumption and reduction in the acid concentration. Therefore, it is really crucial for analysing the performance of acid by studying the effect of different scales of modelling. There are also many other recent modelling studies based on carbonate acidizing (Mahmoodi et al. 2018, Ali and Nasr-El-Din 2018, Alhubail et al. 2017, Baghel and Pravesh 2016, Tabasy and Rashidi 2015) that had contributed remarkably to the enhancement of matrix acidizing technique.

3.4 Proposal of Modelling Methodology

Based on all the available literature reviews, the state-of-art of the modelling study in sandstone matrix acidizing had been preliminarily understood. This is very useful to picture the outlook and to form the basic framework for extended work in this study. Apart from that, this review had also provided a constructive approach for the methodology to perform modelling and simulation of sandstone acidizing process. The implementation of such methodology on HBF_4 acidizing process can be considered.

For the next step, there are several key factors that can be considered to perform the modelling investigation on sandstone acidizing using HBF_4 . Firstly, the modelling of HBF_4 sandstone acidizing is recommended to apply the four-parameter model from HF model. The model will incorporate the porosity-permeability relationship model and many other governing equations. The model is aimed to perform the study for higher temperatures of 200 °F.

In view of the feasibility, practicality, reliability and user friendly perspective, COMSOL Multiphysics in Computational Fluid Dynamics (CFD) software module was suggested to perform further improved modelling of HBF_4 sandstone acid stimulation.

The research methodology used for the research consist of 3 main phases, which include:

- 1) Mechanistic model development using computational fluid dynamics (CFD) approach and validation against experimental data.
- 2) Parametric study for key factors affecting the sandstone acidizing process such as temperature, acid concentration and injection using sensitivity analysis.
- 3) Design optimization using response surface methodology (RSM) and development of empirical model.

3.4.1 Model Development Plan

The recommended steps for model development are described in this section. For further investigation of acidizing process using modelling, COMSOL Multiphysics commercial software of Computational Fluid Dynamics (CFD) is used in the development of core flooding model using

Chapter 3 Comparison and Assessment of Modelling Approach

finite element method (FEM). COMSOL is able to perform detailed 3D simulation. All the model parts, the process parameters and also the simulation control that including the boundary conditions and mesh control can be defined in three stages. In general, the following steps should be considered in order to develop a simulator.

The first step is the pre-processing. The pre-processing of COMSOL is basically the geometry creation, which includes the domain identification, boundary conditions and meshing. The geometry creation is the first step in COMSOL analysis using a commercial software, which builds and describes the shape of the problem to be analyzed. In this research, the geometry that will be created is a 3D cylindrical-shaped model. The geometry dimension can be obtained from the size of the sandstone core-sample used experimentally. It can be created using the same pre-processor software in COMSOL. After that, the area of interest is split into smaller grids or cells. This process is called the meshing. Then, the initial and boundary conditions are defined and specified. A constant flow rate is imposed at the inlet face, and no flow boundary condition is set up at four sides of the model. In this study, a core scale model is adopted.

The second stage is the processing stage. The processing of COMSOL is mainly the numerical solution and computational analysis, which involve the various models developed, discretization and solution of algebraic equations. The developed model will include the effects of homogeneous rock properties and mineralogy distribution on acid propagation. Based on the mass conservations of acids and minerals, an overall mass balance and Darcy's law, a three-dimensional (3D) numerical model will be developed to describe the HBF_4 acid flooding stage. The model will be developed based on kinetic approach. Firstly, the equilibrium between aqueous species will be calculated by using empirical correlations. Then, finite element method (FEM) will be used to numerically solve the equations. In terms of simulation, the initial porosity, initial permeability, density of acids, density of minerals and injection velocity values that are obtained from the experiment data available in the literature will be used as the input parameters.

The final stage is the post-processing step. The post-processing of COMSOL is the visualization, which enables analysis of results to be performed. At the end of the simulation, visualization of the change in porosity and permeability of the 3D core

flooding model will be obtained. In this case, the initial and final porosity and permeability profiles of the model will be shown via the display of domain geometry and grid. Meanwhile, the charts showing the graphical plots of permeability change along the injection time will be exported and clearly visualized.

3.4.2 Model Validation and Design Optimization

In order to verify the core flooding model implemented in COMSOL of CFD, the simulation results and experimental test data will be compared. The core flooding model will be modified, matched and improved until it can correlate with the experimental results well. COMSOL is capable of performing the model validation. The experimental test data can be extracted out as a separated data file. COMSOL has the capacities to import the data file into it and plot the data in its domain. Therefore, the comparison of the experimental and simulation results can be made directly to perform the model validation.

The task of this phase is to perform sensitivity analysis on the sandstone acidizing model which has been validated successfully. The sensitivity analysis would describe the effects of reservoir temperature, acid concentration and injection rate during the reservoir acidizing process. By varying these parameters individually, the performance of the acid in sandstone matrix acidizing will be investigated. Therefore, this would be very helpful for the engineer to have a preliminary understanding if the individual parameters are significant in affecting the acidizing process.

In order to determine the integrated effects of all the significant parameters, a design optimization approach is required. In this study, a response surface methodology (RSM) is being employed using the Design-Expert software. Figure 3.14 – 3.17 shows the flow chart of research methodology overview, which is divided into 6 detailed phases.

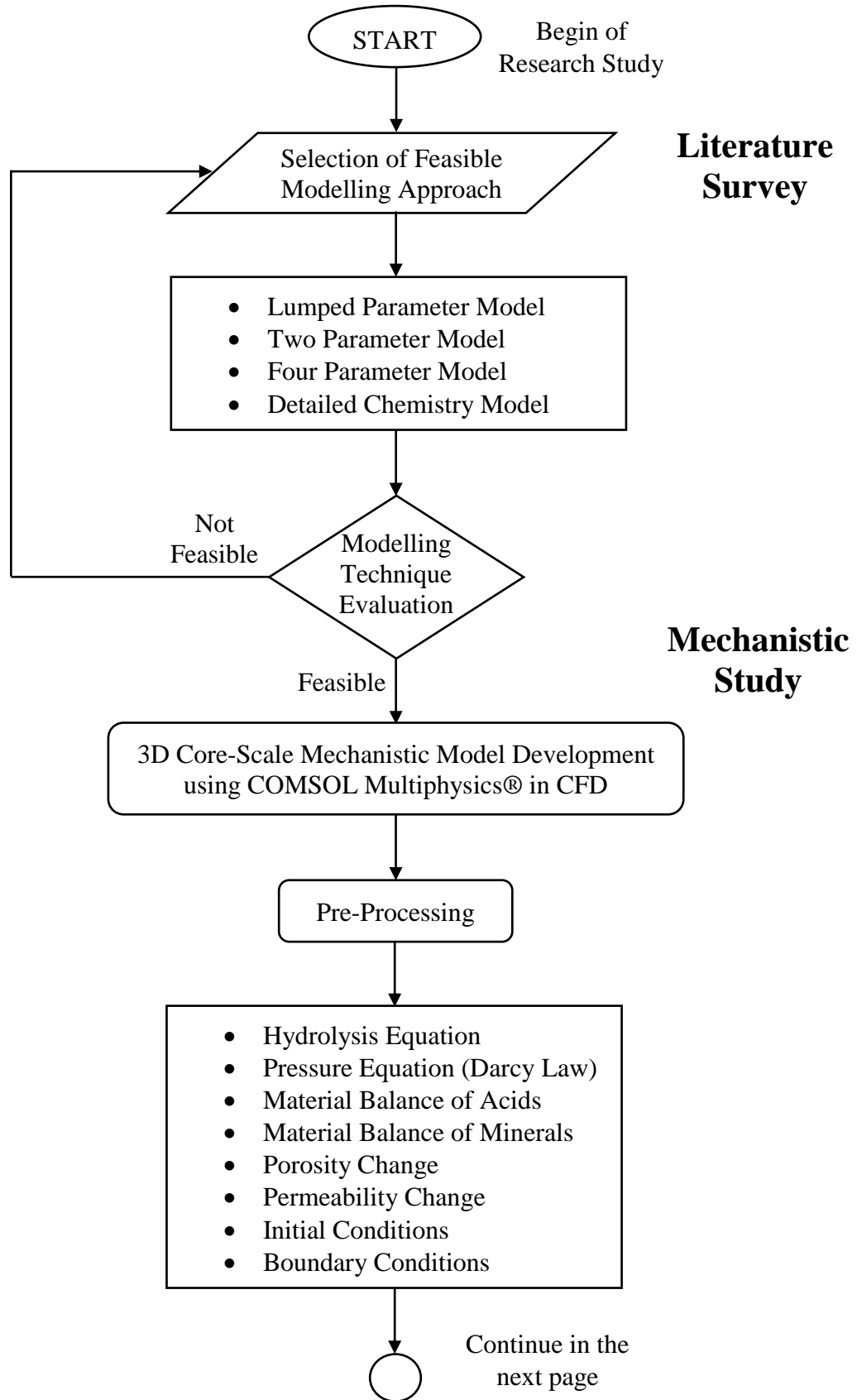


Figure 3.14 Flow chart of research methodology (part 1)

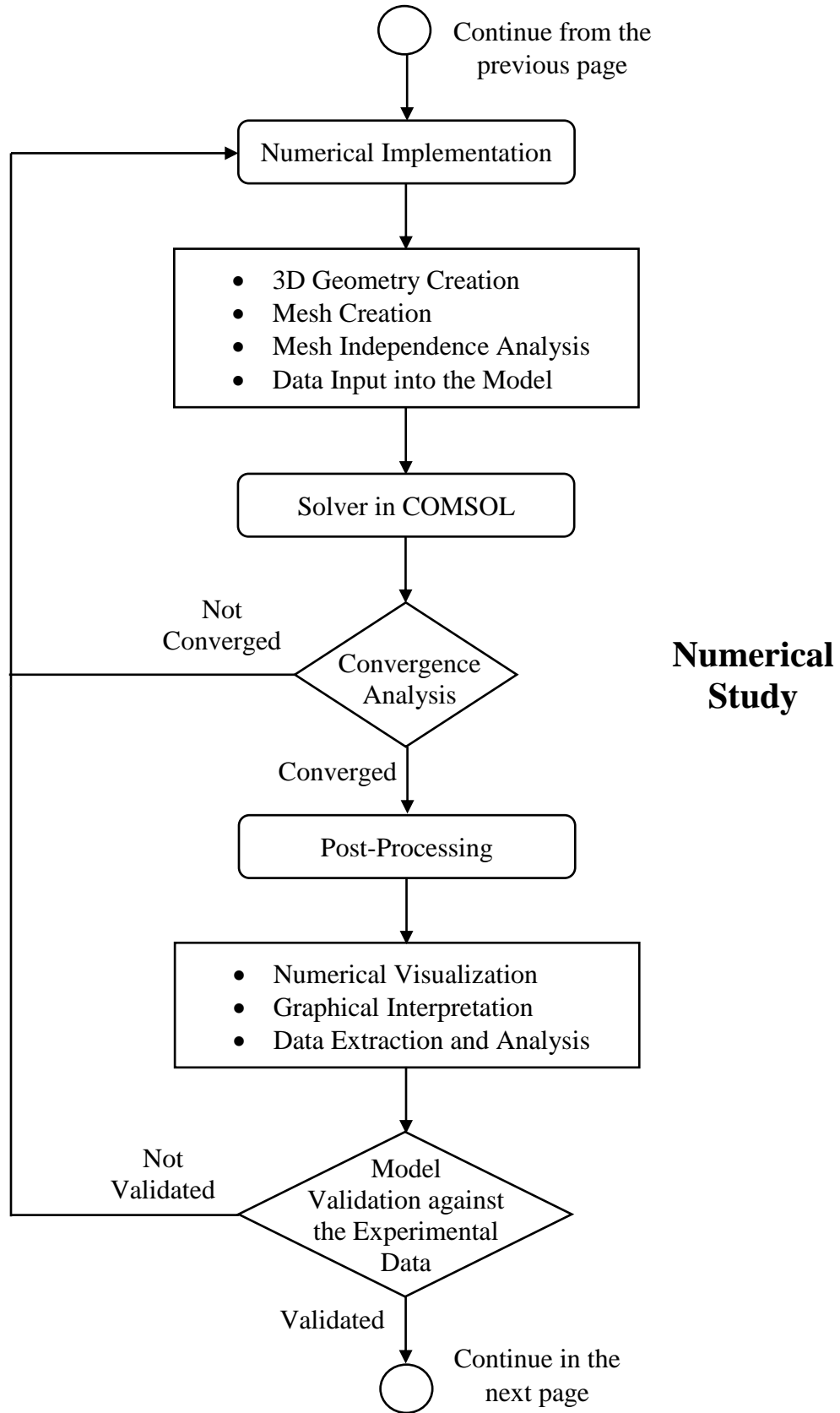


Figure 3.15 Flow chart of research methodology (part 2)

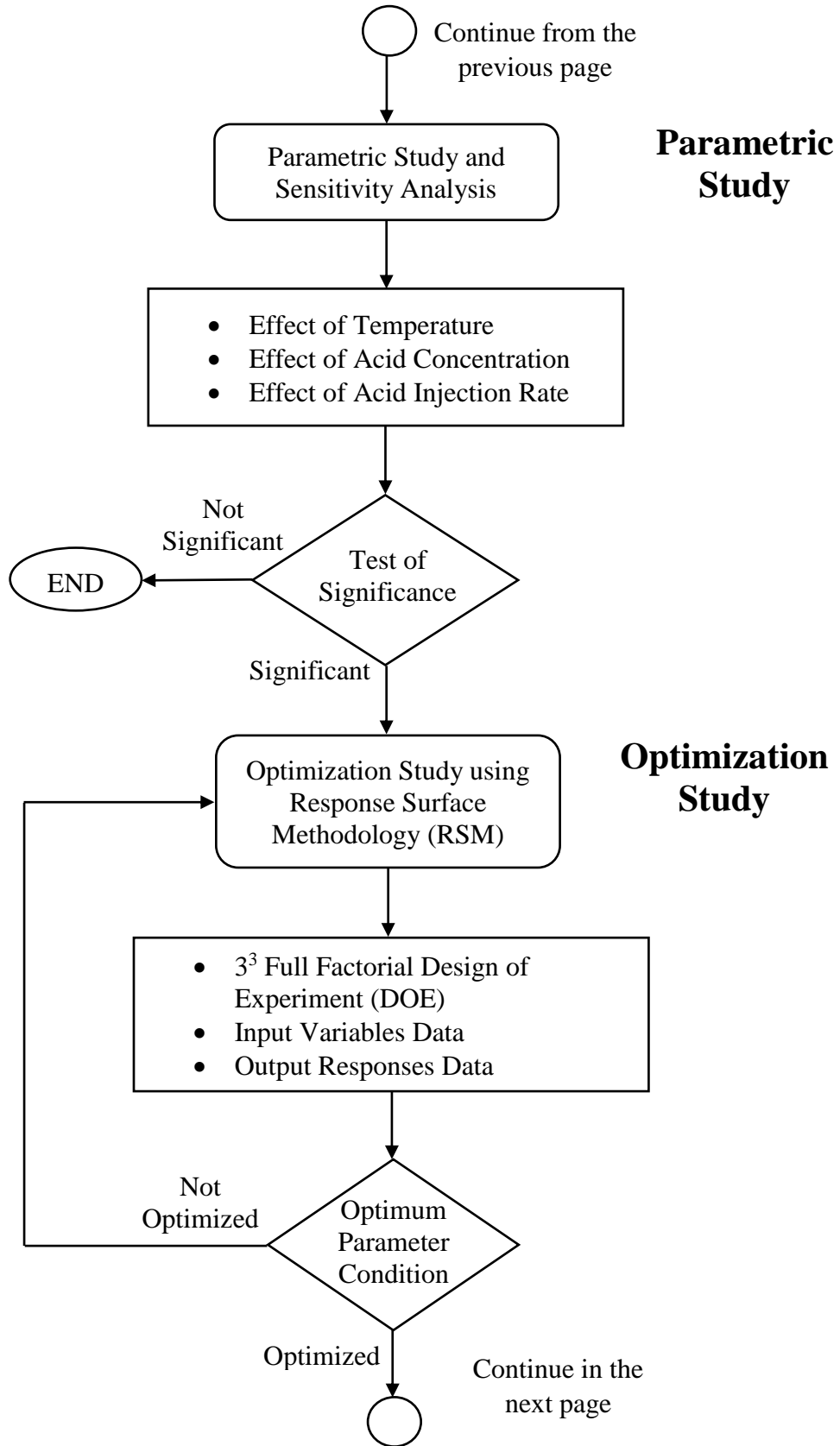


Figure 3.16 Flow chart of research methodology (part 3)

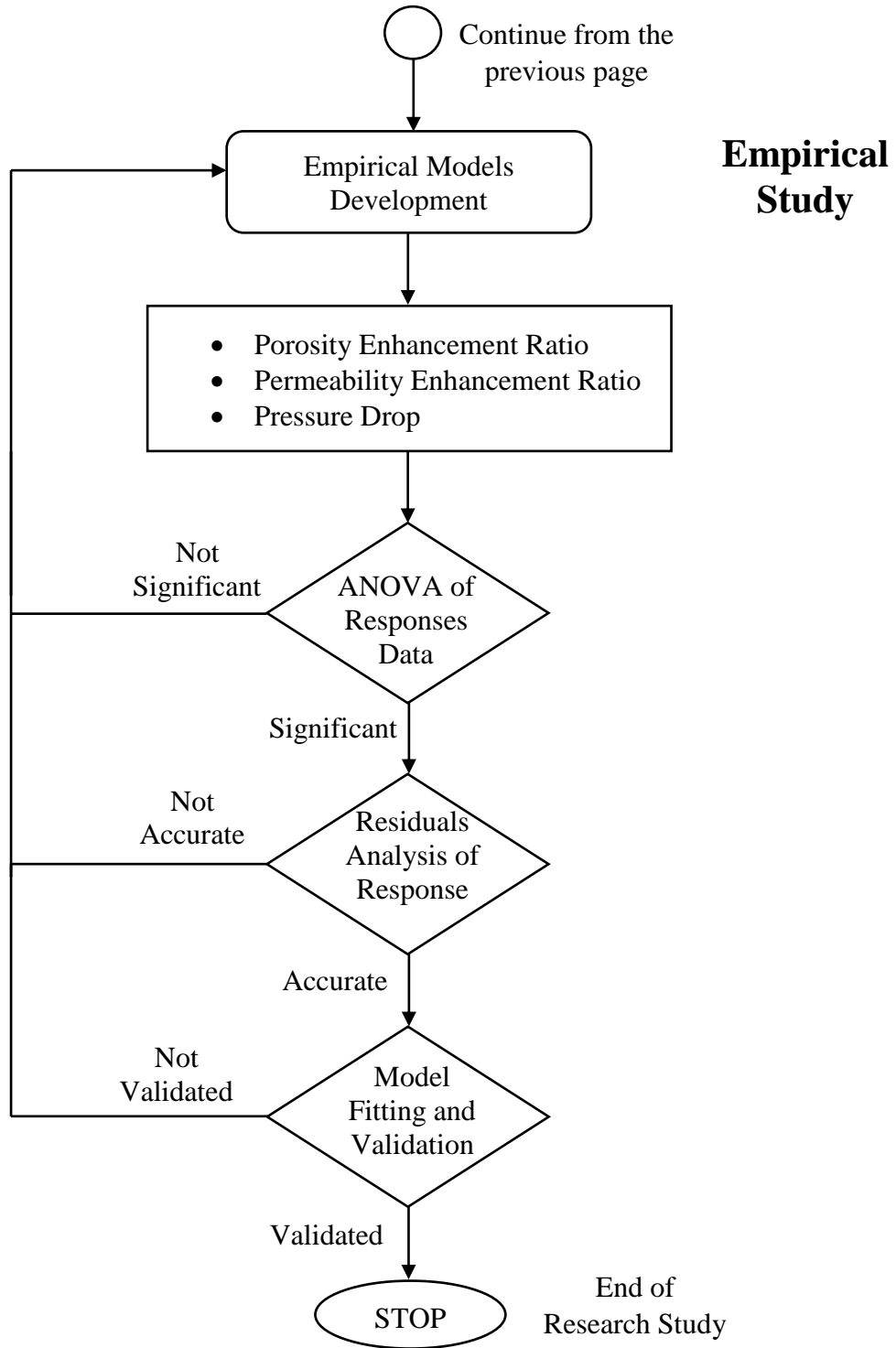


Figure 3.17 Flow chart of research methodology (part 4)

3.5 Summary of Chapter

In this review, the recent advances in the modelling and simulation of the sandstone acidizing process were being summarized. In general, the four main models that had been developed by previous researchers based on the HF acid, namely the lump-parameter model, two-parameter model, four-parameter model and detailed chemistry model. In this chapter, the in depth comparison and assessment of the pros and cons of all these models revealed that the four-parameter model is the most representative model to simulate the sandstone acidizing process as it matched the experimental results at different acid flow rates. Therefore, the four-parameter modelling approach had been proposed to be adopted in present work for HBF_4 acidizing.

For the modelling of HBF_4 , it was found that there are not many investigations that have been done. Hence, the information about the acidizing process of HBF_4 at high temperature sandstone conditions was very little and insufficient. Moreover, the HBF_4 modelling had only study the effect of temperature up to 65 °C. This is not representative enough for the deeper sandstone formation with temperature higher than 200 °F. It is worthy to conduct further investigation in this area of research with an appropriate modelling technique. A complete research methodology is then formulated at the end of this chapter. The literature survey provided in chapter 3 had achieved research objective 2, which is to propose a feasible modelling approach for sandstone acidizing using HBF_4 .

Relevant publications that had been derived from chapter 3 are:

1. **Leong, V. H.**, Mahmud, H. B., Law, M. C., Foo, C. Y. H. and Tan, I. S. (2018). A comparison and assessment of the modelling and simulation of the sandstone matrix acidizing process: a critical methodology study. *Journal of Natural Gas Science and Engineering*. 57. 52-67. Elsevier B. V. <https://doi.org/10.1016/j.jngse.2018.06.044>
2. **Leong, V. H.** and Mahmud, H. B. (2017). A methodological approach to model acidizing process for sandstone well stimulation: a conceptual framework. *In Proceeding: 1st One Curtin International Postgraduate Conference (OCPC) 2017*. Curtin University, Miri, Sarawak, Malaysia. 10th – 12th December 2017.

Chapter 4 Numerical Model Development and Validation

4.1 Introduction

Based on the literature review presented in chapter 3, there had been many applicable models that were developed based on commonly known mud acid stimulation process. However, there is limited focus of numerical studies on fluoroboric, HBF_4 acidizing. Hence, in this chapter, a general 3D core-scale numerical model that is specifically focusing on HBF_4 sandstone acidizing is presented. This model is developed based on the mud acid stimulation modelling approach by [Li et al. \(2004\)](#).

The HBF_4 model has been developed based on the Finite Element Method (FEM). One of the key features of FEM is that it is applicable to unstructured mesh. In terms of the geometry used, FEM is also more flexible. The model is developed based on the kinetics and reaction mechanism of the acids and minerals. Empirical correlation had been used to calculate the equilibrium between the different aqueous species. The model considered the hydrolysis process of HBF_4 , the chemical reactions between acids and minerals; and many other governing equations in it. For instance, the pressure based on Darcy equation, material conservation of acids and mineral components, porosity change and permeability change were modelled. The general description of the model is discussed in this chapter.

Besides, reasonable assumptions were made for model simplification purpose. The important input parameters in describing the sandstone core flooding process were input and set based on the experimental environments so that the model can be validated. A number of simulation sets were conducted using the application of COMSOL® Multiphysics commercial software in CFD to calibrate the simulation results against the experimental data. Generally, this model had been verified and proven to be robust, accurate and reliable for further parametric study. The details of derivations of all governing equations had been included separately in Appendix A at the end of this thesis.

4.2 Model Description and Governing Equations

A three-dimensional (3D) core-scale model had been developed to simulate the sandstone acid treatment process, also known as the core flooding process. The main physics that have been considered in the model included the Darcy's law, mass conservation or transport of acids and minerals and the overall mass balance equations. There are a number of assumptions that were made in order to describe the acidizing process in a simplified way. The assumptions that were considered in the model are as follow. These assumptions had been justified by [Li et al. \(2004\)](#).

- I. Single phase flow
- II. Incompressible fluid and rock
- III. Only liquid phase (the acid) and solid phase (the mineral) present
- IV. No dispersion
- V. No sorption on solid phase
- VI. No effects of gravity

4.2.1 Chemical Reaction Model

In fact, the chemical reactions between the acids and minerals are very complex if they were to be considered independently in a model. This is because there is a large number of mineral components present in a sandstone matrix. Therefore, it is rare to represent these entire chemical reactions separately. Commonly, the reacting minerals in the sandstone were being classified and lumped into several groups according to their reactivity with the acids. In other words, minerals having the similar reaction rate while reacting with the acids would be lumped together.

In the formerly developed two parameter model, the minerals were lumped into two groups only, which were the fast-reacting mineral and slow-reacting minerals based on their reactivity. In the early stage of sandstone acidizing model development, these models had been broadly applied successfully. Nevertheless, this modelling technique is insufficient to represent the acid-rock reactions when the precipitations had to be

considered. The inadequacy of these model under certain condition such as high temperature resulted in the demand in improvement of the subsequent model developed by researchers. The four-parameter model, also known as the two-acid, three-mineral acidizing model was developed for the simulation of high temperature sandstone acidizing. In this model, the precipitation reaction of amorphous silica had been considered. The simulation results of the model had been validated against the experimental data by Lindsay (1976) at high temperature condition with good agreement of the results.

In this HBF_4 acidizing simulation, the four-parameter modelling technique was adopted due to its popularity, accuracy and reliability. Firstly, in this model, the fast-reacting minerals included the feldspar, clays and amorphous silicon as they have relatively rapid or fast reaction rate with the HF. Secondly, the quartz represents the slow reacting mineral due to its relatively slow reaction rate with the HF. Lastly, the silica gel is classified as the third mineral group. It is the precipitated products during the reactions.

Apart from the reactions between HF and the minerals, the reactions between fluorosilicic acid, H_2SiF_6 and the fast-reacting minerals is also included in the model. H_2SiF_6 is the product of primary reactions. During its reaction, H_2SiF_6 would react with the Al in the aluminosilicate mineral to form aluminium fluoride, AlF_3 . At the same time, the Si in H_2SiF_6 will be precipitated as silica gel. This silica gel would have damaged the sandstone formation. The detail chemical reaction processes are shown in Equations (4.1) – (4.4) (Li et al. 2004).



Where v_i are the stoichiometric coefficients [1]. M_1 is the lumped group of fast-reacting minerals, representing feldspar, clays and amorphous silicon. M_2 is the lumped group of slow-reacting minerals, representing the quartz and other detrital clay. M_3 is the

precipitated silica gel, Si(OH)_4 . Some assumptions were made for these chemical reactions in the model as listed.

- I. The solubility product, $K_{\text{Si(OH)}_4}^{SP}$ of silica gel, Si(OH)_4 is zero
- II. The aluminium fluorides, AlF_3 dissolve completely in the acid solution
- III. All the carbonate minerals in the core sample had dissolved completely during HCl pre-flush stage before HBF_4 main acid injection

4.2.2 Hydrolysis of HBF_4

In the form of aqueous solution, HBF_4 will hydrolyse step by step to produce HF progressively. The first step of the hydrolysis process is known as the slowest reaction, hence determining the rate of hydrolysis. Even though HF reacts with clay minerals at a very fast rate, the yield rate and the quantity of HF is limited by the hydrolysis rate and the concentration of HBF_4 . Theoretically, at room temperature condition, the decomposition rate of HBF_4 is slow, thus allowing deeper acid penetration into the rock (Zhou et al. 2016). The hydrolysis of HBF_4 occurs stepwise as shown in Equations (4.5) – (4.8).



When HF was being consumed by the sandstone minerals during the acidizing process, the equilibrium of Equations (4.5) – (4.8) would be shifted to the right hand side. Therefore, more HBF_4 would be hydrolysed and used up to produce HF. It is clear from the equations that the penetration rate of the acid into the sandstone formation is significantly determined by the rate of HBF_4 decomposition. Experimental data found in

Chapter 4 Numerical Model Development and Validation

the literature had proven that even though the hydrolysis rate of HBF_4 is first order reaction in the concentrations of both hydrogen ion, H^+ and fluoroborate ion, BF_4^- , the overall reaction is a second order reaction. This could be seen in the expression shown in Equation (4.9).

$$r_h = k_h \times C_{\text{H}^+} \times C_{\text{BF}_4^-} \quad (4.9)$$

Where r_h = the hydrolysis rate of HBF_4 [$\text{mol}/(\text{m}^3\text{s})$];

k_h = the equilibrium rate constant [$\text{m}^3/\text{mol.s}$];

C_{H^+} = the concentration of hydrogen ion, H^+ [mol/m^3];

$C_{\text{BF}_4^-}$ = the concentration of fluoroborate ion, BF_4^- [mol/m^3].

Previous experimental studies showed that the hydrolysis rate of HBF_4 is a function of the temperature. Therefore, the effect of temperature must be carefully studied as it would greatly influence the sandstone acid treatment using HBF_4 . The equilibrium constant, k_h was obtained by performing kinetic data fitting into the Arrhenius equation as shown in Equation (4.10) (Zhou et al. 2016).

$$k_h = 2.4 \times 10^{15} e^{-\frac{26183}{RT}} \quad (4.10)$$

Where R = the universal gas constant [$\text{cal}/\text{mol.K}$];

T = the formation temperature [K].

4.2.3 Pressure Equation

The pressure distribution at each time step during the simulation must be updated in order to perform the prediction of acid transport in a sandstone core sample. A cubic control volume was defined in formulating the acidizing model. The acid solution used during sandstone acid core flooding process is composed of acids and water. It is assumed to comply with the law of mass conservation, which stated that in a controlled system, the mass in the closed system cannot change over time. The mass of the reactants (acid inlet) must equal to the mass of the products (acid outlet). The pressure equation used in this model is represented by Equation (4.11).

$$\frac{1}{\alpha} \frac{\partial}{\partial x} \left(k_x \frac{\partial P}{\partial x} \right) + \frac{1}{\alpha} \frac{\partial}{\partial y} \left(k_y \frac{\partial P}{\partial y} \right) + \frac{1}{\alpha} \frac{\partial}{\partial z} \left(k_z \frac{\partial P}{\partial z} \right) = 0 \quad (4.11)$$

Where P = the pressure [Pa], k_x , k_y and k_z are the hydraulic conductivity.

4.2.4 Mass Conservation Equation of HBF₄

Based on the general material balance equation for acid, $i = 3$ for HBF₄. HBF₄ is a strong acid. During sandstone acidizing, HBF₄ underwent a complete ionization process to form H⁺ and BF₄⁻ in aqueous solution. So, the concentration of HBF₄ is the same as the concentration of its subsequent ionization product, BF₄⁻. Hence, the hydrolysis rate of HBF₄ is also referred as the rate of BF₄⁻ reduction. In a function of unit time, the change in concentration of HBF₄ is then equal to the net change in concentration due to both the acid fluid transport as well as the total product of hydrolysis process. Therefore, the mass balance of HBF₄ is shown as Equation (4.12).

$$\frac{\partial(C_3\phi)}{\partial t} + \nabla \cdot (\bar{u}C_3) = -r_h \quad (4.12)$$

Where C_3 = the concentration of HBF_4 acid [mol/m^3];

ϕ = the porosity [1],

\bar{u} = the vector velocity [m/s];

r_h = the hydrolysis rate of HBF_4 [$\text{mol}/\text{m}^3\text{s}$].

4.2.5 Mass Conservation Equation of Acid Components

The other two acid types that are involved in the sandstone acidizing process are HF and H_2SiF_6 . Assuming a single phase flow for the process and no sorption on the solid phase. In the model, the effect of dispersion can be neglected from the equation as the spread of acid front is dominantly controlled by the chemical reactions between the acids and the minerals.

For the overall acid consumption rate as well as the mineral dissolution rate, it is highly dependent on two controlling parameters. These two parameters refer to the acid flow to the surface of mineral and the true rate of reaction with the mineral surface. It is clear that the overall rate of reaction is controlled by the slower parameter. During the sandstone acid treatment, the slower process is the reactions between HF and mineral and the faster process of the transport rate of acid. Therefore, the surface reaction rate governs the overall reaction rate. During the core flooding treatment, the acid is consumed, and the mass conservation equation of acid components is shown in Equation (4.13).

$$\frac{\partial(C_i\phi)}{\partial t} + \bar{\nabla} \cdot (\bar{u}C_i) = - \sum_{j=1}^{N_m} E_{f,i,j} S_j^* V_j (1 - \phi) C_i^\alpha \quad i = 1, 2 \quad (4.13)$$

Where C_i = the concentration of acid [mol/m^3];

ϕ = the porosity [1];

\bar{u} = the vector velocity [m/s];

$E_{f,i,j}$ = the reaction rate between the acid and mineral [m/s];

S_j^* = the reaction surface of mineral [1/m];

V_j = the volume fraction of mineral [1].

4.2.6 Mass Conservation Equation of Minerals

The minerals in the sandstone acidizing process are dissolved and removed by two types of acid. In this model, the mass balance of the mineral species in a sandstone core matrix is represented in terms of volume fraction. Since it is assumed that only solid phase exists, all the mineral groups are in solid form. The change in volume of the mineral corresponds to its mass consumption divided by the density. Equation (4.14) shows the material balance for all the minerals involved in the sandstone acidizing reactions.

$$\frac{\partial((1-\phi)V_j)}{\partial t} = -\sum_{i=1}^{N_{a,j}} \frac{MW_i S_j^* V_j (1-\phi) \beta_{i,j} E_{f,i,j} C_i^\alpha}{\rho_j} \quad j = 1, 3 \quad (4.14)$$

Where C_i = the concentration of acid [mol/m³];

ϕ = the porosity [1];

V_j = the volume fraction of mineral [1];

$N_{a,j}$ = the number of acids reacting with minerals;

MW_i = the molecular weight of acid [kg/kgmol];

S_j^* = the reaction surface of mineral [1/m];

$\beta_{i,j}$ = the dissolving power of mineral by acid [1];

$E_{f,i,j}$ = the reaction rate between the acid and mineral [m/s];

ρ_j = the density of mineral [kg/m³].

4.2.7 Change in Porosity

The change in porosity during the acid core flooding process can be modelled according to the material balance of all the minerals. The porosity change in a control volume can be corresponded to the total volume of pore space being created when the minerals are being dissolved and removed. Therefore, the sum of increase in porosity per unit period of time is the total volume of each mineral dissolution deduct the volume of precipitated product generated per unit period of time. In this case, the precipitate is the silica gel. The part of the sandstone matrix that had been removed by both HF and H₂SiF₆ are included. This can be expressed as Equation (4.15).

$$\frac{\partial \phi}{\partial t} = - \sum_{j=1}^{N_m} \sum_{i=1}^{N_{a,j}} \frac{MW_i S_j^* V_j \beta_{i,j} E_{f,i,j} C_i}{\rho_j} \quad (4.15)$$

Where ϕ = the porosity [1];

N_m = the total number of minerals reacting with acids;

$N_{a,j}$ = the number of acids reacting with minerals;

MW_i = the molecular weight of acid [g/mol];

S_j^* = the reaction surface of mineral [1/m];

V_j = the volume fraction of mineral [1];

$\beta_{i,j}$ = the dissolving power of mineral by acid [1];

$E_{f,i,j}$ = the reaction rate between the acid and mineral [m/s];

C_i = the concentration of acid [mol/m³];

ρ_j = the density of mineral [kg/m³].

4.2.8 Change in Permeability

Apart from the display of the porosity change, the change in permeability is also one of the most important parameters that can be used to analyse the efficiency of sandstone acid treatment. Therefore, other than the chemical reaction and mechanism between the acids and the minerals, the relationship between the porosity and permeability is also a key factor that must be quantified in this model. It is commonly known that there is no single porosity-permeability relationship that can be applied to all porous formation universally.

In this simulation, the permeability enhancement is calculated at each time step and is updated based on the Labrid's equation (Labrid 1975). Some of the other examples of the correlation include the Labrid's equation, Lund and Fogler's equation (Lund and Fogler 1975); and Walsh and Brace's equation (Walsh and Brace 1984). Nevertheless, the Labrid's equation was determined to be a suitable correlation for the relationship between the porosity and permeability for silicate sandstone. So, it is applied explicitly in each of the operation grid cell in this model. Its expression is shown in Equation (4.16).

$$\frac{k_2}{k_1} = \left(\frac{\phi_2}{\phi_1} \right)^n \quad (4.16)$$

Where ϕ_1 = the porosity at the first time step;

ϕ_2 = the porosity at the second time step;

k_1 = the permeability at the first time step;

k_2 = the permeability at the second time step;

n = the coefficient corresponds to the sandstone condition.

In this simulation, the pressure is calculated based on the injection rate of the acid whereas the permeability is calculated according to the Darcy's law. Hence, one can say that the pressure and permeability only depend on the porosity at a constant rate of acid injection.

4.2.9 Initial Conditions

Before the beginning of the core flooding, it is assumed that there is no acid in the core system. Therefore, the initial conditions are shown in Equation (4.17).

$$\left. \begin{aligned} C_{\text{HBF}_4} = C_{\text{HF}} = C_{\text{H}_2\text{SiF}_6} = 0 \\ V_1 = V_1^0 \\ V_2 = V_2^0 \\ V_3 = V_3^0 \\ \phi = \phi^0 \end{aligned} \right\} \text{ at } t = 0 \quad (4.17)$$

Where V_1 = the volume fraction of fast-reacting mineral [1];

V_2 = the volume fraction of slow-reacting mineral [1];

V_3 = the volume fraction of silica gel precipitate [1];

V_1^0 = original volume fraction of fast-reacting mineral [1];

V_2^0 = original volume fraction of slow-reacting mineral [1];

ϕ^0 = original porosity of the core sample [1].

4.2.10 Boundary Conditions

The acid core flooding process occurs such that the acid is constantly being injected from the left side into the inlet face of the sandstone core at a fixed injection rate. However, when the porosity and permeability is updated during the simulation, the rate of acid injection in each mesh would also change with respect to time. This means that this boundary condition is not directly applicable in the model. Hence, this issue is solved by

assigning a guess to the initial pressure values. So, the model equations would be computed and calculated based on the initial inlet pressure being input. As soon as updating the pressure change, the rate of acid injection at each mesh would be calculated based on the Darcy's law in the model. This calculated rate of injection would then be compared against the input value, thus adjusting the initial pressure. The value of subsequent pressure is predicted according to the difference between the calculated injection rate and the input injection rate as well as the latest pressure value updated. The iteration process would continue until successful data convergence, getting correct value. The concentration of acid at the inlet face of the core sample equals to the concentration of acid injected. Then, the acid exits from the right side of the core sample, which is the outlet face. A constant pressure is exerted at the outlet of the core. So, there is only one-dimensional flow of acid across the two ends of the core sample. For the curve or circular side of the cylindrical core plug, it is assumed that there is no flow on that boundary. Thus, the boundary condition of the model is expressed as Equation (4.18) – (4.20).

$$\left. \begin{array}{l} C_{HF} = C_i^0 \\ P = P_0 \\ Q = \text{Constant} \end{array} \right\} \quad \text{at } x = 0 \quad (4.18)$$

$$P = P_{out} \quad \text{at } x = L \quad (4.19)$$

$$\frac{\partial P}{\partial r} = 0 \quad \text{at } r = r_c \quad (4.20)$$

Where Q = injection rate of acid [m/s];

P_{out} = back pressure exerted at the outlet face of the core [Pa];

L = length of core sample [in];

r_c = radius of core sample [in].

4.2.11 Summary of Governing Equations

Finally, all the necessary equations as well as initial and boundary conditions that had been adopted in this model to describe the sandstone acidizing process is summarized in this section. It includes the key equations used to solve the pressure field, concentration of acids and concentration of minerals.

$$\frac{1}{\alpha} \frac{\partial}{\partial x} \left(k_x \frac{\partial P}{\partial x} \right) + \frac{1}{\alpha} \frac{\partial}{\partial y} \left(k_y \frac{\partial P}{\partial y} \right) + \frac{1}{\alpha} \frac{\partial}{\partial z} \left(k_z \frac{\partial P}{\partial z} \right) = 0 \quad (4.11)$$

$$\frac{\partial(C_3\phi)}{\partial t} + \bar{\nabla} \cdot (\bar{u}C_3) = -r_n \quad (4.12)$$

$$\frac{\partial(C_i\phi)}{\partial t} + \bar{\nabla} \cdot (\bar{u}C_i) = -\sum_{j=1}^{N_m} E_{f,i,j} S_j^* V_j (1-\phi) C_i^\alpha \quad i = 1, 2 \quad (4.13)$$

$$\frac{\partial((1-\phi)V_j)}{\partial t} = -\sum_{i=1}^{N_{a,j}} \frac{MW_i S_j^* V_j (1-\phi) \beta_{i,j} E_{f,i,j} C_i^\alpha}{\rho_j} \quad j = 1, 2, 3 \quad (4.14)$$

$$\frac{\partial\phi}{\partial t} = -\sum_{j=1}^{N_m} \sum_{i=1}^{N_{a,j}} \frac{MW_i S_j^* V_j \beta_{i,j} E_{f,i,j} C_i}{\rho_j} \quad (4.15)$$

$$\frac{k_2}{k_1} = \left(\frac{\phi_2}{\phi_1} \right)^n \quad (4.16)$$

$$\left. \begin{aligned} C_{HBF_4} = C_{HF} = C_{H_2SiF_6} = 0 \\ V_1 = V_1^0 \\ V_2 = V_2^0 \\ V_3 = V_3^0 \\ \phi = \phi^0 \end{aligned} \right\} \text{at } t = 0 \quad (4.17)$$

$$\left. \begin{array}{l} C_{HF} = C_i^0 \\ Q = \text{Constant} \end{array} \right\} \quad \text{at } x = 0 \quad (4.18)$$

$$P = P_{out} \quad \text{at } x = L \quad (4.19)$$

$$\frac{\partial P}{\partial r} = 0 \quad \text{at } r = r_c \quad (4.20)$$

4.3 Numerical Solution and Model Implementation

For further investigation of sandstone acidizing process using modelling approach, COMSOL® Multiphysics commercial software of Computational Fluid Dynamics (CFD) is suggested to be used in the development of core flooding model using finite element method (FEM). COMSOL® is a sophisticated and convenient tool that can perform detailed 3D geometric modelling and simulation. All the model parts, the process parameters and the simulation control including the boundary conditions and mesh control can be defined in several stages. In general, the following steps should be considered to develop a simulator.

4.3.1 Geometry Creation

The geometry created is a cylindrical shaped sandstone core plug. The dimension of the geometry is 3 inch long with 1.5 inch diameter. This geometry is simulating a typical sandstone core sample that is commonly used during the core flooding experiments. It is being generated directly in the COMSOL® software by key in the radius and length in the domain interface. Then, the object type is selected as solid, simulating a generalized homogeneous Berea sandstone core.

4.3.2 Grid Blocks Creation and Mesh Independence Analysis

Prior to proceed with the real numerical simulation and model verification, the mesh independence analysis was conducted. In ideal case, the accuracy of the simulation results obtained is higher when the mesh size is finer, and the domain element is denser. At the same time, it must be understood that the period of computational time to complete the simulation run would also be longer. This is due to the significantly increased calculation workload and solving of the governing equations in the model at each time step.

However, at a certain point of mesh size increased, the accuracy of the simulation data becomes insignificant and can be neglected. Hence, selecting an optimum mesh size based on the accuracy of simulation result while taking the computational time into consideration is crucial in a modelling study. It is also a typical procedure for any kind of CFD modelling study.

In present work, the mesh independency was checked to obtain a threshold grid size of the geometry, where the further grid size refinement would only cause ignorable effect on the simulation data. The optimum grid size selected would then be used to simulate all the simulation cases while providing optimum accuracy. A total of four different mesh size had been used for mesh independence analysis and the results of porosity, permeability and pressure after numerical simulation were exported. These include the normal, fine, finer and extra fine meshes. A physics-controlled mesh sequence type was selected while building the mesh.

In order to select the optimum grid size, the porosity profile was observed. The mesh independency analysis results were obtained. Judging from the porosity profiles, it is clearly observed that the porosity increment due to different mesh size is not significantly altered.

Based on the final porosity, permeability and pressure extracted, it is demonstrated that nearly constant values are achieved from normal mesh to extra fine mesh. Therefore, further reduction in the grid size of the geometry is not a necessary step since it does not influence the accuracy of the results. Nevertheless, since the computational time for 1 run of simulation using the extra-fine mesh size is within 30 minutes and is acceptable for this

study, the final mesh size selected is the extra-fine mesh. This would ensure a more accurate result obtained in the subsequent parametric study or sensitivity analysis.

Figure 4.1 shows the schematic diagram for the meshing of the cylindrical sandstone core by selecting the extra-fine element size. Referring to the axis orientation, the x-axis corresponds to the main direction of acid transport whereas the y-axis and z-axis represented the cross-sectional plane of the core where it is assumed there is no flow across them. So, the final mesh is made up of 77516 domain elements, 4068 triangular elements, 212 edge elements and 8 vertex elements. The simulation time required to complete each run is approximately 26 mins. Once the mesh independency is secured, then the subsequent simulations could be run without major concern in relation to the grid size.

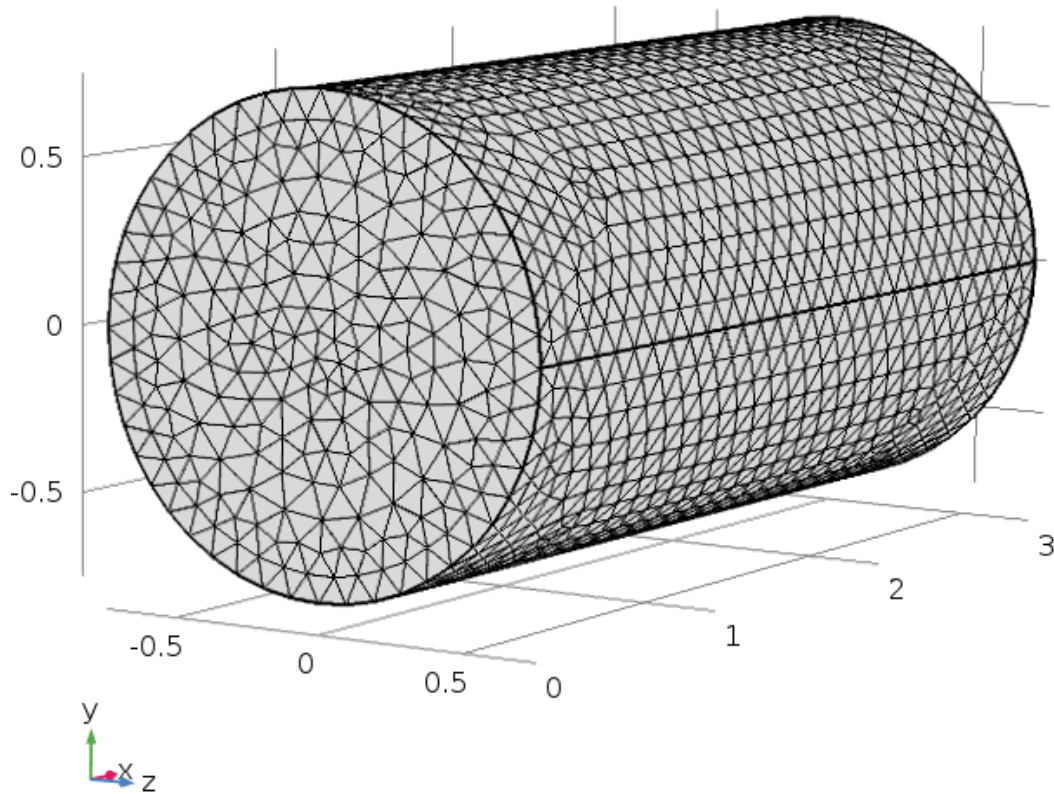


Figure 4.1 The meshing of the geometry using extra-fine element size (unit = inch)

4.3.3 Model Input and Settings

Table 4.1 provided all the required input parameter and necessary coefficients for the simulation. In the numerical simulation, the geometry of the core sample is designed to be the same as the experimentally used core sample in the literature, which is cylindrical-shaped. The dimension of the core sample is set as 3 in long and 1.5 in diameter. This core plug was run throughout all the simulations. The initial porosity and permeability of the core sample were also set based on the experimental condition, which are 12% and 40mD, respectively. In this model, the initial porosity and permeability of the core sample were kept constant along the core plug. Hence, the transport mechanism of the model was simplified to only one dimensional flow, which is only in the direction from the inlet face to the outlet face (x -direction).

For the simulation condition, acid is being injected at constant injection velocity of 2.23×10^{-5} m/s. The temperature condition is set as 25 °C in the first simulation. However, this is a subjective parameter that can be varied and changed later on for parametric study. The reference pressure level and outlet pressure were set as 14.7 psi (101325 Pa) and 1 psi (6894.76 Pa) respectively. Whereas the time step of the simulation was input at 5 mins. It is the time interval between two time steps. Therefore, data of the results generated during the simulation were recorded every 5 mins until the simulation stopped.

The values of reaction rate constant, dissolving power and stoichiometry coefficient listed in Table 1 were determined from the literature data provided by [Da Motta et al. \(1993\)](#). The values are the Damkholer numbers that had been used in fitting the test data by [Lindsay \(1976\)](#). Different chemical reaction between acids and minerals would have different values of reaction rate constant and dissolving power. Four main acid and mineral reactions occurring during the core flooding were considered in this model, which included the reactions between HF and fast reacting minerals, HF and slow reacting minerals, HF and silica gel, as well as H_2SiF_6 and fast reacting minerals. Their respective reaction rate constants are 0.127, 2.32×10^{-8} , 2×10^{-7} and 5×10^{-5} m/s. Whereas their mass dissolving power are 0.486, 0.5, 0.8 and 2.47 respectively. These reaction rate constants and dissolving powers were well understood and could be determined from the literatures ([Economides et al. 2013](#)).

Table 4.1 Required input parameter in the model

| Parameter | Value | Unit | Parameter | Value | Unit |
|-------------------------------------|-----------------------|------|---|-----------------------|--------------------|
| <i>(a) Core Information</i> | | | <i>(b) Kinetic Parameter</i> | | |
| Core length, l | 3 | in | Reaction rate constant of HF and fast reacting minerals | 0.127 | m/s |
| Core diameter, D | 1.5 | in | Reaction rate constant of HF and slow reacting minerals | 2.32×10^{-8} | m/s |
| Initial porosity, ϕ | 0.12 | [1] | Reaction rate constant of HF and silica gel | 2×10^{-7} | m/s |
| Initial permeability, k | 40 | mD | Reaction rate constant of H_2SiF_6 and fast reacting minerals | 5×10^{-5} | m/s |
| <i>(c) Simulation Condition</i> | | | <i>(d) Acid Information</i> | | |
| Injection velocity, v | 2.23×10^{-5} | m/s | Acid viscosity, μ | 8.9×10^{-4} | Pa.s |
| Time step, t | 5 | min | Acid density, ρ_{acid} | 1075 | kg/m ³ |
| Temperature, T | 25 | °C | Acid diffusion coefficient, D_c | 1×10^{-6} | m ² /s |
| Reference pressure level, P_{ref} | 101325 | Pa | Acid Concentration, C_{acid} | 1469 | mol/m ³ |
| Outlet pressure, P_{out} | 6894.76 | Pa | Relative molecular weight of HF | 20 | g/mol |
| <i>(e) Mass dissolving power</i> | | | Relative molecular weight of H_2SiF_6 | 144 | g/mol |

| | | | | | | | |
|---------------------------------------|---|-------|-----|--|---------------------------|--------|-------------------|
| Mass | dissolving | 0.486 | [1] | <i>(f) Mineral Information</i> | | | |
| | power of HF and fast reacting minerals | | | | | | |
| Mass | dissolving | 0.5 | [1] | Relative | molecular | 262 | g/mol |
| | power of HF and slow reacting minerals | | | weight | of fast reacting minerals | | |
| Mass | dissolving | 0.8 | [1] | Relative | molecular | 60 | g/mol |
| | power of HF and silica gel | | | weight | of slow reacting minerals | | |
| Mass | dissolving | 2.47 | [1] | Relative | molecular | 96 | g/mol |
| | power of H ₂ SiF ₆ and fast reacting minerals | | | weight | of silica gel | | |
| <i>(g) Stoichiometry Coefficients</i> | | | | Volume | fraction | of | 0.20 |
| | | | | fast reacting minerals | | | [1] |
| v_1 | | 27 | [1] | Volume | fraction | of | 0.78 |
| | | | | slow reacting minerals | | | [1] |
| v_2 | | 6 | [1] | Volume | fraction | of | 0.02 |
| | | | | silica gel | | | [1] |
| v_3 | | 6 | [1] | Specific | reaction | 235000 | 1/m |
| | | | | surface area of fast reacting minerals | | | |
| v_4 | | 1 | [1] | Specific | reaction | 300000 | 1/m |
| | | | | surface area of slow reacting minerals | | | |
| v_5 | | 3 | [1] | Specific | reaction | 330000 | 1/m |
| | | | | surface area of silica gel | | | |
| v_6 | | 1 | [1] | Density | of fast reacting minerals | 2600 | kg/m ³ |

| | | | | | |
|-------|-----|-----|-----------------------------------|------|-----------------|
| v_7 | 1 | [1] | Density of slow reacting minerals | 2650 | kg/m^3 |
| v_8 | 2.5 | [1] | Density of silica gel | 740 | kg/m^3 |

The stoichiometry coefficients of the four main reactions, v_1-v_8 are 27, 6, 6, 1, 3, 1, 1 and 2.5 respectively (Da Motta et al. 1993). Other information regarding the acids and minerals were all listed in Table 4.1. The main injected acid is HBF_4 . After hydrolysed, it will produce HF, which is the reacting acid. There are two reacting acids and three reacting minerals in the model. The two reacting acids are HF and H_2SiF_6 whereas the three reacting minerals are fast reacting mineral, slow reacting mineral and silica gel (carbonates precipitate). The basic acid information required are the acid viscosity (8.9×10^{-4} Pa.s), acid density (1075 kg/m^3), acid diffusion coefficient ($1 \times 10^{-6} \text{ m}^2/\text{s}$) and acid concentration (1469 mol/m^3). The value of the acid concentration is based on 12% HBF_4 used. The relative molecular weight of HF and H_2SiF_6 are 20 and 144 g/mol respectively (Li et al. 2004).

For the mineral information required in the model, the relative molecular weight of fast reacting minerals, slow reacting minerals and silica gel are 262, 60 and 96 g/mol respectively. The volume fraction of fast reacting minerals, slow reacting minerals and silica gel were set to be 0.20, 0.78 and 0.02. These values are the same as the experimentally used core sample. Different core sample used might have different volume fraction of minerals. The sum of the volume fraction of the three mineral groups is 1. Furthermore, the specific reaction surface of fast reacting minerals, slow reacting minerals and silica gel are 235000, 300000 and 330000 m^{-1} . Last but not least, the last group of parameters input in the model is the density. The density of fast reacting minerals, slow reacting minerals and silica gel are 2600, 2650 and 740 kg/m^3 (Li et al. 2004).

4.4 Model Validation

After modelling all the governing equations describing the sandstone acidizing process, HBF_4 acidizing is simulated in the COMSOL® Multiphysics commercial software. Prior to conduct further simulation investigation at higher temperature as well as performing design optimization study on various parameters affecting the sandstone acidizing process using HBF_4 acid, it is crucial to validate the feasibility of the model. This is very important so that the results obtained from this simulation study would be verified. Hence, the HBF_4 simulation result at 25 °C and 65 °C were being validated against the experimental data obtained from the literature by [Zhou et al. \(2016\)](#).

Figure 4.2 and 4.3 shows the plot of the comparison between HBF_4 acidizing simulation result and experimental data at 25 °C and 65 °C respectively. The plot of permeability ratio, k/k_0 versus time of main acid injection is obtained. The results showed that the simulation results have fairly good agreement with the experimental results. The high consistency of the simulation results fitting the experimental data indicates that the model is reliable for further investigation.

From Figure 4.2 and 4.3, it is clear that the fluoroboric acidizing treatment at 25 °C resulted in permeability enhancement ratio of only 1.2 along the core plug after 35 mins, which is nearly no improvement and not significant. However, at increased temperature of 65 °C, the permeability ratio enhancement after 35 mins is drastically increased to approximately 1.9. The improved permeability to initial permeability of the core sample is almost doubled, which demonstrated significant result.

Comparison of Fluoroboric Acidizing Simulation Result and Experimental Data at 25 °C

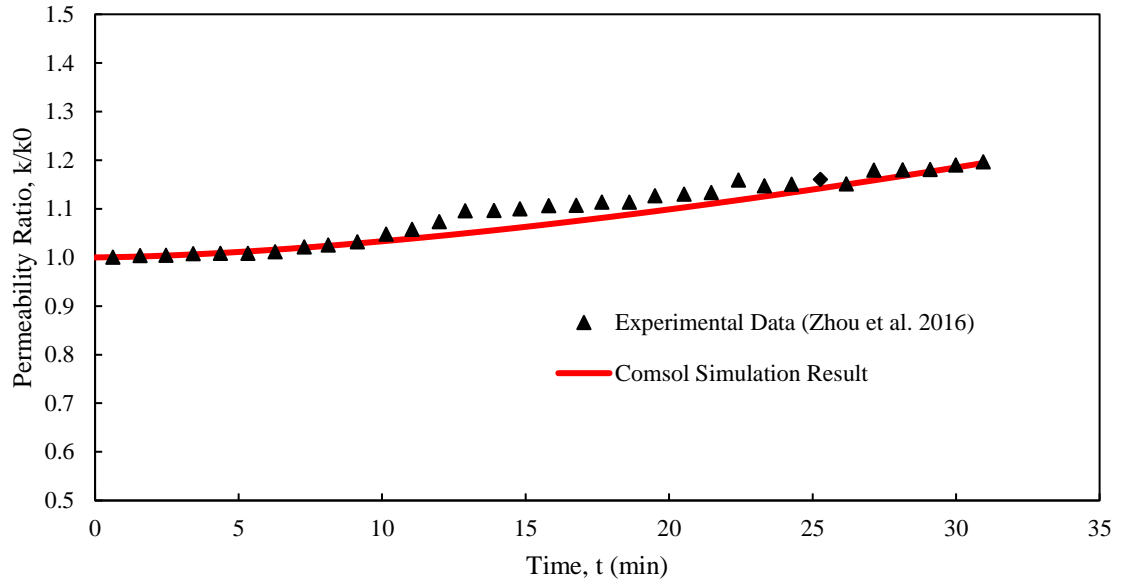


Figure 4.2 Plot of comparison between fluoroboric acidizing simulation result and experimental data at 25 °C

Comparison of Fluoroboric Acidizing Simulation Result and Experimental Data at 65 °C

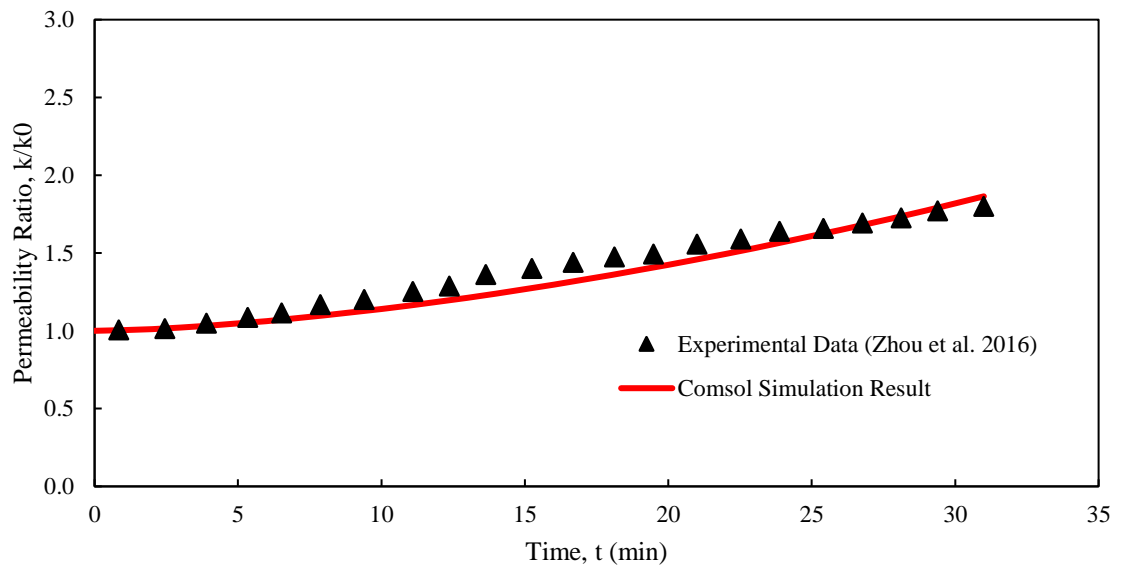


Figure 4.3 Plot of comparison between fluoroboric acidizing simulation result and experimental data at 65 °C

4.5 Summary of Chapter

A 3D mathematical model to simulate the performance of fluoroboric acid, HBF_4 at various range of temperatures had been developed. The numerical simulation process had also been accomplished using the COMSOL® Multiphysics commercial software of computational fluid dynamics (CFD). A finite element method (FEM) was adopted and implemented to perform the numerical solving of the core-scale cylindrical model.

At the end of this chapter, the model had been validated against the measured experimental data by Zhou et al. (2016) in the literature. The results of model verification at both 25 °C and 65 °C were highly satisfying. The plot data of permeability enhancement ratio over the acid injection time fit the experimental test data closely and consistently, indicating good agreement of the results. This mechanistic model is accurate, robust and also time and cost saving. It is confident that the model is feasible and reliable in present study.

Finally, the presented model can be further applied to obtain a number of 3D visualization of the simulation results as well as interpretation. The detail numerical investigation adopting this model will be clearly discussed in the next chapter. The numerical study presented in chapter 4 had achieved research objective 3, which is to develop a mechanistic model for sandstone acidizing and validate it against the experimental data available in the literature.

Relevant publications that had been arisen from chapter 4 are:

1. **Leong, V. H.**, Mahmud, H. B., Law, M. C., Foo, C. Y. H. and Tan, I. S. (2018). A numerical modelling and simulation of core-scale sandstone acidizing process: a study on the effect of temperature. *Journal of Petroleum Exploration and Production Technology*. Springer Nature. <https://doi.org/10.1007/s13202-018-0522-8>
2. **Leong, V. H.** and Mahmud, H. B. (2017). Sandstone acid stimulation using fluoroboric acid. *In Proceeding: 5th Postgraduate Borneo Research Colloquium 2017*. University Malaysia Sarawak (UNIMAS), Kuching, Sarawak, Malaysia. 4th – 6th July 2017.

Chapter 5 Parametric Study and Sensitivity Analysis

Analysis

5.1 Introduction

In this chapter, the technical performance of HBF_4 had been studied intensively. By utilizing the model developed in chapter 4, the acid transport in porous medium was simulated to investigate the performance of HBF_4 in sandstone acidizing. In present work, the effect of temperature on HBF_4 acidizing was determined by conducting the simulation at various of temperatures. This numerical method allowed a cost and time saving alternative to simulate HBF_4 acidizing process. The characterizations of the results in this chapter included the distribution of porosity, permeability, pressure, acids concentration and minerals volume fraction along the core. Overall, this study had extended the boundary of sandstone acidizing research area by extensively studying the effect of elevated temperature up to 105 °C to increase the porosity and permeability of a sandstone formation, which had been lacking in the literature.

Furthermore, this numerical method is also very beneficial and useful to perform a preliminary parametric study. This model had then been implemented to simulate various other parameters conditions that would affect the HBF_4 acidizing performance such as the acid injection rate and acid concentration. Meanwhile, the effect of formation temperature had been coupled and incorporated with the effects of those two factors respectively in affecting sandstone acid stimulation. In this chapter, the range of temperature is set as low (25 °C), moderate (65 °C) and high (105 °C) whereas the range of the other design parameters had been set based on the suitable values in the literature. For instance, the range of acid concentration is set from 1.5% to 12% HBF_4 (Shafiq and Ben Mahmud 2016), whereas the range of acid injection rate is considered from 1.11E-5 m/s to 4.46E-5 m/s (Al-Shaalan and Nasr-El-Din 2000) for sensitivity analysis. The results covered the porosity enhancement, permeability enhancement and pressure drop.

5.2 Design for Parametric Study

The chemical reaction and process is very complex in sandstone acidizing. The success rate of sandstone acidizing is significantly affected by various parameters such as the temperature, acid concentration and acid injection rate. In this model, these parameters are set as the input parameter, allowing the changes in the value for sensitivity analysis. Generally, the effect of temperature the most significant parameter in sandstone acidizing using fluoroboric acid (HBF_4) as the temperature governs the rate of HBF_4 hydrolysis to produce HF, which further reacts with the sandstone minerals. Therefore, in this sensitivity analysis, the effect of temperature is studied by considering 5 sets of simulation with temperatures set as 25 °C, 45 °C, 65 °C, 85 °C and 105 °C.

After that, this factor is incorporated with the other two factors by setting three different temperature conditions, including the low (25 °C), moderate (65 °C) and high (105 °C) temperature. To study the effect of acid concentration on sandstone acid stimulation, the injection rate is set as constant at each of the three temperature conditions. Then, the range of acid concentration is varied from as low as 1.5% HBF_4 to as high as 12% HBF_4 for sensitivity analysis. Hence, an integrated effect of the formation temperature and the acid concentration is presented. Table 5.1 shows the summary of all the simulation cases to study the effect of acid concentration at various temperature condition.

Meanwhile, to study the effect of acid injection rate on sandstone core flooding process, the acid concentration is set as constant at each of the three temperature conditions. Then, the range of acid injection rate is varied between $1.11\text{E-}5$ m/s and $4.46\text{E-}5$ m/s for sensitivity analysis. Therefore, the coupled effect of formation temperature and acid injection rate is studied. Table 5.2 represents the summary of all the simulation cases to evaluate the effect of acid injection rate at various temperature condition.

Generally, in this study, only the parameters that are focused have been changed while all other parameters being kept constant. This would ensure that the difference in the sandstone acidizing result is caused by that parameter. Hence, the impact of the parameters being focused can be clearly observed. In this work, 15 simulation sets had been run for each of the two factors, giving a total of 30 simulation runs.

Table 5.1 Summary of all the simulation cases in the parametric study for the effect of acid concentration

| Case Study | Temperature (°C) | HBF ₄ Concentration (%) | Injection Rate (m/s) |
|--|------------------|------------------------------------|----------------------|
| Effect of HBF ₄ concentration at low temperature 25 °C | | | |
| 1 | 25 | 1.5 | 2.23 E-5 |
| 2 | 25 | 3 | 2.23 E-5 |
| 3 | 25 | 6 | 2.23 E-5 |
| 4 | 25 | 9 | 2.23 E-5 |
| 5 | 25 | 12 | 2.23 E-5 |
| Effect of HBF ₄ concentration at medium temperature 65 °C | | | |
| 6 | 65 | 1.5 | 2.23 E-5 |
| 7 | 65 | 3 | 2.23 E-5 |
| 8 | 65 | 6 | 2.23 E-5 |
| 9 | 65 | 9 | 2.23 E-5 |
| 10 | 65 | 12 | 2.23 E-5 |
| Effect of HBF ₄ concentration at high temperature 105 °C | | | |
| 11 | 105 | 1.5 | 2.23 E-5 |
| 12 | 105 | 3 | 2.23 E-5 |
| 13 | 105 | 6 | 2.23 E-5 |
| 14 | 105 | 9 | 2.23 E-5 |
| 15 | 105 | 12 | 2.23 E-5 |

Table 5.2 Summary of all the simulation cases in the parametric study for the effect of acid injection rate

| Case Study | Temperature (°C) | HBF ₄ Concentration (%) | Injection Rate (m/s) |
|--|------------------|------------------------------------|----------------------|
| Effect of injection rate at low temperature 25 °C | | | |
| 1 | 25 | 12 | 1.11 E-5 |
| 2 | 25 | 12 | 1.67 E-5 |
| 3 | 25 | 12 | 2.23 E-5 |
| 4 | 25 | 12 | 3.34 E-5 |
| 5 | 25 | 12 | 4.46 E-5 |
| Effect of injection rate at medium temperature 65 °C | | | |
| 6 | 65 | 12 | 1.11 E-5 |
| 7 | 65 | 12 | 1.67 E-5 |
| 8 | 65 | 12 | 2.23 E-5 |
| 9 | 65 | 12 | 3.34 E-5 |
| 10 | 65 | 12 | 4.46 E-5 |
| Effect of injection rate at high temperature 105 °C | | | |
| 11 | 105 | 12 | 1.11 E-5 |
| 12 | 105 | 12 | 1.67 E-5 |
| 13 | 105 | 12 | 2.23 E-5 |
| 14 | 105 | 12 | 3.34 E-5 |
| 15 | 105 | 12 | 4.46 E-5 |

5.3 Numerical Visualization of the Effect of Temperature

5.3.1 Porosity and Permeability Distribution

When the temperature increases, the hydrolysis rate of HBF_4 also increases. The chemical reaction shift to the right, producing more HF. Therefore, the hydrolysis rate of HBF_4 acts as the governing factor, controlling the chemical reaction and mechanism between the HBF_4 acid and the sandstone minerals. Therefore, it is known that the porosity and permeability of the sandstone core is eventually affected by the formation temperature.

In this study, all the main parameters are set according to the experimental condition. The acid used is 12% HBF_4 combined with 12% HCl, and is being injected at a constant rate of 2.23×10^{-5} m/s. The initial porosity and permeability are set at 12% and 3.95×10^{-14} m² respectively. The HBF_4 acid is being injected from the left side or the inlet face and breakthrough from the right side or the outlet face of the core plug. When the acid is injected into the core, the acid began to react, and the minerals present in the rock are being dissolved and removed, hence increasing the sandstone porosity and permeability.

After 5, 15, 25, and 35 mins of the fluoroboric acid injection, the results of the 3D numerical visualization are obtained. The porosity and permeability distribution of the core after 25 and 35 mins at 25 °C, 65 °C, and 105 °C due to acid dissolution and precipitation reactions are shown in Figure 5.1 and 5.3 respectively. This simulation is based on homogeneous sandstone condition, therefore the moving of injected acid at the front end of the core plug is observed to be uniform throughout the length of the core plug. There is no preferential flow path being created along the core sample as the porosity and permeability distribution being decreased in a gradual and uniform pattern from the entering side until the exiting end of the core geometry.

Based on the simulation results, the injection of HBF_4 has successfully increased the porosity to 0.1286; and permeability to 4.87×10^{-14} m². This demonstrated that even at

room temperature of 25 °C, porosity and permeability enhancement was observed in the sandstone core, with the porosity and permeability increase of 1.07 times and 1.23 times the initial value respectively. The performance of HBF₄ acid is a function of the temperature. It highly depends on the effect of temperature. The permeability increase is not significant enough due to the slow hydrolysis rate of the HBF₄ acid at room temperature, which limited the speed of acid spending.

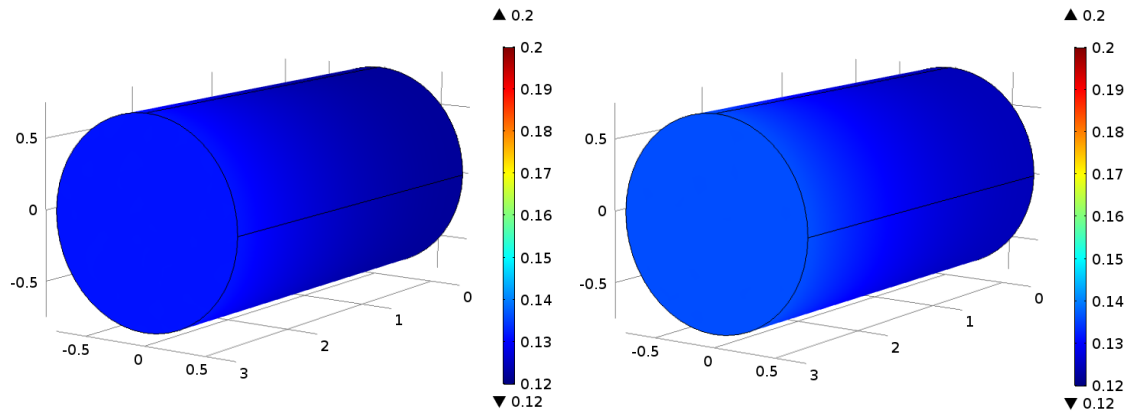
Nevertheless, when the temperature is increased to 65 °C, the hydrolysis rate of HBF₄ increases significantly, hence increasing the porosity and permeability enhancement ratio. Hence, the gradient of the permeability enhancement is also significantly improved. At 65 °C, the porosity of the sandstone core increases to 0.1507, with porosity enhancement ratio of 1.26 times. Whereas for the permeability, an increment to $8.12 \times 10^{-14} \text{ m}^2$ is obtained, with permeability enhancement ratio of 2.06 times.

Meanwhile at 105 °C, which better represents the real high temperature field condition, the HBF₄ acid treatment successfully increases the porosity to 0.2004 and permeability to $2.79 \times 10^{-13} \text{ m}^2$, with their respective porosity and permeability enhancement ratio of 1.67 and 7.06 times. This had proven that at high temperature condition, the acid and rock reactions became more drastic as more HF is being produced from the hydrolysis reaction.

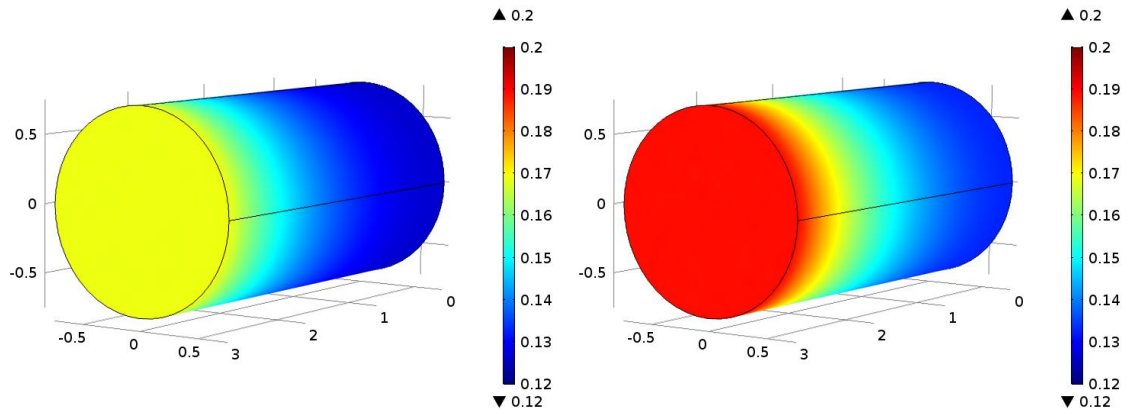
Based on Figure 5.1 and 5.3, it is observed that generally the sandstone core zone that had been dissolved by the acid injected is the one third region of the core length. In other word, most of the acid is being consumed effectively around the inlet face of the core, with porosity and permeability distribution decreases gradually. Also, the slow hydrolysis process of HBF₄ allowed deep penetration into the core. Therefore, a gentle porosity and permeability profile is obtained.

The complete results of simulation based on the five temperatures at 25 °C, 45 °C, 65 °C, 85 °C and 105 °C were tabulated in Table 5.3 and 5.4. The initial and final porosity and permeability as well as their respective porosity and permeability enhancement ratio were shown in the Tables. The graph of porosity and permeability are plotted against the time of acid injection as in Figure 5.2 and 5.4. Generally, it can be seen that the porosity and permeability increase when the formation temperature becomes higher. This is due to higher rate of hydrolysis and the reactivity of acid at higher temperature.

(a)



(b)



(c)

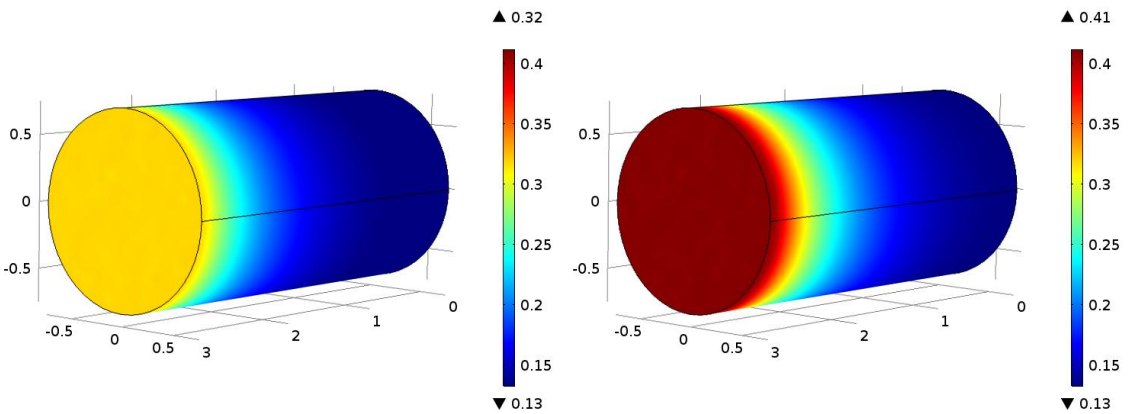


Figure 5.1 Porosity distribution after 25 mins (left) and after 35 mins (right) of fluoroboric acid injection at (a) 25 °C, (b) 65 °C and (c) 105 °C

Table 5.3 Effect of temperature on porosity enhancement ratio

| Temperature, T ($^{\circ}\text{C}$) | Initial Porosity, ϕ_0 | Final Porosity, ϕ_f | Porosity Enhancement Ratio, ϕ_f / ϕ_0 |
|--|-------------------------------|-----------------------------|--|
| 25 | 0.12 | 0.1286 | 1.07 |
| 45 | 0.12 | 0.1369 | 1.14 |
| 65 | 0.12 | 0.1507 | 1.26 |
| 85 | 0.12 | 0.1713 | 1.43 |
| 105 | 0.12 | 0.2004 | 1.67 |

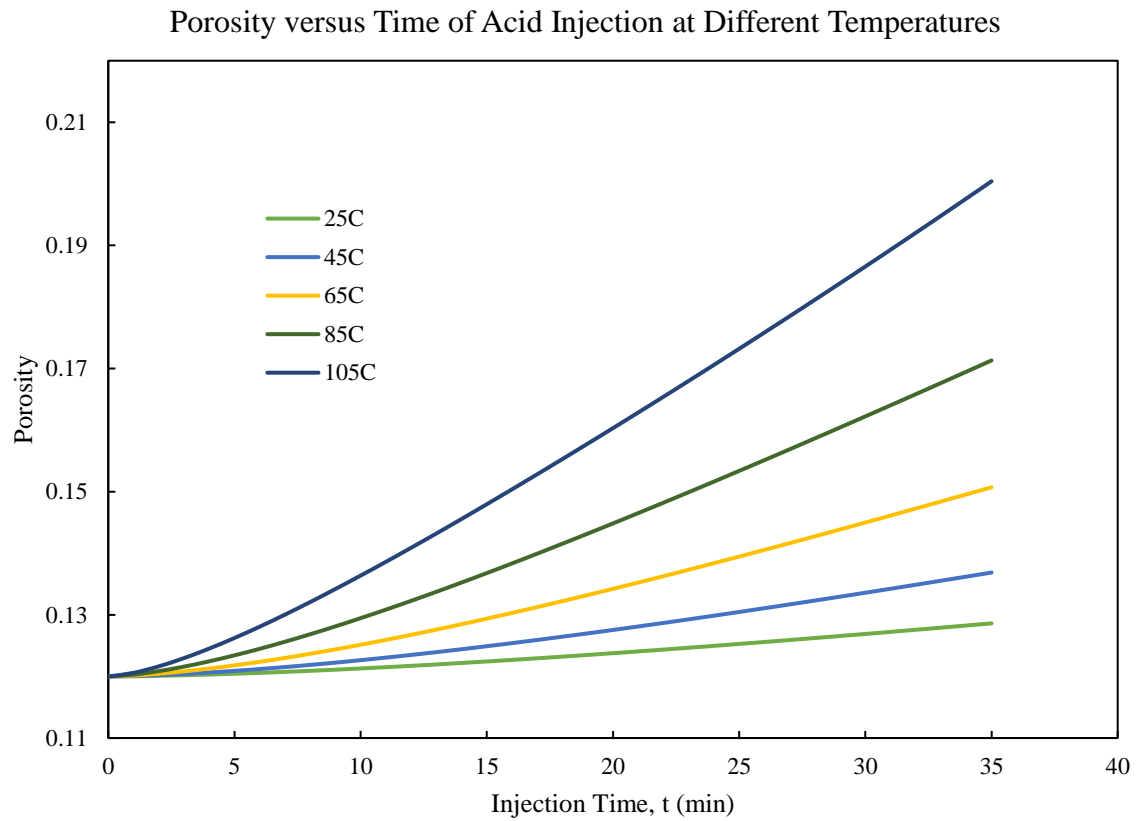


Figure 5.2 The effect of temperatures on sandstone porosity after fluoroboric acidizing

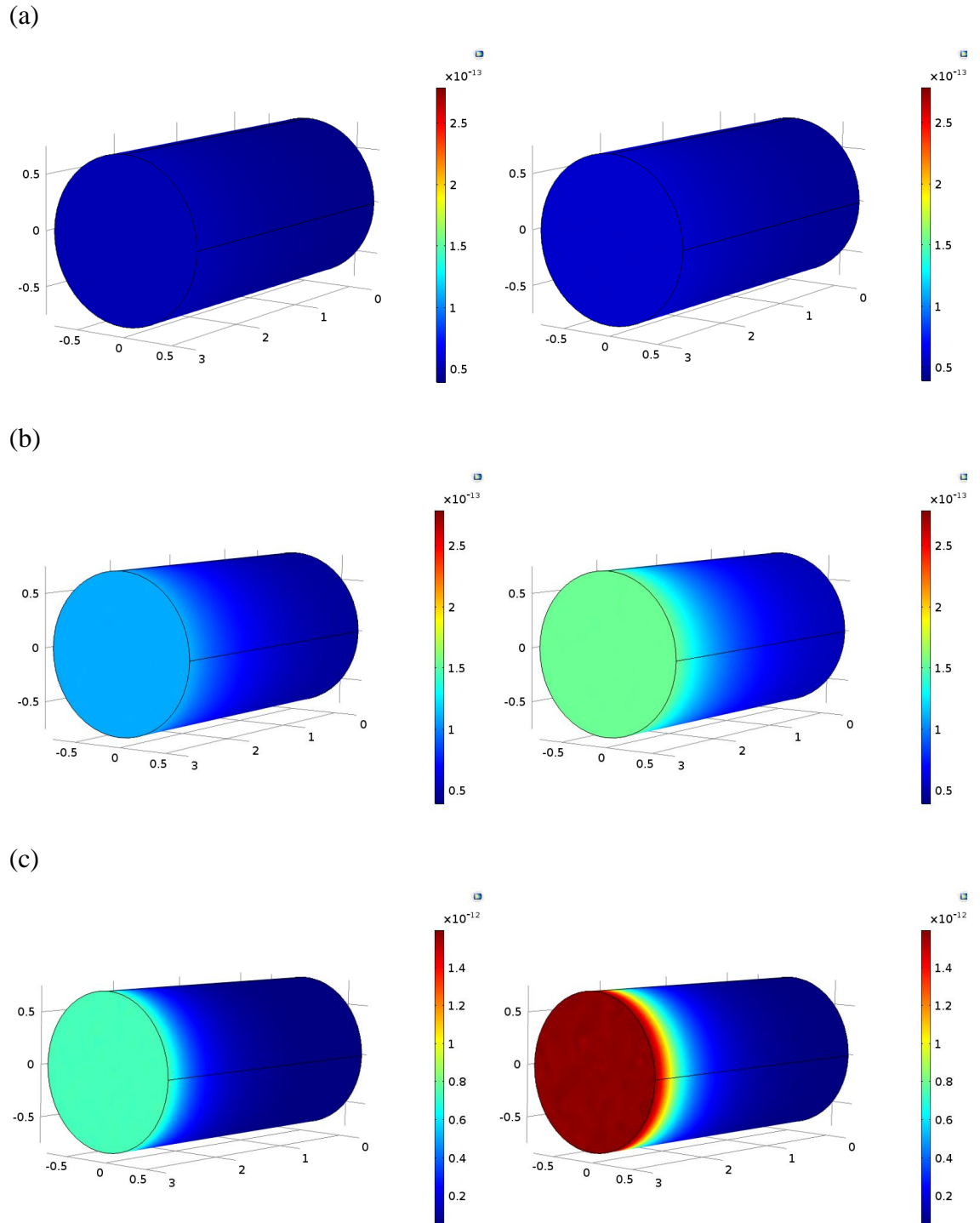


Figure 5.3 Permeability distribution after 25 mins (left) and after 35 mins (right) of fluoroboric acid injection at (a) 25 °C, (b) 65 °C and (c) 105 °C

Table 5.4 Effect of temperature on permeability enhancement ratio

| Temperature, T (°C) | Initial Permeability, k_0 (m^2) ($\times 10^{-14}$) | Final Permeability, k_f (m^2) | Permeability Enhancement Ratio, k_f/k_0 |
|-----------------------|--|--|---|
| 25 | 3.95 | 4.87E-14 | 1.23 |
| 45 | 3.95 | 5.91E-14 | 1.50 |
| 65 | 3.95 | 8.12E-14 | 2.06 |
| 85 | 3.95 | 1.31E-13 | 3.32 |
| 105 | 3.95 | 2.79E-13 | 7.06 |

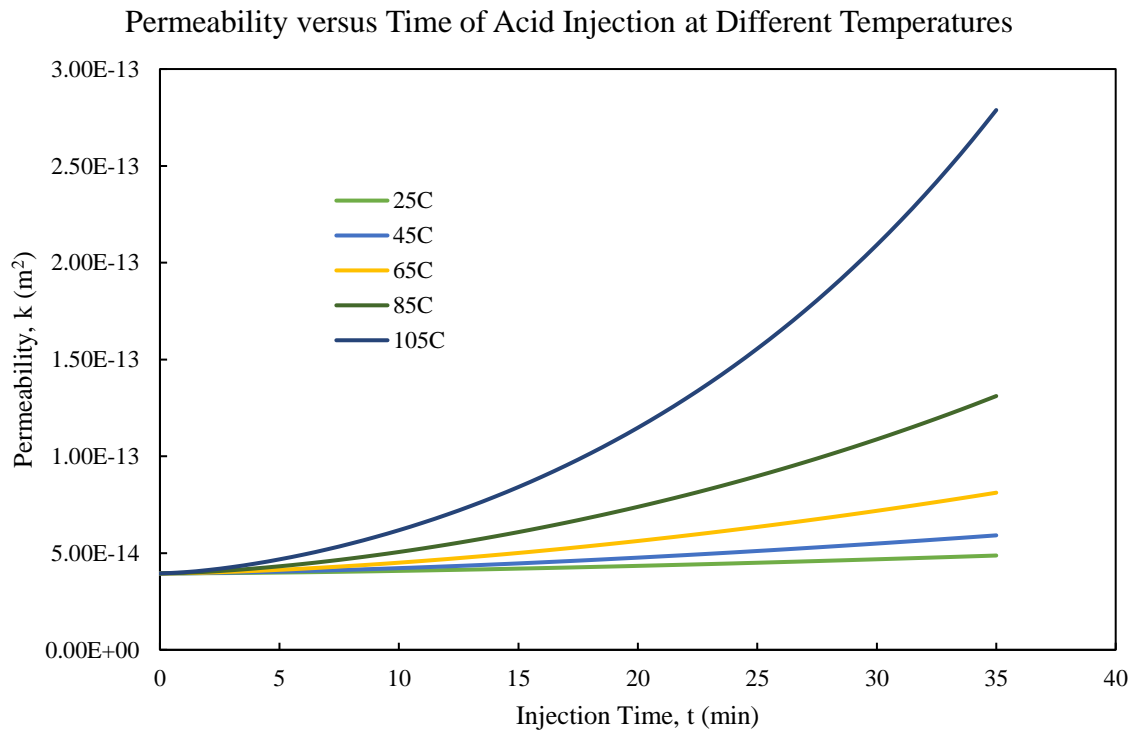


Figure 5.4 The effect of temperatures on sandstone permeability after fluoroboric acidizing

5.3.2 Pressure and Acids Concentration Distribution

Figure 5.5 shows the initial pressure distribution along the core when the acid injection process begins. After the acid treatment process, the pressure drop occurs. The pressure distribution in the sandstone core plug after 25 mins and after 35 mins of acid injection were obtained and shown in Figure 5.7. Based on the 3D visualization result, it is observed that the pressure drops at 25 °C is not so obvious. However, at higher temperatures of 65 °C and 105 °C, the pressure drops significantly due to more acid consumption and mineral dissolution. Due to increased hydrolysis rate, the chemical reaction between the acids and the minerals become more active, hence resulting in higher pressure drop.

The complete pressure drops results of simulation based on the five temperatures were tabulated in Table 5.5. The initial and final pressure and the pressure drop date were shown in the Table. Figure 5.8 illustrated the pressure drop curve for the HBF_4 acid treatment process at different temperatures generated during the simulation. The acidizing treatment resulted in pressure reduction in a gradual pattern along the core flooding process. Based on the pressure response curve, it is clear that when the temperature increases, the pressure drop is more drastic due to the rapid hydrolysis reaction and acid rock reaction.

Figure 5.6 shows the initial HBF_4 acid distribution in the sandstone core at the beginning of the acid core flooding process. From the figure, it is clear that the acid is distributed uniformly along the core, starting from the inlet face of the core. Then, slowly along the core flooding process, the HBF_4 acid distribution after 25 mins and 35 mins of acid injection were shown in Figure 5.9. From the figure, the HBF_4 acid penetrated more evenly and slowly along the sandstone core length at 25 °C because the hydrolysis rate is slow. At 65 °C, the hydrolysis rate increases and the reduction of HBF_4 acid concentration becomes faster. Whereas at even higher temperature of 105 °C, most of the HBF_4 acid is spent at the region near the inlet face. This is due to a faster acid spending speed.

Meanwhile, it is also noticeable that the acid front penetrated more than one third of the core region. This scenario had proven that the chemical reactions between the acid and rock resulted in more acid front spreading or penetration into the core as compared to the effect of dispersion. Therefore, it is valid and reasonable to assume there is no dispersion.

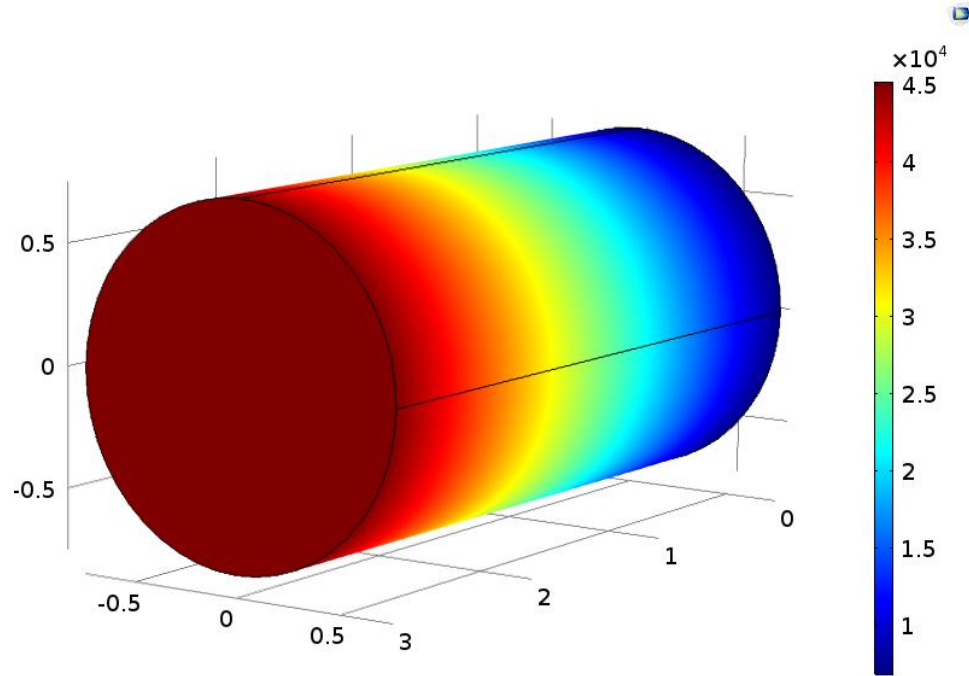


Figure 5.5 Initial pressure distribution at the beginning of acid injection

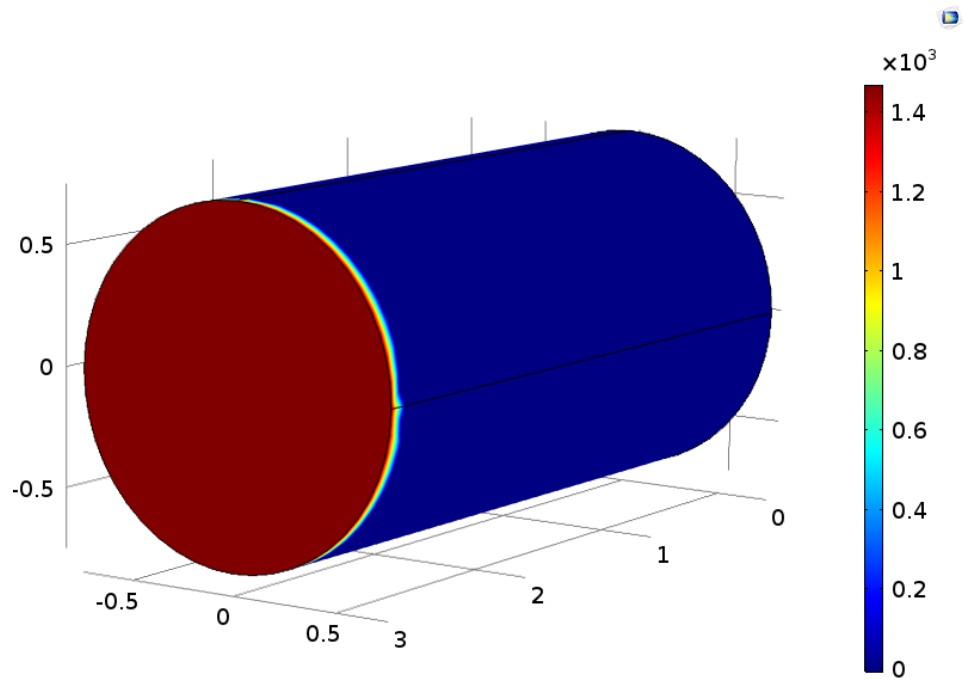


Figure 5.6 Initial HBF_4 acid distribution at the beginning of acid injection

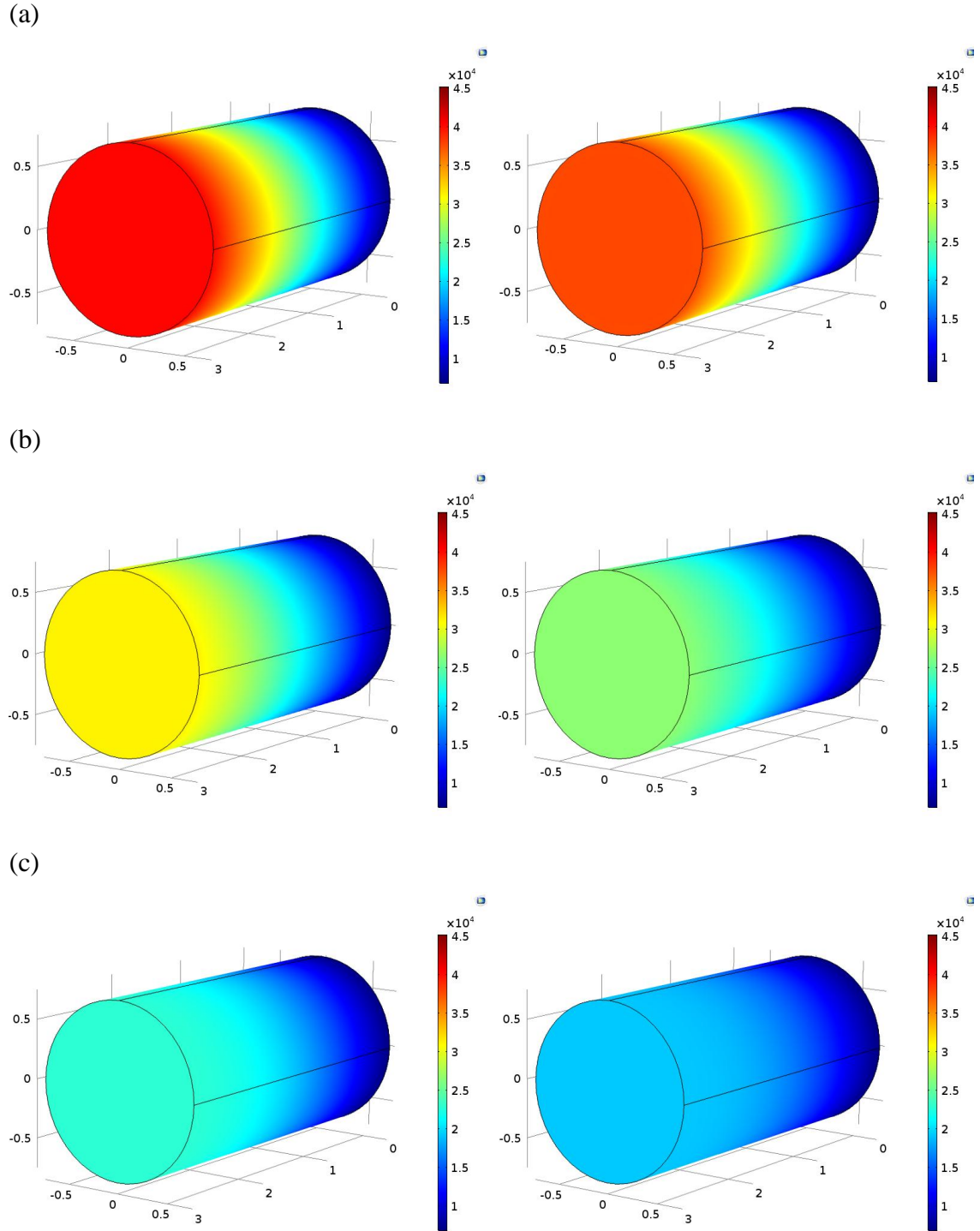


Figure 5.7 Pressure distribution after 25 mins (left) and after 35 mins (right) of fluoroboric acid injection at (a) 25 °C, (b) 65 °C and (c) 105 °C

Table 5.5 Effect of temperature on pressure drop

| Temperature, T ($^{\circ}\text{C}$) | Initial Pressure, P_0 (Pa) | Final Pressure, P_f (Pa) | Pressure Drop, ΔP (Pa) |
|--|---------------------------------|-------------------------------|-----------------------------------|
| 25 | 26039.68168 | 22965.60533 | 3074.076347 |
| 45 | 26040.40886 | 20778.51802 | 5261.890847 |
| 65 | 26041.84560 | 18267.21372 | 7774.631886 |
| 85 | 26044.60449 | 16268.37189 | 9776.232603 |
| 105 | 26049.89308 | 15354.20302 | 10695.69005 |

Pressure versus Time of Acid Injection at Different Temperatures

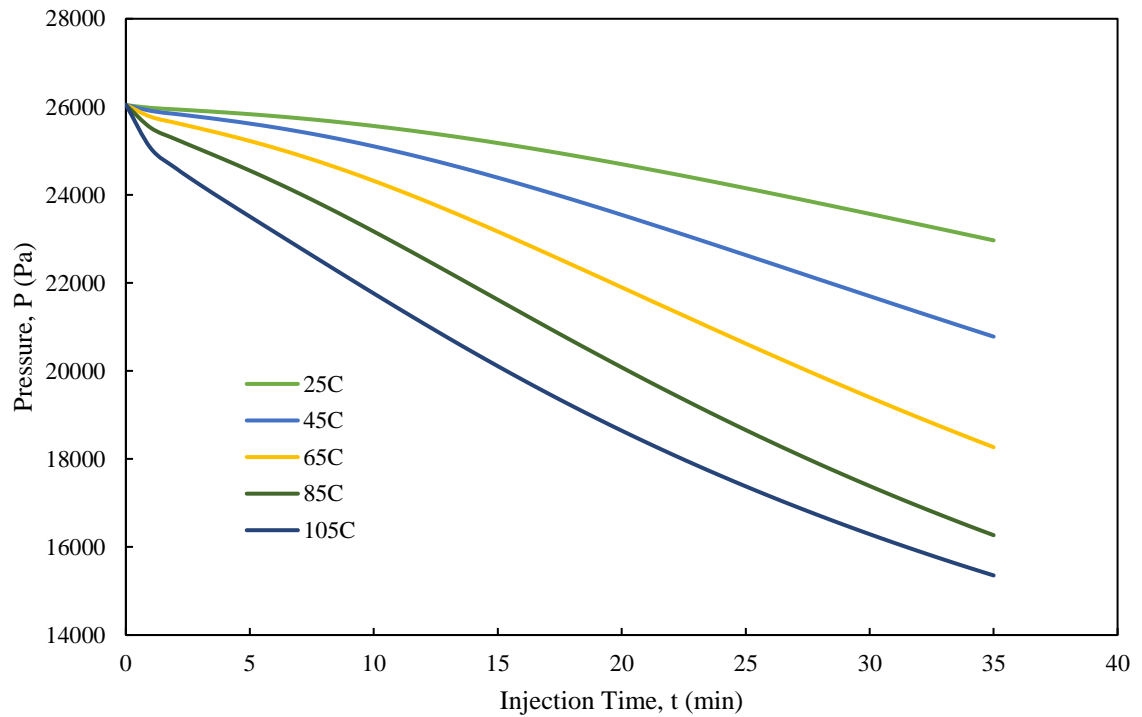


Figure 5.8 The effect of temperatures on sandstone pressure drop after fluoroboric acidizing

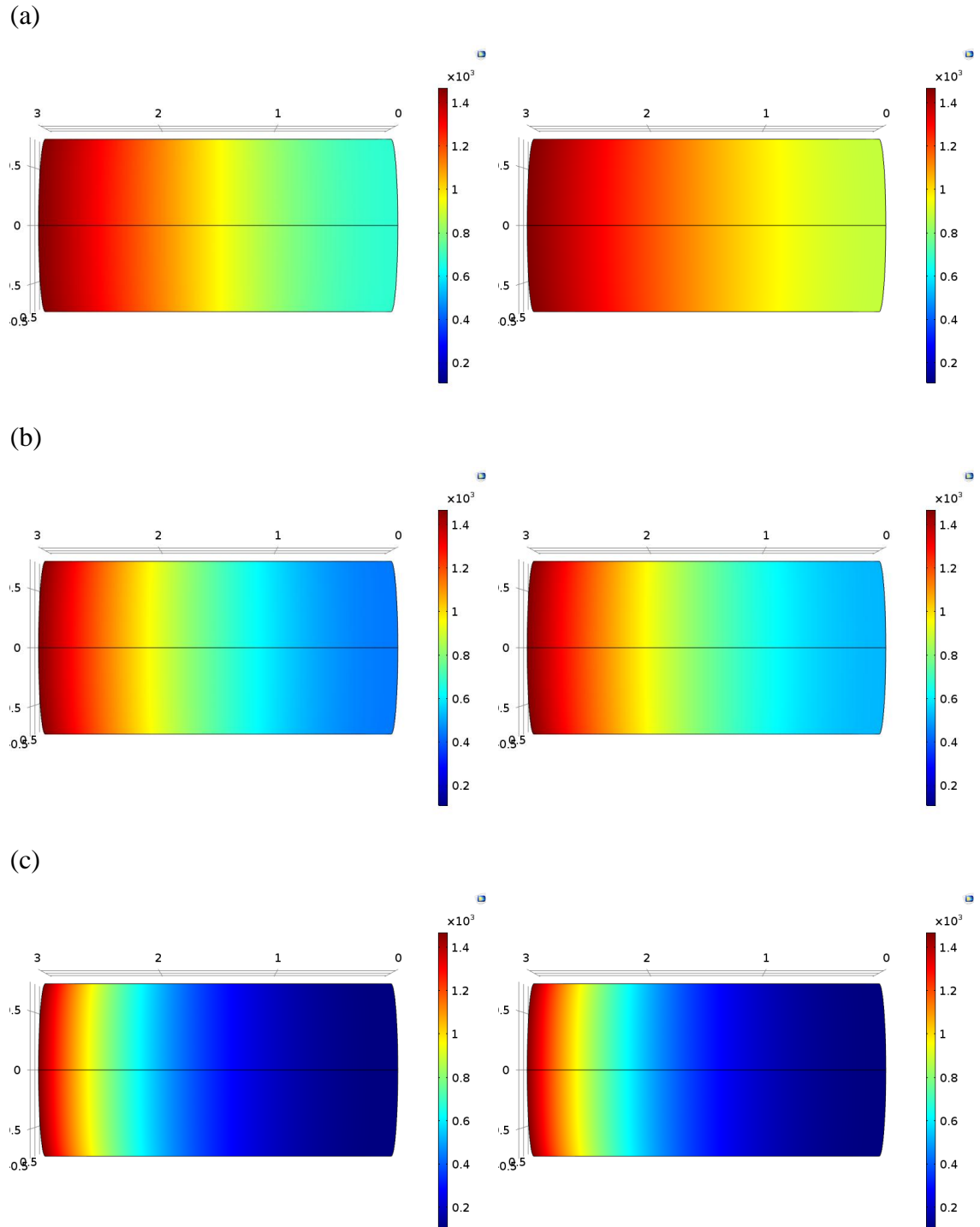


Figure 5.9 HBF₄ acid distribution after 25 mins (left) and after 35 mins (right) of fluoroboric acid injection at (a) 25 °C, (b) 65 °C and (c) 105 °C

The full results of initial and final HBF_4 concentration after acid core flooding simulation at the five temperatures of 25 °C, 45 °C, 65 °C, 85 °C and 105 °C were tabulated in Table 5.6. The higher the temperature, the lower the final HBF_4 concentration because of the increased rate of hydrolysis, causing more acid consumption.

Figure 5.10 illustrated the HBF_4 concentration curve during acid treatment process at different temperatures generated. In general, the curve pattern of the concentration of HBF_4 along the core flooding process showed a sharp increment at the beginning of the acid injection. Then, it continues to increase progressively until it reached the equilibrium concentration, which eventually leads to a nearly constant concentration value. Based on the HBF_4 concentration curve, it indicates that effective acidizing occurs as soon as the acid begins to be injected and slowly weakens. Furthermore, when the temperature increases, it is noticeable that the HBF_4 would be spent more quickly and therefore, reaching an equilibrium constant sooner. This is also due to the rapid hydrolysis rate.

Referring to Table 5.6, the initial HBF_4 concentration at all the temperature ranges are the same, which is 16.9 mol/m^3 . This is the acid concentration calculated as soon as the core flooding process begins. Its initial value depends on the initial injected value. However, it is not the same case for HF and H_2SiF_6 concentrations. Table 5.7 and 5.8 shows the results of HF and H_2SiF_6 concentration respectively at different temperatures. It could be seen that the initial values for HF and H_2SiF_6 are different for varied temperature conditions. This is because their initial and final concentrations depend on the hydrolysis rate of HBF_4 and subsequent chemical reactions, which are strongly affected by the temperature parameter.

In plot form, the respective HF and H_2SiF_6 concentration curves were graphically shown in Figure 5.11 and 5.12. Overall, the concentration of HF would increase simultaneously with the consumption of HBF_4 main acid through hydrolysis process. On the other hand, the concentration of H_2SiF_6 would increase synchronously with the consumption of HF acid through the chemical reaction with the sandstone minerals during acid treatment. At increased temperature environments, the rate of hydrolysis rate would increase. Hence, this would also lead to an increase in subsequent HF and H_2SiF_6 concentration reasonably.

Table 5.6 Effect of temperature on HBF₄ concentration

| Temperature, <i>T</i> (°C) | Initial HBF ₄ Concentration (mol/m ³) | Final HBF ₄ Concentration (mol/m ³) |
|-------------------------------|---|---|
| 25 | 16.9 | 1.11E+03 |
| 45 | 16.9 | 1.01E+03 |
| 65 | 16.9 | 8.48E+02 |
| 85 | 16.9 | 6.51E+02 |
| 105 | 16.9 | 4.62E+02 |

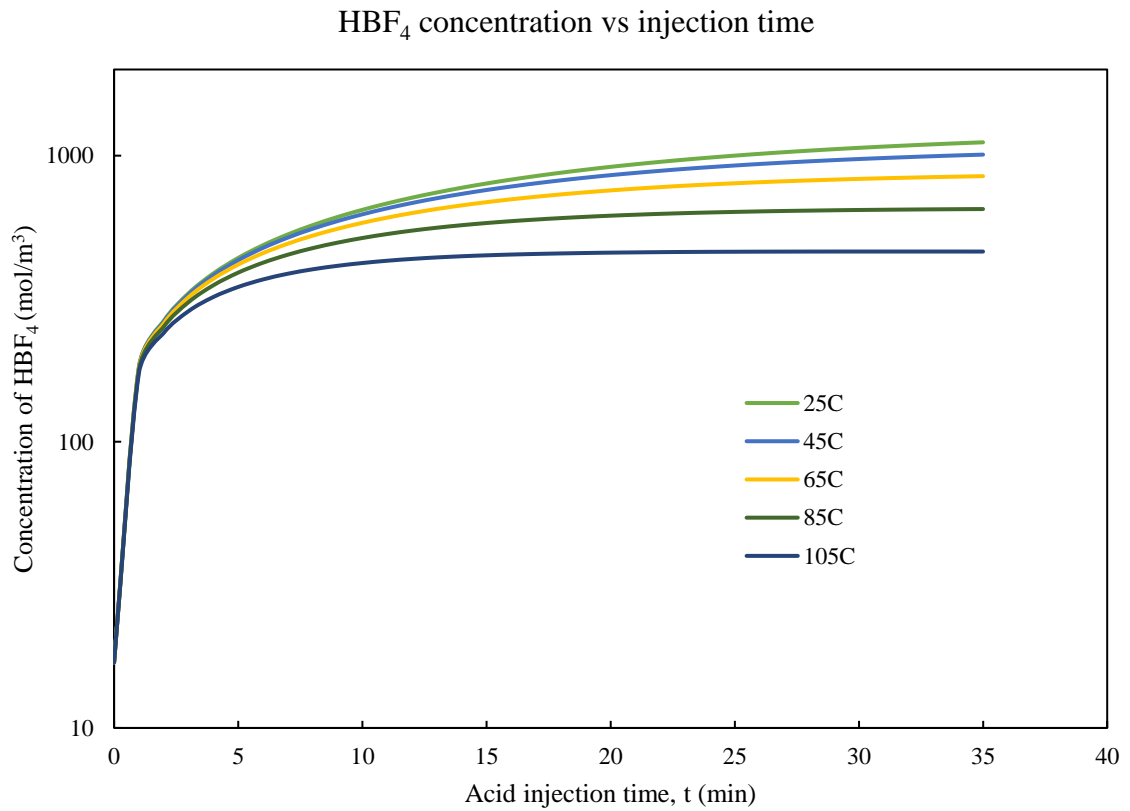


Figure 5.10 The effect of temperatures on HBF₄ concentration along acid injection time

Table 5.7 Effect of temperature on HF concentration

| Temperature, T ($^{\circ}\text{C}$) | Initial HF Concentration (mol/m^3) | Final HF Concentration (mol/m^3) |
|--|---|---|
| 25 | 5.01E-07 | 3.36E-05 |
| 45 | 1.04E-06 | 6.58E-05 |
| 65 | 2.11E-06 | 1.21E-04 |
| 85 | 4.16E-06 | 2.15E-04 |
| 105 | 8.09E-06 | 4.76E-04 |

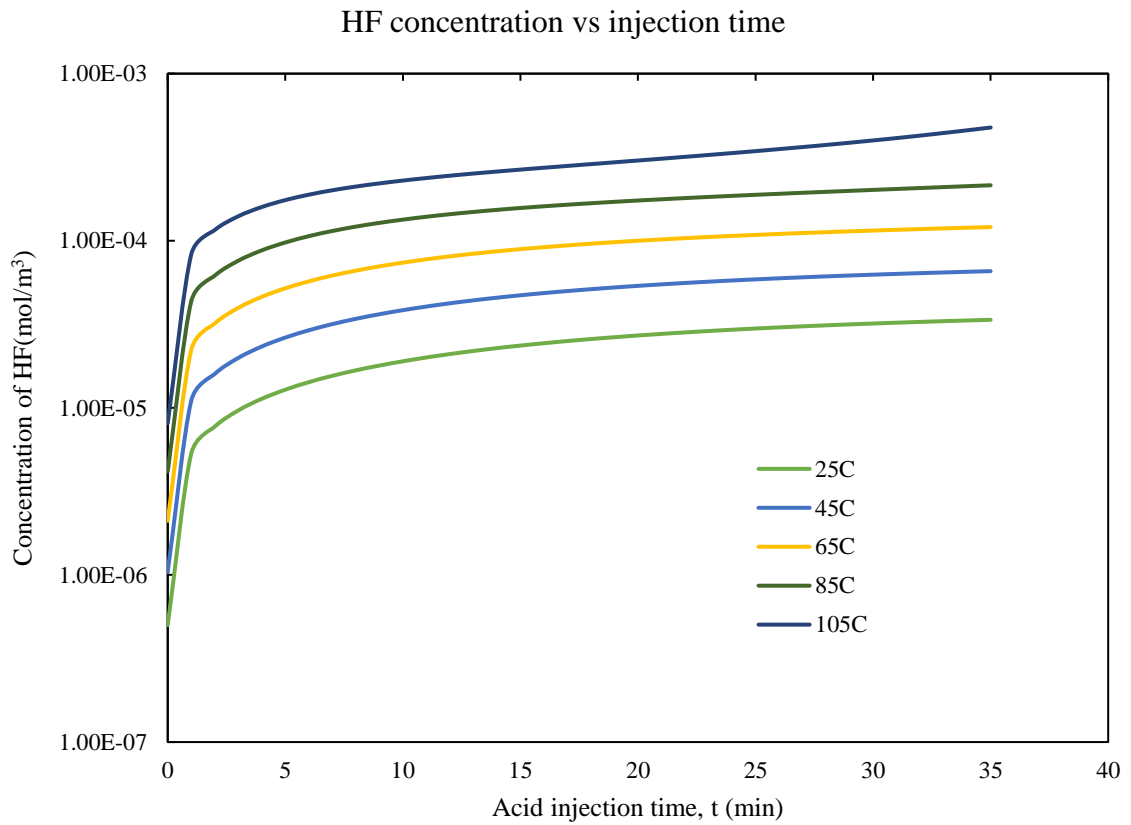


Figure 5.11 The effect of temperatures on HF concentration along acid injection time

Table 5.8 Effect of temperature on H_2SiF_6 concentration

| Temperature, T ($^{\circ}C$) | Initial H_2SiF_6 Concentration (mol/m^3) | Final H_2SiF_6 Concentration (mol/m^3) |
|-------------------------------------|---|---|
| 25 | 1.24E-06 | 9.49E-03 |
| 45 | 2.58E-06 | 1.86E-02 |
| 65 | 5.22E-06 | 3.41E-02 |
| 85 | 1.03E-05 | 6.06E-02 |
| 105 | 2.00E-05 | 1.33E-01 |

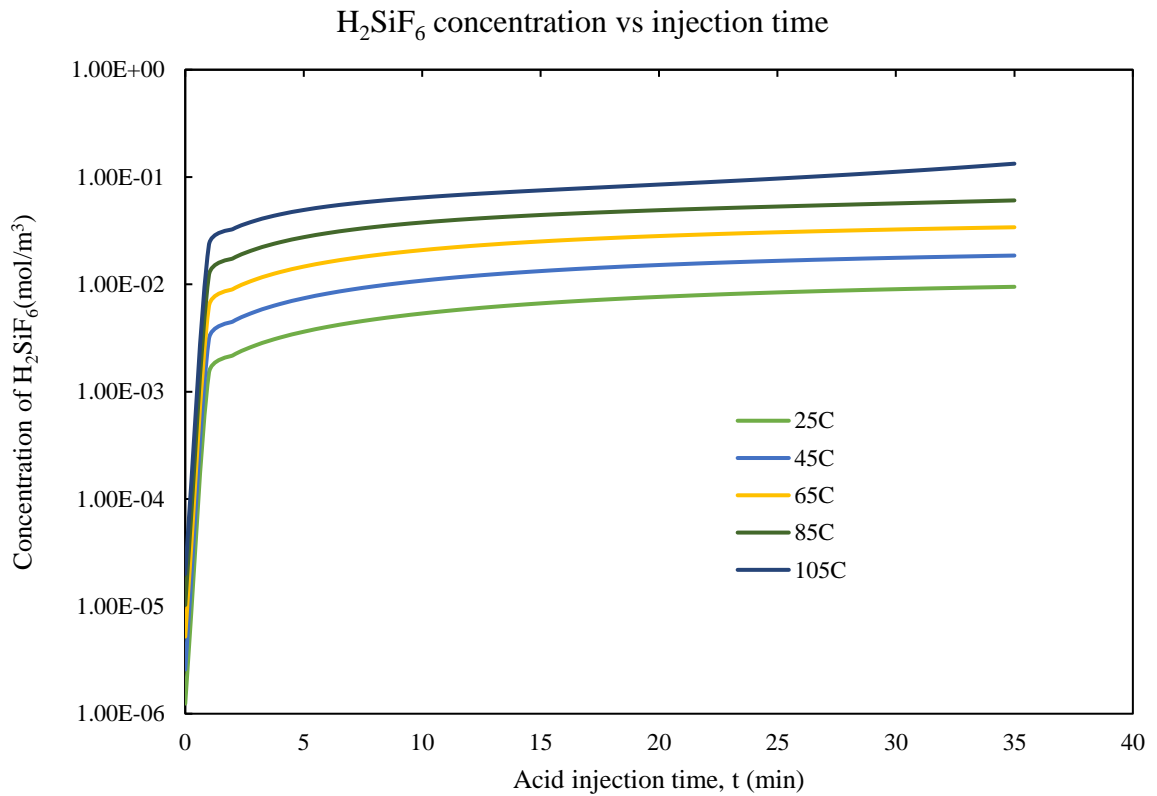


Figure 5.12 The effect of temperatures on H_2SiF_6 concentration along acid injection time

5.3.3 Minerals Volume Fraction Distribution

In this simulation, the acid spread gradually along the core sample. By the time 35 mins of acid injection, the simulation process stops converging and end the simulation. This is an indication that the effluent acid begins to be produced from the outlet face of the core at that point of time. For the homogeneous case, the time of acid breakthrough is 35 mins.

Apart from the mineral dissolution of the fast-reacting and slow-reacting minerals, there is also a zone of precipitation reaction, resulting the formation of the precipitated products, which is the silica gel, Si(OH)_4 . In present study, it is observed that the variation in the volume fraction of slow-reacting mineral is not significant at low temperature of 25 °C. There is only subtle change in quartz concentration contributed in the simulation. Hence, this is a clear indication that the chemical reaction the acid with the slow-reacting minerals is not helpful in porosity and permeability enhancement. The similar results were observed at increased temperature conditions of 45 °C to 105 °C. Thus, the results for slow-reacting mineral volume fraction is excluded and neglected in this section due to insignificance.

Figure 5.13 and 5.14 show the initial fast-reacting mineral and silica gel precipitate distribution in the sandstone core once the acid core flooding process started. From Figure 5.13, the fast-reacting mineral would begin to decrease as it is being consumed in the acid-rock chemical reaction. In the other hand, the silica gel precipitate would begin to increase as it is being produced in the acid-rock chemical reaction as demonstrated in Figure 5.14.

After 35 mins of HBF_4 acid injection, the distribution of both this minerals inside the core plug at 25 °C, 65 °C and 105 °C were depicted in Figure 5.15. According to the figure, it is observed that at 25 °C, the consumption rate of the fast-reacting mineral is not significant due to lower reactivity of the acid. At moderate temperature condition of 65 °C, the consumption rate of the fast-reacting mineral increases. When the temperature is very high at 105 °C, a drastic reduction in the composition of fast-reacting mineral is observed from the 3D numerical visualization results. This is because the acid reactivity is very high at such a high temperature formation environment. The similar trend is obtained for the rate of silica gel precipitation or generation during the sandstone core flooding process as clearly shown in the figure.

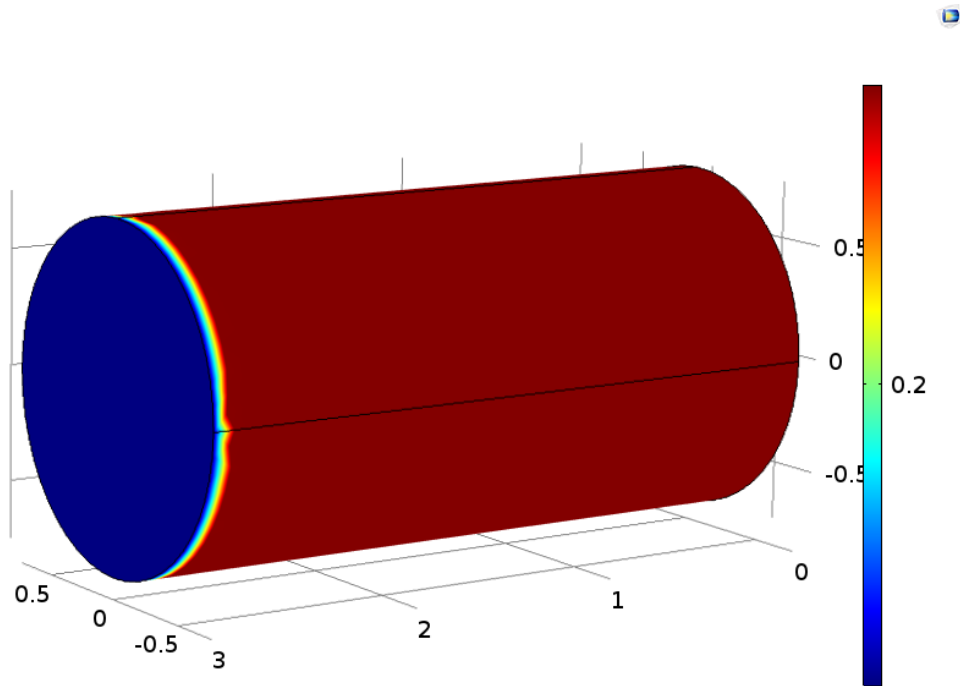


Figure 5.13 Initial fast-reacting mineral distribution at the beginning of acid injection

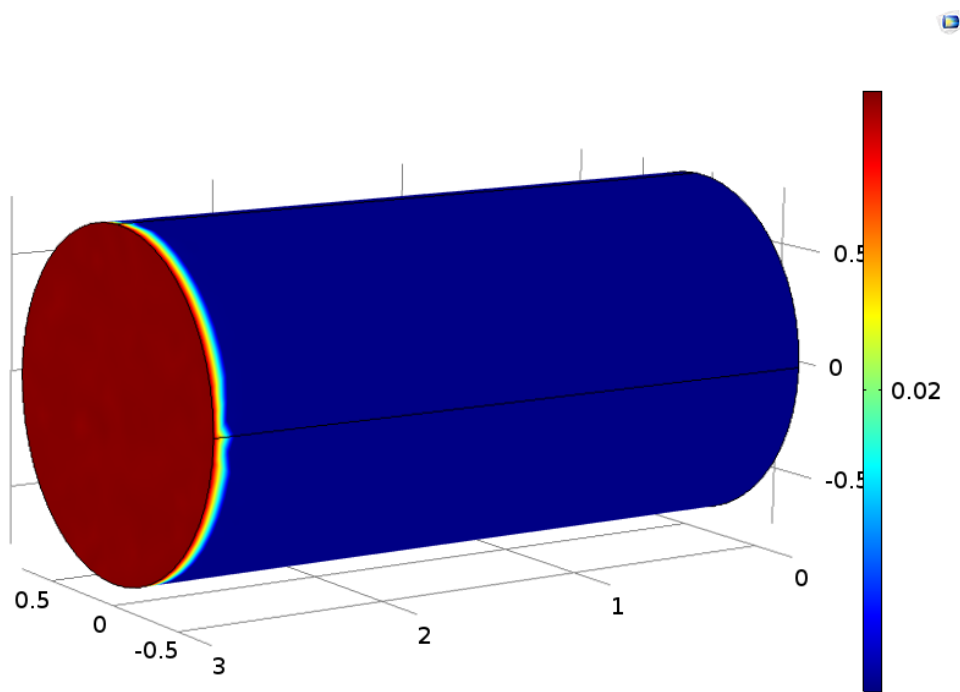


Figure 5.14 Initial silica gel precipitate distribution at the beginning of acid injection

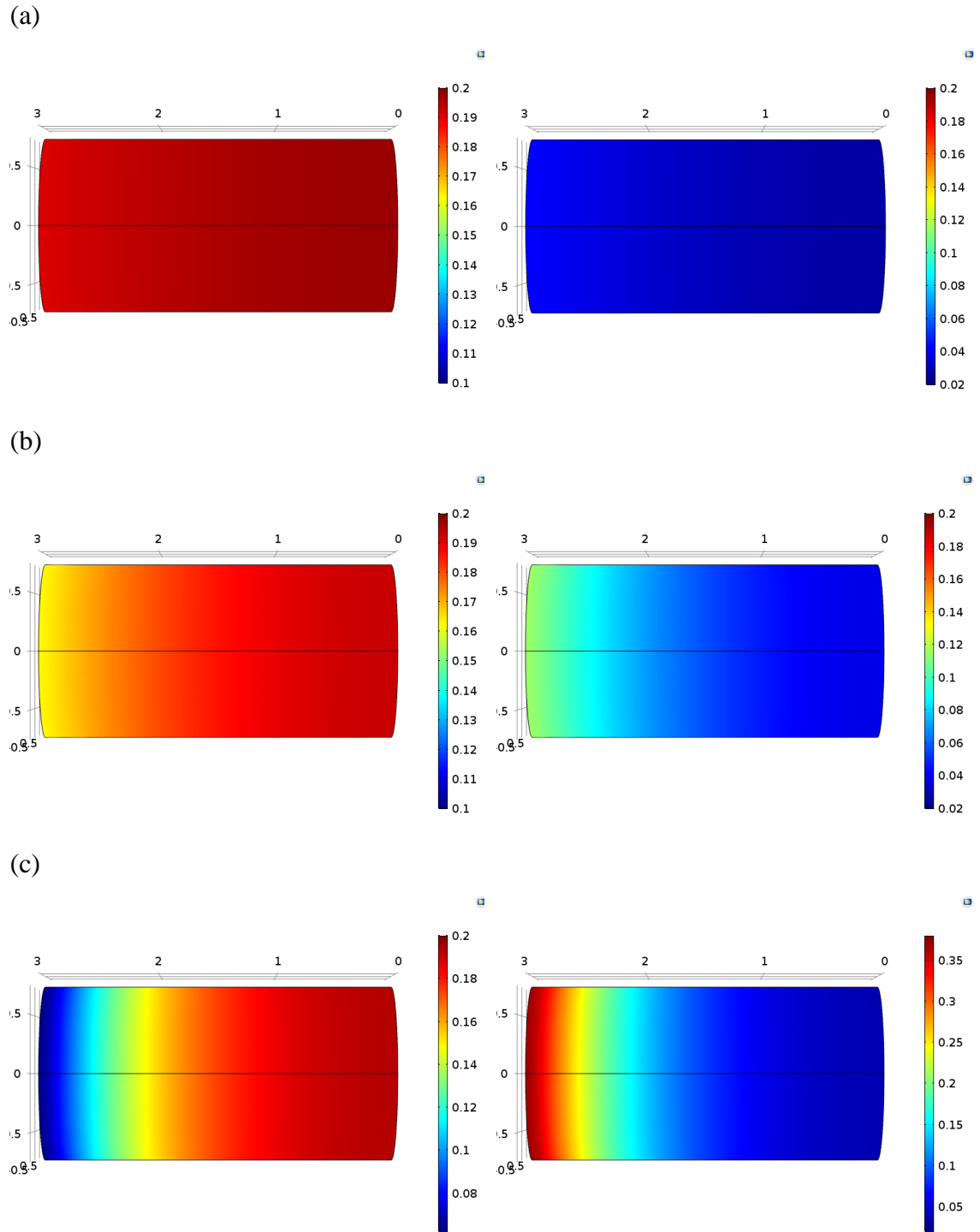


Figure 5.15 Fast-reacting mineral (left) and silica gel (right) distribution after 35 mins of fluoroboric acid injection at (a) 25 °C, (b) 65 °C and (c) 105 °C

In this simulation, the fast-reacting mineral would be consumed throughout the acid-rock chemical reactions whereas the silica gel would be produced from the reaction between H_2SiF_6 and fast-reacting mineral. At the same time, silica gel would also be consumed in its reaction with HF. Table 5.9 and 5.10 shows the results of the effect of temperature on fast-reacting mineral and silica gel respectively. The initial fast-reacting mineral volume fraction and silica gel volume fraction values are constant for various temperatures. These values are determined from the initial input to the simulation. Their respective response curves over acid injection time were also plotted graphically in Figure 5.16 and 5.17.

According to Figure 5.16, at 25 °C, the volume fraction of fast-reacting mineral slowly decreases upon consumption by both HF and H_2SiF_6 . A less steep trend is observed from the graph along the acid injection time. However, as the formation temperature increases, the volume fraction response curve indicated that the reduction in fast-reacting mineral volume fraction becomes faster and more drastically. This is due to the higher rapidity of the chemical reactions. The higher the temperature, the faster the chemical equilibrium to shift to the right hand side. Hence, this causes more fast-reacting mineral dissolution.

Referring to Figure 5.17, the precipitation of silica gel at 25 °C is not so much. Therefore, the increment of the silica gel volume fraction is not significant. Nevertheless, at higher temperatures, the volume fraction of silica gel would also be getting higher. The trend of the volume fraction response curve became steeper, with an increased slope. Theoretically, this is resulted from the higher acid-rock reactivity at higher temperature. Therefore, the equilibrium for the chemical reaction between H_2SiF_6 and fast-reacting mineral is shifting to the right hand side at a faster speed, forming more silica gel precipitate.

According to the overall increase in the silica gel precipitation, one could also understand that the chemical reaction between the H_2SiF_6 and fast-reacting mineral is more significant than the chemical reaction between HF and silica gel to produce H_2SiF_6 , which would otherwise result in an overall decrease curve in the silica gel volume fraction. In other word, the rate of silica gel production is more rapid than the rate of silica gel consumption during the acid core flooding stimulation process.

Table 5.9 Effect of temperature on fast-reacting mineral volume fraction

| Temperature, T (°C) | Initial Fast-reacting Mineral Volume Fraction | Final Fast-reacting Mineral Volume Fraction |
|--------------------------|--|--|
| 25 | 0.2 | 0.1952 |
| 45 | 0.2 | 0.1907 |
| 65 | 0.2 | 0.1833 |
| 85 | 0.2 | 0.1727 |
| 105 | 0.2 | 0.1592 |

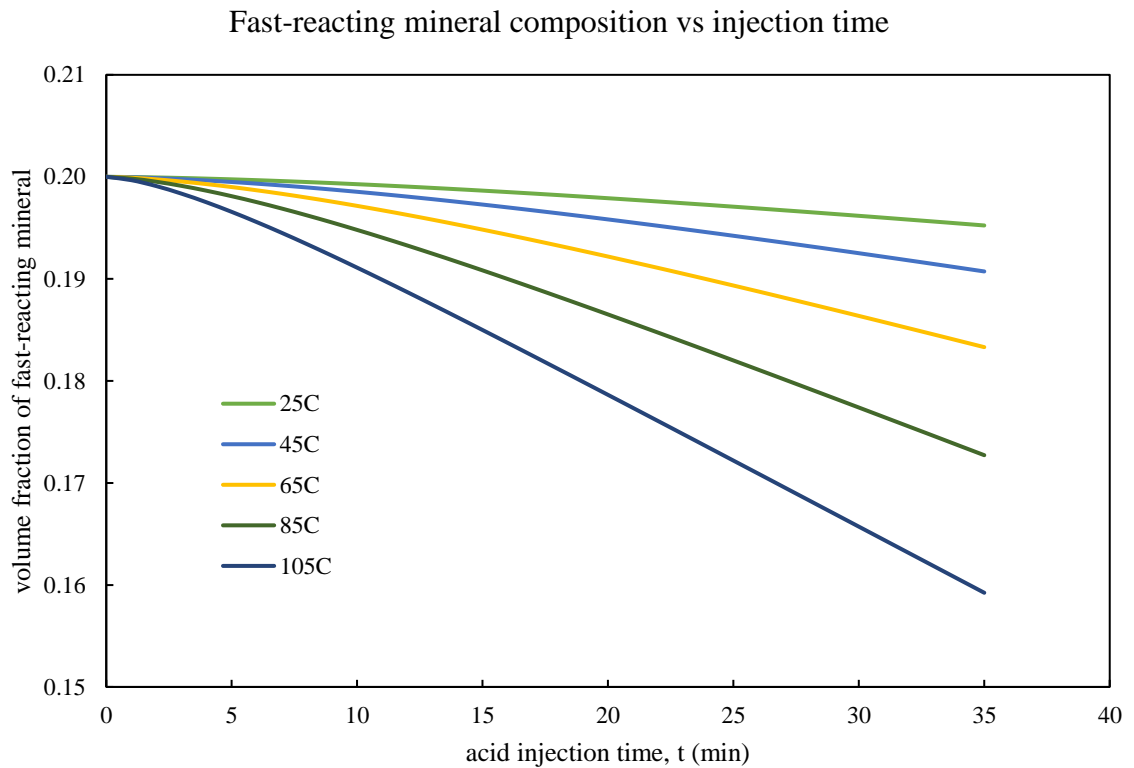


Figure 5.16 The effect of temperatures on fast-reacting mineral composition over injection time

Table 5.10 Effect of temperature on silica gel volume fraction

| Temperature, T ($^{\circ}\text{C}$) | Initial Silica Gel volume fraction | Final Silica Gel volume fraction |
|--|---------------------------------------|-------------------------------------|
| 25 | 0.02 | 0.0323 |
| 45 | 0.02 | 0.0440 |
| 65 | 0.02 | 0.0631 |
| 85 | 0.02 | 0.0905 |
| 105 | 0.02 | 0.1253 |

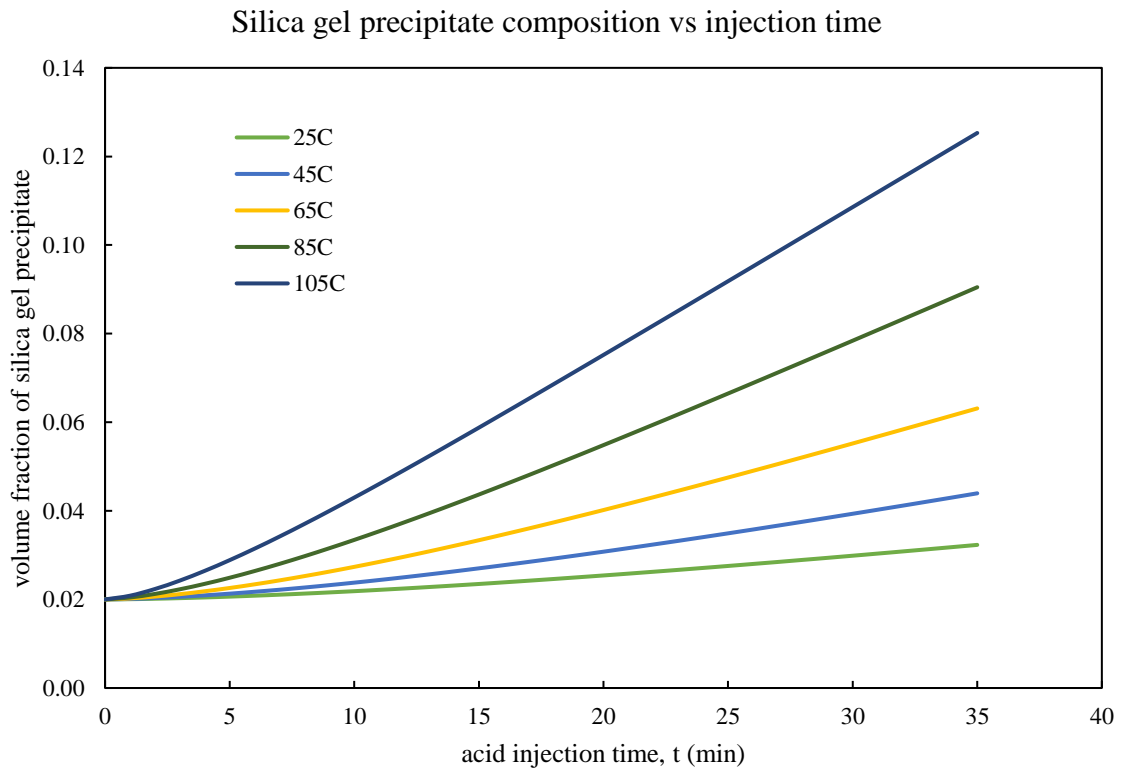


Figure 5.17 The effect of temperatures on silica gel precipitate composition over injection time

5.4 Effect of Acid Concentration at different Temperatures

5.4.1 Porosity and Permeability Enhancement Ratio

The acid concentration has a great impact on the porosity and permeability profile of sandstone acidizing. In conventional mud acid application in sandstone acidizing, it is proven that an increased HF concentration achieved more significant results of acid stimulation. This is due to a deeper depth of penetration by the acid with higher concentration (Kalfayan and Metcalf 2000).

In this simulation, the effect of HBF_4 acid concentration is studied. Table 5.11 and 5.12 showed the results of porosity and permeability increment due to increased acid concentration at low, moderate and high temperature condition. According to the simulation at 25 °C, the porosity enhancement ratio due to increased acid concentration increases from 1.01 to 1.07; and the permeability enhancement ratio increases from 1.03 to 1.23. However, at 105 °C, the porosity enhancement ratio due to increased acid concentration increases from 1.08 to 1.67; and the permeability enhancement ratio increases from 1.27 to 7.06.

Figure 5.18 to 5.20 represented the graph of porosity against the acid injection time at 25 °C, 65 °C and 105°C respectively. Meanwhile, figure 5.21 to 5.23 demonstrated the graph of permeability against the acid injection time at 25 °C, 65 °C and 105 °C respectively. Generally, the trend of all these plots showed a uniform and steady increment along the acid injection time during the acid stimulation process.

Based on the results of simulation, the porosity and permeability increase when the acid concentration increases at all temperature ranges. This is because when the acid concentration increases, the penetration of acid into the sandstone matrix also increases. Also, the higher the acid concentration, the higher the amount of sandstone minerals being dissolved by the acid. Even though more precipitation would occur at the same time, the

precipitates will be dissolved again by the acid. Therefore, a high HBF_4 acid concentration is favoured in sandstone acidizing.

Furthermore, this increment became more significant when the temperature increases. Therefore, a steeper trend is observed in figure 5.20 and 5.23 as compared to a relatively less steep trend in figure 5.18 and 5.21 respectively. This scenario is caused by the increase hydrolysis rate of HBF_4 at higher temperature. Therefore, the integrated effects of temperature and acid concentration is found to be very important as both the parameters would remarkably affect the acid stimulation results.

Porosity versus time of acid injection at different acid concentration (25 °C)

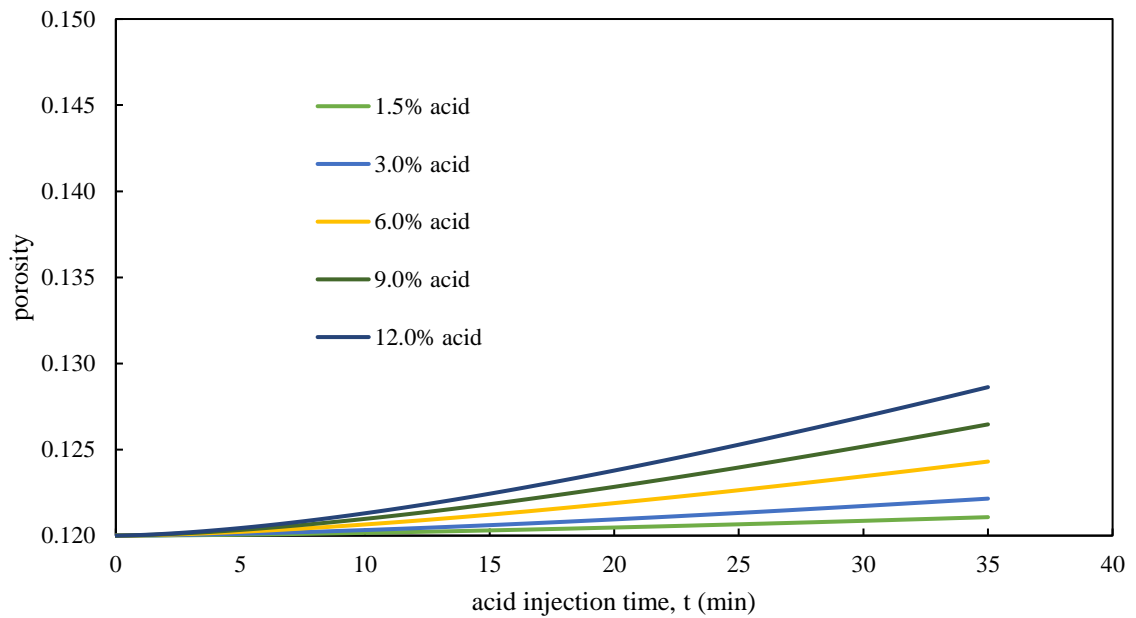


Figure 5.18 The effect of acid concentration on sandstone porosity after acidizing at 25 °C

Table 5.11 Effect of acid concentration on porosity enhancement ratio

| Temperature, T (°C) | Acid Concentration, c (%) | Initial Porosity, ϕ_0 | Final Porosity, ϕ_f | Porosity Enhancement Ratio, ϕ_f/ϕ_0 |
|--------------------------|-----------------------------------|-------------------------------|-----------------------------|---|
| 25 | 1.5 | 0.12 | 0.1211 | 1.01 |
| | 3.0 | 0.12 | 0.1221 | 1.02 |
| | 6.0 | 0.12 | 0.1243 | 1.04 |
| | 9.0 | 0.12 | 0.1265 | 1.05 |
| | 12.0 | 0.12 | 0.1286 | 1.07 |
| 65 | 1.5 | 0.12 | 0.1238 | 1.03 |
| | 3.0 | 0.12 | 0.1276 | 1.06 |
| | 6.0 | 0.12 | 0.1352 | 1.13 |
| | 9.0 | 0.12 | 0.1429 | 1.19 |
| | 12.0 | 0.12 | 0.1507 | 1.26 |
| 105 | 1.5 | 0.12 | 0.1294 | 1.08 |
| | 3.0 | 0.12 | 0.1389 | 1.16 |
| | 6.0 | 0.12 | 0.1585 | 1.32 |
| | 9.0 | 0.12 | 0.1790 | 1.49 |
| | 12.0 | 0.12 | 0.2004 | 1.67 |

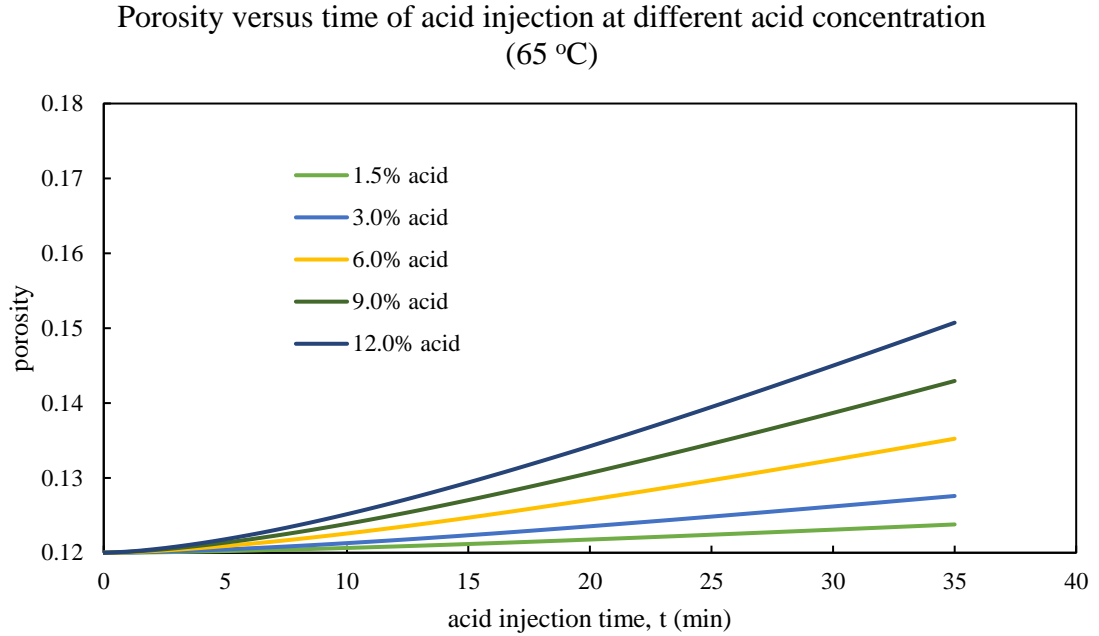


Figure 5.19 The effect of acid concentration on sandstone porosity after acidizing at 65 °C

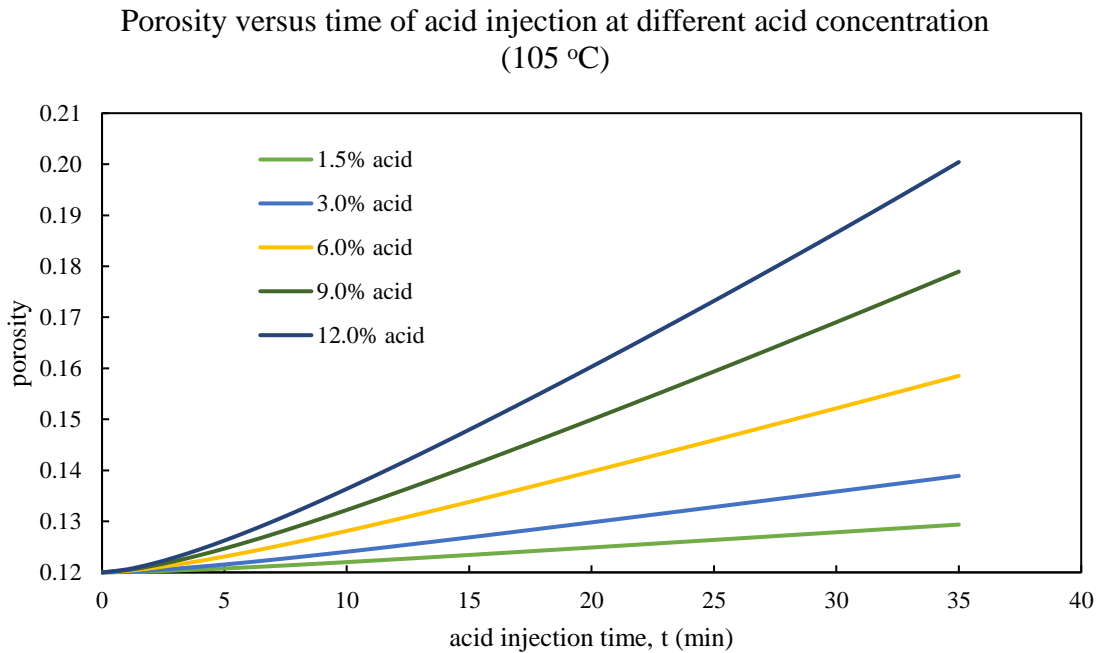


Figure 5.20 The effect of acid concentration on sandstone porosity after acidizing at 105 °C

Table 5.12 Effect of acid concentration on permeability enhancement ratio

| Temperature, T (°C) | Acid Concentration, c (%) | Initial Permeability, k_0 (m ²) ($\times 10^{-14}$) | Final Permeability, k_f (m ²) | Permeability Enhancement Ratio, k_f/k_0 |
|--------------------------|-----------------------------------|---|---|---|
| 25 | 1.5 | 3.95 | 4.05×10^{-14} | 1.03 |
| | 3.0 | 3.95 | 4.16×10^{-14} | 1.05 |
| | 6.0 | 3.95 | 4.39×10^{-14} | 1.11 |
| | 9.0 | 3.95 | 4.63×10^{-14} | 1.17 |
| | 12.0 | 3.95 | 4.87×10^{-14} | 1.23 |
| 65 | 1.5 | 3.95 | 4.34×10^{-14} | 1.10 |
| | 3.0 | 3.95 | 4.76×10^{-14} | 1.21 |
| | 6.0 | 3.95 | 5.71×10^{-14} | 1.45 |
| | 9.0 | 3.95 | 6.82×10^{-14} | 1.73 |
| | 12.0 | 3.95 | 8.12×10^{-14} | 2.06 |
| 105 | 1.5 | 3.95 | 5.01×10^{-14} | 1.27 |
| | 3.0 | 3.95 | 6.42×10^{-14} | 1.63 |
| | 6.0 | 3.95 | 1.06×10^{-13} | 2.68 |
| | 9.0 | 3.95 | 1.73×10^{-13} | 4.39 |
| | 12.0 | 3.95 | 2.79×10^{-13} | 7.06 |

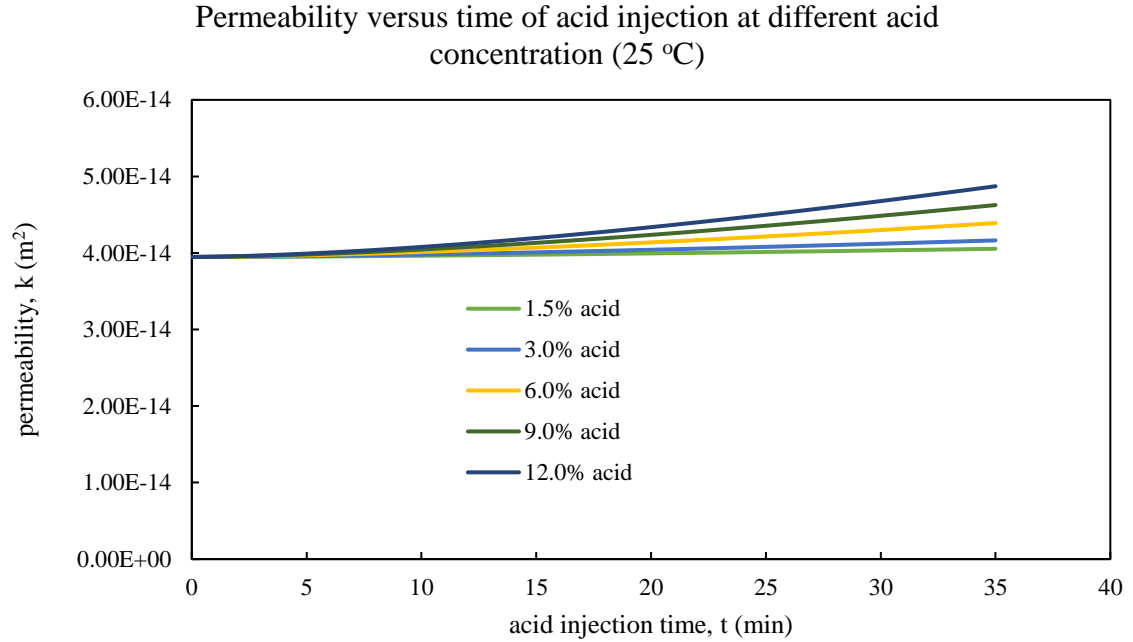


Figure 5.21 The effect of acid concentration on sandstone permeability after acidizing at 25 °C

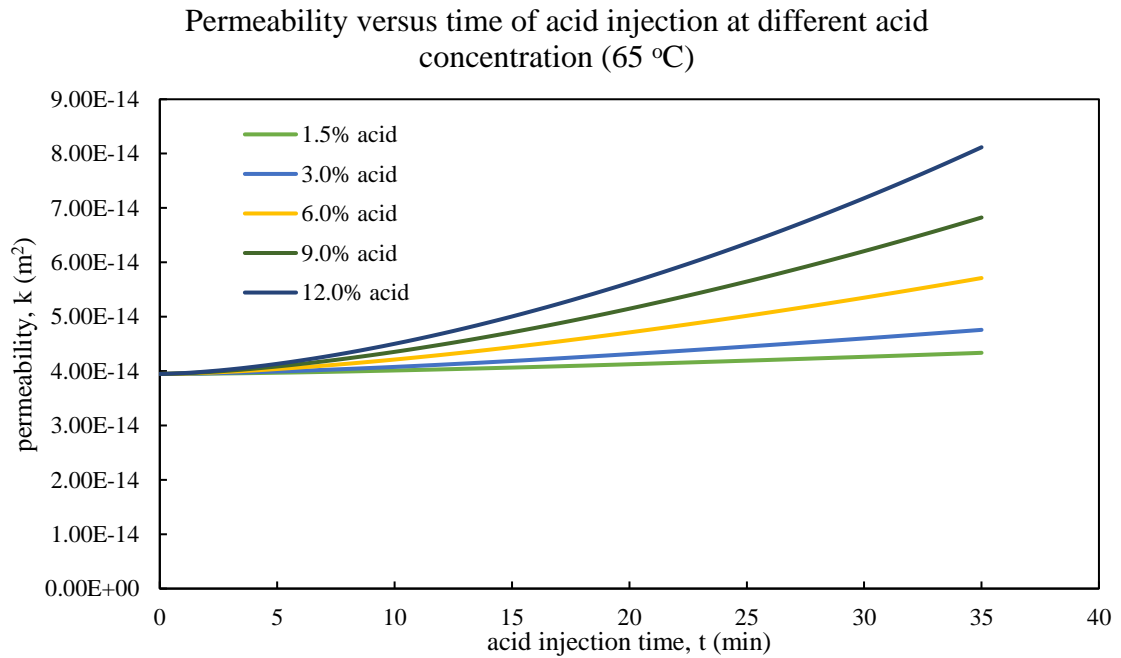


Figure 5.22 The effect of acid concentration on sandstone permeability after acidizing at 65 °C

Permeability versus time of acid injection at different acid concentration (105 °C)

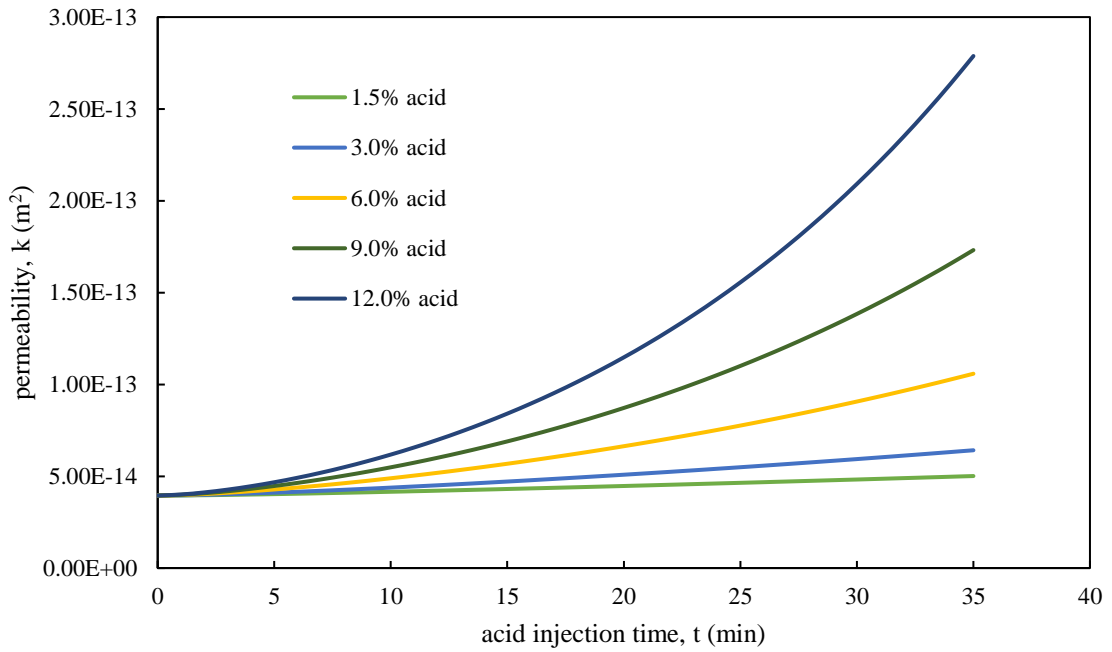


Figure 5.23 The effect of acid concentration on sandstone permeability after acidizing at 105 °C

5.4.2 Pressure Drop

Pressure drop is another indication of the sandstone acidizing performance. The initial pressure computed by the model is a function of the acid injection rate. Since the acid injection rate is kept constant in this sensitivity analysis, the initial pressure is found to be nearly the same. The pressure drop across the core sample during sandstone core flooding process is due to the increase in porosity and permeability in the core.

The result of pressure drop due to increased acid concentration at low, moderate and high temperature condition is showed in Table 5.13. Based on the simulation at 25 °C, the pressure drop due to increased acid concentration increases from 425.67 Pa to 3074.08 Pa. At 65 °C, the pressure drop is recorded from 1323.77 Pa to 7774.63 Pa when the acid concentration is varied. However, at 105 °C, the pressure drop due to increased acid

concentration increases from 2317.09 Pa to 10695.69 Pa. The graph of pressure against the acid injection time at 25, 65 and 105 °C respectively are represented in Figure 5.24 to 5.26. Overall, the trend of all these plots showed a gradual pressure reduction pattern along the acid injection time.

As indicated by the results of simulation, there is clearly a more rapid pressure drop response when the acid concentration increases at all temperature ranges. This is due to an increased rate of mineral dissolution when the acid concentration increases. More acid is being reacted with the sandstone minerals. Thus, the acid penetration becomes deeper as the strength of acid is higher.

Moreover, this pressure reduction is observed to become more remarkable when the temperature increases. This is indicated by a sharper pressure drop response as shown in figure 5.26 as compared to a relatively less sharp pressure reduction pattern in figure 5.24. This increment in pressure drop is due to the increased HBF_4 hydrolysis rate to produce HF at higher temperature. Hence, this further proves that the coupling effects of temperature and acid concentration is significant.

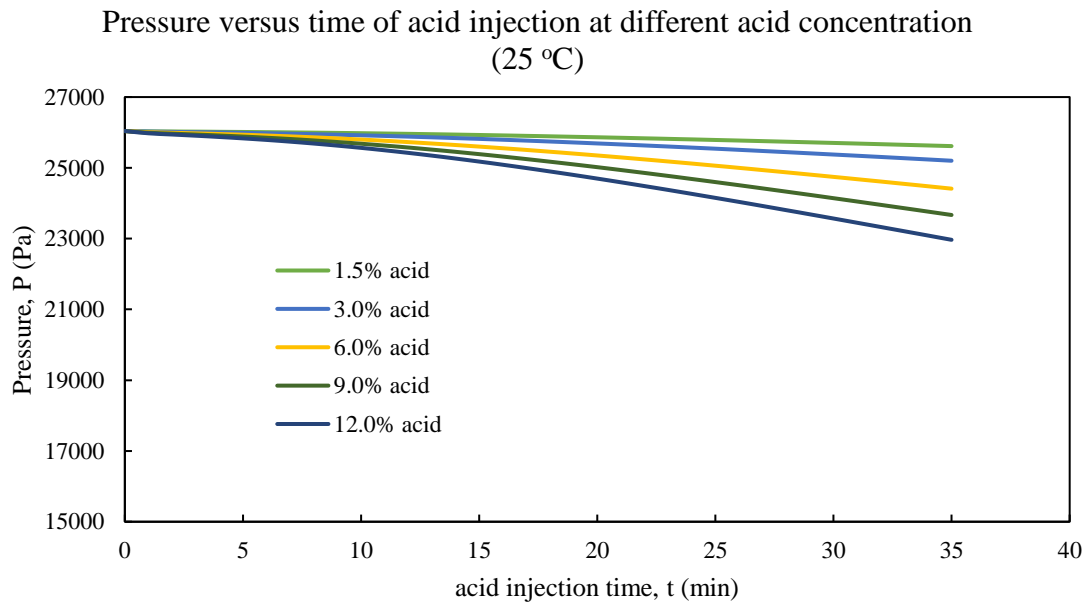


Figure 5.24 The effect of acid concentration on pressure drop after acidizing at 25 °C

Table 5.13 Effect of acid concentration on pressure drop

| Temperature, T ($^{\circ}\text{C}$) | Acid Concentration, c (%) | Initial Pressure, P_0 (Pa) | Final Pressure, P_f (Pa) | Pressure Drop, ΔP (Pa) |
|--|--------------------------------|------------------------------|----------------------------|--------------------------------|
| 25 | 1.5 | 26039.09 | 25613.42 | 425.67 |
| | 3.0 | 26039.18 | 25200.43 | 838.75 |
| | 6.0 | 26039.34 | 24411.30 | 1628.04 |
| | 9.0 | 26039.51 | 23667.38 | 2372.13 |
| | 12.0 | 26039.68 | 22965.61 | 3074.08 |
| 65 | 1.5 | 26039.36 | 24715.60 | 1323.77 |
| | 3.0 | 26039.72 | 23520.68 | 2519.03 |
| | 6.0 | 26040.43 | 21452.34 | 4588.09 |
| | 9.0 | 26040.14 | 19725.85 | 6315.28 |
| | 12.0 | 26041.85 | 18267.21 | 7774.63 |
| 105 | 1.5 | 26040.37 | 23723.28 | 2317.09 |
| | 3.0 | 26041.73 | 21886.41 | 4155.32 |
| | 6.0 | 26044.45 | 19088.72 | 6955.73 |
| | 9.0 | 26047.17 | 17004.72 | 9042.45 |
| | 12.0 | 26049.89 | 15354.20 | 10695.69 |

Pressure versus time of acid injection at different acid concentration
(65 °C)

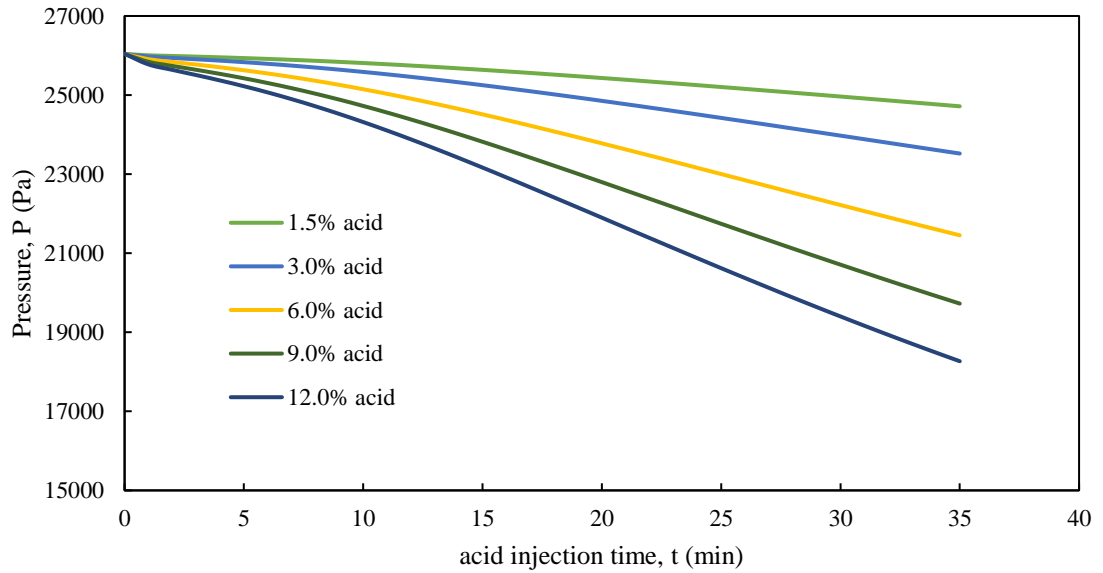


Figure 5.25 The effect of acid concentration on pressure drop after acidizing at 65 °C

Pressure versus time of acid injection at different acid concentration
(105 °C)

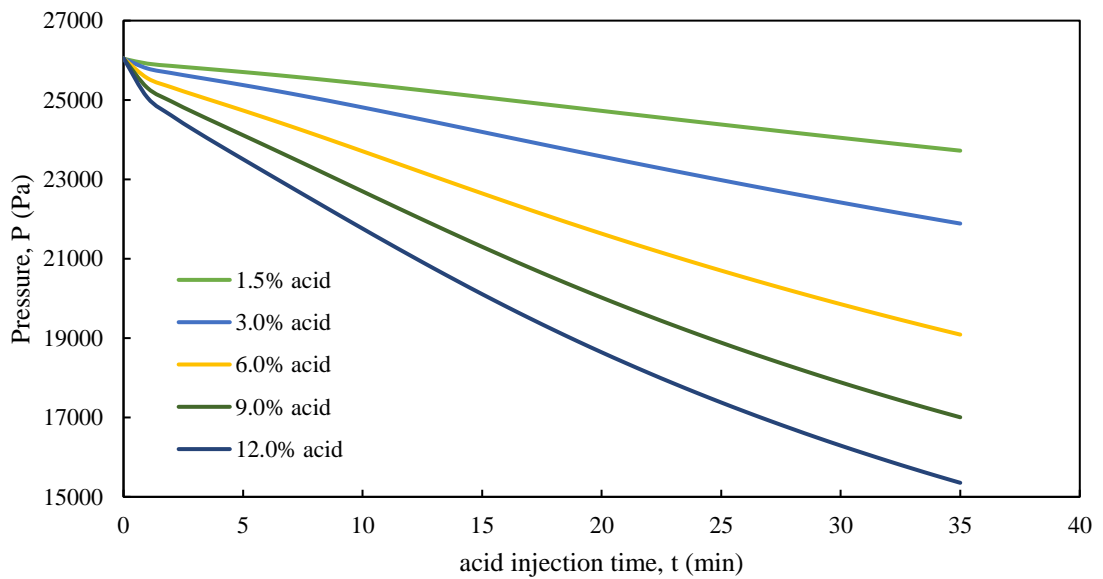


Figure 5.26 The effect of acid concentration on pressure drop after acidizing at 105 °C

5.5 Effect of Acid Injection Rate at different Temperatures

5.5.1 Porosity and Permeability Enhancement Ratio

As the acid is being injected into the sandstone matrix, the reaction between the acid and minerals is occurring. In this simulation, the effect of HBF_4 acid injection rate is analysed by obtaining the porosity and permeability profile of sandstone acidizing. Table 5.14 and 5.15 showed the results of porosity and permeability increment due to increased acid injection rate at low, moderate and high temperature condition. According to the simulation at 25 °C, the porosity enhancement ratio due to increased acid injection rate increases from 1.06 to 1.09; and the permeability enhancement ratio increases from 1.21 to 1.28. However, at 105 °C, the porosity enhancement ratio due to increased acid injection rate increases from 1.61 to 1.79; and the permeability enhancement ratio increases from 6.49 to 8.31.

Figure 5.27 to 5.29 showed the graph of porosity against the acid injection time at 25 °C, 65 °C and 105 °C respectively. Meanwhile, figure 5.30 to 5.32 showed the graph of permeability against the acid injection time at 25 °C, 65 °C and 105 °C respectively. Overall, the pattern of all these plots demonstrated a slow and steady increment along the acid injection time.

As indicated by the results of simulation, the porosity and permeability increase when the acid injection rate increases at all temperature ranges. This is because when the acid injection rate increases, the penetration rate of the acid into the sandstone matrix at a specific time also increases. This would increase the exposure sectors of the sandstone core to the acid, hence improving the acid stimulation process. Whereas while the acid injection rate is slow, a face dissolution would occur at the inlet face of the core, resulting in less acid penetration depth. At the same time, a slow acid injection rate would result in the creation of more precipitates. Thus, a high HBF_4 acid injection rate has a positive influence in sandstone acidizing.

In addition, this increment became more significant when the temperature increases. Therefore, a steeper trend is observed in figure 5.29 and 5.32 as compared to a relatively less steep trend in figure 5.27 and 5.30 respectively. This scenario is because an increased in temperature would enhance the hydrolysis rate of HBF_4 to produce HF. Therefore, the coupled effects of temperature and acid injection rate is clearly remarkable as both the parameters would affect the performance of acidizing.

Porosity versus time of acid injection at different acid injection rate
(25 °C)

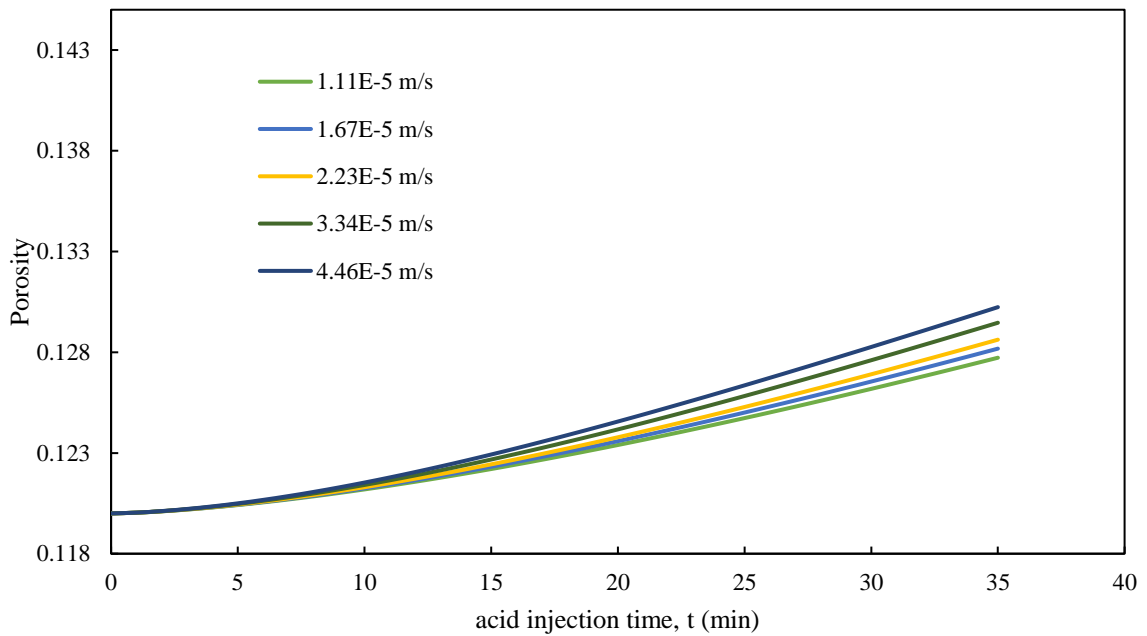


Figure 5.27 The effect of acid injection rate on sandstone porosity after acidizing at 25 °C

Table 5.14 Effect of acid injection rate on porosity enhancement ratio

| Temperature, T ($^{\circ}\text{C}$) | Acid Injection Rate, ν (m/s) ($\times 10^{-5}$) | Initial Porosity, ϕ_0 | Final Porosity, ϕ_f | Porosity Enhancement Ratio, ϕ_f / ϕ_0 |
|--|--|----------------------------|--------------------------|---|
| 25 | 1.11 | 0.12 | 0.1277 | 1.06 |
| | 1.67 | 0.12 | 0.1282 | 1.07 |
| | 2.23 | 0.12 | 0.1286 | 1.07 |
| | 3.34 | 0.12 | 0.1295 | 1.08 |
| | 4.46 | 0.12 | 0.1302 | 1.09 |
| 65 | 1.11 | 0.12 | 0.1476 | 1.23 |
| | 1.67 | 0.12 | 0.1492 | 1.24 |
| | 2.23 | 0.12 | 0.1507 | 1.26 |
| | 3.34 | 0.12 | 0.1538 | 1.28 |
| | 4.46 | 0.12 | 0.1567 | 1.31 |
| 105 | 1.11 | 0.12 | 0.1934 | 1.61 |
| | 1.67 | 0.12 | 0.1969 | 1.64 |
| | 2.23 | 0.12 | 0.2004 | 1.67 |
| | 3.34 | 0.12 | 0.2076 | 1.73 |
| | 4.46 | 0.12 | 0.2151 | 1.79 |

Porosity versus time of acid injection at different acid injection rate (65 °C)

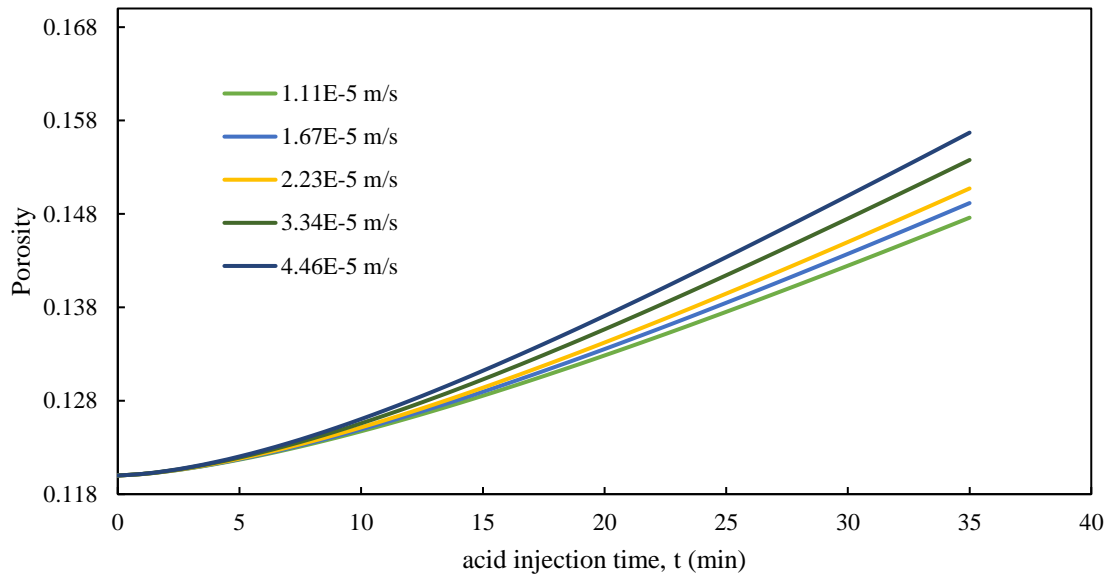


Figure 5.28 The effect of acid injection rate on sandstone porosity after acidizing at 65 °C

Porosity versus time of acid injection at different acid injection rate (105 °C)

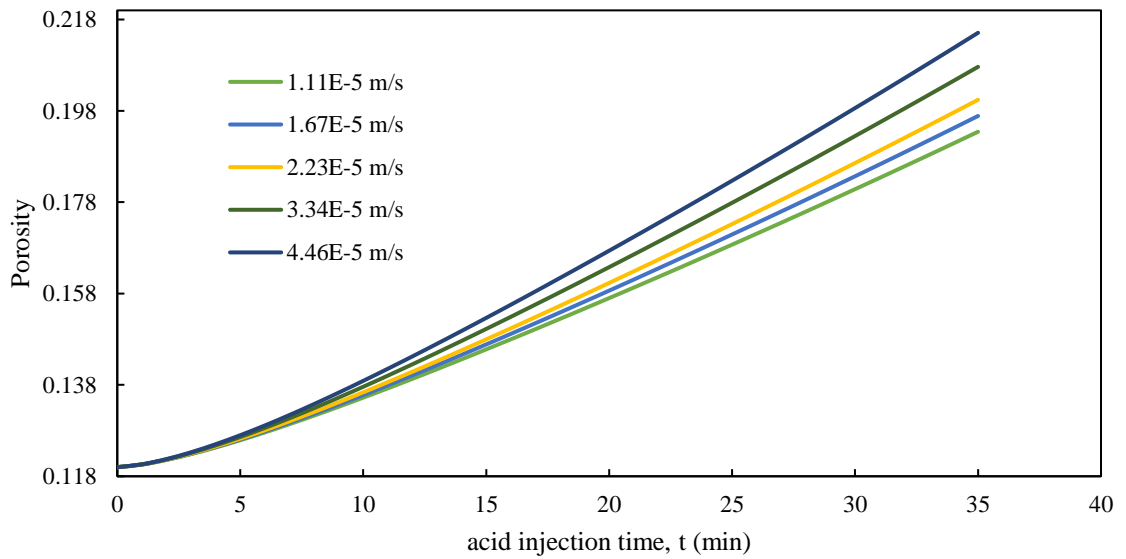


Figure 5.29 The effect of acid injection rate on sandstone porosity after acidizing at 105 °C

Table 5.15 Effect of acid injection rate on permeability enhancement ratio

| Temperature, T (°C) | Acid Injection Rate, v (m/s) ($\times 10^{-5}$) | Initial Permeability, k_0 (m^2) ($\times 10^{-14}$) | Final Permeability, k_f (m^2) | Permeability Enhancement Ratio, k_f/k_0 |
|--------------------------|---|---|---|---|
| 25 | 1.11 | 3.95 | 4.77×10^{-14} | 1.21 |
| | 1.67 | 3.95 | 4.82×10^{-14} | 1.22 |
| | 2.23 | 3.95 | 4.87×10^{-14} | 1.23 |
| | 3.34 | 3.95 | 4.97×10^{-14} | 1.26 |
| | 4.46 | 3.95 | 5.05×10^{-14} | 1.28 |
| 65 | 1.11 | 3.95 | 7.65×10^{-14} | 1.94 |
| | 1.67 | 3.95 | 7.88×10^{-14} | 2.00 |
| | 2.23 | 3.95 | 8.12×10^{-14} | 2.06 |
| | 3.34 | 3.95 | 8.58×10^{-14} | 2.17 |
| | 4.46 | 3.95 | 9.05×10^{-14} | 2.29 |
| 105 | 1.11 | 3.95 | 2.56×10^{-13} | 6.49 |
| | 1.67 | 3.95 | 2.67×10^{-13} | 6.77 |
| | 2.23 | 3.95 | 2.79×10^{-13} | 7.06 |
| | 3.34 | 3.95 | 3.03×10^{-13} | 7.67 |
| | 4.46 | 3.95 | 3.28×10^{-13} | 8.31 |

Permeability versus time of acid injection at different acid injection rate (25 °C)

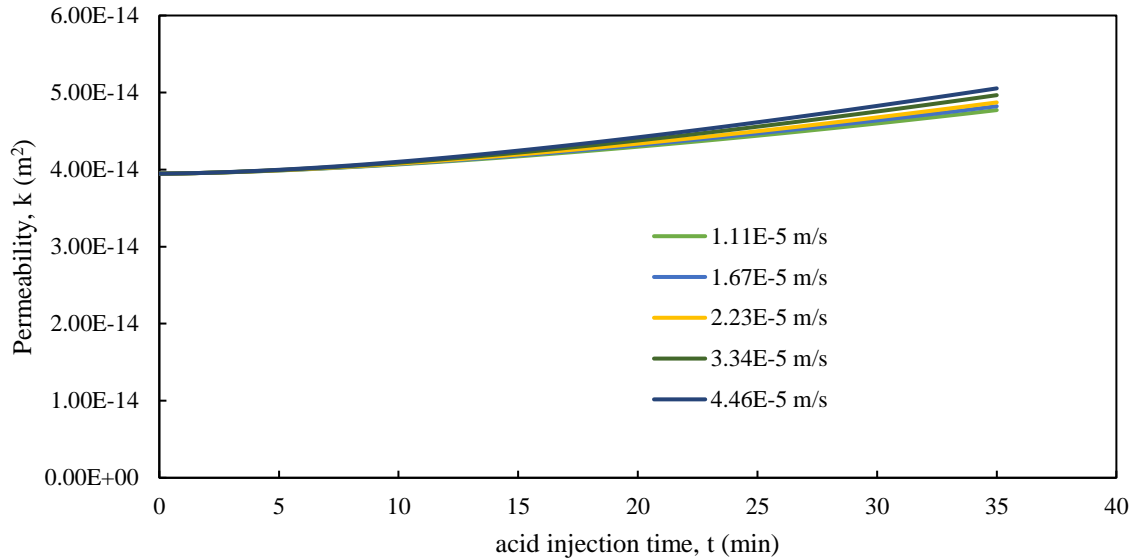


Figure 5.30 The effect of acid injection rate on sandstone permeability after acidizing at 25 °C

Permeability versus time of acid injection at different acid injection rate (65 °C)

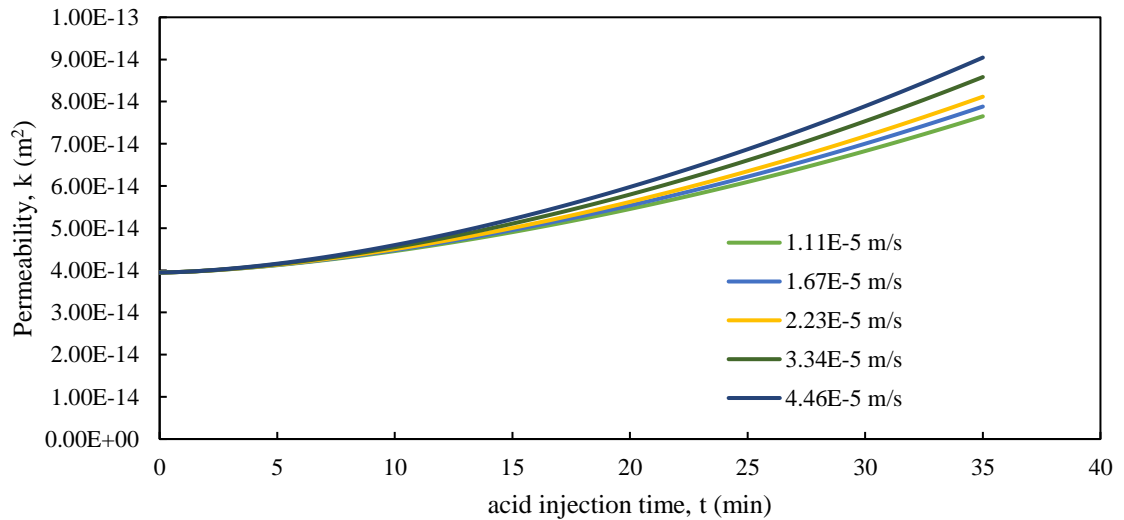


Figure 5.31 The effect of acid injection rate on sandstone permeability after acidizing at 65 °C

Permeability versus time of acid injection at different acid injection rate (105 °C)

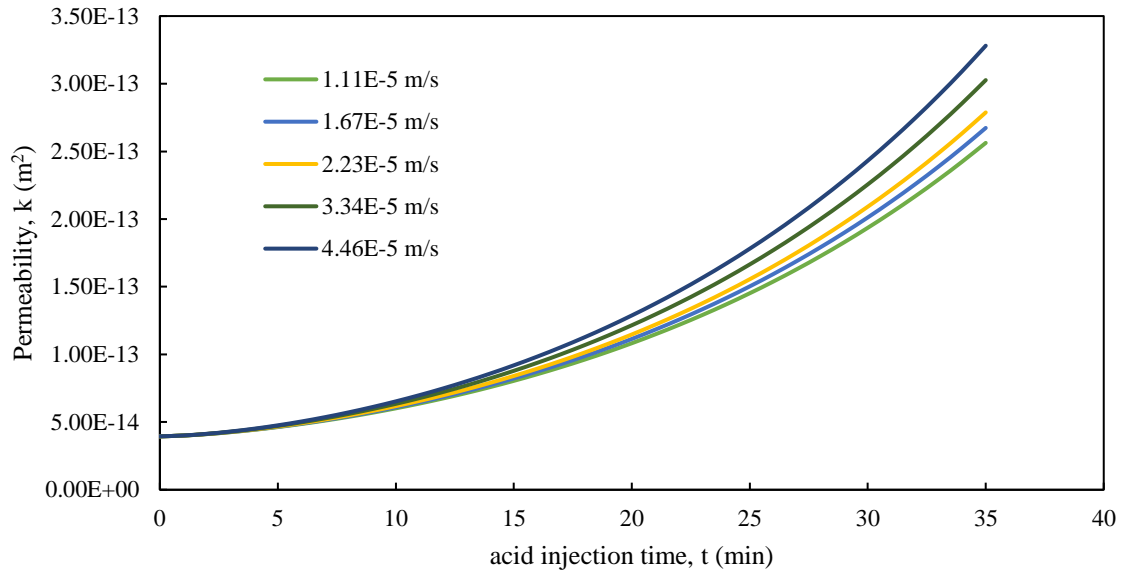


Figure 5.32 The effect of acid injection rate on sandstone permeability after acidizing at 105 °C

5.5.2 Pressure Drop

As mentioned earlier, the initial pressure calculated by the model is governed by the acid injection rate. So, since the acid injection rate is varied over a range of 1.11E-5 to 4.46E-5 m/s in this sensitivity analysis, the initial pressure is found to be different, unlike in the previous cases studying the effect of acid concentration. An increase in the porosity and permeability in the sandstone core sample would result in the pressure reduction across the core sample during acid flooding.

The result of pressure drop due to increased acid injection rate at low, moderate and high temperature condition is tabulated in Table 5.16. According to the simulation at 25 °C, the pressure drop due to increased acid injection rate increases from 1439.65 Pa to 7351.59 Pa. At 65 °C, the pressure drop is recorded from 3736.96 Pa to 18046.46 Pa when the acid injection rate is changed. However, at 105 °C, the pressure drop due to increased acid injection rate increases from 5564.08 Pa to 23828.49 Pa. The plot of pressure against the

acid injection time at 25 °C, 65 °C and 105 °C respectively are represented in Figure 5.33 to 5.35. Overall, the trend of all these plots showed a gradual pressure drop pattern along the acid injection time.

The simulation results showed that the pressure drop response increases when the acid injection rate increases at all temperatures. Initially at 25 °C, the pressure drop at each acid injection rate is not obvious. But at higher temperature of 105 °C, there is clearly a more significant and rapid pressure drop response particularly at higher acid injection rate. This is shown by a steeper pressure drop pattern in figure 5.35 as compared to a relatively less sharp pressure reduction pattern in figure 5.33. This increment in pressure drop is attributed to the increased HBF_4 hydrolysis rate at higher temperature, allowing more acid-mineral reaction. Hence, this indicated that the joint effects of temperature and acid injection rate is significant.

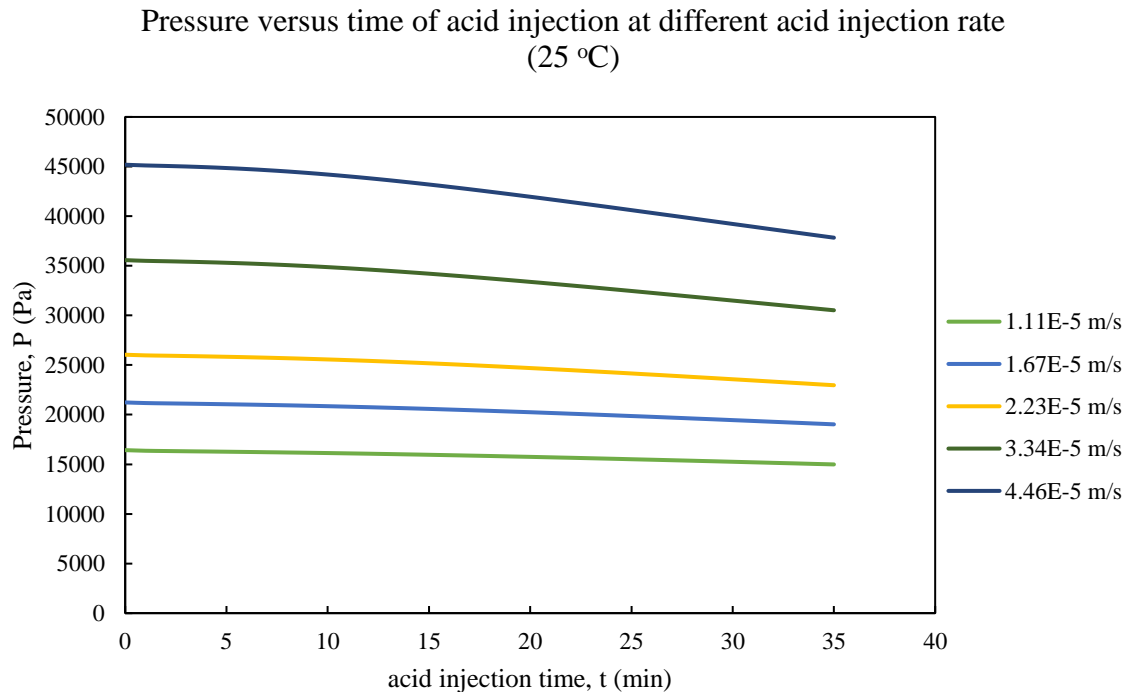


Figure 5.33 The effect of acid injection rate on pressure drop after acidizing at 25 °C

Table 5.16 Effect of acid injection rate on pressure drop

| Temperature, T (°C) | Acid Injection Rate, v (m/s) ($\times 10^{-5}$) | Initial Pressure, P_0 (Pa) | Final Pressure, P_f (Pa) | Pressure Drop, ΔP (Pa) |
|--------------------------|---|------------------------------------|----------------------------------|-----------------------------------|
| 25 | 1.11 | 16424.67 | 14985.01 | 1439.65 |
| | 1.67 | 21323.19 | 19023.24 | 2208.95 |
| | 2.23 | 26039.68 | 22965.61 | 3074.08 |
| | 3.34 | 35568.88 | 30517.08 | 5051.80 |
| | 4.46 | 45183.93 | 37832.34 | 7351.59 |
| 65 | 1.11 | 16426.94 | 12689.98 | 3736.96 |
| | 1.67 | 21234.46 | 15584.53 | 5649.92 |
| | 2.23 | 26041.85 | 18267.21 | 7774.63 |
| | 3.34 | 35571.05 | 23010.91 | 12560.13 |
| | 4.46 | 45186.09 | 27139.64 | 18046.46 |
| 105 | 1.11 | 16435.37 | 10871.30 | 5564.08 |
| | 1.67 | 21242.90 | 13243.23 | 7999.66 |
| | 2.23 | 26049.89 | 15354.20 | 10695.69 |
| | 3.34 | 35579.09 | 18797.06 | 16782.04 |
| | 4.46 | 45194.14 | 21365.65 | 23828.49 |

Pressure versus time of acid injection at different acid injection rate (65 °C)

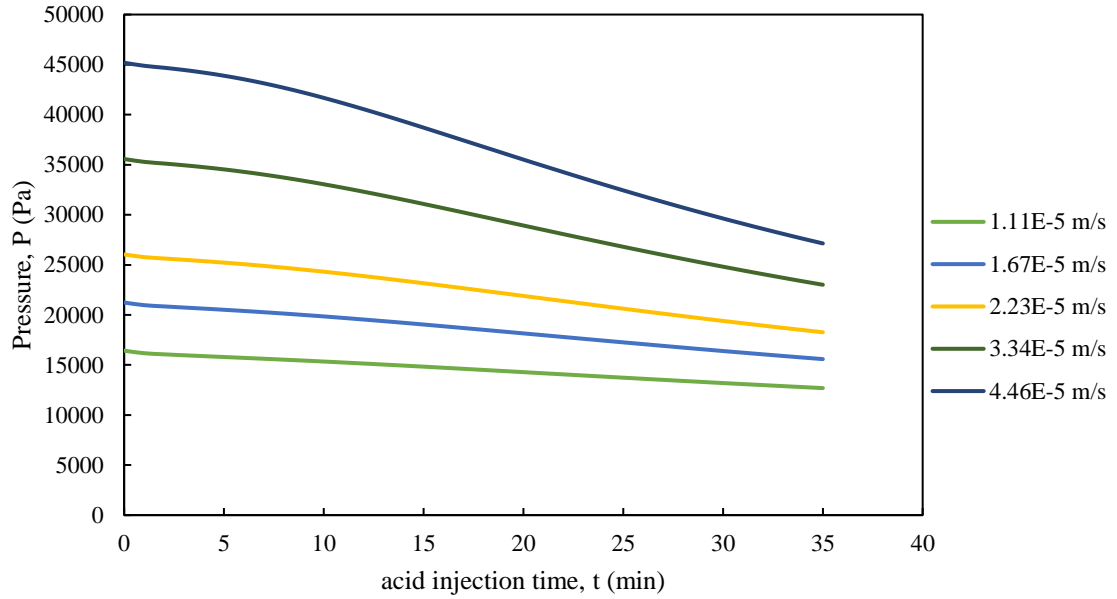


Figure 5.34 The effect of acid injection rate on pressure drop after acidizing at 65 °C

Pressure versus time of acid injection at different acid injection rate (105 °C)

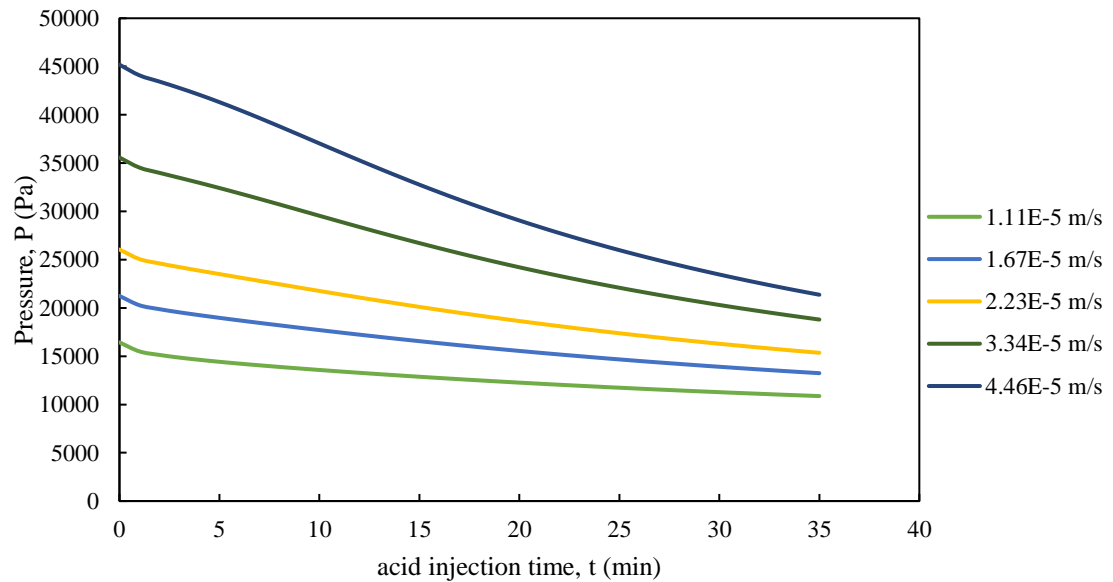


Figure 5.35 The effect of acid injection rate on pressure drop after acidizing at 105 °C

5.6 Summary of Chapter

The simulation results showed that porosity increases at low (25 °C), medium (65 °C) and high (105 °C) temperature conditions were 1.07, 1.26 and 1.67 times the initial value respectively; whereas the permeability increases at low, medium and high temperature conditions were 1.23, 2.06 and 7.06 times the initial value respectively. Overall, it is concluded that the efficiency and performance of HBF₄ acid in sandstone matrix stimulation became better at increased temperature. In general, the hydrolysis reaction of HBF₄ that had been included in this model became the governing model that controlled the acid performance at various temperatures.

Besides, the parametric study on acid concentration and acid injection rate implied that both these factors had a significant effect on the performance of sandstone acidizing. However, it is noticed that the effect of acid concentration is more remarkable than that of acid injection rate. Therefore, it is recommended that a more detailed optimization study to be performed on these three main factors that had significantly influenced sandstone acid stimulation results. The detail discussion on the optimization study will be shown in the next chapter. In a nutshell, the parametric study based on the mechanistic model presented in chapter 5 had completed research objective 4, which is to perform a sensitivity analysis on various factors affecting the sandstone acidizing efficiency.

Relevant publications that had been derived from chapter 5 are:

1. **Leong, V. H.**, Mahmud, H. B., Law, M. C., Foo, C. Y. H. and Tan, I. S. (2018). A sensitivity analysis and parametric study of factors affecting sandstone acidizing using numerical simulation. *Journal of Petroleum Exploration and Production Technology*. Springer Nature. (Under review)
2. **Leong, V. H.**, Mahmud, H. B., Law, M. C., Foo, C. Y. H. and Tan, I. S. (2018). A study on the effect of acid concentration at various temperatures on sandstone acidizing: a numerical simulation. *In Proceeding: One Curtin International Postgraduate Conference (OCPC) 2018*. Curtin University, Miri, Sarawak, Malaysia. 26th – 28th November 2018.

Chapter 6 Optimization Study using Response Surface Methodology (RSM)

6.1 Introduction

Since a modelling platform to study the HBF_4 acidizing process had already been provided in chapter 4, it is also very helpful to consider a further optimization work in this study. In this chapter, an optimization approach known as the response surface methodology (RSM) is being adopted in order to performance design optimization for sandstone acidizing process. A 3^3 full factorial simulation design had been proposed. In the present study, the input variables or the factors include the temperature, acid concentration and acid injection rate, whereas the output variables or the responses include the porosity enhancement ratio, permeability enhancement ratio and the pressure drop. This study aimed to evaluate the possible joint effects of formation temperature, acid concentration and acid injection rate on the porosity, permeability and pressure drop of the sandstone core subjected to simultaneous variation of these parameters. These factors had been proven to be significant in affecting the sandstone acidizing performance according to the preliminary parametric study conducted in chapter 5.

In this work, empirical equations had been derived from the models. The empirical approximation based on reaction kinetics and mechanisms are used to describe the relationship between the input and output variables that affects the performance of a sandstone acidizing process. However, it should be noted that the validity of an empirical model is only within the range of value set in this study. It is not to be used to predict and optimize the process beyond this particular range. Overall, the empirical models developed in this study could be utilized as an optimization tool for sandstone acidizing in the future. This study would also enhance the understanding of different chemical reactions and mechanisms that occur during sandstone acidizing process in a detailed perspective to produce an optimized process outcome.

6.2 Optimization Methodology for Process Analysis and Modelling

Apart of experimental investigation, process modelling is one of the most popular scientific approach to study and understand a concept, a chemical process and a physical behaviour of science and engineering field (Vishnudas and Chaudhuri 2017). Although the development of a model is often challenging, it is not deniable that various scientific models based on the kinetics, chemical reactions and mechanisms had enhanced and facilitated the understanding of sandstone acidizing process. There are two major classification of models, which are known as the mechanistic model and the empirical model.

Generally, the development of a mechanistic model depends of the solid understanding of a chemical and physical knowledge of a process (Leong et al. 2018b). Meanwhile, the construction of an empirical model is mainly derived from an observed profile of a mathematical equation or function. Empirical correlations are used to describe the relationship between the independent variables and the response of outcome. The independent variables are the input variables manipulated by a user whereas the output response represented the performance measure of a chemical process. It is also applied to predict, improve and also optimize the future trends of a process. In this study, response surface methodology (RSM) is adopted to study the relationships between various independent factors and the response variables. A quality characterization of a process could be obtained from RSM optimization approach.

6.2.1 Response Surface Methodology (RSM)

RSM is being introduced by Box and Wilson (1951) and is particularly popular in designing an experiment setting. It had gained wide application in the field of chemical engineering (Almashjary et al. 2018). This method is developed based upon the statistical analysis and fitting of models such as the linear, quadratic, cubic, polynomial and many other mathematical functions into the designed experimental results. In this study, the

Chapter 6 Optimization Study using Response Surface Methodology (RSM)

optimization of sandstone acidizing process using RSM is being divided into six different stages described in Figure 6.1.

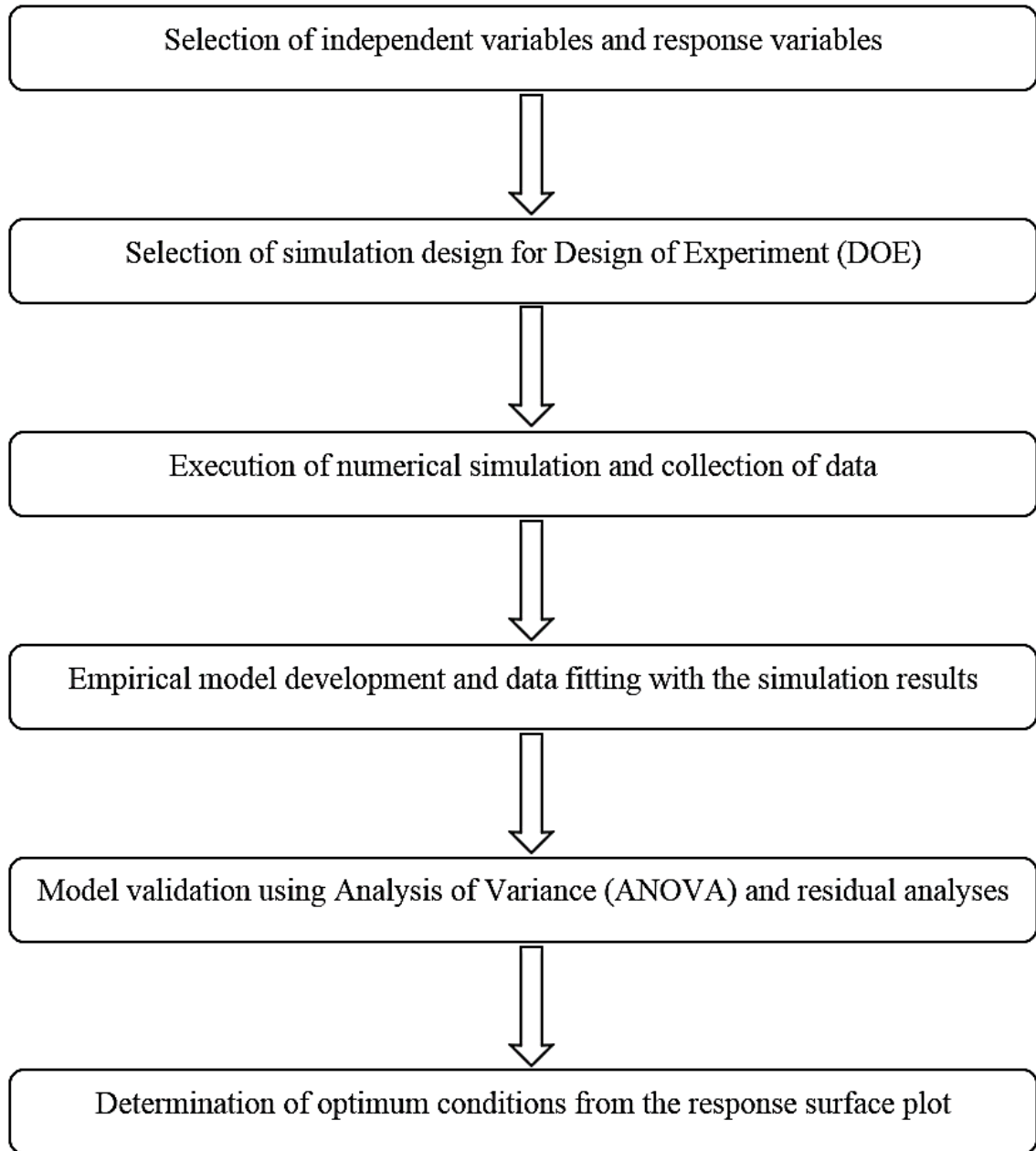


Figure 6.1 A flow chart for optimization process

Chapter 6 Optimization Study using Response Surface Methodology (RSM)

The performance sandstone acidizing process is significantly affected by the formation temperature, acid concentration and acid injection rate. Hence, these three parameters are selected as the independent variables in this optimization study. In order to measure the performance of sandstone acidizing, the porosity, permeability and pressure drop across the sandstone core after core flooding could be characterized. Thus, these three output parameters are selected as the response variables.

Table 6.1 tabulated a summary of factors used in this optimization study. Three different temperatures (25 °C, 65 °C and 105 °C), acid concentrations (1.5%, 6.75% and 12%) and acid injection rates (1.11E-5 m/s, 2.785E-5 m/s and 4.46E-6 m/s) were used in this study. Each of the three independent factors are input as a numerical variable with their corresponding units. RSM worked in such a way that the input values are being coded as +1 for high, 0 for moderate and -1 as low instead of the actual data.

Table 6.1 Summary of factors

| Factor | A | B | C |
|---------------|-------------|--------------------|---------------------|
| Name | Temperature | Acid Concentration | Acid Injection Rate |
| Units | °C | % | m/s |
| Type | Numeric | Numeric | Numeric |
| Minimum | 25.00 | 1.50 | 0.0000111 |
| Maximum | 105.00 | 12.00 | 0.0000446 |
| Coded Low | -1 ↔ 25.00 | -1 ↔ 1.50 | -1 ↔ 0.0000111 |
| Coded High | +1 ↔ 105.00 | +1 ↔ 12.00 | +1 ↔ 0.0000446 |
| Mean | 65.00 | 6.75 | 0.00002785 |
| Std. Dev. | 30.48 | 4.00 | 0.00001276 |

There are some options for the selection of response surface design such as the Central Composite Design (CCD), Box-Behnken Design, Optimal (Custom) Design and 3 Level Factorial Design. The difference between these designs are the points in 3 dimensions considered in the design and the number of simulations required. Table 6.2 presented a

Chapter 6 Optimization Study using Response Surface Methodology (RSM)

summary of build information for the optimization approach. The Design Expert version 11 software was used to perform the design optimization and the file version is 11.0.3.0. A full 3^3 factorial design as shown in Figure 6.2 was adopted to design the simulation experiment and the results obtained were optimized using response surface methodology. In this study, the x_1 , x_2 and x_3 in figure 6.2 represented the variables of formation temperature, acid concentration and acid injection rate respectively. A number of 32 simulation runs had been designed and the design model selected is quadratic model.

Table 6.2 Summary of build information

| | | | |
|---------------------|-------------------|----------------|------------|
| File Version | 11.0.3.0 | | |
| Study Type | Response Surface | Subtype | Randomized |
| Design Type | 3 Level Factorial | Runs | 32 |
| Design Model | Quadratic | Blocks | No Blocks |

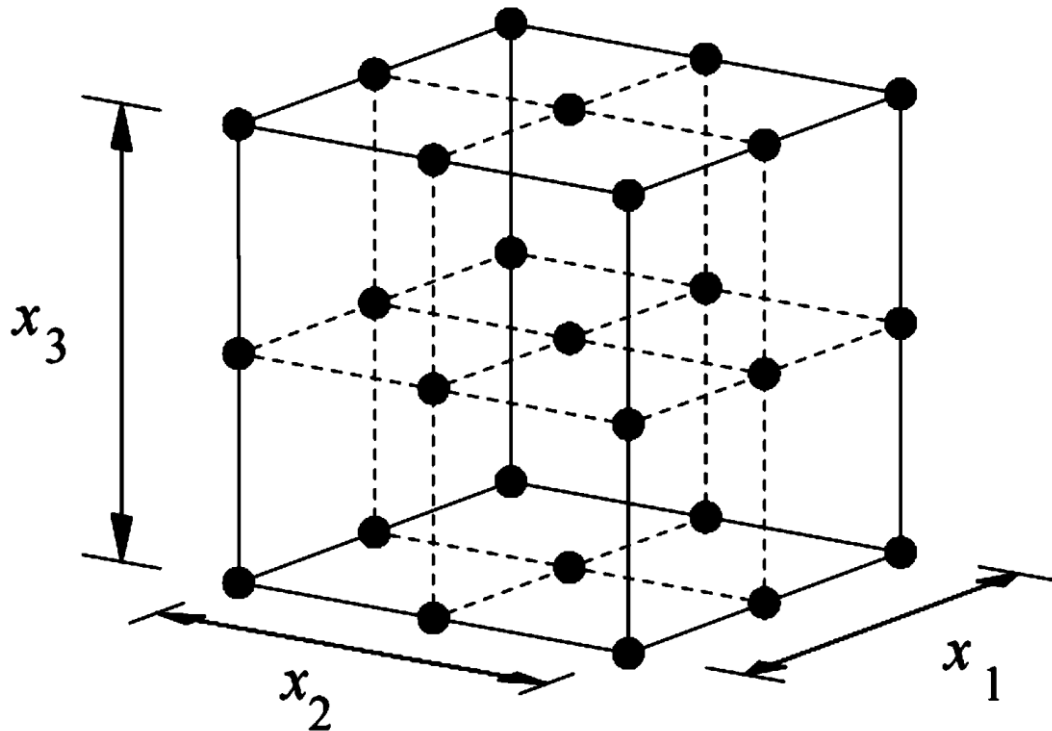


Figure 6.2 A 3^3 full factorial design of experiment

Chapter 6 Optimization Study using Response Surface Methodology (RSM)

The relationship between different independent variables can be expressed in Equation (6.1).

$$Y = f(x_1, x_2, x_3) + \varepsilon \quad (6.1)$$

Where Y is the predicted response, f is the function of the true response variable which is usually a first or second order polynomial function, x_1 , x_2 and x_3 are the three independent variables, and ε is the statistical error term, also known as the noise.

Through a linear regression analysis, a suitable empirical prediction of the function for the response variables will be suggested. Usually, a lower order of polynomial is suggested to be used for the independent variables with narrower range for simplicity purpose. If the response map is showing only a small or slight curvature, a first-order polynomial is recommended.

A first order model considering several independent variables are shown in Equation (6.2).

$$Y = \beta_0 + \beta_1 x_1 + \beta_2 x_2 + \beta_3 x_3 + \varepsilon \quad (6.2)$$

Where β_0 is the constant coefficient, and β_1 , β_2 and β_3 are the linear coefficients.

Equation (6.3) is formed by adding the interaction terms into Equation (6.2).

$$Y = \beta_0 + \beta_1 x_1 + \beta_2 x_2 + \beta_3 x_3 + \beta_{11} x_1^2 + \beta_{22} x_2^2 + \beta_{33} x_3^2 + \beta_{12} x_1 x_2 + \beta_{13} x_1 x_3 + \beta_{23} x_2 x_3 + \varepsilon \quad (6.3)$$

Where β_{11} , β_{22} and β_{33} are the quadratic coefficients, and β_{12} , β_{13} and β_{23} are the interaction coefficients.

In generalized form, a first order model having interaction terms are defined as Equation (6.4)

$$Y = \beta_0 + \sum_{i=1}^k \beta_i x_i + \sum_{i=1}^k \sum_{j>1}^k \beta_{ij} x_i x_j + \varepsilon \quad (6.4)$$

Chapter 6 Optimization Study using Response Surface Methodology (RSM)

Where β_i is the linear coefficient, β_{ij} is the interaction coefficient, x_i and x_j are the independent variables, and k is the number of factors ($k=3$ in this case).

However, a second order polynomial regression analysis is applied in present RSM study. It could be represented in Equation (6.5).

$$Y = \beta_0 + \sum_{i=1}^k \beta_i x_i + \sum_{i=1}^k \beta_{ii} x_i^2 + \sum_{i=1}^k \sum_{j>1}^k \beta_{ij} x_i x_j + \varepsilon \quad (6.5)$$

Where β_{ii} is the quadratic coefficient of the model.

6.2.2 Design of Experiment (DOE)

Design of Experiment (DOE) is one of the fundamental techniques in engineering applications to enhance the efficiency of a chemical process or system. DOE is being adopted to vary all the important parameters simultaneously into a set of experiments. The results obtained are then being used to develop an empirical model for interpretation, prediction and optimization purposes. DOE considered only the most simplified combinations of all the significant variables just sufficient for process optimization, hence saving experimental cost and operational time.

In present work, the simulation results from the porosity enhancement ratio, permeability enhancement ratio and pressure drop at different conditions were obtained and input into the Design Expert software for analysis. Several steps are taken to select the most suitable response model to fit the data. The significant terms and their interactions are determined while the insignificant terms are eliminated from the model. This would ensure that the model selected are accurate to predict all the responses. Table 6.3 showed the simulation design layout as determined by the design of experiment (DOE) software. There are a total number of 32 simulation runs required in the design and all of which are being simulated in COMSOL Multiphysics software of computational fluid dynamics (CFD).

Table 6.3 Simulation design layout

| Run | Factor 1 | Factor 2 | Factor 3 |
|-----|----------------|-----------------------|--------------------------|
| | A: Temperature | B: Acid Concentration | C: Acid Injection Rate |
| | °C | % | ($\times 10^{-5}$) m/s |
| 1 | 25 | 1.5 | 1.11 |
| 2 | 25 | 1.5 | 2.785 |
| 3 | 25 | 1.5 | 4.46 |
| 4 | 25 | 6.75 | 1.11 |
| 5 | 25 | 6.75 | 2.785 |
| 6 | 25 | 6.75 | 4.46 |
| 7 | 25 | 12 | 1.11 |
| 8 | 25 | 12 | 2.785 |
| 9 | 25 | 12 | 4.46 |
| 10 | 65 | 1.5 | 1.11 |
| 11 | 65 | 1.5 | 2.785 |
| 12 | 65 | 1.5 | 4.46 |
| 13 | 65 | 6.75 | 1.11 |
| 14 | 65 | 6.75 | 2.785 |
| 15 | 65 | 6.75 | 2.785 |
| 16 | 65 | 6.75 | 2.785 |
| 17 | 65 | 6.75 | 2.785 |
| 18 | 65 | 6.75 | 2.785 |
| 19 | 65 | 6.75 | 2.785 |
| 20 | 65 | 6.75 | 4.46 |
| 21 | 65 | 12 | 1.11 |
| 22 | 65 | 12 | 2.785 |
| 23 | 65 | 12 | 4.46 |
| 24 | 105 | 1.5 | 1.11 |
| 25 | 105 | 1.5 | 2.785 |
| 26 | 105 | 1.5 | 4.46 |

| | | | |
|----|-----|------|-------|
| 27 | 105 | 6.75 | 1.11 |
| 28 | 105 | 6.75 | 2.785 |
| 29 | 105 | 6.75 | 4.46 |
| 30 | 105 | 12 | 1.11 |
| 31 | 105 | 12 | 2.785 |
| 32 | 105 | 12 | 4.46 |

6.2.3 Empirical Modelling and Determination of Optimal Conditions

The data obtained from the numerical simulation is used to develop three empirical models. The relationships showing the effects of the integrated factors including the temperature, acid concentration and injection rate on the porosity enhancement ratio, permeability enhancement ratio and pressure drop respectively are defined. Analysis of Variance (ANOVA) is then performed to evaluate the model F-value, p-value and other statistical data to verify the validity of the empirical models developed. Meanwhile, several residual analyses such as the normal plot, predicted vs. actual plot, residual vs. predicted plot, leverage plot and Box-cox plot are all conducted to further ensure the reliability of the data predicted using the model. Finally, the optimum conditions could be determined from the response surface plot, which included the 2D contour map and the 3D surface plot.

6.3 Results and Discussion

The summary of responses for porosity enhancement ratio, permeability enhancement ratio and pressure drop are being presented in Table 6.4. A total number of 32 observations had been made and polynomial function analysis was conducted. The detail statistical analyses of the empirical approximation for each of the responses were presented in this section. Generally, an inverse power transformation, an inverse square root power transformation and a natural logarithm power transformation had been made on porosity

Chapter 6 Optimization Study using Response Surface Methodology (RSM)

enhancement ratio, permeability enhancement ratio and pressure drop responses respectively. A response transformation was required because the error or residuals is a function of the predicted response magnitude, which is not favourable in the empirical modelling. The final model terms selection and development had indicated that a quadratic model is the most appropriate for the empirical approximation for all the three response models. The range of responses obtained from the simulation are 1.01 to 1.71 for porosity enhancement ratio, 1.02 to 8.31 for permeability enhancement ratio and 197 Pa to 23829 Pa for pressure drop. The complete simulation results of all the responses were tabulated in Table 6.5.

Table 6.4 Summary of responses

| Response | R1 | R2 | R3 |
|-----------------|----------------------------|--------------------------------|---------------|
| Name | Porosity Enhancement Ratio | Permeability Enhancement Ratio | Pressure Drop |
| Units | 1 | 1 | Pa |
| Observations | 32 | 32 | 32 |
| Analysis | Polynomial | Polynomial | Polynomial |
| Minimum | 1.00802 | 1.0243 | 197.25 |
| Maximum | 1.79242 | 8.31091 | 23828.5 |
| Mean | 1.19 | 2.11 | 6168.62 |
| Std. Dev. | 0.2017 | 1.84 | 5643.59 |
| Ratio | 1.78 | 8.11 | 120.80 |
| Transformation | Inverse | Inverse Sqrt | Natural Log |
| Model | Quadratic | Quadratic | Quadratic |

Chapter 6 Optimization Study using Response Surface Methodology (RSM)

Table 6.5 Tabulation of simulation results

| Run | Factor 1 | Factor 2 | Factor 3 | Response 1 | Response 2 | Response 3 |
|------------|---------------------|--------------------------|------------------------------|----------------------------------|--------------------------------------|-----------------------|
| | A: Temperature | B: Acid Concentration | C: Acid Injection Rate | Porosity Enhancement Ratio | Permeability Enhancement Ratio | Pressure Drop |
| | °C | % | ($\times 10^{-5}$) m/s | 1 | 1 | Pa |
| 1 | 25 | 1.5 | 1.11 | 1.00802 | 1.02430 | 197.25 |
| 2 | 25 | 1.5 | 2.785 | 1.00939 | 1.02847 | 559.734 |
| 3 | 25 | 1.5 | 4.46 | 1.01061 | 1.03221 | 1038.45 |
| 4 | 25 | 6.75 | 1.11 | 1.03616 | 1.11338 | 847.106 |
| 5 | 25 | 6.75 | 2.785 | 1.04234 | 1.13324 | 2384.37 |
| 6 | 25 | 6.75 | 4.46 | 1.04788 | 1.15121 | 4390.28 |
| 7 | 25 | 12 | 1.11 | 1.06439 | 1.20893 | 1439.65 |
| 8 | 25 | 12 | 2.785 | 1.07542 | 1.24628 | 4021.34 |
| 9 | 25 | 12 | 4.46 | 1.08531 | 1.28035 | 7351.59 |
| 10 | 65 | 1.5 | 1.11 | 1.02834 | 1.08838 | 616.906 |
| 11 | 65 | 1.5 | 2.785 | 1.03308 | 1.10339 | 1740.85 |
| 12 | 65 | 1.5 | 4.46 | 1.03756 | 1.11770 | 3250.81 |
| 13 | 65 | 6.75 | 1.11 | 1.12844 | 1.45839 | 2392.56 |
| 14 | 65 | 6.75 | 2.785 | 1.15004 | 1.54066 | 6586.97 |
| 15 | 65 | 6.75 | 2.785 | 1.15004 | 1.54066 | 6586.97 |
| 16 | 65 | 6.75 | 2.785 | 1.15004 | 1.54066 | 6586.97 |
| 17 | 65 | 6.75 | 2.785 | 1.15004 | 1.54066 | 6586.97 |
| 18 | 65 | 6.75 | 2.785 | 1.15004 | 1.54066 | 6586.97 |
| 19 | 65 | 6.75 | 2.785 | 1.15004 | 1.54066 | 6586.97 |
| 20 | 65 | 6.75 | 4.46 | 1.17052 | 1.62101 | 12021 |
| 21 | 65 | 12 | 1.11 | 1.23000 | 1.93868 | 3736.96 |
| 22 | 65 | 12 | 2.785 | 1.26888 | 2.11516 | 10077.1 |

Chapter 6 Optimization Study using Response Surface Methodology (RSM)

| | | | | | | |
|----|-----|------|-------|---------|---------|---------|
| 23 | 65 | 12 | 4.46 | 1.30589 | 2.29126 | 18046.5 |
| 24 | 105 | 1.5 | 1.11 | 1.07141 | 1.24588 | 1122.64 |
| 25 | 105 | 1.5 | 2.785 | 1.08160 | 1.28158 | 3025.59 |
| 26 | 105 | 1.5 | 4.46 | 1.09218 | 1.31901 | 5653.31 |
| 27 | 105 | 6.75 | 1.11 | 1.33143 | 2.84991 | 3790.3 |
| 28 | 105 | 6.75 | 2.785 | 1.37891 | 3.13174 | 9697.47 |
| 29 | 105 | 6.75 | 4.46 | 1.42844 | 3.43551 | 17460.5 |
| 30 | 105 | 12 | 1.11 | 1.61190 | 6.49199 | 5564.08 |
| 31 | 105 | 12 | 2.785 | 1.70002 | 7.36020 | 13619.2 |
| 32 | 105 | 12 | 4.46 | 1.79242 | 8.31091 | 23828.5 |

6.3.1 ANOVA of Response and Empirical Model Development

The simulation data are analysed and fitted into different model, such as the linear model, two-factor interaction (2FI) model, quadratic model and cubic polynomials model. The most suitable source is identified for fitting the model. Table 6.6 and 6.7 showed the fit summary and sequential model sum of squares of all the three responses in this study respectively. For each source, the probability (Prob > F) or sequential p-value is checked to ensure that it is below 0.05 significance benchmark. At the same time, the highest order of polynomial showing the significance of additional terms should be chosen. From the results, it is shown that the quadratic model with sequential p-value of <0.0001 is suggested to be used for fitting the three models. It should be noted that the cubic model had been identified as aliased, therefore is not suitable for model fitting.

Table 6.6 Fit summary of responses

| Response | Source | Sequential p-value | Adjusted R ² | Predicted R ² | |
|--------------------------------|------------------|--------------------|-------------------------|--------------------------|------------------|
| Porosity Enhancement Ratio | Linear | < 0.0001 | 0.8377 | 0.7841 | |
| | 2FI | < 0.0001 | 0.9831 | 0.9777 | |
| Ratio | Quadratic | < 0.0001 | 0.9950 | 0.9909 | Suggested |
| | Cubic | < 0.0001 | 0.9994 | 0.9976 | Aliased |
| Permeability Enhancement Ratio | Linear | < 0.0001 | 0.8323 | 0.7783 | |
| | 2FI | < 0.0001 | 0.9742 | 0.9665 | |
| Ratio | Quadratic | < 0.0001 | 0.9922 | 0.9862 | Suggested |
| | Cubic | < 0.0001 | 0.9987 | 0.9951 | Aliased |
| Pressure Drop | Linear | < 0.0001 | 0.8903 | 0.8725 | |
| | 2FI | 0.7581 | 0.8827 | 0.8173 | |
| Drop | Quadratic | < 0.0001 | 0.9997 | 0.9994 | Suggested |
| | Cubic | < 0.0001 | 1.0000 | 0.9998 | Aliased |

Table 6.7 Sequential Model Sum of Squares of responses

| Response | Source | Sum of Squares | df | Mean Square | F-value | p-value | |
|----------------------------|-------------------------|----------------|----------|---------------|--------------|--------------------|------------------|
| Porosity Enhancement Ratio | Mean vs Total | 23.78 | 1 | 23.78 | | | |
| | Linear vs Mean | 0.3749 | 3 | 0.1250 | 54.32 | < 0.0001 | |
| Ratio | 2FI vs Linear | 0.0584 | 3 | 0.0195 | 81.47 | < 0.0001 | |
| | Quadratic vs 2FI | 0.0044 | 3 | 0.0015 | 21.02 | < 0.0001 | Suggested |
| Cubic vs Quadratic | Cubic vs Quadratic | 0.0014 | 7 | 0.0002 | 23.42 | < 0.0001 | Aliased |

Chapter 6 Optimization Study using Response Surface Methodology (RSM)

| | | | | | | | |
|--------------|------------------|---------------|----------|---------------|----------------|---------------|------------------|
| | Residual | 0.0001 | 15 | 8.640E- | | | |
| | | | | 06 | | | |
| | Total | 24.22 | 32 | 0.7569 | | | |
| Permeability | Mean vs | 19.99 | 1 | 19.99 | | | |
| Enhancement | Total | | | | | | |
| Ratio | Linear vs | 0.8843 | 3 | 0.2948 | 52.29 | < | |
| | Mean | | | | | 0.0001 | |
| | 2FI vs | 0.1361 | 3 | 0.0454 | 52.24 | < | |
| | Linear | | | | | 0.0001 | |
| | Quadratic | 0.0159 | 3 | 0.0053 | 20.16 | < | Suggested |
| | vs 2FI | | | | | 0.0001 | |
| | Cubic vs | 0.0052 | 7 | 0.0007 | 17.18 | < | Aliased |
| | Quadratic | | | | | 0.0001 | |
| | Residual | 0.0006 | 15 | 0.0000 | | | |
| | Total | 21.03 | 32 | 0.6572 | | | |
| Pressure | Mean vs | 2180.89 | 1 | 2180.89 | | | |
| Drop | Total | | | | | | |
| | Linear vs | 34.85 | 3 | 11.62 | 84.88 | < | |
| | Mean | | | | | 0.0001 | |
| | 2FI vs | 0.1732 | 3 | 0.0577 | 0.3944 | 0.7581 | |
| | Linear | | | | | | |
| | Quadratic | 3.65 | 3 | 1.22 | 3370.95 | < | Suggested |
| | vs 2FI | | | | | 0.0001 | |
| | Cubic vs | 0.0071 | 7 | 0.0010 | 17.92 | < | Aliased |
| | Quadratic | | | | | 0.0001 | |
| | Residual | 0.0008 | 15 | 0.0001 | | | |
| | Total | 2219.58 | 32 | 69.36 | | | |

Chapter 6 Optimization Study using Response Surface Methodology (RSM)

Table 6.8 represented the model summary statistics of the responses. According to the results, the quadratic model is suggested to fit the data for all three responses. A low standard deviation, high R-squared and low PRESS value indicated that the quadratic model has the best fit summary for the empirical approximation of responses. The maximum Adjusted R² and the Predicted R² value would favour the model selection. The PRESS value is defined as the residual sum of squares. It is the difference between the actual data determined from the simulation run and the predicted data from the design expert. It is represented in Equation (6.6).

$$PRESS = \sum_{i=1}^k (y_i - \hat{y}_{i,-i})^2 \quad (6.6)$$

Table 6.8 Model summary statistics of responses

| Response | Source | Std. Dev. | R ² | Adjusted R ² | Predicted R ² | PRESS | |
|--------------------------------------|------------------|--------------|----------------|-------------------------|--------------------------|---------------|------------------|
| Porosity Enhancement Ratio | Linear | 0.048 | 0.853 | 0.8377 | 0.7841 | 0.0948 | |
| | | 0 | 4 | | | | |
| | 2FI | 0.015 | 0.986 | 0.9831 | 0.9777 | 0.0098 | |
| | | 5 | 4 | | | | |
| | Quadratic | 0.008 | 0.995 | 0.9950 | 0.9909 | 0.0040 | Suggested |
| | c | 4 | 0 | | | | d |
| | Cubic | 0.002 | 0.999 | 0.9994 | 0.9976 | 0.0010 | Aliased |
| | | 9 | 7 | | | | |
| Permeability Enhancement Ratio | Linear | 0.075 | 0.848 | 0.8323 | 0.7783 | 0.2310 | |
| | | 1 | 5 | | | | |
| | 2FI | 0.029 | 0.979 | 0.9742 | 0.9665 | 0.0349 | |
| | | 5 | 2 | | | | |
| | Quadratic | 0.016 | 0.994 | 0.9922 | 0.9862 | 0.0144 | Suggested |
| | c | 2 | 4 | | | | d |

Chapter 6 Optimization Study using Response Surface Methodology (RSM)

| | | | | | | | |
|----------|-----------------|--------------|--------------|---------------|---------------|---------------|-----------------|
| | Cubic | 0.006 | 0.999 | 0.9987 | 0.9951 | 0.0051 | Aliased |
| | | 5 | 4 | | | | |
| Pressure | Linear | 0.370 | 0.900 | 0.8903 | 0.8725 | 4.93 | |
| Drop | | 0 | 9 | | | | |
| | 2FI | 0.382 | 0.905 | 0.8827 | 0.8173 | 7.07 | |
| | | 6 | 4 | | | | |
| | Quadrati | 0.019 | 0.999 | 0.9997 | 0.9994 | 0.0236 | Suggeste |
| | c | 0 | 8 | | | | d |
| | Cubic | 0.007 | 1.000 | 1.0000 | 0.9998 | 0.0075 | Aliased |
| | | 5 | 0 | | | | |

In the development of the empirical model, the backward elimination method is employed to identify all the significant terms for the model. Referring to the backward elimination regression as well as the probability value, justification will be made whether to include the terms into the model, or to be removed from it. Table 6.9 to 6.11 showed the Analysis of Variance (ANOVA) results for quadratic model of porosity enhancement ratio, permeability enhancement ratio and pressure drop response respectively. Analysis of Variance was aimed to determine the accuracy of the three empirical models developed. From the ANOVA results, the model F-value is 692.16, 437.29 and 11902.36 for the three response models respectively. This gave an implication that the models are significant. There is only 0.01% chance that a noise would result in such a large F-value.

The P-values of the three models are all less than 0.0001, implying that the model terms are very significant. Based on the results for porosity enhancement ratio quadratic model as shown in Table 6.9, the terms A, B, C, AB, and A^2 are all highly significant model terms, showing the P-value of less than 0.0001. Besides, the terms AC, BC and B^2 are also significant terms as their P-values are less than 0.05. On the other hand, the P-value greater than 0.10 indicated that the model terms are not significant. In this case, the model term C^2 is having P-value greater than 0.05, indicating that this term is less significant. However, since there are not many insignificant model terms, model reduction is not required in this case. For permeability enhancement ratio quadratic model as shown in

Chapter 6 Optimization Study using Response Surface Methodology (RSM)

Table 6.10, the significant terms included A, B, C, AB, A² and B². Meanwhile, the less significant model terms are AC, BC and C². For pressure drop response model in Table 6.11, all the model terms A, B, C, AB, AC, BC, A², B² and C² are identified as significant terms. Hence, the overall model does not need to be reduced.

Table 6.9 ANOVA for quadratic model of porosity enhancement ratio response

| Source | Sum of Squares | df | Mean Square | F-value | p-value | |
|-----------------------|----------------|----|-------------|---------|----------|-------------|
| Model | 0.4378 | 9 | 0.0486 | 692.16 | < 0.0001 | significant |
| A-Temperature | 0.2060 | 1 | 0.2060 | 2930.71 | < 0.0001 | |
| B-Acid Concentration | 0.1655 | 1 | 0.1655 | 2354.55 | < 0.0001 | |
| C-Acid Injection Rate | 0.0035 | 1 | 0.0035 | 49.58 | < 0.0001 | |
| AB | 0.0568 | 1 | 0.0568 | 808.11 | < 0.0001 | |
| AC | 0.0008 | 1 | 0.0008 | 11.81 | 0.0024 | |
| BC | 0.0008 | 1 | 0.0008 | 11.60 | 0.0025 | |
| A ² | 0.0039 | 1 | 0.0039 | 54.90 | < 0.0001 | |
| B ² | 0.0012 | 1 | 0.0012 | 16.59 | 0.0005 | |
| C ² | 6.265E-07 | 1 | 6.265E-07 | 0.0089 | 0.9256 | |
| Residual | 0.0015 | 22 | 0.0001 | | | |
| Lack of Fit | 0.0015 | 17 | 0.0001 | | | |
| Pure Error | 0.0000 | 5 | 0.0000 | | | |
| Cor Total | 0.4393 | 31 | | | | |

Table 6.10 ANOVA for quadratic model of permeability enhancement ratio response

| Source | Sum of Squares | df | Mean Square | F-value | p-value |
|--------|----------------|----|-------------|---------|---------|
|--------|----------------|----|-------------|---------|---------|

Chapter 6 Optimization Study using Response Surface Methodology (RSM)

| | | | | | |
|--------------------------|-----------|----|-----------|---------|-------------------------|
| Model | 1.04 | 9 | 0.1151 | 437.29 | < significant 0.0001 |
| A-Temperature | 0.5039 | 1 | 0.5039 | 1913.71 | < 0.0001 |
| B-Acid Concentration | 0.3760 | 1 | 0.3760 | 1427.81 | < 0.0001 |
| C-Acid Injection Rate | 0.0044 | 1 | 0.0044 | 16.74 | 0.0005 |
| AB | 0.1350 | 1 | 0.1350 | 512.57 | < 0.0001 |
| AC | 0.0005 | 1 | 0.0005 | 1.95 | 0.1770 |
| BC | 0.0006 | 1 | 0.0006 | 2.41 | 0.1348 |
| A ² | 0.0139 | 1 | 0.0139 | 52.92 | < 0.0001 |
| B ² | 0.0040 | 1 | 0.0040 | 15.21 | 0.0008 |
| C ² | 7.803E-06 | 1 | 7.803E-06 | 0.0296 | 0.8649 |
| Residual | 0.0058 | 22 | 0.0003 | | |
| Lack of Fit | 0.0058 | 17 | 0.0003 | | |
| Pure Error | 0.0000 | 5 | 0.0000 | | |
| Cor Total | 1.04 | 31 | | | |

Table 6.11 ANOVA for quadratic model of pressure drop response

| Source | Sum of Squares | df | Mean Square | F-value | p- value |
|---------------|-------------------|----|----------------|----------|-------------------------|
| Model | 38.68 | 9 | 4.30 | 11902.36 | < significant 0.0001 |
| A-Temperature | 9.61 | 1 | 9.61 | 26607.48 | < 0.0001 |

Chapter 6 Optimization Study using Response Surface Methodology (RSM)

| | | | | | | |
|-----------------------|--------|----|--------|----------|--------|--------|
| B-Acid Concentration | 13.75 | 1 | 13.75 | 38077.71 | < | 0.0001 |
| C-Acid Injection Rate | 11.50 | 1 | 11.50 | 31843.60 | < | 0.0001 |
| AB | 0.1571 | 1 | 0.1571 | 435.14 | < | 0.0001 |
| AC | 0.0095 | 1 | 0.0095 | 26.40 | < | 0.0001 |
| BC | 0.0065 | 1 | 0.0065 | 18.06 | 0.0003 | |
| A ² | 0.6433 | 1 | 0.6433 | 1781.56 | < | 0.0001 |
| B ² | 1.42 | 1 | 1.42 | 3935.49 | < | 0.0001 |
| C ² | 0.2880 | 1 | 0.2880 | 797.55 | < | 0.0001 |
| Residual | 0.0079 | 22 | 0.0004 | | | |
| Lack of Fit | 0.0079 | 17 | 0.0005 | | | |
| Pure Error | 0.0000 | 5 | 0.0000 | | | |
| Cor Total | 38.69 | 31 | | | | |

Table 6.12 tabulated the fit statistics of the responses. The R^2 value of the empirical models of porosity enhancement ratio, permeability enhancement ratio and pressure drop responses are 0.9965, 0.9944 and 0.9998. This means that 99.65%, 99.44% and 99.98% of the variability of the response data around the mean could be approximated by the porosity, permeability and pressure drop model respectively. From the table, the difference between the R^2 value and the Adjusted R^2 value is only 0.0015 for porosity mode, 0.0022 for permeability model and 0.0001 for pressure model. These little differences indicated that there are no insignificant and unnecessary terms added into the three empirical models. The difference between the Adjusted R^2 value and the Predicted R^2 values for the three models are also very small and are all less than 0.2, which is only

0.0041, 0.0061 and 0.0003 respectively. The highly reasonable agreement between these two values implied that the empirical models are having a good fit with the simulation data obtained. Moreover, the Adequate Precision of the models, which is the measure of the signal to noise ratio are 93.6369, 72.2048 and 452.5859 respectively. In general, the desired ratio should be greater than 4. Therefore, the high ratio indicated an adequate signal for the models to navigate the design space.

Table 6.12 Fit statistics of response

| Response | Porosity Enhancement Ratio | Permeability Enhancement Ratio | Pressure Drop |
|--------------------------|---------------------------------------|---|--------------------------|
| Std. Dev. | 0.0084 | 0.0162 | 0.0190 |
| Mean | 0.8621 | 0.7904 | 8.26 |
| C.V. % | 0.9724 | 2.05 | 0.2302 |
| R ² | 0.9965 | 0.9944 | 0.9998 |
| Adjusted R ² | 0.9950 | 0.9922 | 0.9997 |
| Predicted R ² | 0.9909 | 0.9862 | 0.9994 |
| Adeq. Precision | 93.6369 | 72.2048 | 452.5859 |

6.3.2 Empirical Model Development

Table 6.13 to 6.15 tabulated the coefficients in terms of coded factors of porosity enhancement ratio, permeability enhancement ratio and pressure drop response respectively. The empirical equations described in terms of the coded factors can be adopted to predict the responses for a given level of each factors. The estimated coefficients are defined as the expected change in responses per unit change in the factor value. Meanwhile, all the other factors being kept constant. The default code for the high level of a factor is +1 whereas that for the low level of a factor is -1.

Chapter 6 Optimization Study using Response Surface Methodology (RSM)

The intercept in the orthogonal design of the models represented the overall average response of all the simulated data. According to the value of factor set, the coefficients are being adjusted around the average response value. By making comparisons between the factor coefficients, the coded empirical equation is very useful to evaluate the effect or impact of the relative factors. As mentioned previously, this empirical model is only valid within the range of data used in the simulation, which are 25 °C to 105 °C for temperature, 1.5% to 12% for acid concentration and 1.11E-5 to 4.46E-5 for acid injection rate. All the combined conditions set for the sandstone acidizing operation within the range in this study can be applied to predict the porosity enhancement ratio. The Variance Inflation Factor (VIF) quantified the severity of the multi-collinearity in an ordinary least squares regression analysis. VIF of 1 indicated that the factors are orthogonal, whereas VIF larger than 1 indicated multi-collinearity. The correlation of factors is more severe when the VIF value is higher. Generally, a VIF of less than 10 are acceptable.

Table 6.13 Coefficients in terms of coded factors of porosity enhancement ratio response

| Factor | Coefficient | df | Standard | 95% CI | | VIF |
|--------------------------|-------------|----|----------|---------|---------|--------|
| | Estimate | | Error | Low | High | |
| Intercept | 0.8681 | 1 | 0.0028 | 0.8623 | 0.8740 | |
| A-Temperature | -0.1070 | 1 | 0.0020 | -0.1111 | -0.1029 | 1.0000 |
| B-Acid Concentration | -0.0959 | 1 | 0.0020 | -0.1000 | -0.0918 | 1.0000 |
| C-Acid Injection Rate | -0.0139 | 1 | 0.0020 | -0.0180 | -0.0098 | 1.0000 |
| AB | -0.0688 | 1 | 0.0024 | -0.0738 | -0.0638 | 1.0000 |
| AC | -0.0083 | 1 | 0.0024 | -0.0133 | -0.0033 | 1.0000 |
| BC | -0.0082 | 1 | 0.0024 | -0.0133 | -0.0032 | 1.0000 |
| A ² | -0.0232 | 1 | 0.0031 | -0.0297 | -0.0167 | 1.10 |
| B ² | 0.0128 | 1 | 0.0031 | 0.0063 | 0.0193 | 1.10 |
| C ² | -0.0003 | 1 | 0.0031 | -0.0068 | 0.0062 | 1.10 |

Table 6.14 Coefficients in terms of coded factors of permeability enhancement ratio response

| Factor | Coefficient | df | Standard | 95% CI | | VIF |
|--------------------------|-------------|----|----------|---------|---------|--------|
| | Estimate | | Error | Low | High | |
| Intercept | 0.8025 | 1 | 0.0055 | 0.7912 | 0.8138 | |
| A-Temperature | -0.1673 | 1 | 0.0038 | -0.1752 | -0.1594 | 1.0000 |
| B-Acid Concentration | -0.1445 | 1 | 0.0038 | -0.1525 | -0.1366 | 1.0000 |
| C-Acid Injection Rate | -0.0157 | 1 | 0.0038 | -0.0236 | -0.0077 | 1.0000 |
| AB | -0.1061 | 1 | 0.0047 | -0.1158 | -0.0963 | 1.0000 |
| AC | -0.0065 | 1 | 0.0047 | -0.0162 | 0.0032 | 1.0000 |
| BC | -0.0073 | 1 | 0.0047 | -0.0170 | 0.0024 | 1.0000 |
| A ² | -0.0441 | 1 | 0.0061 | -0.0567 | -0.0316 | 1.10 |
| B ² | 0.0237 | 1 | 0.0061 | 0.0111 | 0.0362 | 1.10 |
| C ² | -0.0010 | 1 | 0.0061 | -0.0136 | 0.0115 | 1.10 |

Table 6.15 Coefficients in terms of coded factors of pressure drop response

| Factor | Coefficient | df | Standard | 95% CI | | VIF |
|--------------------------|-------------|----|----------|---------|---------|--------|
| | Estimate | | Error | Low | High | |
| Intercept | 8.79 | 1 | 0.0064 | 8.77 | 8.80 | |
| A-Temperature | 0.7306 | 1 | 0.0045 | 0.7213 | 0.7399 | 1.0000 |
| B-Acid Concentration | 0.8740 | 1 | 0.0045 | 0.8647 | 0.8833 | 1.0000 |
| C-Acid Injection Rate | 0.7992 | 1 | 0.0045 | 0.7900 | 0.8085 | 1.0000 |
| AB | -0.1144 | 1 | 0.0055 | -0.1258 | -0.1031 | 1.0000 |
| AC | -0.0282 | 1 | 0.0055 | -0.0396 | -0.0168 | 1.0000 |
| BC | -0.0233 | 1 | 0.0055 | -0.0347 | -0.0119 | 1.0000 |

Chapter 6 Optimization Study using Response Surface Methodology (RSM)

| | | | | | | |
|----------------|---------|---|--------|---------|---------|------|
| A ² | -0.2999 | 1 | 0.0071 | -0.3146 | -0.2851 | 1.10 |
| B ² | -0.4457 | 1 | 0.0071 | -0.4604 | -0.4310 | 1.10 |
| C ² | -0.2006 | 1 | 0.0071 | -0.2154 | -0.1859 | 1.10 |

In the empirical models, the estimated coefficients for all the terms are at a 95% Confidence Interval (CI). The developed empirical model in terms of coded factors for the porosity enhancement ratio (PORO), permeability enhancement ratio (PERM) and pressure drop (PRDR) are shown in Equations (6.7), (6.8) and (6.9) respectively.

$$1/\text{PORO} = 0.8681 - 0.1070 A - 0.0959 B - 0.0139 C - 0.0688 AB - 0.0083 AC - 0.0082 BC - 0.0232 A^2 + 0.0128 B^2 - 0.0003 C^2 \quad (6.7)$$

$$1/\sqrt{\text{PERM}} = 0.8025 - 0.1673 A - 0.1445 B - 0.0157 C - 0.1061 AB - 0.0065 AC - 0.0073 BC - 0.0441 A^2 + 0.0237 B^2 - 0.0010 C^2 \quad (6.8)$$

$$\ln(\text{PRDR}) = 8.79 + 0.7306 A + 0.8740 B + 0.7992 C - 0.1144 AB - 0.0282 AC - 0.0233 BC - 0.2999 A^2 - 0.4457 B^2 - 0.2006 C^2 \quad (6.9)$$

Where PORO represented the porosity enhancement ratio [1], PERM is the permeability enhancement ratio [1], PRDR is the pressure drop [Pa], A is the coded factor of temperature (°C), B is the coded factor of acid concentration (%) and C is the coded factor acid injection rate (m/s).

As stated previously, an inverse power transform had been applied for the porosity response, therefore the empirical equation in Equation (6.7) is given in term of 1/PORO. Since an inverse square root power transform was adopted for the permeability response, so the empirical equation given in Equation (6.8) is written in term of $1/\sqrt{\text{PERM}}$. Whereas for the pressure drop response, a natural log power transform was applied, given the empirical equation in Equation (6.9) as $\ln(\text{PRDR})$.

6.3.3 Residuals Analysis of Response Data

One of the most important steps in empirical modelling of the validation of the model. Various residual analyses are vital to be conducted in order to ensure that the developed models could be adequately applied. Before the residual analyses of data, it is assumed that the predicted empirical model is correct, the error term has a zero mean and a constant variance, and the errors are normally distributed as well as uncorrelated to one another. The residual analyses that had been conducted are the normal probability plot, predicted versus actual plot, residual versus predicted plot, leverage plot and box-cox plot. These analyses had given further confirmation that the simulation data are well fitted to the empirical models. Therefore, the predicted models are accurate and reliable as an optimization tool for sandstone acidizing performance.

Figure 6.3, 6.4 and 6.5 depicted the normal plot of residuals and the predicted vs. actual plot for the responses of porosity, permeability and pressure drop respectively. The normal plot would evaluate if a set of data is in line or linear with the normal distribution by observing the characteristics of a model residuals. The plots of simulation data versus the empirical normal distribution are shown and an approximately straight line is observed from Figure 6.3 and 6.4. Since there is no significant deviation of the scattered points from the straight line, this indicated that the data followed the normality of the plot. Nevertheless, it is denoted from the normal plot of Figure 6.5 that there is a point located at the far right, slightly further from the linear line. As there is no obvious non-linear S-curve pattern observed from the plot, that error point could be deemed negligible.

The predicted vs. actual plot of the porosity enhancement ratio response data represented in Figure 6.3, 6.4 and 6.5 is a useful plot as it also acted as an indication on how well the simulation data fit with the empirical model. The 45 ° diagonal straight line as shown in the figures is known as the locus showing that the predicted data and actual data are the same. From the figure, it is observed that all of the points are nicely fitted to the diagonal line. Hence, it is proven that the data obtained from the simulation are close to the one predicted by the empirical models. Also, there is no identifiable outliers in the plot. This relatively close data fitting indicated that a strong correlation existed between the predicted and actual data for all the three response models.

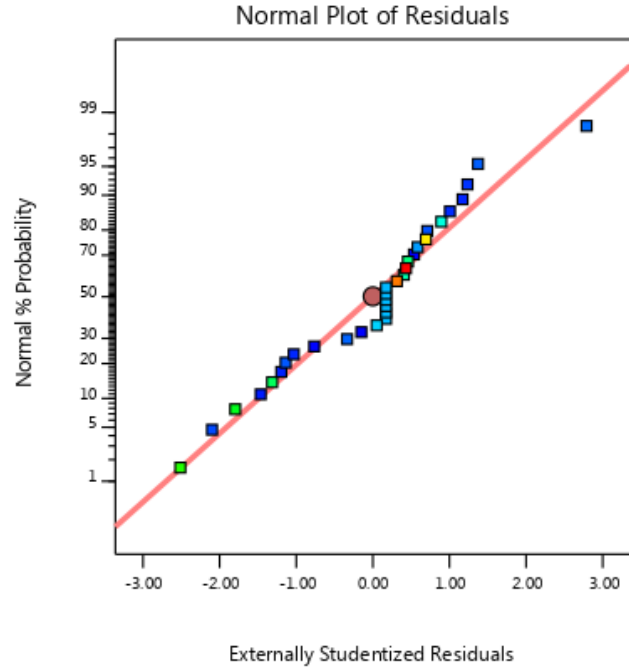
Chapter 6 Optimization Study using Response Surface Methodology (RSM)

Design-Expert® Software

1/(Porosity Enhancement Ratio)

Color points by value of
1/(Porosity Enhancement Ratio):

0.992  0.558



Design-Expert® Software

1/(Porosity Enhancement Ratio)

Color points by value of
1/(Porosity Enhancement Ratio):

0.992  0.558

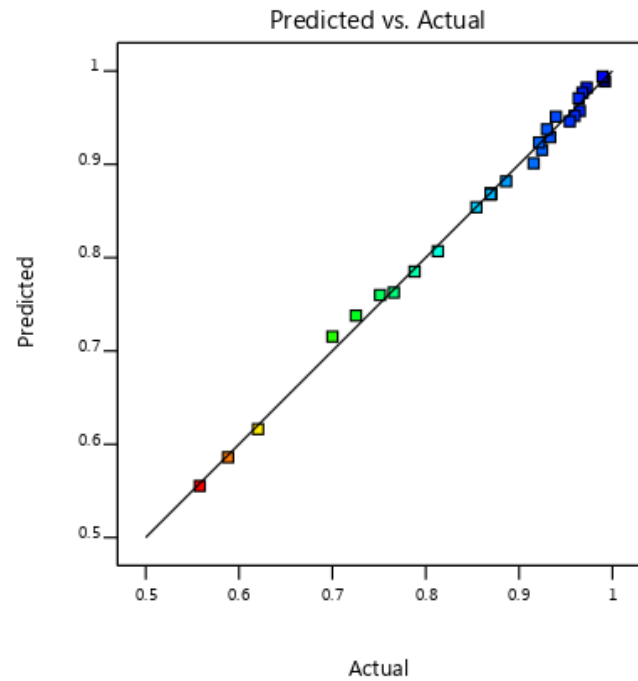


Figure 6.3 Normal probability plot of residuals (upper) and predicted vs. actual plot (bottom) for porosity enhancement ratio response

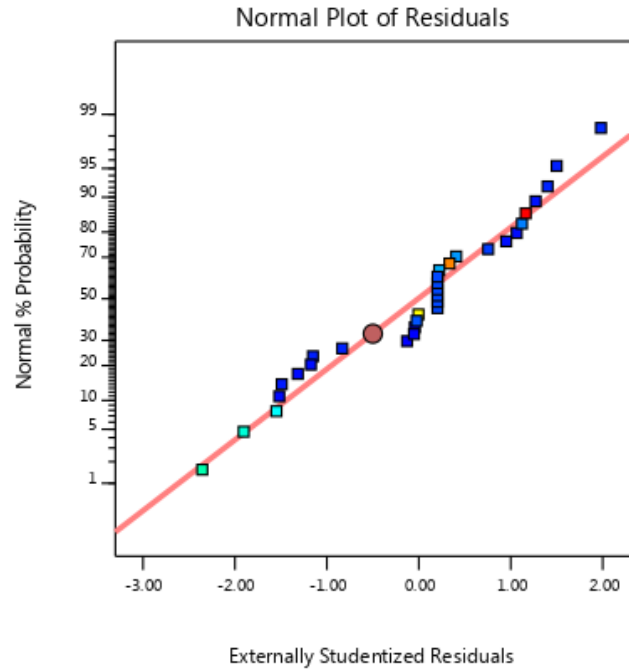
Chapter 6 Optimization Study using Response Surface Methodology (RSM)

Design-Expert® Software

1/Sqrt(Permeability Enhancement Ratio)

Color points by value of
1/Sqrt(Permeability Enhancement Ratio):

0.988  0.347



Design-Expert® Software

1/Sqrt(Permeability Enhancement Ratio)

Color points by value of
1/Sqrt(Permeability Enhancement Ratio):

0.988  0.347

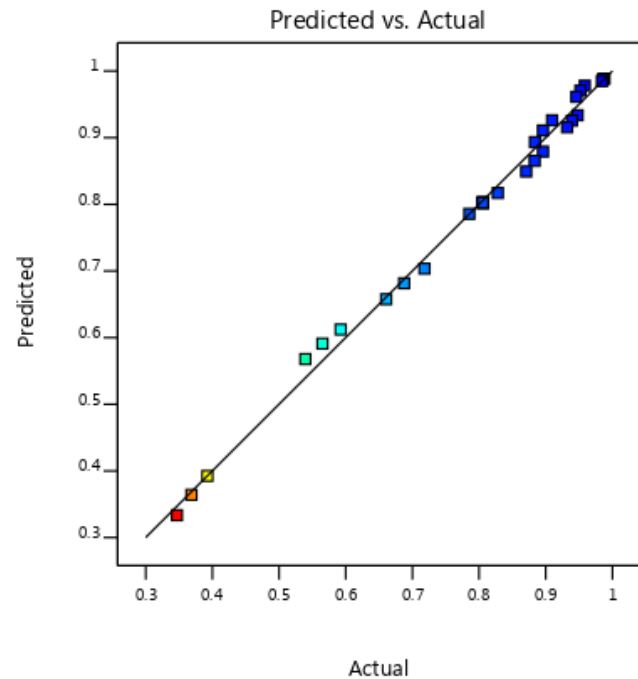


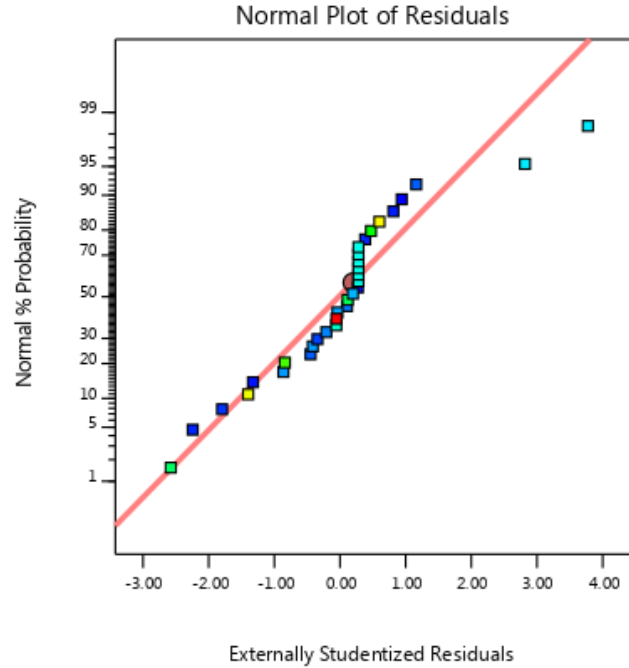
Figure 6.4 Normal probability plot of residuals (upper) and predicted vs. actual plot (bottom) for permeability enhancement ratio response

Design-Expert® Software

In(Pressure Drop)

Color points by value of
In(Pressure Drop):

5.284  10.079



Design-Expert® Software

In(Pressure Drop)

Color points by value of
In(Pressure Drop):

5.284  10.079

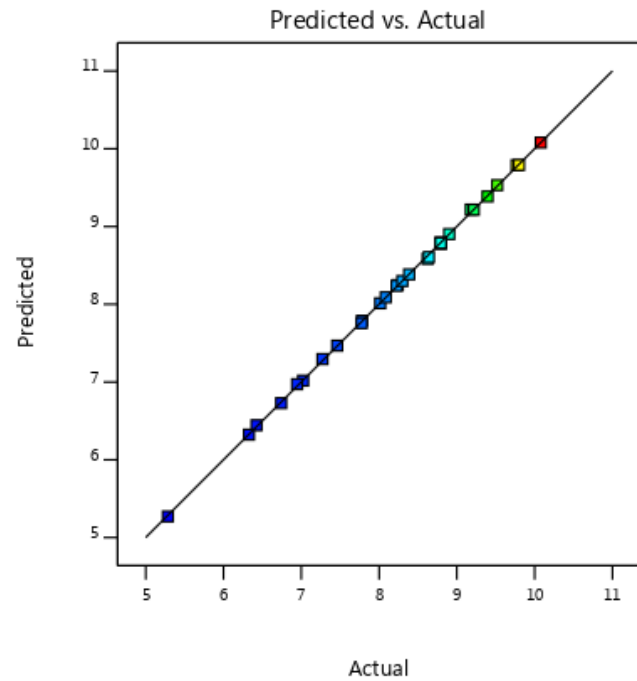


Figure 6.5 Normal probability plot of residuals (upper) and predicted vs. actual plot (bottom) for pressure drop response

Chapter 6 Optimization Study using Response Surface Methodology (RSM)

Figure 6.6, 6.7 and 6.8 showed the residuals vs. predicted plot and the leverage plot for porosity enhancement ratio, permeability enhancement ratio and pressure drop responses. The residuals vs. predicted plot is a scatter plot of residuals that is commonly used to identify the non-linearity, unequal variances of error and any outliers of the simulation data. As shown in the figures, the plot of residuals is randomly scattered, and a horizontal band is roughly formed close to the zero line. Besides, all the residuals are well fitted within the limits of the data as shown by the two red lines (-3.6315, 3.6315) and there are no outliers observed from the plot. Therefore, this indicated that the data are well fitted, and the fitted data are independent of each other. In other words, the data is not biased and is homoscedastic. However, in Figure 6.8, there is only one point that fell outside the limits of data and is slightly above the red line. It is noted that this is exactly the point that corresponds with the error point as shown in the previous Figure 6.5. Therefore, it will be ignored as it does not affect the accuracy of empirical approximation in overall.

The leverage plot for the three responses revealed in Figure 6.6, 6.7 and 6.8 is an added variable plot, which is generalized from partial regression method. Thus, it revealed the influence of each individual model terms. The range of plot from 0 to 1 would show the effect of each of the full 3^3 factorial design points on the predicted empirical model. From the figures, it is shown that all the points were scattered in the plot, with the leverage value ranged from 0.10 to 0.50. The red horizontal line in the plot indicated the maximum leverage value, which is 0.625. Since all the leverage values are within the range, it is confident that the empirical model developed will not be influenced by the model terms.

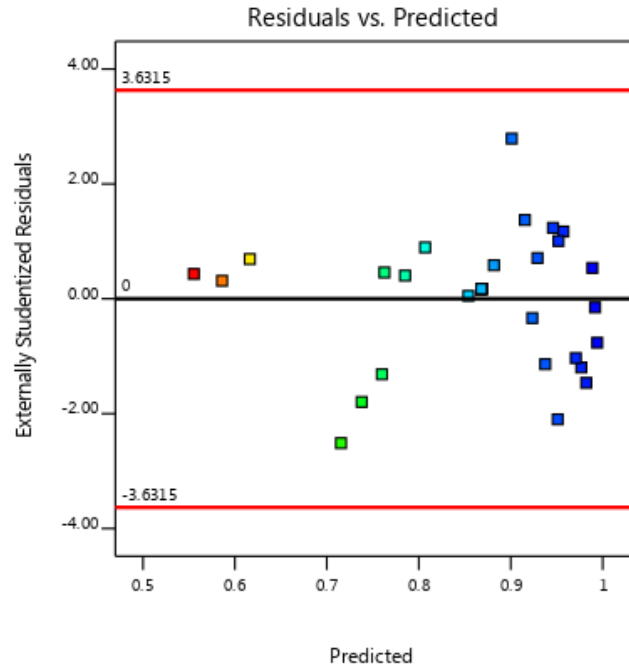
Chapter 6 Optimization Study using Response Surface Methodology (RSM)

Design-Expert® Software

1/(Porosity Enhancement Ratio)

Color points by value of
1/(Porosity Enhancement Ratio):

0.992  0.558



Design-Expert® Software

1/(Porosity Enhancement Ratio)

Color points by value of
1/(Porosity Enhancement Ratio):

0.992  0.558

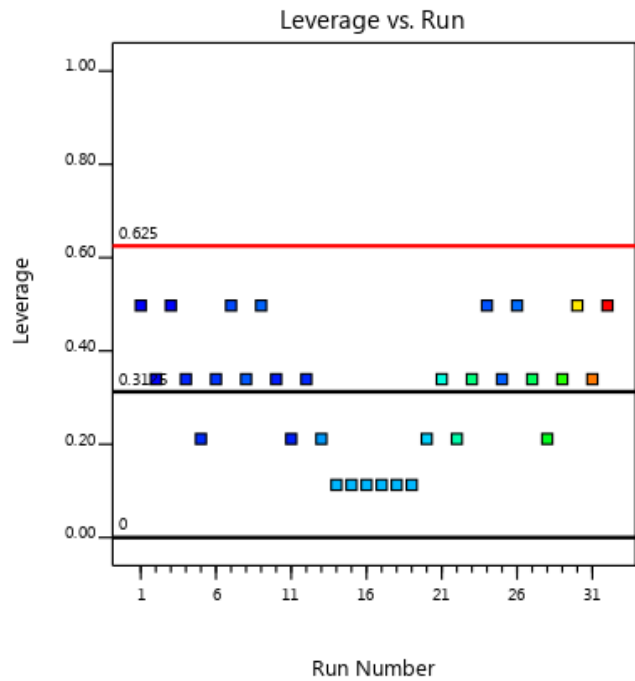


Figure 6.6 Residuals vs. predicted plot (upper) and leverage plot (bottom) for porosity enhancement ratio response

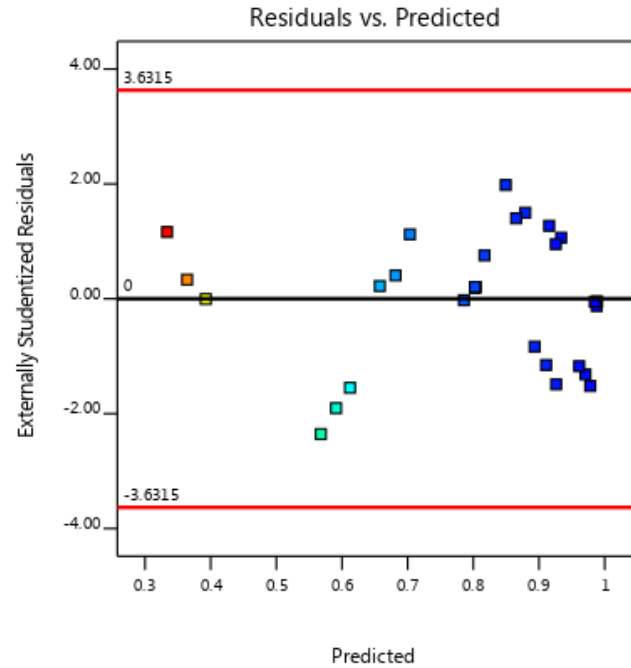
Chapter 6 Optimization Study using Response Surface Methodology (RSM)

Design-Expert® Software

1/Sqrt(Permeability Enhancement Ratio)

Color points by value of
1/Sqrt(Permeability Enhancement Ratio):

0.988  0.347



Design-Expert® Software

1/Sqrt(Permeability Enhancement Ratio)

Color points by value of
1/Sqrt(Permeability Enhancement Ratio):

0.988  0.347

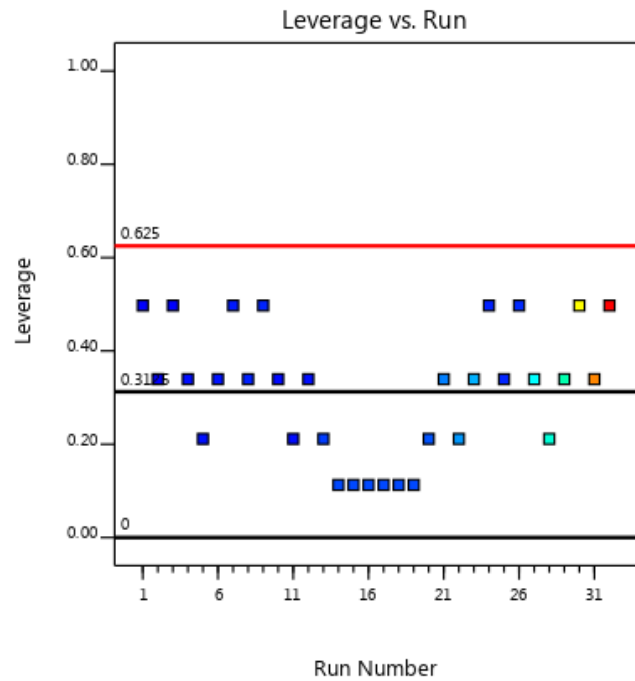


Figure 6.7 Residuals vs. predicted plot (upper) and leverage plot (bottom) for permeability enhancement ratio response

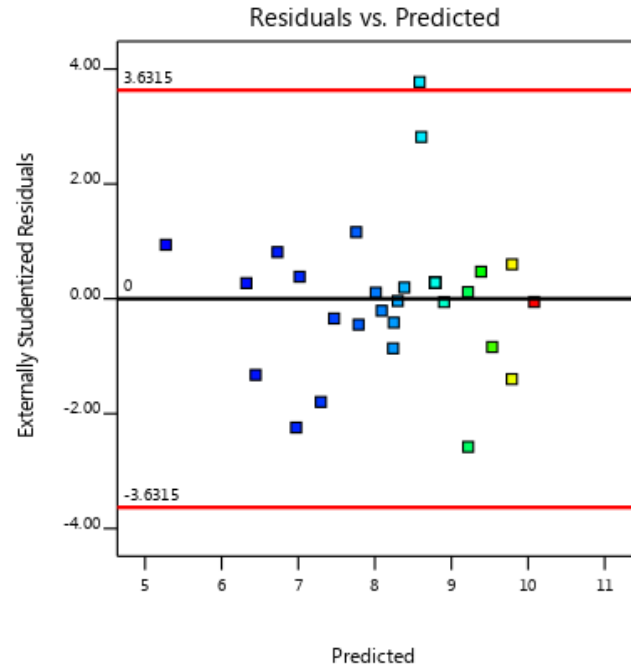
Chapter 6 Optimization Study using Response Surface Methodology (RSM)

Design-Expert® Software

In(Pressure Drop)

Color points by value of
In(Pressure Drop):

5.284  10.079



Design-Expert® Software

In(Pressure Drop)

Color points by value of
In(Pressure Drop):

5.284  10.079

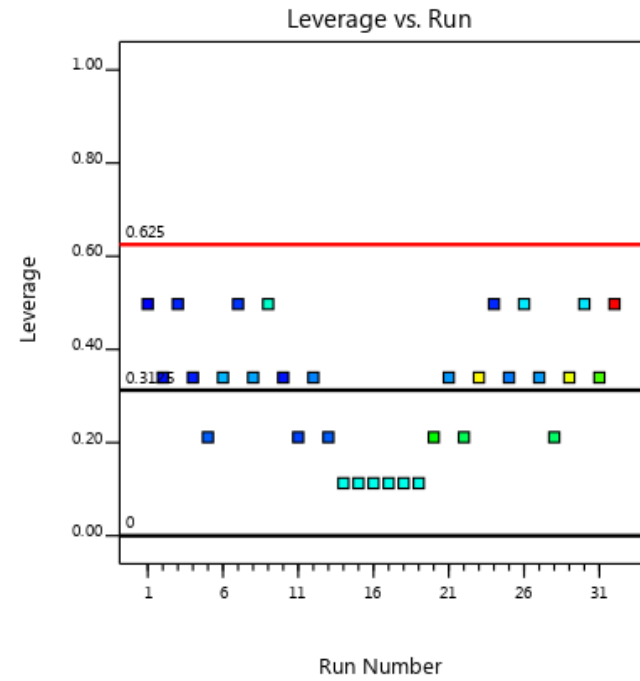


Figure 6.8 Residuals vs. predicted plot (upper) and leverage plot (bottom) for pressure drop response

Chapter 6 Optimization Study using Response Surface Methodology (RSM)

Figure 6.9, 6.10 and 6.11 demonstrated the Box-Cox plot before and after power transformation for porosity enhancement ratio, permeability enhancement ratio and pressure drop responses respectively. The x-axis of the plot is represented the lambda value while the y-axis is represented by taking the log function of the sum of squares of residuals. The lambda value is the power of which all data should raise to fit the trend of normality. The Box-Cox power transformation checked for the finest standard deviation of the data, instead of the normality. Therefore, this does not ensure normality of data.

Based on Figure 6.9, the lambda value before transformation is 1 as shown by the blue vertical line. Meanwhile, the green vertical line represented the best lambda value obtained from the analysis of data, which is -1.06. The value obtained is not within the 95% confidence interval (CI) of lambda, which ranges from -1.76 to -0.48. Thereafter, an inverse transformation is recommended to be made in order to ensure that the power of the empirical model is valid for the real data. Then, the new lambda value became -1, which is within the 95% confidence interval. Thus, an inverse transformation had improved the empirical approximation for the porosity enhancement ratio model.

Referring to Figure 6.10, the lambda value before transformation is 1 as indicated by the blue vertical line. However, the best lambda value represented in the green vertical line is -0.51. The marked value is beyond the 95% confidence interval (CI) of lambda, which had the range of -0.77 to -0.24. Consequently, an inverse square root power transformation is recommended for the empirical model of permeability. After transformation, the new lambda value is marked within the 95% confidence interval, which is -0.5. Thus, an inverse square root transformation being adopted had enhanced the empirical prediction for the permeability enhancement ratio model.

According to Figure 6.11, the lambda value before transformation is 1 as evidenced in the blue line but the best lambda value as shown in the green vertical line is 0.02. This means that the value obtained had exceeded the 95% confidence interval (CI) of lambda, ranging from -0.03 to 0.07. So, a natural log transformation is suggested to be made for the pressure drop prediction model. The new lambda value became 0 after such a transformation, ensuring that it is within the 95% confidence interval. Therefore, a natural log transformation had increased the validity of the pressure drop empirical approximation.

Chapter 6 Optimization Study using Response Surface Methodology (RSM)

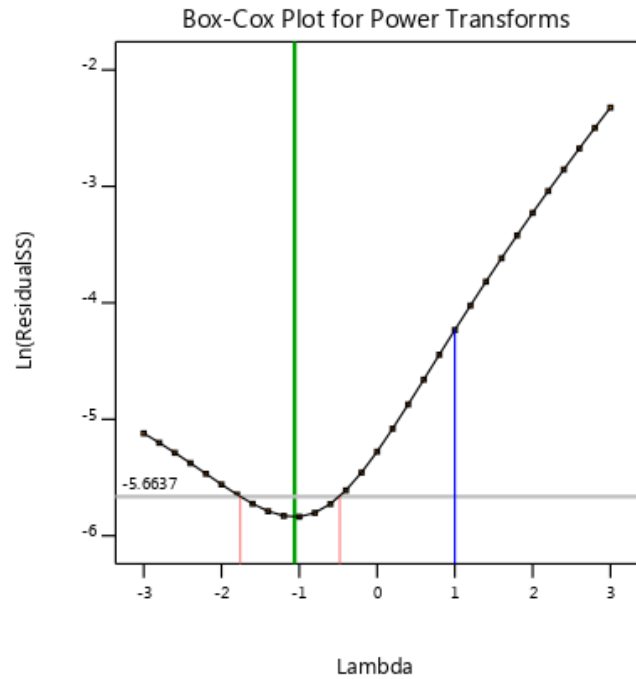
Design-Expert® Software

Porosity Enhancement Ratio

Current Lambda = 1
Best Lambda = -1.06
CI for Lambda: (-1.76, -0.48)

Recommend transform:
Inverse
(Lambda = -1)

Current Transform:
None



Design-Expert® Software

1/(Porosity Enhancement Ratio)

Current Lambda = -1
Best Lambda = -1.06
CI for Lambda: (-1.76, -0.48)

Recommend transform:
Inverse
(Lambda = -1)

Current Transform:
Inverse

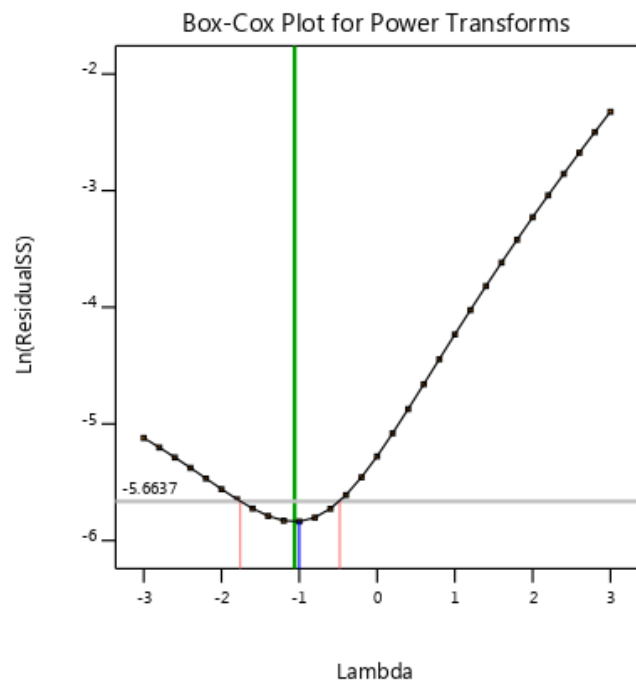


Figure 6.9 Box-cox plot before (upper) and after (bottom) an inverse power transformation for porosity enhancement ratio response

Chapter 6 Optimization Study using Response Surface Methodology (RSM)

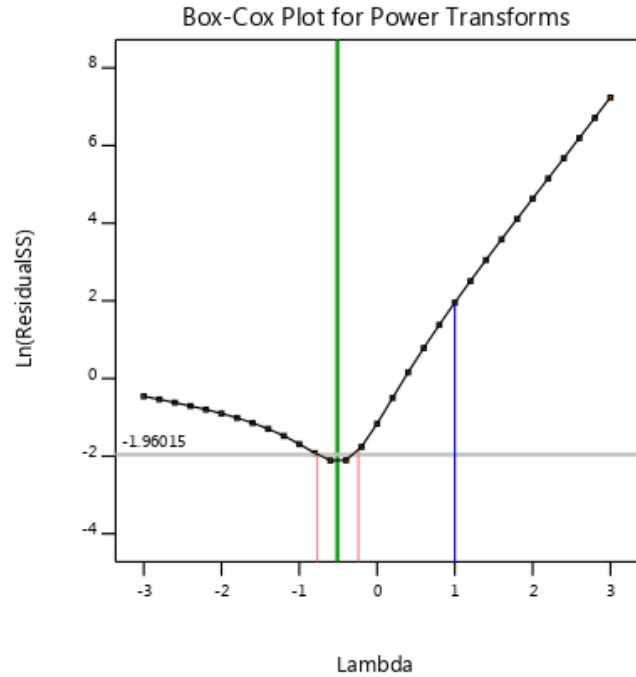
Design-Expert® Software

Permeability Enhancement Ratio

Current Lambda = 1
Best Lambda = -0.51
CI for Lambda: (-0.77, -0.24)

Recommend transform:
Inverse Sqrt
(Lambda = -0.5)

Current Transform:
None



Design-Expert® Software

1/Sqrt(Permeability Enhancement Ratio)

Current Lambda = -0.5
Best Lambda = -0.51
CI for Lambda: (-0.77, -0.24)

Recommend transform:
Inverse Sqrt
(Lambda = -0.5)

Current Transform:
Inverse Sqrt

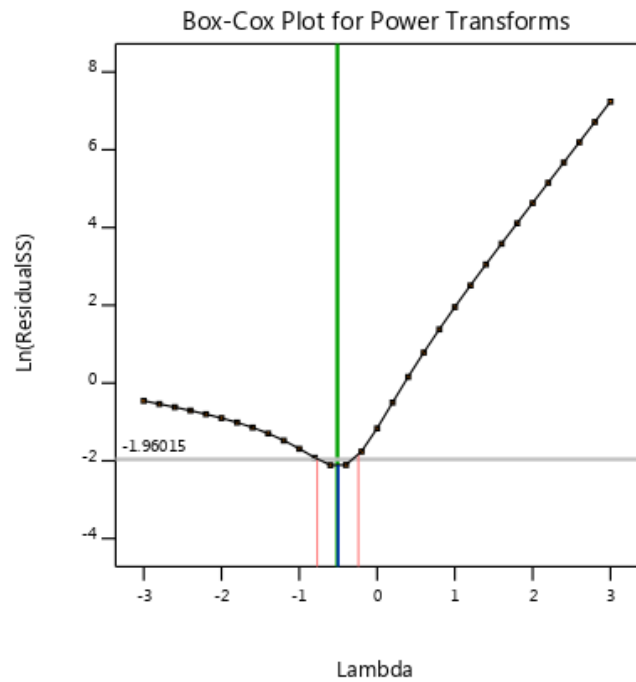


Figure 6.10 Box-cox plot before (upper) and after (bottom) an inverse square root power transformation for permeability enhancement ratio response

Chapter 6 Optimization Study using Response Surface Methodology (RSM)

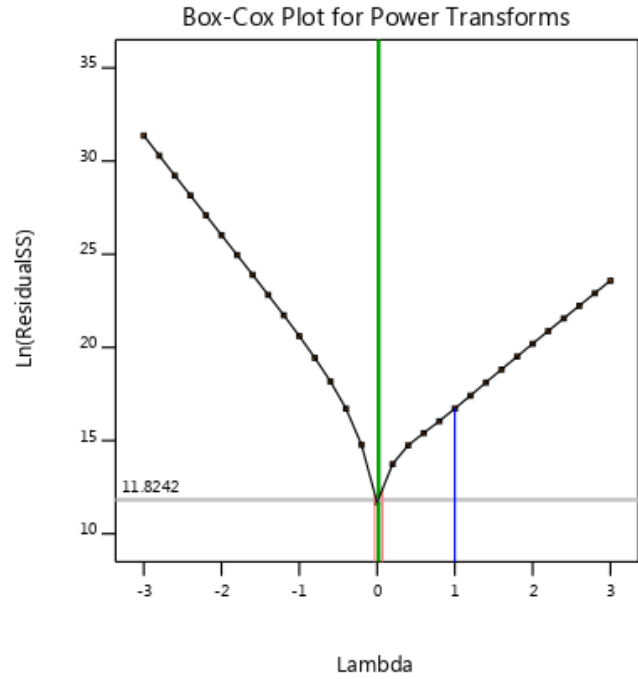
Design-Expert® Software

Pressure Drop

Current Lambda = 1
Best Lambda = 0.02
CI for Lambda: (-0.03, 0.07)

Recommend transform:
Log
(Lambda = 0)

Current Transform:
None



Design-Expert® Software

In(Pressure Drop)

Current Lambda = 0
Best Lambda = 0.02
CI for Lambda: (-0.03, 0.07)

Recommend transform:
Log
(Lambda = 0)

Current Transform:
Natural Log

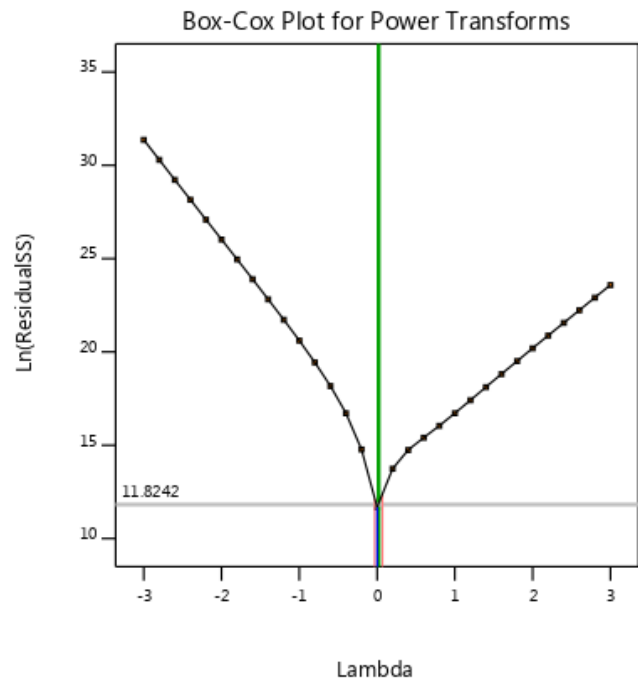


Figure 6.11 Box-cox plot before (upper) and after (bottom) a natural log power transformation for pressure drop response

6.3.4 Empirical Model Fitting and Validation

Table 6.16, 6.17 and 6.18 showed the comparison of predicted data and the actual data for porosity enhancement ratio, permeability enhancement ratio and pressure drop response respectively at different sandstone acidizing conditions. As stated previously, the coded value -1 represented the low level of all factors, 0 is the moderate level of factors and +1 as the high level factors. The percentage of difference between the actual simulation data and the predicted data based on the empirical equations developed had been calculated and tabulated. These tables served as an additional prove that further confirmed and validated the accuracy of the empirical models in predicting the porosity, permeability and pressure drop.

From Table 6.16, the highest percentage of difference recorded is 2.14% only while most of the percentage of difference is below 1.00%. This showed a clear evidence that the predicted model is fairly accurate to perform the prediction for porosity enhancement ratio based on the sets of sandstone acidizing conditions set in the simulation. In Table 6.17, the recorded highest percentage of difference for permeability response is 9.75%, which is slightly higher than that of porosity response. Nevertheless, the percentage difference is still below 10%. Since most of the percentage of difference data ranges around 0.09% to 4.19%, the few slightly higher values would not significantly affect the accuracy of the empirical approximation. Further evaluation had been made based on Table 6.18. The largest value of percentage difference for the pressure drop response is denoted at 4.19%. Most of the calculated data are around 1.00% difference. An overall percentage of below 5.00% would imply that the empirical predictions are highly accurate and reliable.

Table 6.16 Comparison of predicted data and actual data for porosity enhancement ratio response

| Run | Coded Values | | | Simulation Data | Predicted Data | Percentage of Difference |
|-----|--------------|---|---|----------------------------|----------------|--------------------------|
| | A | B | C | Porosity Enhancement Ratio | | |
| 1 | 1 | 1 | 1 | 1 | 1 | % |

Chapter 6 Optimization Study using Response Surface Methodology (RSM)

| | | | | | | |
|----|----|----|----|---------|--------|------|
| 1 | -1 | -1 | -1 | 1.00802 | 1.0112 | 0.32 |
| 2 | -1 | -1 | 0 | 1.00939 | 1.0083 | 0.11 |
| 3 | -1 | -1 | +1 | 1.01061 | 1.0059 | 0.46 |
| 4 | -1 | 0 | -1 | 1.03616 | 1.0447 | 0.83 |
| 5 | -1 | 0 | 0 | 1.04234 | 1.0505 | 0.79 |
| 6 | -1 | 0 | +1 | 1.04788 | 1.0571 | 0.88 |
| 7 | -1 | +1 | -1 | 1.06439 | 1.0514 | 1.22 |
| 8 | -1 | +1 | 0 | 1.07542 | 1.0666 | 0.82 |
| 9 | -1 | +1 | +1 | 1.08531 | 1.0828 | 0.23 |
| 10 | 0 | -1 | -1 | 1.02834 | 1.0181 | 0.99 |
| 11 | 0 | -1 | 0 | 1.03308 | 1.0238 | 0.90 |
| 12 | 0 | -1 | +1 | 1.03756 | 1.0301 | 0.72 |
| 13 | 0 | 0 | -1 | 1.12844 | 1.1342 | 0.51 |
| 14 | 0 | 0 | 0 | 1.15004 | 1.1519 | 0.17 |
| 15 | 0 | 0 | 0 | 1.15004 | 1.1519 | 0.17 |
| 16 | 0 | 0 | 0 | 1.15004 | 1.1519 | 0.17 |
| 17 | 0 | 0 | 0 | 1.15004 | 1.1519 | 0.17 |
| 18 | 0 | 0 | 0 | 1.15004 | 1.1519 | 0.17 |
| 19 | 0 | 0 | 0 | 1.15004 | 1.1519 | 0.17 |
| 20 | 0 | 0 | +1 | 1.17052 | 1.1711 | 0.05 |
| 21 | 0 | +1 | -1 | 1.23000 | 1.2395 | 0.77 |
| 22 | 0 | +1 | 0 | 1.26888 | 1.2739 | 0.39 |
| 23 | 0 | +1 | +1 | 1.30589 | 1.3113 | 0.41 |
| 24 | +1 | -1 | -1 | 1.07141 | 1.0763 | 0.46 |
| 25 | +1 | -1 | 0 | 1.08160 | 1.0924 | 1.00 |
| 26 | +1 | -1 | +1 | 1.09218 | 1.1098 | 1.61 |
| 27 | +1 | 0 | -1 | 1.33143 | 1.3161 | 1.15 |
| 28 | +1 | 0 | 0 | 1.37891 | 1.3552 | 1.72 |
| 29 | +1 | 0 | +1 | 1.42844 | 1.3978 | 2.14 |
| 30 | +1 | +1 | -1 | 1.61190 | 1.6231 | 0.70 |

Chapter 6 Optimization Study using Response Surface Methodology (RSM)

| | | | | | | |
|----|----|----|----|---------|--------|------|
| 31 | +1 | +1 | 0 | 1.70002 | 1.7065 | 0.38 |
| 32 | +1 | +1 | +1 | 1.79242 | 1.8088 | 0.47 |

Table 6.17 Comparison of predicted data and actual data for permeability enhancement ratio response

| Run | Coded Values | | | Simulation Data | Predicted Data | Percentage of Difference |
|-----|--------------|----|----|--------------------------------|----------------|--------------------------|
| | A | B | C | Permeability Enhancement Ratio | | % |
| | 1 | 1 | 1 | 1 | 1 | % |
| 1 | -1 | -1 | -1 | 1.02430 | 1.0230 | 0.13 |
| 2 | -1 | -1 | 0 | 1.02847 | 1.0249 | 0.35 |
| 3 | -1 | -1 | +1 | 1.03221 | 1.0309 | 0.13 |
| 4 | -1 | 0 | -1 | 1.11338 | 1.1466 | 2.98 |
| 5 | -1 | 0 | 0 | 1.13324 | 1.1670 | 2.98 |
| 6 | -1 | 0 | +1 | 1.15121 | 1.1931 | 3.64 |
| 7 | -1 | +1 | -1 | 1.20893 | 1.1650 | 3.64 |
| 8 | -1 | +1 | 0 | 1.24628 | 1.2049 | 3.32 |
| 9 | -1 | +1 | +1 | 1.28035 | 1.2526 | 2.17 |
| 10 | 0 | -1 | -1 | 1.08838 | 1.0453 | 3.96 |
| 11 | 0 | -1 | 0 | 1.10339 | 1.0613 | 3.82 |
| 12 | 0 | -1 | +1 | 1.11770 | 1.0821 | 3.18 |
| 13 | 0 | 0 | -1 | 1.45839 | 1.4974 | 2.68 |
| 14 | 0 | 0 | 0 | 1.54066 | 1.5528 | 0.79 |
| 15 | 0 | 0 | 0 | 1.54066 | 1.5528 | 0.79 |
| 16 | 0 | 0 | 0 | 1.54066 | 1.5528 | 0.79 |
| 17 | 0 | 0 | 0 | 1.54066 | 1.5528 | 0.79 |
| 18 | 0 | 0 | 0 | 1.54066 | 1.5528 | 0.79 |
| 19 | 0 | 0 | 0 | 1.54066 | 1.5528 | 0.79 |
| 20 | 0 | 0 | +1 | 1.62101 | 1.6195 | 0.09 |

Chapter 6 Optimization Study using Response Surface Methodology (RSM)

| | | | | | | |
|----|----|----|----|---------|--------|------|
| 21 | 0 | +1 | -1 | 1.93868 | 2.0194 | 4.16 |
| 22 | 0 | +1 | 0 | 2.11516 | 2.1519 | 1.73 |
| 23 | 0 | +1 | +1 | 2.29126 | 2.3118 | 0.90 |
| 24 | +1 | -1 | -1 | 1.24588 | 1.2934 | 3.81 |
| 25 | +1 | -1 | 0 | 1.28158 | 1.3353 | 4.19 |
| 26 | +1 | -1 | +1 | 1.31901 | 1.3857 | 5.06 |
| 27 | +1 | 0 | -1 | 2.84991 | 2.6673 | 6.41 |
| 28 | +1 | 0 | 0 | 3.13174 | 2.8621 | 8.61 |
| 29 | +1 | 0 | +1 | 3.43551 | 3.1007 | 9.75 |
| 30 | +1 | +1 | -1 | 6.49199 | 6.4845 | 0.11 |
| 31 | +1 | +1 | 0 | 7.36020 | 7.5391 | 2.43 |
| 32 | +1 | +1 | +1 | 8.31091 | 8.9802 | 8.05 |

Table 6.18 Comparison of predicted data and actual data for pressure drop response

| Run | Coded Values | | | Simulation Data | Predicted Data | Percentage of Difference |
|-----|--------------|----|----|-----------------|----------------|--------------------------|
| | A | B | C | Pressure drop | | |
| | 1 | 1 | 1 | Pa | Pa | % |
| 1 | -1 | -1 | -1 | 197.25 | 195.21 | 1.03 |
| 2 | -1 | -1 | 0 | 559.734 | 558.58 | 0.21 |
| 3 | -1 | -1 | +1 | 1038.45 | 1070.09 | 3.05 |
| 4 | -1 | 0 | -1 | 847.106 | 838.40 | 1.03 |
| 5 | -1 | 0 | 0 | 2384.37 | 2343.73 | 1.70 |
| 6 | -1 | 0 | +1 | 4390.28 | 4386.56 | 0.08 |
| 7 | -1 | +1 | -1 | 1439.65 | 1476.60 | 2.57 |
| 8 | -1 | +1 | 0 | 4021.34 | 4032.73 | 0.28 |
| 9 | -1 | +1 | +1 | 7351.59 | 7373.89 | 0.30 |
| 10 | 0 | -1 | -1 | 616.906 | 630.93 | 2.27 |
| 11 | 0 | -1 | 0 | 1740.85 | 1755.13 | 0.82 |

Chapter 6 Optimization Study using Response Surface Methodology (RSM)

| | | | | | | |
|----|----|----|----|---------|----------|------|
| 12 | 0 | -1 | +1 | 3250.81 | 3268.87 | 0.56 |
| 13 | 0 | 0 | -1 | 2392.56 | 2416.80 | 1.01 |
| 14 | 0 | 0 | 0 | 6586.97 | 6568.23 | 0.28 |
| 15 | 0 | 0 | 0 | 6586.97 | 6568.23 | 0.28 |
| 16 | 0 | 0 | 0 | 6586.97 | 6568.23 | 0.28 |
| 17 | 0 | 0 | 0 | 6586.97 | 6568.23 | 0.28 |
| 18 | 0 | 0 | 0 | 6586.97 | 6568.23 | 0.28 |
| 19 | 0 | 0 | 0 | 6586.97 | 6568.23 | 0.28 |
| 20 | 0 | 0 | +1 | 12021 | 11951.36 | 0.58 |
| 21 | 0 | +1 | -1 | 3736.96 | 3796.37 | 1.59 |
| 22 | 0 | +1 | 0 | 10077.1 | 10079.91 | 0.03 |
| 23 | 0 | +1 | +1 | 18046.5 | 17918.70 | 0.71 |
| 24 | +1 | -1 | -1 | 1122.64 | 1119.35 | 0.29 |
| 25 | +1 | -1 | 0 | 3025.59 | 3027.22 | 0.05 |
| 26 | +1 | -1 | +1 | 5653.31 | 5481.31 | 3.04 |
| 27 | +1 | 0 | -1 | 3790.3 | 3824.18 | 0.89 |
| 28 | +1 | 0 | 0 | 9697.47 | 10104.13 | 4.19 |
| 29 | +1 | 0 | +1 | 17460.5 | 17873.96 | 2.37 |
| 30 | +1 | +1 | -1 | 5564.08 | 5357.75 | 3.71 |
| 31 | +1 | +1 | 0 | 13619.2 | 13830.06 | 1.55 |
| 32 | +1 | +1 | +1 | 23828.5 | 23901.57 | 0.31 |

6.3.5 Optimization of Response Data

The results of final model fitting and optimization of data were presented in graphical image, which included the 2D contour plot and the 3D surface plot. A 2D contour plot graphically represented a constant z-slice of a 3D surface. The plot consisted of 1 independent variable on the y-axis and another 1 independent variable on the x-axis. A 3D surface plot showed the response data at the z-axis with respect to the change in two independent variables at the x-axis and y-axis. The response is then represented by a

Chapter 6 Optimization Study using Response Surface Methodology (RSM)

gradient of colours in the curved response surface. A navy blue gradually changes to a light green region for low desirability area. In contrast, a yellow gradually change to a warm red region represented the high desirability area, also known as the optimal response condition. The medium desirability is demonstrated by a light blue to a pale green area. A detailed graphical interpretation based on the response displayed had been made for different sandstone acidizing conditions. Based on the data interpretation, the optimal response within the ranges or the boundaries set for simulation could be visualized and determined directly from the plots. Generally, the contour plot agrees and correspond to the 3D surface plot.

Figure 6.12 and 6.13 showed the contour plot and 3D surface plot for porosity and permeability enhancement ratio respectively of factors A: temperature and B: acid concentration. Based on the depicted figures, it is clear that both the formation temperature and acid concentration had a significant impact on the porosity and permeability enhancement ratio of the sandstone. A higher porosity enhancement ratio is resulted from both high formation temperature and acid concentration. At a high injection rate, the highest porosity and permeability enhancement ratio are recorded at 1.79 and 8.31 respectively at temperature 105 °C and 12% acid concentration. At a low and moderate injection rate, the respective highest porosity enhancement ratio is 1.61 and 1.70, and permeability enhancement ratio is 6.49 and 7.36 respectively.

Figure 6.14 displayed the contour plot and 3D surface plot for pressure drop response of factors AB. It is observed that there is a correspondence between the pressure drop response with the porosity and permeability responses. A gradual increment in both temperature and acid concentration used had resulted in increased pressure drop, corresponding to porosity and permeability improvement due to mineral dissolution. The highest pressure drop was found to be 5564.08Pa, 13619.2Pa and 23828.5Pa at low, moderate and high injection rate respectively.

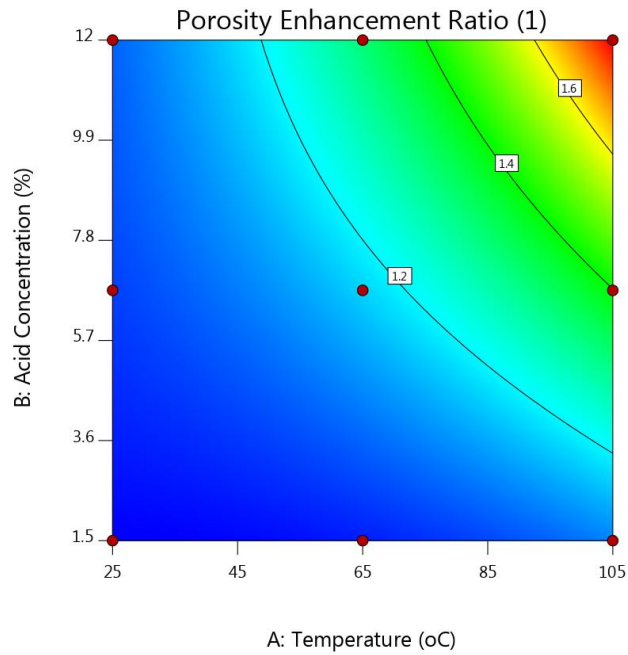
Chapter 6 Optimization Study using Response Surface Methodology (RSM)

Design-Expert® Software
 Factor Coding: Actual
 Original Scale

Porosity Enhancement Ratio (1)
 ● Design Points
 1.00802 1.79242

X1 = A: Temperature
 X2 = B: Acid Concentration

Actual Factor
 C: Acid Injection Rate = 4.46E-05



Design-Expert® Software
 Factor Coding: Actual
 Original Scale

Porosity Enhancement Ratio (1)
 ● Design points above predicted value
 ○ Design points below predicted value
 1.00802 1.79242

X1 = A: Temperature
 X2 = B: Acid Concentration

Actual Factor
 C: Acid Injection Rate = 4.46E-05

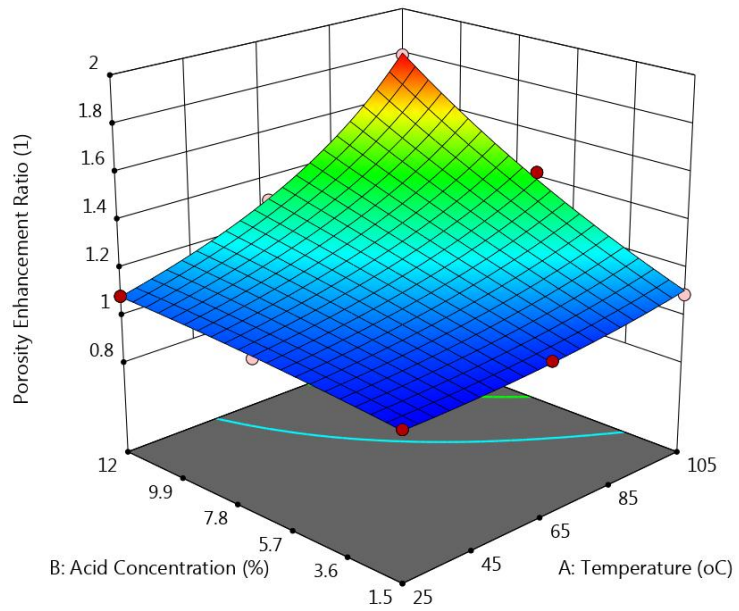


Figure 6.12 2D contour plot (upper) and 3D surface plot (bottom) for porosity enhancement ratio response of Factors AB

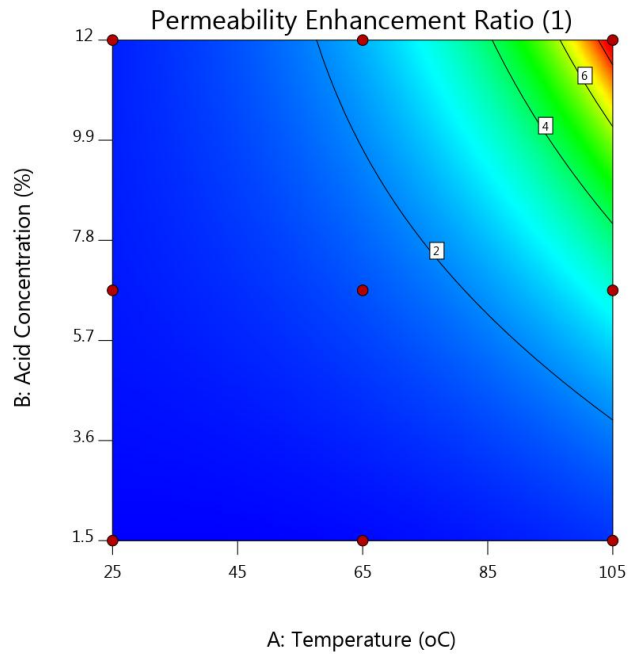
Chapter 6 Optimization Study using Response Surface Methodology (RSM)

Design-Expert® Software
 Factor Coding: Actual
 Original Scale

Permeability Enhancement Ratio (1)
 ● Design Points
 1.0243 8.31091

X1 = A: Temperature
 X2 = B: Acid Concentration

Actual Factor
 C: Acid Injection Rate = 4.46E-05



Design-Expert® Software
 Factor Coding: Actual
 Original Scale

Permeability Enhancement Ratio (1)
 ● Design points above predicted value
 ○ Design points below predicted value
 1.0243 8.31091

X1 = A: Temperature
 X2 = B: Acid Concentration

Actual Factor
 C: Acid Injection Rate = 4.46E-05

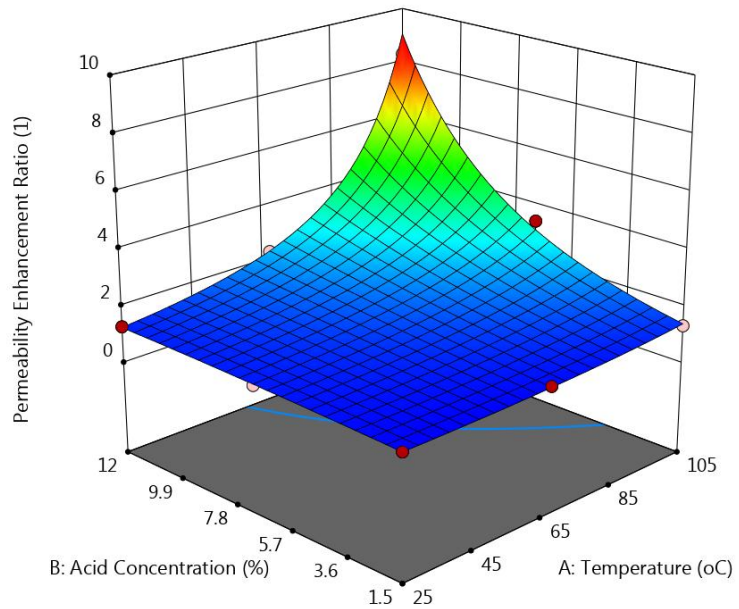


Figure 6.13 2D contour plot (upper) and 3D surface plot (bottom) for permeability enhancement ratio response of Factors AB

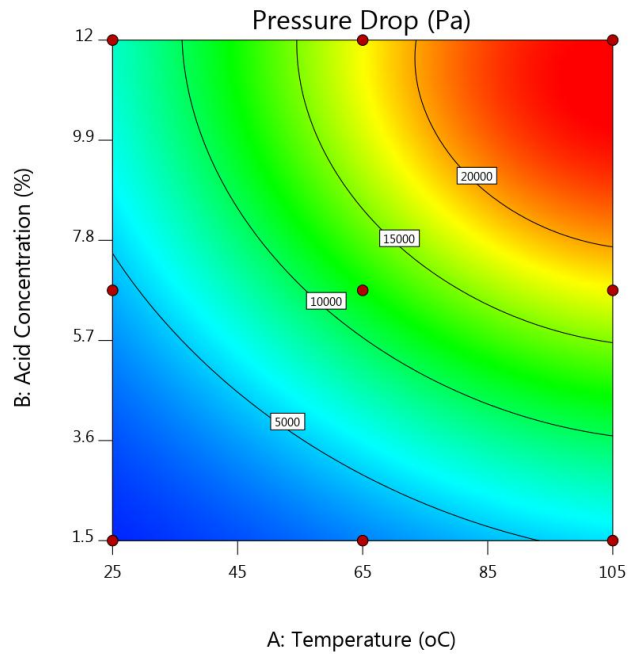
Chapter 6 Optimization Study using Response Surface Methodology (RSM)

Design-Expert® Software
 Factor Coding: Actual
 Original Scale

Pressure Drop (Pa)
 ● Design Points
 197.25 23828.5

X1 = A: Temperature
 X2 = B: Acid Concentration

Actual Factor
 C: Acid Injection Rate = 4.46E-05



Design-Expert® Software
 Factor Coding: Actual
 Original Scale

Pressure Drop (Pa)
 ● Design points above predicted value
 ○ Design points below predicted value
 197.25 23828.5

X1 = A: Temperature
 X2 = B: Acid Concentration

Actual Factor
 C: Acid Injection Rate = 4.46E-05

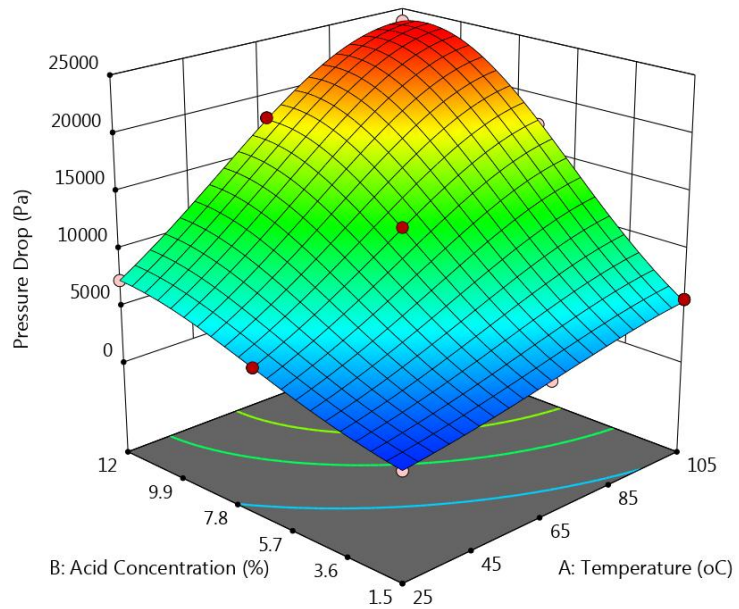


Figure 6.14 2D contour plot (upper) and 3D surface plot (bottom) for pressure drop response of Factors AB

Chapter 6 Optimization Study using Response Surface Methodology (RSM)

Figure 6.15 and 6.16 represented the contour plot and 3D surface plot for porosity and permeability enhancement ratio respectively of factors A: temperature and C: acid injection rate. According to the depicted figures, it is shown that both the formation temperature and acid injection rate had positively affected the porosity and permeability enhancement ratio of the sandstone. A higher porosity enhancement ratio is resulted from both high formation temperature and acid injection rate. However, the effect of change of acid injection rate is not as significant as the effect of change of formation temperature comparatively. At a high acid concentration, the highest porosity and permeability enhancement ratio is found to be 1.79 and 8.31 respectively at temperature 105°C and acid injection rate of 4.46×10^{-5} . At a low acid concentration, the highest porosity and permeability enhancement ratio are 1.09 and 1.32 respectively. Whereas at moderate acid concentration, the highest porosity and permeability enhancement ratio are recorded as 1.43 and 3.44 respectively.

Figure 6.17 illustrated the contour plot and 3D surface plot for pressure drop response of factors AC. Generally, the response curve showed that the pressure drop value is having a gradual increment trend when both the formation temperature and acid injection rate increased. However, the increase of pressure drop is less significant at low temperature and injection rate region. The higher the value of both the factors, the higher the pressure drop across the sandstone core. From the figure, the highest pressure drops determined at low, moderate and high acid concentration are 5653.31Pa, 17460.5Pa and 23828.5Pa respectively.

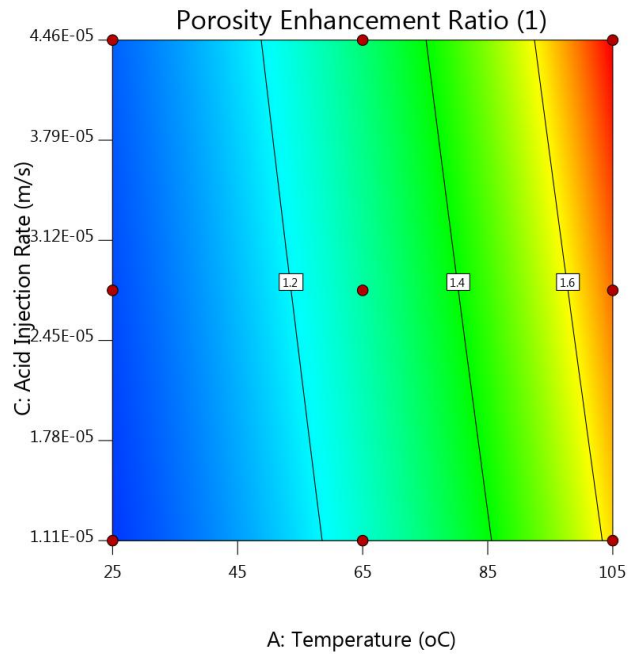
Chapter 6 Optimization Study using Response Surface Methodology (RSM)

Design-Expert® Software
 Factor Coding: Actual
 Original Scale

Porosity Enhancement Ratio (l)
 ● Design Points
 1.00802 1.79242

X1 = A: Temperature
 X2 = C: Acid Injection Rate

Actual Factor
 B: Acid Concentration = 12



Design-Expert® Software
 Factor Coding: Actual
 Original Scale

Porosity Enhancement Ratio (l)
 ● Design points above predicted value
 ○ Design points below predicted value
 1.00802 1.79242

X1 = A: Temperature
 X2 = C: Acid Injection Rate

Actual Factor
 B: Acid Concentration = 12

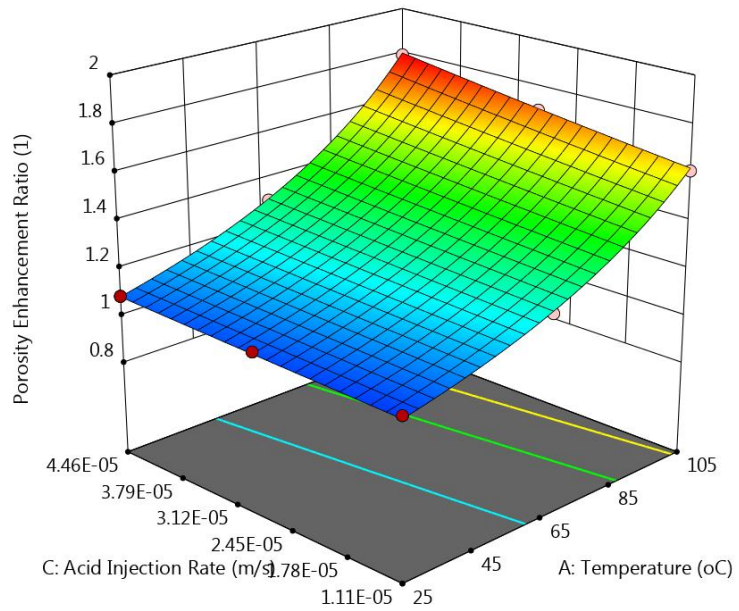


Figure 6.15 2D contour plot (upper) and 3D surface plot (bottom) for porosity enhancement ratio response of Factors AC

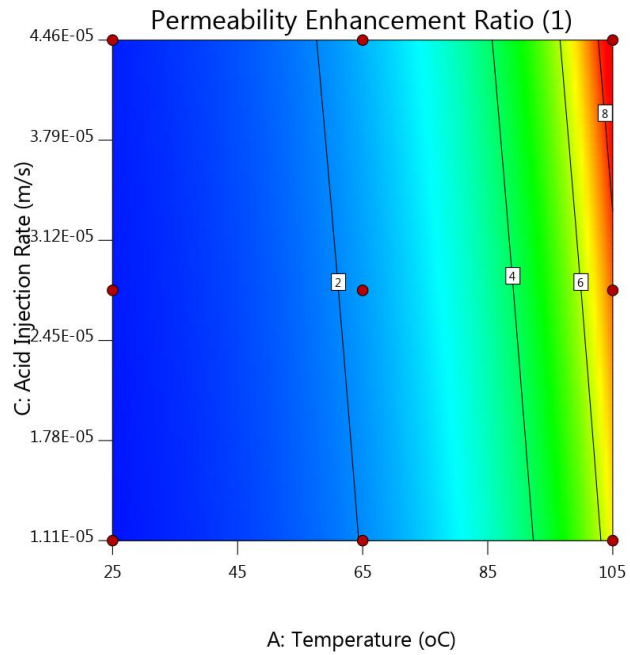
Chapter 6 Optimization Study using Response Surface Methodology (RSM)

Design-Expert® Software
 Factor Coding: Actual
 Original Scale

Permeability Enhancement Ratio (1)
 ● Design Points
 1.0243 8.31091

X1 = A: Temperature
 X2 = C: Acid Injection Rate

Actual Factor
 B: Acid Concentration = 12



Design-Expert® Software
 Factor Coding: Actual
 Original Scale

Permeability Enhancement Ratio (1)
 ● Design points above predicted value
 ○ Design points below predicted value
 1.0243 8.31091

X1 = A: Temperature
 X2 = C: Acid Injection Rate

Actual Factor
 B: Acid Concentration = 12

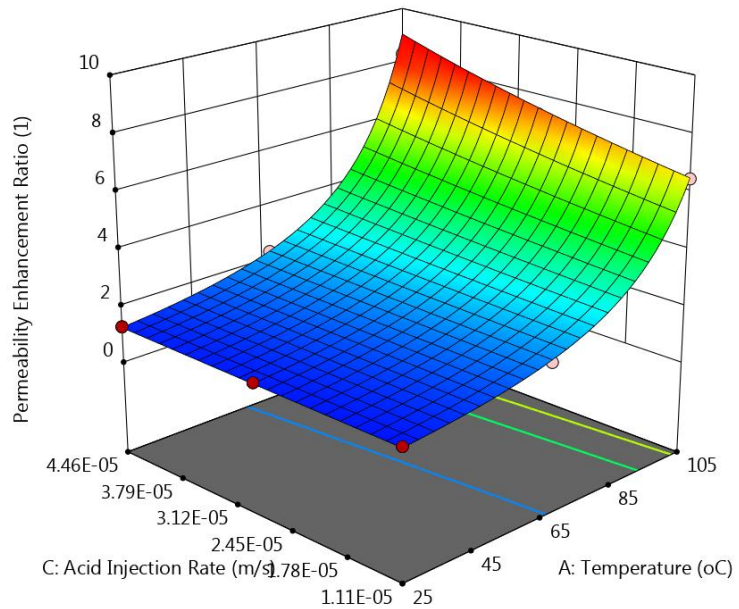


Figure 6.16 2D contour plot (upper) and 3D surface plot (bottom) for permeability enhancement ratio response of Factors AC

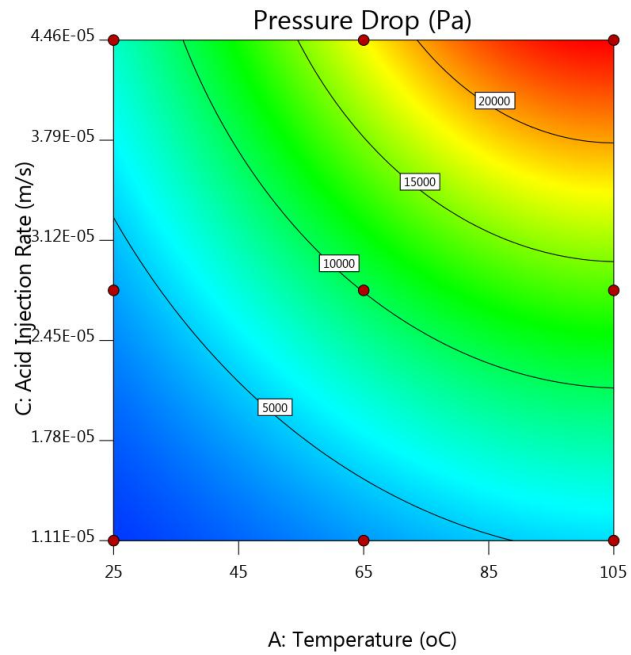
Chapter 6 Optimization Study using Response Surface Methodology (RSM)

Design-Expert® Software
Factor Coding: Actual
Original Scale

Pressure Drop (Pa)
● Design Points
197.25 23828.5

X1 = A: Temperature
X2 = C: Acid Injection Rate

Actual Factor
B: Acid Concentration = 12



Design-Expert® Software
Factor Coding: Actual
Original Scale

Pressure Drop (Pa)
● Design points above predicted value
○ Design points below predicted value
197.25 23828.5

X1 = A: Temperature
X2 = C: Acid Injection Rate

Actual Factor
B: Acid Concentration = 12

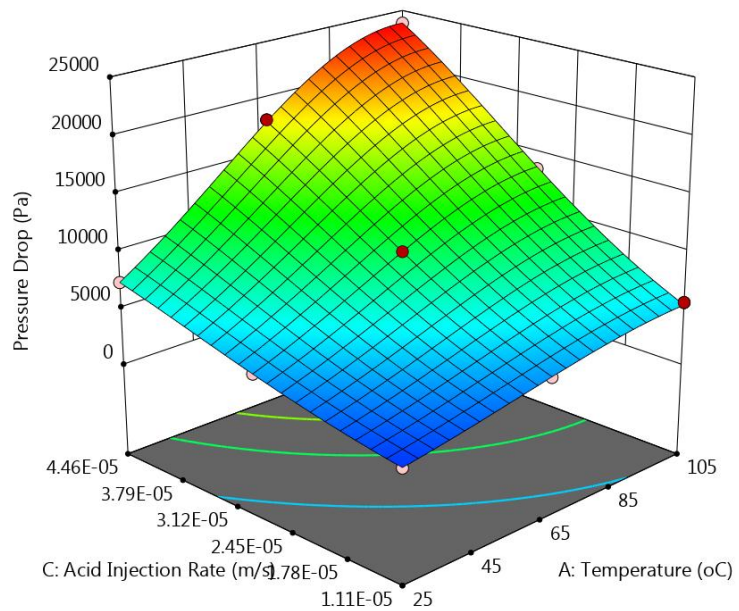


Figure 6.17 2D contour plot (upper) and 3D surface plot (bottom) for pressure drop response of Factors AC

Chapter 6 Optimization Study using Response Surface Methodology (RSM)

Figure 6.18 and 6.19 revealed the contour plot and 3D surface plot for porosity and permeability enhancement ratio respectively of factors B: acid concentration and C: acid injection rate. In view of the depicted figures, it is observed that both the acid concentration and acid injection rate showed a positive influence on the porosity and permeability enhancement ratio of the sandstone. A higher porosity and permeability enhancement ratio are indicated from both high acid concentration and acid injection rate. Nevertheless, the effect of change of acid injection rate is relatively less significant than that of change of acid concentration. At a high temperature, the highest porosity and permeability enhancement ratio is denoted at 1.79 and 8.31 respectively at 12% acid concentration and acid injection rate of 4.46×10^{-5} m/s. At a low and moderate temperature, the highest porosity enhancement ratio is 1.09 and 1.31 respectively; and the highest permeability enhancement ratio is 1.28 and 2.29 respectively.

Figure 6.20 represented the contour plot and 3D surface plot for pressure drop response of factors BC. In general, the response curve showed that the pressure drop value is having a gradual increment trend due to an increase in both the acid concentration and acid injection rate. Nevertheless, the magnitude of pressure drop is less significant at low acid concentration and injection rate condition. A higher pressure drop is recorded at a higher the value of both the variables. As shown in the figure, the highest pressure drops denoted at low, moderate and high formation temperature are 7351.59Pa, 18046.5Pa and 23828.5Pa respectively.

Overall, it is concluded that the highest porosity enhancement ratio was resulted from high temperature range of 100 °C to 105 °C. A high temperature would increase the hydrolysis rate of the acid, hence producing more reactants to react with the minerals presented in the sandstone core. The optimum acid concentration used should be ranging from 11% – 12% and the optimum acid injection rate is having the range of 4.00×10^{-5} to 4.46×10^{-5} . A high acid concentration would favour the acidizing process as a more rapid reactions would occur between the acid and the rock. Meanwhile, a high acid injection rate would enhance the penetration distance, hence increase the reaction surface between the acid and the minerals.

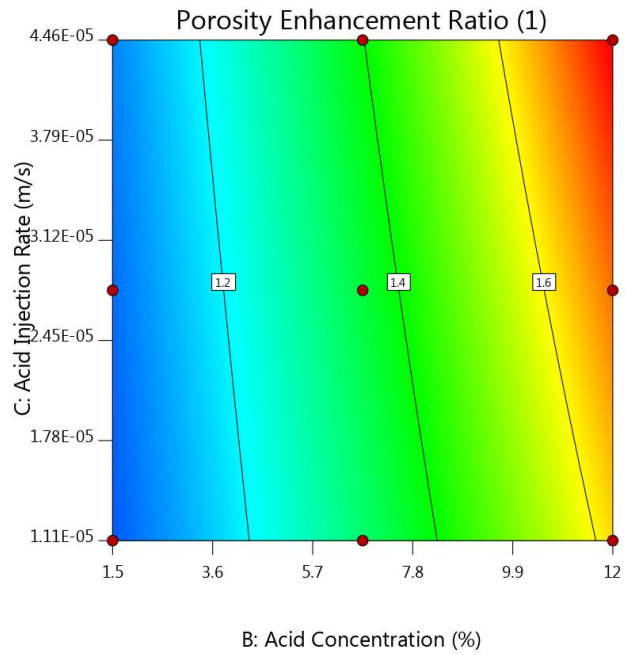
Chapter 6 Optimization Study using Response Surface Methodology (RSM)

Design-Expert® Software
 Factor Coding: Actual
 Original Scale

Porosity Enhancement Ratio (1)
 ● Design Points
 1.00802 1.79242

X1 = B: Acid Concentration
 X2 = C: Acid Injection Rate

Actual Factor
 A: Temperature = 105



Design-Expert® Software
 Factor Coding: Actual
 Original Scale

Porosity Enhancement Ratio (1)
 ● Design points above predicted value
 ○ Design points below predicted value
 1.00802 1.79242

X1 = B: Acid Concentration
 X2 = C: Acid Injection Rate

Actual Factor
 A: Temperature = 105

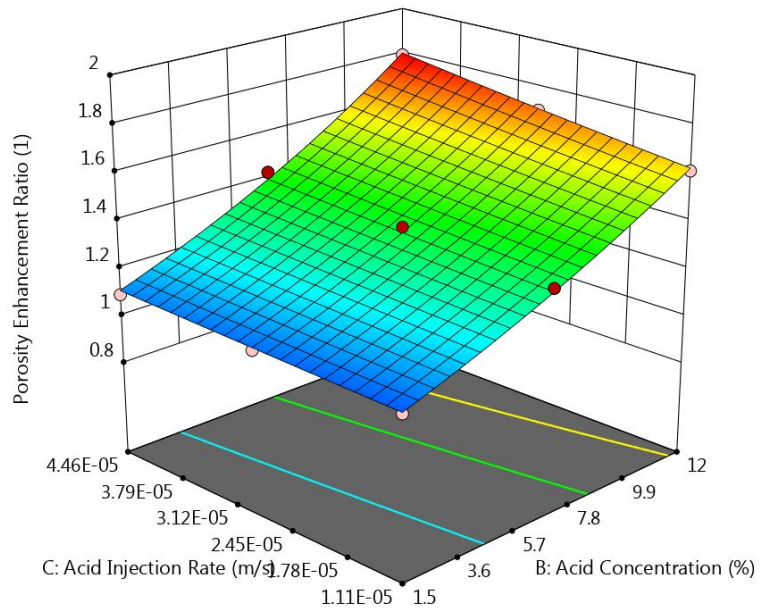


Figure 6.18 2D contour plot (upper) and 3D surface plot (bottom) for porosity enhancement ratio response of Factors BC

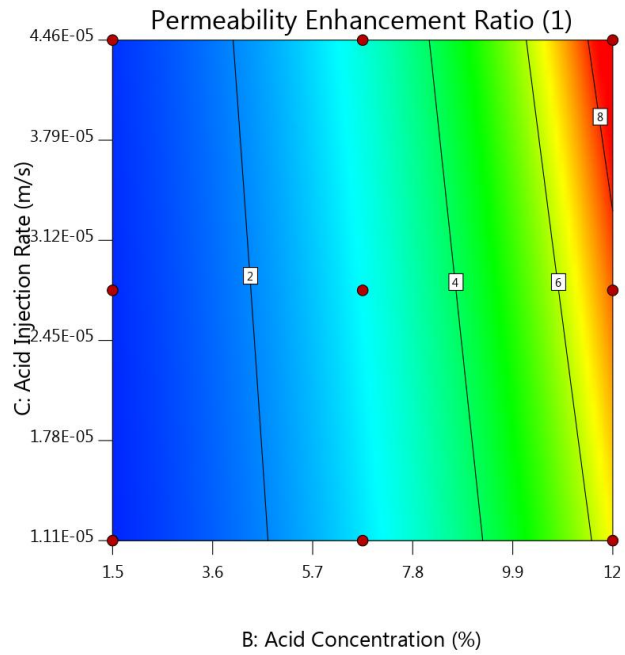
Chapter 6 Optimization Study using Response Surface Methodology (RSM)

Design-Expert® Software
 Factor Coding: Actual
 Original Scale

Permeability Enhancement Ratio (1)
 ● Design Points
 1.0243 8.31091

X1 = B: Acid Concentration
 X2 = C: Acid Injection Rate

Actual Factor
 A: Temperature = 105



Design-Expert® Software
 Factor Coding: Actual
 Original Scale

Permeability Enhancement Ratio (1)
 ● Design points above predicted value
 ○ Design points below predicted value
 1.0243 8.31091

X1 = B: Acid Concentration
 X2 = C: Acid Injection Rate

Actual Factor
 A: Temperature = 105

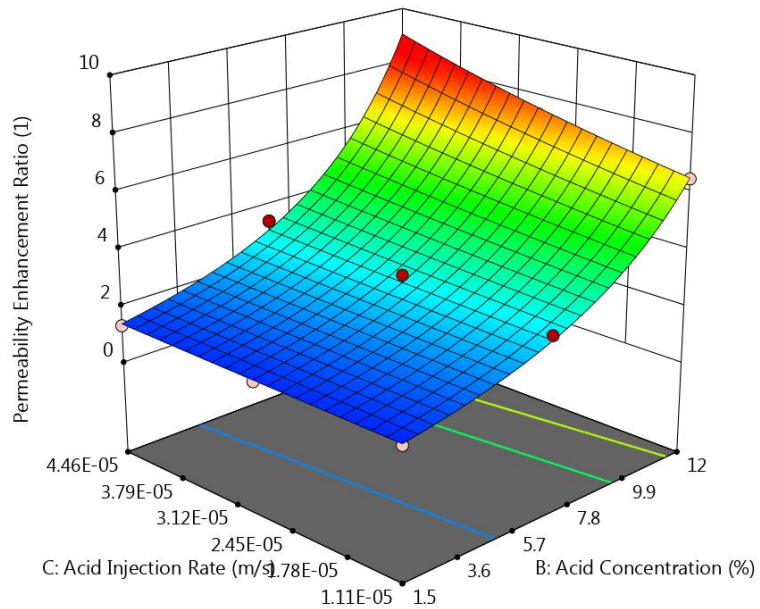


Figure 6.19 2D contour plot (upper) and 3D surface plot (bottom) for permeability enhancement ratio response of Factors BC

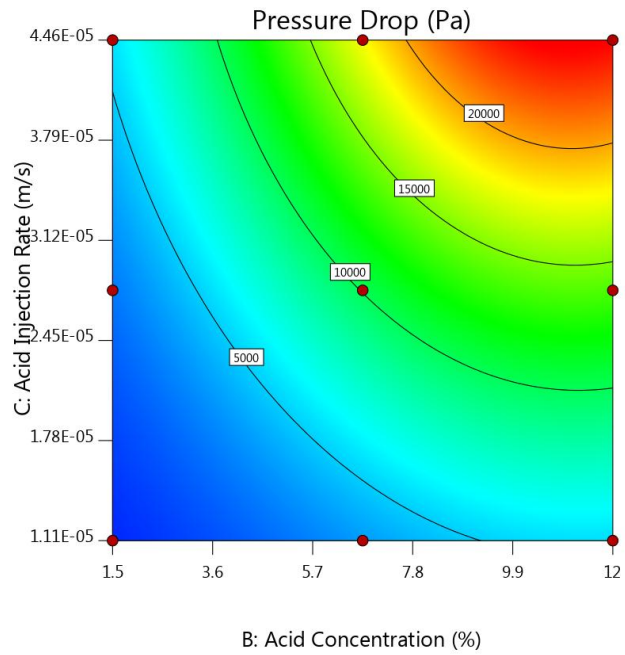
Chapter 6 Optimization Study using Response Surface Methodology (RSM)

Design-Expert® Software
Factor Coding: Actual
Original Scale

Pressure Drop (Pa)
● Design Points
197.25 23828.5

X1 = B: Acid Concentration
X2 = C: Acid Injection Rate

Actual Factor
A: Temperature = 105



Design-Expert® Software
Factor Coding: Actual
Original Scale

Pressure Drop (Pa)
● Design points above predicted value
○ Design points below predicted value
197.25 23828.5

X1 = B: Acid Concentration
X2 = C: Acid Injection Rate

Actual Factor
A: Temperature = 105

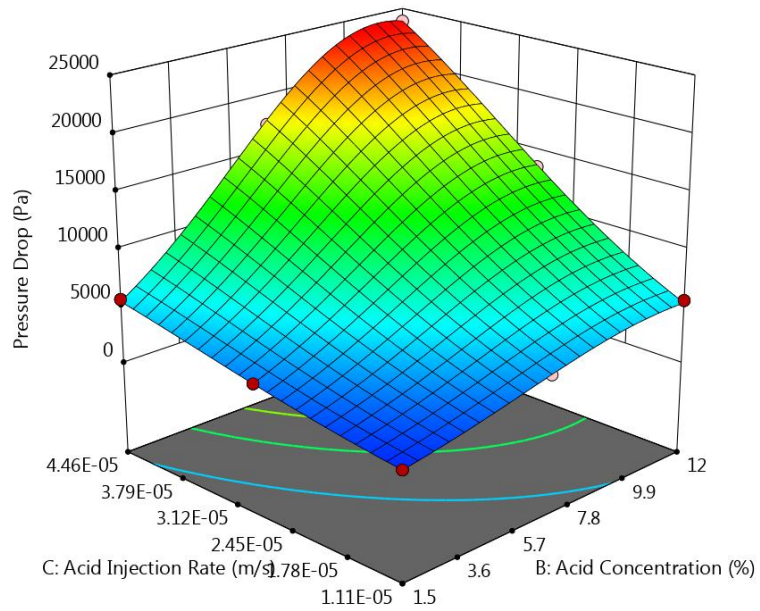


Figure 6.20 2D contour plot (upper) and 3D surface plot (bottom) for pressure drop response of Factors BC

6.4 Summary of Chapter

In conclusion, a study of the integrated effects of temperature, acid concentration and acid injection rate on sandstone acidizing performance have been presented. A response surface methodology (RSM) have been employed as an optimization approach to perform the empirical modelling and statistical analysis. A 3^3 full factorial design of experiment (DOE) had been applied and all the simulation runs were conducted using the mechanistic model developed in chapter 3 using COMSOL Multiphysics. Three responses had been obtained as the quality indication of the efficiency of sandstone acidizing, which included the porosity enhancement ratio, permeability enhancement ratio and the pressure drop.

Three quadratic empirical models that considered the combined effects of the three independent variables had been developed for the porosity, permeability and pressure drop responses. The results from the analysis of variance (ANOVA) had reflected that the predicted models are accurate, significant, reliable and well fitted with the actual simulation results. Therefore, these empirical models could be further applied to predict, improve and optimize the efficiency of sandstone acidizing. In summary, the optimization study based on the response surface methodology (RSM) presented in chapter 6 had fulfilled research objective 5, which is to determine an optimal solution for sandstone acidizing process as well as development of empirical models.

Relevant publications that had been arisen from chapter 4 are:

1. **Leong, V. H.**, Mahmud, H. B., Law, M. C., Foo, C. Y. H. and Tan, I. S. (2018). An optimization approach for sandstone acidizing process using response surface methodology (RSM) and numerical simulation. *Journal of Petroleum Science and Engineering*. Elsevier B. V. (Under review)
2. **Leong, V. H.**, Mahmud, H. B., Law, M. C., Foo, C. Y. H. and Tan, I. S. (2018). An optimization framework for sandstone acidizing using design of experiment (DOE) and mathematical modelling. *In Proceeding: 11th Curtin University Technology, Science and Engineering (CUTSE) International Conference 2018*. Curtin University, Miri, Sarawak, Malaysia. 26th – 28th November 2018.

Chapter 7 Conclusions and Recommendations

7.1 Conclusion

This study was carried out to determine the optimum design of sandstone acidizing process for a successful core stimulation purpose. This study had focused on the use of the fluoroboric acid (HBF_4) in improving the porosity and permeability of the sandstone core. The ultimate goals of this research were to conduct a preliminary screening on all acids, proposal of suitable modelling approach, development of a mechanistic model, parametric study using sensitivity analysis as well as optimization of the sandstone acidizing design. The three main aspects that had been considered in this study included the numerical study, parametric study and optimization study. Based on these major aspects, there are a few conclusions that were drawn to attention as highlighted in the following sub-sections. These conclusions served as the major contribution to the knowledge generated from this thesis.

7.1.1 Numerical Study

At room temperature of 25°C , the porosity and permeability enhancement ratio obtained by using fluoroboric acid were 1.07 and 1.23 respectively. The results were not significant due to low hydrolysis rate that limits the acid penetration speed. When the temperature increases to 105°C , the acid-rock chemical reaction shift to the right more drastically, hence producing more HF to dissolve more minerals content. Then, this resulted in significant porosity and permeability improvement in the sandstone matrix of 1.67 and 7.06 respectively. This had proven that the efficiency of HBF_4 is more remarkable at high temperature as compared to low temperature condition. Hence, research question 1 had been answered and hypothesis 1 was accepted.

7.1.2 Parametric Study

Based on the results of parametric study, an overall enhancement in porosity and permeability were observed when the acid concentration is increased at all three temperature conditions. This is because higher rate of mineral dissolution by the acid is achieved when the acid concentration increases. However, the level of increment is comparatively more significant at higher temperatures. From the pressure drop curve, it is also shown that a greater pressure drop is obtained at high temperatures. This is due to increase hydrolysis rate at high temperatures to produce HF acid. Hence, a high HBF_4 acid concentration is better for sandstone acidizing performance especially at high temperature.

Furthermore, in general, porosity and permeability were improved when the acid injection rate is increased at the three ranges of temperatures. Clearly, this is due to an increased penetration rate into the sandstone matrix when the injection rate is higher. Nevertheless, the trend of increment becomes steeper as the temperature increases. A sharper pressure drop pattern is also observed. This is governed by the increased rate of hydrolysis that allowed increase overall reactions. Thus, it is deduced that a high acid injection rate is more favourable for sandstone acidizing results, particularly at high formation temperature.

Therefore, the conclusion made had clearly addressed research question 2 and hypothesis 2 had also been accepted. Although both acid concentration and acid injection rate revealed positive effects to the porosity and permeability enhancement of sandstone matrix, it is observed that the effect of acid concentration is more remarkable as compared to that of acid injection rate. Therefore, it is recommended for optimization approach to be conducted to extensively study the integrated effects of formation temperature, acid concentration and acid injection rate in sandstone acidizing.

7.1.3 Optimization Study

The optimization study had indicated that all the three variables had significant effects on the enhancement of porosity and permeability of sandstone after acid stimulation. Nevertheless, it is observed from the contour map and response curve that the change in formation temperature and acid concentration are more significant on sandstone porosity and permeability improvement. Meanwhile, it is implied that the effect of change in acid injection rate is less significant under comparison with the other two factors. The optimum conditions that would favour the sandstone acidizing performance determined from this study included a formation temperature ranged from 95 °C – 105 °C, acid concentration ranged from 10% – 12% and acid injection rate ranged from 4.0E-5 m/s to 4.5E-5 m/s.

Generally, this study had proven the reliability and robustness of RSM as an optimization tool for sandstone acid stimulation. The empirical models could also be further modified and improved by considering more aspects that might influence the efficiency of sandstone acidizing. Thus, this conclusion had solved research question 3 and had proven hypothesis 3 made in Chapter 1.

7.1.4 Overall Remarks

Overall, this research had narrowed down the research gap identified in the introductory Chapter 1. The conclusions derived from this study had clearly answered all three research questions and their respective hypotheses are also accepted. This thesis had contributed to the development of a new mechanistic model for HBF_4 sandstone acidizing process using COMSOL® Multiphysics approach. Furthermore, this research had newly incorporated the RSM optimization approach in optimizing the sandstone acidizing parameters using HBF_4 , which was not done previously. In addition, this thesis had thrown some insights into the use of fluoroboric acid for sandstone acidizing at elevated temperature, replacing the mud acid. This research also made some contributions by identifying parameters that are significant in affecting sandstone acidizing using HBF_4 . These findings would help the petroleum engineers to diversify the choice of acid in designing the sandstone acid stimulation method.

7.2 Recommendations

There are a few recommendations for future work that had been identified from this study. The recommendations are made based on two areas of research, which included the modelling work and the experimental work.

In terms of modelling study, it is suggested to study the upscaling of the current core scale model to a field scale model. In fact, it is vital to model the field scale situation for accurate prediction and better understanding of the sandstone acidizing process. However, this work would require the availability of the real field data to obtain the necessary information about the reservoir. Also, detailed characterization of the reservoir would be needed prior to perform the study on acid stimulation on a field scale. This would definitely be more beneficial for the engineer to plan a successful matrix acidizing treatment design.

Besides, it is recommended to further study other parameters or sandstone conditions. For instance, the effect of reservoir heterogeneity could be studied and compared against the homogeneous condition. A more detailed analysis of the sandstone mineralogy and the composition of different minerals could be obtained and modelled. Moreover, it is recommended to integrate the CT-scanned of an actual sandstone core into current model to study the effect of sandstone porosity heterogeneity and mineral heterogeneity. Approaches adopted by [Liu et al. \(2017\)](#) and [Mostaghimi et al. \(2016\)](#) could be referred in future study in these areas of research.

In term of experimental study, it is also recommended to conduct a core flooding experiment to recheck the validity of the model. There are a number of characterization test and analysis than can be performed in the future to characterize the effectiveness of HBF_4 under various conditions such as Poro-Perm, FESEM, CT Scan, ICP and ^{19}F NMR. These outlooks would be able to make a significant breakthrough and positive growth in the oil and gas industry by improving the HBF_4 acidizing model, in order to predict and forecast the sandstone acidizing process at elevated temperatures.

References

- Abdelmoneim, S. S., & Nasr-El-Din, H. A. 2015. Determining the Optimum HF Concentration for Stimulation of High Temperature Sandstone Formations. *SPE European Formation Damage Conference and Exhibition, 3-5 June, Budapest, Hungary*. Society of Petroleum Engineers. <https://doi.org/10.2118/174203-MS>
- Aboud, R. S., Smith, K. L., Forero Pachon, L., & Kalfayan, L. J. 2007. Effective Matrix Acidizing in High-Temperature Environments. *SPE Annual Technical Conference and Exhibition, 11-14 November, Anaheim, California, U.S.A.* Society of Petroleum Engineers. <https://doi.org/10.2118/109818-MS>
- Al-Dahlan, M. N., Nasr-El-Din, H. A., & Al-Qahtani, A. A. 2001. Evaluation of Retarded HF Acid Systems. *SPE International Symposium on Oilfield Chemistry, 13-16 February, Houston, Texas*. Society of Petroleum Engineers. <https://doi.org/10.2118/65032-MS>
- Al-harbi B. G., Al Dahlan, M. N., & Khaldi, M. H. 2012. Aluminum and Iron Precipitation During Sandstone Acidizing Using Organic-HF Acids. *SPE International Symposium and Exhibition on Formation Damage Control, 15-17 February, Lafayette, Louisiana, USA*. Society of Petroleum Engineers. <https://doi.org/10.2118/151781-MS>
- Al-Harbi, B. G., Al-Khaldi, M. H., & AlDossary, K. A. 2011. Interactions of Organic-HF Systems with Aluminosilicates: Lab Testing and Field Recommendations. *SPE European Formation Damage Conference, 7-10 June, Noordwijk, The Netherlands*. Society of Petroleum Engineers. <https://doi.org/10.2118/144100-MS>
- Al-Harthy, S., Bustos. O. A., Fuller, M. J., Hamzah, N. E., Ismail, M. I., & Parapat, A. 2009. Options for High-Temperature Well Stimulation. *Oilfield Review*. **20**(4). 52-53. Schlumberger

- Al-Shaalan, T. M., & Nasr-El-Din, H. A. 2000. Mathematical Modeling of Sandstone Stimulation: A Critical Review of Available Models. *CORROSION 2000*, 26-31 March, Orlando, Florida. NACE International.
- Alhubail, M. M., Misra, A., & Barati, R. 2017. A Novel Acid Transport Model with Robust Finite Element Discretization. *SPE Kingdom of Saudi Arabia Annual Technical Symposium and Exhibition*, 24-27 April, Dammam, Saudi Arabia. Society of Petroleum Engineers. <https://doi.org/10.2118/188030-MS>
- Almashjary, K. H., Khalid, M., Dharaskar, S., Jagadish, P., Walvekar, R. & Gupta, T. C. S. M. 2018. Optimisation of extractive desulfurization using Chline Chloride-based deep eutectic solvents. *Fuel*. **234**. 1388-1400. Elsevier B.V. <https://doi.org/10.1016/j.fuel.2018.08.005>
- Ali, M. T., & Nasr-El-Din, H. A. 2018. A Robust Model to Simulate Dolomite-Matrix Acidizing. *SPE Production & Operations*. Society of Petroleum Engineers. <https://doi.org/10.2118/191136-PA>
- Ali, S. A., Ermel, E., Clarke, J., Fuller, M. J., Xiao, Z., & Malone, B. 2008. Stimulation of High-Temperature Sandstone Formations from West Africa with Chelating Agent-Based Fluids. *SPE Production & Operations*. **23**(01). 32-38. Society of Petroleum Engineers. <https://doi.org/10.2118/93805-PA>
- Ali, S., Frenier, W.W., Lecerf, B., Ziauddin, M., Kotlar, H.K., Nasr-el-din, H.A., & Vikane, O. 2004. Virtual Testing: The Key to a Stimulating Process. *Oilfield Review*. **16**(1). 58-68. Schlumberger
- Ameri, A., Nick, H. M., Ilangovan, N., & Peksa, A. 2016. A Comparative Study on the Performance of Acid Systems for High Temperature Matrix Stimulation. *Abu Dhabi International Petroleum Exhibition & Conference*, 7-10 November, Abu Dhabi, UAE. Society of Petroleum Engineers. <https://doi.org/10.2118/183399-MS>
- Andotra, G. 2014. Investigating the Use of Chelating Agents for Clay Dissolution and Sandstone Acidizing Purposes. *Master's thesis*. Texas A&M University. <http://hdl.handle.net/1969.1/153620>

References

- Aneto, N. 2012. An In-depth Investigation of an Aluminum Chloride Retarded Mud Acid System on Sandstone Reservoirs. *Master's thesis*. Texas A&M University. <http://hdl.handle.net/1969.1/ETD-TAMU-2012-05-10779>
- Ayorinde, A., Granger, C., & Thomas, R. L. 1992. The application of Fluoroboric Acid in Sandstone Matrix Acidizing: A Case Study. *21st Annual Convention Proceedings*. **2**. 235-261. Indonesian Petroleum Association
- Ayotte, P., Hebert, M., & Marchand, P. 2005. Why is hydrofluoric acid a weak acid? *The Journal of Chemical Physics*. **123**(18). <https://doi.org/10.1063/1.2090259>
- Baghel, V. S., & Pravesh, J. 2016. A Semi-Empirical Carbonate Acidizing Model for Chelating-Agent-Based Fluids. *IADC/SPE Asia Pacific Drilling Technology Conference, 22-24 August, Singapore*. Society of Petroleum Engineers. <https://doi.org/10.2118/180590-MS>
- Bartko, K. M., Acock, A. M., Robert, J. A., & Thomas, R. L. 1997. A Field Validated Matrix Acidizing Simulator for Production Enhancement in Sandstone and Carbonates. *SPE European Formation Damage Conference, 2-3 June, The Hague, Netherlands*. Society of Petroleum Engineers. <https://doi.org/10.2118/38170-MS>
- Bernabe, Y., Mok, U., & Evans, B. 2003. Permeability-porosity relationships in tocks subjected to various evolution processes. *Pure and Applied Geophysics*. **160**(5-6). 937-960. Springer Nature. <https://doi.org/10.1007/PL00012574>
- Bertaux, J. 1989. Treatment-Fluid Selection for Sandstone Acidizing: Permeability Impairment in Potassic Mineral Sandstones. *SPE Production Engineering*. **4**(1). 41-48. Society of Petroleum Engineers. <https://doi.org/10.2118/15884-PA>
- Box, G. E. P. & Wilson, K. B. 1951. On the Experimental Attainment of Optimum Conditions. *Journal of the Royal Statistical Society. Series B (Methodological)*. **13**(1). 1-45. Wiley. <https://www.jstor.org/stable/2983966>
- Bryant, S. L. 1991. An Improved Model of Mud Acid/Sandstone Chemistry. *SPE Annual Technical Conference and Exhibition, 6-9 October, Dallas, Texas*. Society of Petroleum Engineers. <https://doi.org/10.2118/22855-MS>

- Bybee, K. 2003. Matrix Acid Stimulation. *Journal of Petroleum Technology*. **55**(7). 49-50. Society of Petroleum Engineers. <https://doi.org/10.2118/0703-0049-JPT>
- Cipolla, C. L. 2003. Overview: Well Stimulation. *Journal of Petroleum Technology*. **55**(7). 40-40. Society of Petroleum Engineers. <https://doi.org/10.2118/0703-0040-JPT>
- Conservancy. 2016. Risks of Fracking and Other Well Stimulation Treatments. <https://www.conservancy.org/our-work/policy/oil/hydraulic-fracturing-acidizing>
- Coulter, G. 2011. Technology Focus: Well Stimulation. *Journal of Petroleum Technology*. **63**(6). 62-62. Society of Petroleum Engineers. <https://doi.org/10.2118/0611-0062-JPT>
- Coulter, G. 2012. Technology Focus: Well Stimulation. *Journal of Petroleum Technology*. **64**(6). 90-90. Society of Petroleum Engineers. <https://doi.org/10.2118/0612-0090-JPT>
- Crowe, C. W. 1986. Precipitation of Hydrated Silica from Spent Hydrofluoric Acid: How Much of a Problem Is It? *Journal of Petroleum Technology*. **38**(1). 1234-1240. Society of Petroleum Engineers. <https://doi.org/10.2118/13083-PA>
- Crowe, C., Masmonteil, J., & Thomas, R. 1992. Trends in matrix acidizing. *Oilfield Review*. **4**(4). 24-40. Schlumberger
- Da Motta, E. P., Plavnik, B., Schechter, R. S., & Hill, A. D. 1993. Accounting for Silica Precipitation in the Design of Sandstone Acidizing. *SPE Production & Facilities*. **8**(2). 138-144. Society of Petroleum Engineers. <https://doi.org/10.2118/23802-PA>
- De Oliveira, T. J. L., De Melo, A. R., Oliveira, J. A. A., & Pereira, A. Z. I. 2012. Numerical Simulation of the Acidizing Process and PVBT Extraction Methodology Including Porosity/Permeability and Mineralogy Heterogeneity. *SPE International Symposium and Exhibition on Formation Damage Control, 15-17 February, Lafayette, Louisiana, USA*. Society of Petroleum Engineers. <https://doi.org/10.2118/151823-MS>
- Dehghani, M. 2010. Matrix Acidizing Stimulation. *The 1st International Applied Geological Congress, 26-28 April 2010, Iran*

References

- Dong, K., Jin, X., Zhu, D., & Hill, A. D. 2014. The Effect of Core Dimensions on the Optimal Acid Flux in Carbonate Acidizing. *SPE International Symposium and Exhibition on Formation Damage Control*, 26-28 February, Lafayette, Louisiana, USA. Society of Petroleum Engineers. <https://doi.org/10.2118/168146-MS>
- Dong, K., Zhu, D., & Hill, A.D. 2017. Theoretical and Experimental Study on Optimal Injection Rates in Carbonate Acidizing. *SPE Journal*. **22**(3). 892-901. Society of Petroleum Engineers. <https://doi.org/10.2118/178961-PA>
- Ebrahim, A. S., Garrouch, A. A. & Lababidi, H. M. S. 2014. Automating sandstone acidizing using a rule-based system. *Journal of Petroleum Exploration and Production Technology*. **4**(4). 381-396. Springer Nature. <https://doi.org/10.1007/s13202-014-0104-3>
- Economides, M. J., & Nolte, K. G. 2000. *Reservoir stimulation* (3rd edition). Chichester, England: Wiley
- Economides, M. J., Hill, A. D., Ehlig-Economides, C., & Zhu, D. 2013, *Petroleum Production Systems* (2nd edition). Upper Saddle River, NJ: Prentice Hall
- Farley, J. T., Miller, B. M., & Schoettle, V. 1970. Design Criteria for Matrix Stimulation with Hydrochloric-Hydrofluoric Acid. *Journal of Petroleum Technology*. **22**(4). 433-440. Society of Petroleum Engineers. <https://doi.org/10.2118/2621-PA>
- Feng, P., Wang, D., Liu, G., Wang, H., & Economides, M. J. 2011. Sandstone Reservoir Stimulation Using High-Temperature Deep-Penetrating Acid. *SPE Western North America Region Meeting*, 7-11 May, Anchorage, Alaska, USA. Society of Petroleum Engineers. <https://doi.org/10.2118/143942-MS>
- Flood, D. T. 1933. Fluorobenzene. *Organic Syntheses*. **13**. 46. <https://doi.org/10.15227/orgsyn.013.0046>
- Fogler, H. S., Lund, K., & McCune, C. C. 1976. Predicting the Flow and Reaction of HCl/HF Acid Mixtures in Porous Sandstone Cores. *Society of Petroleum Engineers Journal*. **16**(5). 248-260. Society of Petroleum Engineers. <https://doi.org/10.2118/5646-PA>

References

- Frenier, W., Brady, M., Al-Harthy, S., Arangath, R., Chan, K. S., Flamant, N., & Samuel, M. 2004. Hot Oil and Gas Wells Can Be Stimulated Without Acids. *SPE Production & Facilities*. **19**(4). 189-199. Society of Petroleum Engineers. <https://doi.org/10.2118/86522-PA>
- Garcia, E. A. R., LaBlanc, A., Beuterbaugh, A., & Calabrese, T. 2016. Developments in Sandstone HF Acidizing: HF Fluid Compatible with Na or K Brines and Carbonate-Laden Mineralogy for High Temperatures (360 °F). *SPE International Conference and Exhibition on Formation Damage Control*, 24-26 February, Lafayette, Louisiana, USA. Society of Petroleum Engineers. <https://doi.org/10.2118/178999-MS>
- Gdanski, R. D. 1998. Kinetics of Tertiary Reactions of Hydrofluoric Acid on Aluminosilicates. *SPE Production & Facilities*. **13**(2). 75-80. Society of Petroleum Engineers. <https://doi.org/10.2118/31076-PA>
- Gdanski, R. D. 1999. Kinetics of the Secondary Reaction of HF on Alumino-Silicates. *SPE Production & Facilities*. **14**(4). 260-268. Society of Petroleum Engineers. <https://doi.org/10.2118/59094-PA>
- Gdanski, R. D. 2000. Kinetics of the Primary Reaction of HF on Alumino-Silicates. *SPE Production & Facilities*. **15**(4). 279-287. Society of Petroleum Engineers. <https://doi.org/10.2118/66564-PA>
- Gidley, J. L. 1985. Acidizing Sandstone Formations: A Detailed Examination of Recent Experience. *SPE Annual Technical Conference and Exhibition*, 22-26 September, Las Vegas, Nevada. Society of Petroleum Engineers. <https://doi.org/10.2118/14164-MS>
- Golfier, F., Bazin, B., Lenormand, R. & Quintard, M. 2004. Core-scale description of porous media dissolution during acid injection - part I: Theoretical development. *Computational & Applied Mathematics*. **23**(2-3). 173-194. <https://doi.org/10.1590/S0101-82052004000200005>
- Golfier, F., Quintard, M., Bazin, B. & Lenormand, R. 2006. Core-scale description of porous media dissolution during acid injection - part II: Calculation of the

References

- Effective Properties. *Computational & Applied Mathematics*. **25**(1). 55-78.
<https://doi.org/10.1590/S1807-03022006000100003>
- Gomaa, A. M., Cutler, J., Qu, Q., Boles, J., & Wang, X. 2013. An Effective Single-Stage Acid System for Sandstone Formations. *SPE European Formation Damage Conference & Exhibition, 5-7 June, Noordwijk, The Netherlands*. Society of Petroleum Engineers. <https://doi.org/10.2118/165147-MS>
- Guimarães, M. S., Grana, T. de A., & Matos Sarkis, S. R. 2017. Study and Simulation of Matrix Acidizing in Sandstones Reservoirs Applied to Injection Wells of the Mature Fields. *SPE Latin America and Caribbean Mature Fields Symposium, 15-16 March, Salvador, Bahia, Brazil*. Society of Petroleum Engineers. <https://doi.org/10.2118/184928-MS>
- Guo, B. Y., Lyons, W. C., & Ghalambor, A. 2007. Chapter 16 - Matrix Acidizing. *Petroleum Production Engineering, A Computer Assisted Approach* (1st edition). Burlington: Gulf Professional Publishing
- Hanafy, A., Ali, A., Nasr-El-Din, H. A., & Heidari, Z. 2015. Evaluating the Effects of Acid Stimulation Treatment before and After Fines Migration on Petrophysical Properties in Sandstone Reservoirs. *International Petroleum Technology Conference, 6-9 December, Doha, Qatar*. International Petroleum Technology Conference. <https://doi.org/10.2523/IPTC-18569-MS>
- Hanafy, A. M., & Nasr-El-Din, H. A. 2016. NMR Study to Assess Fines Migration Damage and Its Removal Using Regular Mud Acid in Different Sandstone Cores. *Abu Dhabi International Petroleum Exhibition & Conference, 7-10 November, Abu Dhabi, UAE*. Society of Petroleum Engineers. <https://doi.org/10.2118/182976-MS>
- Hashem, M. K., Nasr-El-Din, H. A., & Hopkins, J. A. 1999. An Experience in Acidizing Sandstone Reservoirs: A Scientific Approach. *SPE Annual Technical Conference and Exhibition, 3-6 October, Houston, Texas*. Society of Petroleum Engineers. <https://doi.org/10.2118/56528-MS>

References

- Hekim, Y., Fogler, H. S., & McCune, C. C. 1982. The Radial Movement of Permeability Fronts and Multiple Reaction Zones in Porous Media. *Society of Petroleum Engineers Journal*. **22**(1). 99-107. Society of Petroleum Engineers. <https://doi.org/10.2118/9495-PA>
- Hill, A. D., Lindsay, D. M., Silberberg, I. H., & Schechter, R. S. 1981. Theoretical and Experimental Studies of Sandstone Acidizing. *Society of Petroleum Engineers Journal*. **21**(1). 30-42. Society of Petroleum Engineers. <https://doi.org/10.2118/6607-PA>
- Hill, A. D., Sepehrnoori, K., & Wu, P. Y. 1994. Design of the HCl Preflush in Sandstone Acidizing. *SPE Production & Facilities*. **9**(2). 115-120. Society of Petroleum Engineers. <https://doi.org/10.2118/21720-PA>
- Holman, G. B. 1982. State-of-the-Art Well Stimulation. *Journal of Petroleum Technology*. **34**(2). 239-241. Society of Petroleum Engineers. <https://doi.org/10.2118/10868-PA>
- Houseworth, J. E. 2014. Advanced Well Stimulation Technologies in California: An Independent Review of Scientific and Technical Information, Executive Summary. *California Council on Science and Technology*. ISBN:978-1-930117-94-5
- Hsi, C. D., Bryant, S. L., & Neira, R. D. 1993. Experimental Validation of Sandstone Acidization Models. *SPE International Symposium on Oilfield Chemistry, 2-5 March, New Orleans, Louisiana*. Society of Petroleum Engineers. <https://doi.org/10.2118/25212-MS>
- Jaramillo, O. J., Romero, R., Ortega, A., Milne, A. W., & Lastre Buelvas, M. 2010. Matrix Acid Systems for Formations with High Clay Content. *SPE International Symposium and Exhibition on Formation Damage Control, 10-12 February, Lafayette, Louisiana, USA*. Society of Petroleum Engineers. <https://doi.org/10.2118/126719-MS>
- Ji, Q., Zhou, L., & Nasr-El-Din, H. A. 2014. Acidizing Sandstone Reservoirs Using Fines Control Acid. *SPE Latin America and Caribbean Petroleum Engineering*

References

- Conference, 21-23 May, Maracaibo, Venezuela.* Society of Petroleum Engineers.
<https://doi.org/10.2118/169395-MS>
- Ji, Q., Zhou, L., & Nasr-El-Din, H. 2016. Acidizing Sandstone Reservoirs with Aluminum-Based Retarded Mud Acid. *SPE Journal*. **21**(3). 1050-1060. Society of Petroleum Engineers. <https://doi.org/10.2118/169395-PA>
- Kalfayan, L.J. 2008. *Production Enhancement with Acid Stimulation* (2nd edition). Houston, USA: PennWell Books.
- Kalfayan, L. J., & Metcalf, A. S. 2000. Successful Sandstone Acid Design Case Histories: Exceptions to Conventional Wisdom. *SPE Annual Technical Conference and Exhibition, 1-4 October, Dallas Texas*. Society of Petroleum Engineers.
<https://doi.org/10.2118/63178-MS>
- King, G. E. 1986. Acidizing Concepts - Matrix vs. Fracture Acidizing. *Journal of Petroleum Technology*. **38**(5). 507-508. Society of Petroleum Engineers.
<https://doi.org/10.2118/15279-PA>
- Kume, N., Van Melsen, R., Erhahon, L., & Abiodun, A. F. 1999. New HF Acid System Improves Sandstone Matrix Acidizing Success Ratio By 400% Over Conventional Mud Acid System in Niger Delta Basin. *SPE Annual Technical Conference and Exhibition, 3-6 October, Houston, Texas*. Society of Petroleum Engineers.
<https://doi.org/10.2118/56527-MS>
- Kunze, K. R., Shaughnessy, C. M. 1983. Acidizing Sandstone Formations with Fluoroboric Acid. *Society of Petroleum Engineers Journal*. **23**(1). 65-72. Society of Petroleum Engineers. <https://doi.org/10.2118/9387-PA>
- Labrid, J. C. 1975. Thermodynamic and Kinetic Aspects of Argillaceous Sandstone Acidizing. *Society of Petroleum Engineers Journal*. **15**(2). 117-128. Society of Petroleum Engineers. <https://doi.org/10.2118/5156-PA>
- Lamb, W. 1998. Topics for Production Chemistry-High HF acid. *Paris meeting, 10-12 March*

References

- Lea, C.-M., Hill, A. K., & Sepehrnoori, K. 1992. Simulation of Sandstone Acidizing of a Damaged Perforation. *SPE Production Engineering*. 7(2). 212-218. Society of Petroleum Engineers. <https://doi.org/10.2118/19419-PA>
- Legemah, M. U., Gomaa, A., Bilden, D., Lowe, C., Boles, J., Qu, Q., & Li, L. 2015. Sequential Injection Process Enhances Acidizing Treatment of High-Temperature Wells. *SPE Production and Operations Symposium, 1-5 March, Oklahoma City, Oklahoma, USA*. Society of Petroleum Engineers. <https://doi.org/10.2118/173626-MS>
- Leong, V. H. & Mahmud, H. B. 2017. A Comparative Study of Different Acids used for Sandstone Acid Stimulation: A Literature Review. *IOP Conference Series: Material Science and Engineering*. 217. 012018. IOP Publishing. <https://doi.org/10.1088/1757-899X/217/1/012018>
- Leong, V. H. & Mahmud, H. B. 2018. A preliminary screening and characterization of suitable acids for sandstone matrix acidizing technique: a comprehensive review. *Journal of Petroleum Exploration and Production Technology*. Springer Nature. <https://doi.org/10.1007/s13202-018-0496-6>
- Leong, V. H., Mahmud, H. B., Law, M. C., Foo, H. C. Y. & Tan, I. S. 2018a. A numerical modelling and simulation of core-scale sandstone acidizing process: a study on the effect of temperature. *Journal of Petroleum Exploration and Production Technology*. Springer Nature. <https://doi.org/10.1007/s13202-018-0522-8>
- Leong, V. H., Mahmud, H. B., Law, M. C., Foo, H. C. Y. & Tan, I. S. 2018b. A comparison and assessment of the modelling and simulation of the sandstone matrix acidizing process: A critical methodology study. *Journal of Natural Gas Science and Engineering*. 57. 52-67. Elsevier B. V. <https://doi.org/10.1016/j.jngse.2018.06.044>
- LePage, J. N., De Wolf, C., Bemelaar, J., & Nasr-El-Din, H. A. 2009. An Environmentally Friendly Stimulation Fluid for High-Temperature Applications. *SPE International Symposium on Oilfield Chemistry, 20-22 April, The Woodlands, Texas*. Society of Petroleum Engineers. <https://doi.org/10.2118/121709-MS>

References

- Li, C. 2004. Fine scale sandstone acidizing coreflood simulation. *Doctoral Thesis*. University of Texas at Austin, Austin. <http://hdl.handle.net/2152/1235>
- Li, C., Xie, T., Pournik, M., Zhu, D., & Hill, A. D. 2004. Fine-Scale Simulation of Sandstone Acidizing. *SPE Annual Technical Conference and Exhibition, 26-29 September, Houston, Texas*. Society of Petroleum Engineers. <https://doi.org/10.2118/90428-MS>
- Li, N., Zeng, F. B., Li, J., Zhang, Q., Feng, Y., & Liu, P. 2016. Kinetic mechanics of the reactions between HCl/HF acid mixtures and sandstone minerals. *Journal of Natural Gas Science and Engineering*. **34**. 792-802. Elsevier B. V. <https://doi.org/10.1016/j.jngse.2016.07.044>
- Li, Y.-H., Fambrough, J. D., & Montgomery, C. T. 1998. Mathematical Modeling of Secondary Precipitation from Sandstone Acidizing. *SPE Journal*. **3**(4). 393-401. Society of Petroleum Engineers. <https://doi.org/10.2118/53001-PA>
- Lindsay, D. M. 1976. An Experimental Study of Sandstone Acidization, Report No. UT 76-1, Texas Petroleum Research Committee. Austin
- Liu, M., Shabaninejad, M., & Mostaghimi, P. 2017. Impact of mineralogical heterogeneity on reactive transport modelling. *Computers and Geosciences*. **104**. 12-19. Elsevier B. V. <https://doi.org/10.1016/j.cageo.2017.03.020>
- Lund, K., Fogler, H. S., & Ault, J. W. 1975. A new model of the physical and chemical changes in sandstone during acidizing. *SPE Journal*. **15**(5). 361-370. Society of Petroleum Engineers. <https://doi.org/10.2118/5157-PA>
- Lund, K., Fogler, H. S., McCune, C. C., & Ault, J. W. 1973. Kinetic Rate Expressions for Reactions of Selected Minerals with HCl and HF Mixtures. *SPE Oilfield Chemistry Symposium, 24-25 May, Denver, Colorado*. Society of Petroleum Engineers. <https://doi.org/10.2118/4348-MS>
- Mahmoodi, A., Javadi, A., & Sola, B. S. 2018. Porous media acidizing simulation: New two-phase two-scale continuum modelling approach. *Journal of Petroleum*

References

- Science and Engineering*. **166**. 679-692. Elsevier B. V.
<https://doi.org/10.1016/j.petrol.2018.03.072>
- Mahmoud, M. A. 2011. Removing of Formation Damage and Enhancement of Formation Productivity Using Environmentally Friendly Chemicals. *Doctoral dissertation*. Texas A&M University
- Mahmoud, M. A., Nasr-El-Din, H. A., De Wolf, C., & Alex, A. 2011. Sandstone Acidizing Using a New Class of Chelating Agents. *SPE International Symposium on Oilfield Chemistry, 11-13 April, The Woodlands, Texas, USA*. Society of Petroleum Engineers. <https://doi.org/10.2118/139815-MS>
- Mahmoud, M. A., Nasr-El-Din, H. A., & De Wolf, C. A. 2015. High-Temperature Laboratory Testing of Illitic Sandstone Outcrop Cores with HCl-Alternative Fluids. *SPE Production & Operations*. **30**(1). 43-51. Society of Petroleum Engineers. <https://doi.org/10.2118/147395-PA>
- Martin, A. N. 2004. Stimulating Sandstone Formations with non-HF Treatment Systems. *SPE Annual Technical Conference and Exhibition, 26-29 September, Houston, Texas*. Society of Petroleum Engineers. <https://doi.org/10.2118/90774-MS>
- McBride, J. R., Rathbone, M. J., & Thomas, R. L. 1979. Evaluation of Fluoboric Acid Treatment in The Grand Isle Offshore Area Using Multiple Rate Flow Test. *SPE Annual Technical Conference and Exhibition, 23-26 September, Las Vegas, Nevada*. Society of Petroleum Engineers. <https://doi.org/10.2118/8399-MS>
- McCune, C. C., Fogler, H. S., & Cunningham, J. R. 1975. A New Model of the Physical and Chemical Changes in Sandstone During Acidizing. *Society of Petroleum Engineers Journal*. **15**(5). 361-370. Society of Petroleum Engineers. <https://doi.org/10.2118/5157-PA>
- McLeod, H. O. 1984. Matrix Acidizing. *Journal of Petroleum Technology*. **36**(12). 2055-2069. Society of Petroleum Engineers. <https://doi.org/10.2118/13752-PA>
- Melo, A. R. de, & de Oliveira, T. J. L. 2013. CFD as a Tool for Pumping Strategy Evaluation on Matrix Acidizing Treatments. *SPE European Formation Damage*

References

- Conference & Exhibition, 5-7 June, Noordwijk, The Netherlands.* Society of Petroleum Engineers. <https://doi.org/10.2118/165100-MS>
- Milligan, M. 1994. Well Stimulation Using Acids. *Journal of Canadian Petroleum Technology*. **33**(1). Petroleum Society of Canada. <https://doi.org/10.2118/94-01-01>
- Morgenthaler, L. N., Zhu, D., Mou, J., & Hill, A. D. 2006. Effect of Reservoir Mineralogy and Texture on Acid Response in Heterogeneous Sandstones. *SPE Annual Technical Conference and Exhibition, 24-27 September, San Antonio, Texas, USA.* Society of Petroleum Engineers. <https://doi.org/10.2118/102672-MS>
- Mostaghimi, P., Liu, M., & Arns, C. H. 2016. Numerical Simulation of Reactive Transport on Micro-CT Images. *Mathematical Geosciences*. **48**(8). 963-983. Springer Nature. <https://doi.org/10.1007/s11004-016-9640-3>
- Muecke, T. W. 1982. Principles of Acid Stimulation. *International Petroleum Exhibition and Technical Symposium, 17-24 March, Beijing, China.* Society of Petroleum Engineers. <https://doi.org/10.2118/10038-MS>
- Murtaza, Z., Berndt, O., & Robert, J. 1999. An Improved Sandstone Acidizing Model: The Importance of Secondary and Tertiary Reactions. *SPE European Formation Damage Conference, 31 May-1 June, The Hague, Netherlands.* Society of Petroleum Engineers. <https://doi.org/10.2118/54728-MS>
- Nasr-El-Din, H. A. 2013. HT Stimulation Fluid Based on GLDA Meets Productivity, Environmental Need. *Journal of Petroleum Technology*. **65**(1). 28-31. Society of Petroleum Engineers. <https://doi.org/10.2118/0113-0028-JPT>
- Nasr-El-Din, H. A., Al-Nasser, A. H., Al-Habib, N. S., Jemmali, M., Zoraia, G., & Sunbul, A. 2005. New Methodology to Effectively Stimulate Water Disposal Wells Drilled in Acid Sensitive Sandstone formations in Saudi Arabia. *SPE Middle East Oil and Gas Show and Conference, 12-15 March, Kingdom of Bahrain.* Society of Petroleum Engineers. <https://doi.org/10.2118/93502-MS>

References

- Nasr-El-Din, H. A., Hopkins, J. A., Shuchart, C. E., & Wilkinson, T. 1998. Aluminum Scaling and Formation Damage due to Regular Mud Acid Treatment. *SPE Formation Damage Control Conference, 18-19 February, Lafayette, Louisiana*. Society of Petroleum Engineers. <https://doi.org/10.2118/39483-MS>
- Nasr-El-Din, H. A., Zhou, L., & Al-harbi Bader Ghazi. 2013. Interactions of a Sandstone Acid Systems with Clays. *SPE Production and Operations Symposium, 23-26 March, Oklahoma City, Oklahoma, USA*. Society of Petroleum Engineers. <https://doi.org/10.2118/164472-MS>
- Nevito Gomez, J. 2006. Design, set up, and testing of a matrix acidizing apparatus. *Master's thesis*. Texas A&M University. <https://hdl.handle.net/1969.1/4282>
- O'Driscoll, K. P., Stolyarov, S., & Kalfayan, L. 2005. A Review of Matrix Acidizing Sandstones in Western Siberia Russia. *SPE European Formation Damage Conference, 25-27 May, Sheveningen, The Netherlands*. Society of Petroleum Engineers. <https://doi.org/10.2118/94790-MS>
- Okabe, H. 2005. Bridging Pore to Core-Scale Flow Properties Using Pore-Scale Modeling and Coreflood Simulation. *International Symposium of the Society of Core Analysts, 21-25 Aug, Toronto, Canada*. Report No. SCA2005-33
- Paccaloni, G., & Tambini, M. 1993. Advances in Matrix Stimulation Technology. *Journal of Petroleum Technology*. **45**(3). 256-263. Society of Petroleum Engineers. <https://doi.org/10.2118/20623-PA>
- Parkinson, M., Munk, T. K., Brookley, J. G., Caetano, A. D., Albuquerque, M. A., Cohen, D., & Reekie, M. R. 2010. Stimulation of Multi-layered High-Carbonate-Content Sandstone Formations in West Africa Using Chelant-Based Fluids and Mechanical Diversion. *SPE International Symposium and Exhibition on Formation Damage Control, 10-12 February, Lafayette, Louisiana, USA*. Society of Petroleum Engineers. <https://doi.org/10.2118/128043-MS>
- Perthuis, H., Touboul, E., & Piot, B. 1989. Acid Reactions and Damage Removal in Sandstones: A Model for Selecting the Acid Formulation. *SPE International*

References

- Symposium on Oilfield Chemistry, 8-10 February, Houston, Texas*. Society of Petroleum Engineers. <https://doi.org/10.2118/18469-MS>
- Pituckchon, A. 2014. Further Investigation of Fluoboric Acid in Sandstone Acidizing Using ^{11}B and ^{19}F NMR. *Master's thesis*. Texas A&M University. <https://hdl.handle.net/1969.1/152823>
- Ponce da Motta, E., Plavnik, B., & Schechter, R. S. 1992. Optimizing Sandstone Acidization. *SPE Reservoir Engineering*. **7**(1). 149-153. Society of Petroleum Engineers. <https://doi.org/10.2118/19426-PA>
- Portier, S., Andr e L., Vuataz, F. D. 2007. Review on chemical stimulation techniques in oil. Switzerland. Centre for Geothermal Research, Neuch atel, Switzerland.
- Quinn, M. A., Lake, L. W., & Schechter, R. S. 1997. Designing Effective Sandstone Acidizing Treatments Through Geochemical Modeling. *SPE European Formation Damage Conference, 2-3 June, The Hague, Netherlands*. Society of Petroleum Engineers. <https://doi.org/10.2118/38173-MS>
- Rabie, A. I., & Nasr-El-Din, H. A. 2015. Effect of Acid Additives on the Reaction of Stimulating Fluids during Acidizing Treatments. *SPE North Africa Technical Conference and Exhibition, 14-16 September, Cairo, Egypt*. Society of Petroleum Engineers. <https://doi.org/10.2118/175827-MS>
- Rahman, S. S. 2000. A 3-D Numerical Model for Designing and Planning of Matrix Acid Stimulation in Low-Permeability Rocks. *SPE Asia Pacific Oil and Gas Conference and Exhibition, 16-18 October, Brisbane, Australia*. Society of Petroleum Engineers. <https://doi.org/10.2118/64403-MS>
- Restrepo, A., Lastre, M., Milne, A. W., Penaloza, S. J. & Castro, E. 2012. Effective Kaolinite Damage Control under Unfavourable Chemical Environment: Field Case. *SPE International Symposium and Exhibition on Formation Damage Control, 15-17 February, Lafayette, Louisiana, USA*. Society of Petroleum Engineers. <https://doi.org/10.2118/151841-MS>

References

- Reyes, E. A., Smith, A. L., Beuterbaugh, A., & Calabrese, T. 2015. GLDA/HF Facilitates High Temperature Acidizing and Coiled Tubing Corrosion Inhibition. *SPE European Formation Damage Conference and Exhibition, 3-5 June, Budapest, Hungary*. Society of Petroleum Engineers. <https://doi.org/10.2118/174264-MS>
- Rignol, J., Ounsakul, T., Kharrat, W., Fu, D., Teng, L. K., Lomovskaya, I., & Boonjai, P. 2015. Improved Fluid Technology for Stimulation of Ultrahigh-Temperature Sandstone Formation. *SPE International Symposium on Oilfield Chemistry, 13-15 April, The Woodlands, Texas, USA*. Society of Petroleum Engineers. <https://doi.org/10.2118/173755-MS>
- Rodoplu, S., Zhu, D., Hill, A. D., & Zhou, H. 2003. Development and Validation of a Sandstone Acidizing Model with a New Permeability Response Model. *SPE Annual Technical Conference and Exhibition, 5-8 October, Denver, Colorado*. Society of Petroleum Engineers. <https://doi.org/10.2118/84132-MS>
- Rogers, B. A., Burk, M. K., & Stonecipher, S. A. 1998. Designing a Remedial Acid Treatment for Gulf of Mexico Deepwater Turbidite Sands Containing Zeolite Cement. *SPE Formation Damage Control Conference, 18-19 February, Lafayette, Louisiana*. Society of Petroleum Engineers. <https://doi.org/10.2118/39595-MS>
- Ryss, I. G. 1956. *The Chemistry of Fluorine and Its Inorganic Compounds* (Reprint). Moscow: State Publishing House of Scientific, Technical, and Chemical Literature
- Sanchez, T. 2016. Operating Manual, Core Flooding – V 1.5740. <http://www.stfrance.fr>
- Sayed, M. A. I., & Nasr-El-Din, H. A. 2013. Acid Treatments in High Temperature Dolomitic Carbonate Reservoirs Using Emulsified Acids: A Coreflood Study. *SPE Production and Operations Symposium, 23-26 March, Oklahoma City, Oklahoma, USA*. Society of Petroleum Engineers. <https://doi.org/10.2118/164487-MS>
- Schechter, R. S. 1992. *Oil Well Stimulation* (Illustrated). Englewood Cliffs, New Jersey, USA: Prentice Hall

References

- Schechter, R. S. & Gidley, J. L. 1969. The Change in Pore Size Distribution from Surface Reactions in Porous Media. *AIChE Journal*. **15**(3). 339-350. Wiley. <https://doi.org/10.1002/aic.690150309>
- Schmid, W., Martin, A., & Palacios, J. M. 2016. Comprehensive Approach of Reservoir Characterization has Allowed Successful Stimulation of Sandstone Formations in Bachaquero Field-Lake Maracaibo, Venezuela. *SPE Trinidad and Tobago Section Energy Resources Conference, 13-15 June, Port of Spain, Trinidad and Tobago*. Society of Petroleum Engineers. <https://doi.org/10.2118/180842-MS>
- Sevougian, S. D., Lake, L. W., & Schechter, R. S. 1995. A New Geochemical Simulator to Design More Effective Sandstone Acidizing Treatments. *SPE Production & Facilities*. **10**(1). 13-19. Society of Petroleum Engineers. <https://doi.org/10.2118/24780-PA>
- Shafiq, M. U., Ben Mahmud, H. K., & Hamid, M. A. 2015. Comparison of Buffer Effect of Different Acids During Sandstone Acidizing. *IOP Conference Series: Material Science and Engineering*. **78**. 012008. IOP Publishing. <https://doi.org/10.1088/1757-899X/78/1/012008>
- Shafiq, M. U., & Ben Mahmud, H. K. 2016. An Effective Acid Combination for Enhanced Properties and Corrosion Control of Acidizing Sandstone Formation. *IOP Conference Series: Material Science and Engineering*. **121**. 012002. IOP Publishing. <https://doi.org/10.1088/1757-899X/121/1/012002>
- Shafiq, M. U., & Ben Mahmud, H. K. 2017. Sandstone matrix acidizing knowledge and future development. *Journal of Petroleum Exploration & Production Technology*. **7**(4). 1205-1216. Springer Nature. <https://doi.org/10.1007/s13202-017-0314-6>
- Shafiq, M. U., Ben Mahmud, H., & Arif, M. 2018. Mineralogy and pore topology analysis during matrix acidizing of tight sandstone and dolomite formations using chelating agents. *Journal of Petroleum Science and Engineering*. **167**. 869-876. Elsevier B.V. <https://doi.org/10.1016/j.petrol.2018.02.057>
- Shafiq, M. U., Ben Mahmud, H., Rezaee, R., & Testamandi, N. 2017. Investigation of Changing Pore Topology and Porosity During Matrix Acidizing using Different

References

- Chelating Agents. *IOP Conference Series: Material Science and Engineering*. **217**. 012023. <https://doi.org/10.1088/1757-899X/217/1/012023>
- Shafiq, M. U., & Shuker, M.T. 2013. Finding Suitable Acid for Acidizing of Low Permeable Sandstone Formation: A Research. *SPE/PAPG Annual Technical Conference, 26-27 November, Islamabad, Pakistan*. Society of Petroleum Engineers. <https://doi.org/10.2118/169641-MS>
- Shafiq, M. U., Shuker, M. T., & Kyaw, A. 2013a. Comparison of Using Combination of Acetic Acid and Hydrochloric Acid with Only Hydrochloric Acid as Matrix Pre Flush. *International Journal of Petroleum and Geoscience Engineering*. **1**(1). 41-49. Academic Research Online Publisher
- Shafiq, M. U., Shuker, M. T., & Kyaw, A. 2013b. Performance Prediction of Acids on Sandstone Acidizing. *ASJ International Journal of Advances in Scientific Research and Reviews*. **1**(2). 7-12. Academia Scholarly Journal
- Shafiq, M. U., Shuker, M. T., & Kyaw, A. 2014. Performance comparison of new combinations of acids with mud acid in sandstone acidizing. *Research Journal of Applied Sciences, Engineering & Technology*. **7**(2). 324–328. MAXWELL Scientific
- Shaughnessy, C. M., & Kunze, K. R. 1981. Understanding Sandstone Acidizing Leads to Improved Field Practices. *Journal of Petroleum Technology*. **33**(7). 1196-1202. Society of Petroleum Engineers. <https://doi.org/10.2118/9388-PA>
- Shuchart, C. E. 1997. Chemical Study of Organic-HF Blends Leads to Improved Fluids. *International Symposium on Oilfield Chemistry, 18-21 February, Houston, Texas*. Society of Petroleum Engineers. <https://doi.org/10.2118/37281-MS>
- Shuchart, C. E., & Buster, D. C. 1995. Determination of the Chemistry of HF Acidizing with the Use of F NMR Spectroscopy. *SPE International Symposium on Oilfield Chemistry, 14-17 February, San Antonio, Texas*. Society of Petroleum Engineers. <https://doi.org/10.2118/28975-MS>

References

- Shuchart, C. E., & Gdanski, R. D. 1996. Improved Success in Acid Stimulations with a New Organic-HF System. *European Petroleum Conference, 22-24 October, Milan, Italy*. Society of Petroleum Engineers. <https://doi.org/10.2118/36907-MS>
- Smith, C. F., Hendrickson, A. R. 1965. Hydrofluoric Acid Stimulation of Sandstone Reservoirs. *Journal of Petroleum Technology*. **17**(2). 215-222. Society of Petroleum Engineers. <https://doi.org/10.2118/980-PA>
- Sumotarto, U., Hill, A. D., & Sepehrnoori, K. 1995. An Integrated Sandstone Acidizing Fluid Selection and Simulation to Optimize Treatment Design. *SPE Annual Technical Conference and Exhibition, 22-25 October, Dallas, Texas*. Society of Petroleum Engineers. <https://doi.org/10.2118/30520-MS>
- Svendsen, O. B., Kleven, R., Hartley, I. P. R., & Aksnes, N. 1992. Stimulation of High-Rate Gravel-Packed Oil Wells Damaged by Clay and Fines Migration: A Case Study, Gullfaks Field, North Sea. *European Petroleum Conference, 16-18 November, Cannes, France*. Society of Petroleum Engineers. <https://doi.org/10.2118/24991-MS>
- Tabasy, M. & Rashidi, F. 2015. A qualitative simulation of a face dissolution pattern in acidizing process using rotating disk apparatus for a carbonate gas reservoir. *Journal of Natural Gas Science and Engineering*. **26**. 1460-1469. Elsevier B. V. <https://doi.org/10.1016/j.jngse.2015.08.014>
- Taha, R., Hill, A. D., & Sepehrnoori, K. 1986. Simulation of Sandstone-Matrix Acidizing in Heterogeneous Reservoirs. *Journal of Petroleum Technology*. **38**(7). 753-767. Society of Petroleum Engineers. <https://doi.org/10.2118/13218-PA>
- Taha, R., Hill, A. D., & Sepohrnoori, K. 1989. Sandstone Acidizing Design with a Generalized Model. *SPE Production Engineering*. **4**(1). 49-55. Society of Petroleum Engineers. <https://doi.org/10.2118/16885-PA>
- Tan, X., Weng, X., & Cohen, C. E. 2016. An Improved Wormhole Propagation Model with a Field Example. *SPE International Conference and Exhibition on Formation Damage Control, 24-26 February, Lafayette, Louisiana, USA*. Society of Petroleum Engineers. <https://doi.org/10.2118/179017-MS>

References

- Templeton, C. C., Richardson, E. A., Karnes, G. T., & Lybarger, J. H. 1975. Self-Generating Mud Acid. *Journal of Petroleum Technology*. **27**(10). 1199-1203. Society of Petroleum Engineers. <https://doi.org/10.2118/5153-PA>
- Thomas, R. L., & Crowe, C. W. 1978. Single-Stage Chemical Treatment Provides Stimulation and Clay Control in Sandstone Formations. *SPE California Regional Meeting, 12-14 April, San Francisco, California*. Society of Petroleum Engineers. <https://doi.org/10.2118/7124-MS>
- Thomas, R. L., & Crowe, C. W. 1981. Matrix Treatment Employs New Acid System for Stimulation and Control of Fines Migration in Sandstone Formations. *Journal of Petroleum Technology*. **33**(8). 1491-1500. Society of Petroleum Engineers. <https://doi.org/10.2118/7566-PA>
- Thomas, R. L., Nasr-El-Din, H. A., Lynn, J. D., Mehta, S., & Zaidi, S. R. 2001. Precipitation During the Acidizing of a HT/HP Illitic Sandstone Reservoir in Eastern Saudi Arabia: A Laboratory Study. *SPE Annual Technical Conference and Exhibition, 30 September-3 October, New Orleans, Louisiana*. Society of Petroleum Engineers. <https://doi.org/10.2118/71690-MS>
- Thomas, R. L., Nasr-El-Din, H. A., Lynn, J. D., Mehta, S., Muhareb, M., & Ginest, N. 2002a. Channel vs. Matrix Sandstone Acidizing of a HT/HP Reservoir in Saudi Arabia. *International Symposium and Exhibition on Formation Damage Control, 20-21 February, Lafayette, Louisiana*. Society of Petroleum Engineers. <https://doi.org/10.2118/73702-MS>
- Thomas, R. L., Nasr-El-Din, H. A., Mehta, S., Hilab, V., & Lynn, J. D. 2002b. The Impact of HCl to HF Ratio on Hydrated Silica Formation During the Acidizing of a High Temperature Sandstone Gas Reservoir in Saudi Arabia. *SPE Annual Technical Conference and Exhibition, 29 September-2 October, San Antonio, Texas*. Society of Petroleum Engineers. <https://doi.org/10.2118/77370-MS>
- Tuedor, F. E., Xiao, Z., Frenier, W. W., Fu, D., Salamat, G., Davies, S. N., & Lecerf, B. 2006. A Breakthrough Fluid Technology in Stimulation of Sandstone Reservoirs. *SPE International Symposium and Exhibition on Formation Damage Control, 15-*

References

- 17 February, Lafayette, Louisiana, USA. Society of Petroleum Engineers. <https://doi.org/10.2118/98314-MS>
- Van Domelen, M. S., & Jennings, A. R. 1995. Alternate Acid Blends for HPHT Applications. *Offshore Europe, 5-8 September, Aberdeen, United Kingdom*. Society of Petroleum Engineers. <https://doi.org/10.2118/30419-MS>
- Van Domelen, M. S., Reddingius, A. A., Faber, M. J., & Buijse, M. A. 1997. High-Temperature Acid Stimulation Offshore the Netherlands. *SPE European Formation Damage Conference, 2-3 June, The Hague, Netherlands*. Society of Petroleum Engineers. <https://doi.org/10.2118/38171-MS>
- Veldkam, J.G.H., & Boxem, T.A.P.T. 2015. Sector Outlook: Geothermal power increase in the Netherland by enhancing the capacity. TNO.
- Vishnudas, R. & Chaudhuri, A. 2017. A comprehensive numerical study of immiscible and miscible viscous fingers during chemical enhanced oil recovery. *Fuel*. **194**. 480-490. Elsevier B. V. <https://doi.org/10.1016/j.fuel.2017.01.014>
- Walsh, J. B., & Brace, W. F. 1984. The effect of pressure on porosity and the transport properties of rock. *Journal of Geophysical Research: Solid Earth Banner*. **89**. 9425-9431. Wiley. <https://doi.org/10.1029/JB089iB11p09425>
- Walsh, M. P., Lake, L. W., & Schechter, R. S. 1982. A Description of Chemical Precipitation Mechanisms and Their Role in Formation Damage during Stimulation by Hydrofluoric Acid. *Journal of Petroleum Technology*. **34**(9). 2097-2112. Society of Petroleum Engineers. <https://doi.org/10.2118/10625-PA>
- Wamser, C. A. 1948. Hydrolysis of Fluoboric Acid in Aqueous Solution. *Journal of the American Chemical Society*. **70**(3). 1209-1215. ACS. <https://doi.org/10.1021/ja01183a101>
- Wamser, C. A. 1951. Equilibria in the System Boron Trifluoride-Water at 25 °. *Journal of the American Chemical Society*. **73**(1). 409-416. ACS. <https://doi.org/10.1021/ja01145a134>

References

- Wang, X. L., Qu, Q., Boles, J. L., Gomaa, A. M., & Cutler, J. L. 2013. Matrix Stimulation: An Effective One-Step Sandstone Acid System. *SPE Production and Operations Symposium, 23-26 March, Oklahoma City, Oklahoma, USA*. Society of Petroleum Engineers. <https://doi.org/10.2118/164491-MS>
- Wehunt, C. D., Van Arsdale, H., Warner, J. L., & Ali, S. A. 1993. Laboratory Acidization of an Eolian Sandstone at 380F. *SPE International Symposium on Oilfield Chemistry, 2-5 March, New Orleans, Louisiana*. Society of Petroleum Engineers. <https://doi.org/10.2118/25211-MS>
- Williams, B. B., Gidley, J. L., & Schechter R. S. 1979. *Acidizing Fundamentals* (Illustrated edition). New York: Henry L. Doberty Memorial Fund of AIME
- Williams, B. B., & Whiteley, M. E. 1971. Hydrofluoric Acid Reaction with a Porous Sandstone. *Society of Petroleum Engineers Journal*. **11**(3). 306-314. Society of Petroleum Engineers. <https://doi.org/10.2118/3112-PA>
- Xie, T. 2004. A Parametric Study of Sandstone Acidizing using Fine-scale Simulator. *Master's thesis*. University of Texas at Austin, Austin
- Xie, T., Li, C., Pournik, M., Zhu, D., Hill, A. D., & Devine, C. 2005. A Laboratory and Modeling Investigation of Acid-Created Wormholes in Sandstones. *SPE European Formation Damage Conference, 25-27 May, Sheveningen, The Netherlands*. Society of Petroleum Engineers. <https://doi.org/10.2118/94566-MS>
- Yang, C., & Zheng, L. H. 2014. Modelling acidizing process in lab-scale sandstone core. *Energy Education Science and Technology Part A: Energy Science and Research*. **32**(3). 2037-2046
- Yang, F. 2012. Acidizing of Sandstone Reservoirs Using HF and Organic Acids. *Master's thesis*. Texas A&M University. <http://hdl.handle.net/1969.1/ETD-TAMU-2012-08-11631>
- Yang, F., Nasr-El-Din, H. A., & Al-Harbi, B. M. 2012a. Acidizing Sandstone Reservoirs Using HF and Formic Acids. *SPE International Symposium and Exhibition on*

References

- Formation Damage Control, 15-17 February, Lafayette, Louisiana, USA.* Society of Petroleum Engineers. <https://doi.org/10.2118/150899-MS>
- Yang, F., Nasr-El-Din, H. A., & Harbi, B. A. 2012b. Acidizing Sandstone Reservoirs Using HF and Organic Acids. *SPE International Production and Operations Conference & Exhibition, 14-16 May, Doha, Qatar.* Society of Petroleum Engineers. <https://doi.org/10.2118/157250-MS>
- Ying-Hsiao, L., Fambrough, J. D., & Montgomery, C. T. 1998. Mathematical Modeling of Secondary Precipitation from Sandstone Acidizing. *SPE Formation Damage Control Conference, 18-19 February, Lafayette, Louisiana.* Society of Petroleum Engineers. <https://doi.org/10.2118/39420-MS>
- Zakaria, H. 2013. Acidizing Operation Modelling in Sandstone Formations. *International Journal of Petroleum and Geoscience Engineering.* **1**(4). 261-275. Academic Research Online Publisher
- Zeit, B. 2005. Stimulation of Sandstone Reservoirs. *SPE Technology Transfer Workshop.* A Presentation.
- Zhou, L., & Nasr-El-Din, H. A. 2013. Acidizing Sandstone Formations Using a Sandstone Acid System for High Temperatures. *SPE European Formation Damage Conference & Exhibition, 5-7 June, Noordwijk, The Netherlands.* Society of Petroleum Engineers. <https://doi.org/10.2118/165084-MS>
- Zhou, L., & Nasr-El-Din, H. A. 2016. Phosphonic-Based Hydrofluoric Acid: Interactions with Clay Minerals and Flow in Sandstone Cores. *SPE Journal.* **21**(1). 264-279. Society of Petroleum Engineers. <https://doi.org/10.2118/164472-PA>
- Zhou, X., Zhang, S.C., Zhang, X., Wang, F., & Lin, H. 2016. Core-Scale Experimental and Numerical Investigation on Fluoroboric Acidizing of a Sandstone Reservoir. *Energy Technology.* **4**(7). 870-879. Wiley. <https://doi.org/10.1002/ente.201600005>

“Every reasonable effort has been made to acknowledge the owners of copyright material. I would be pleased to hear from any copyright owner who has been omitted or incorrectly acknowledged.”

Appendix

Appendix A. Derivation of Governing Equations

A.1 Pressure Equation

Figure A.1 depicted a cubic control volume was defined in formulating the acidizing model.

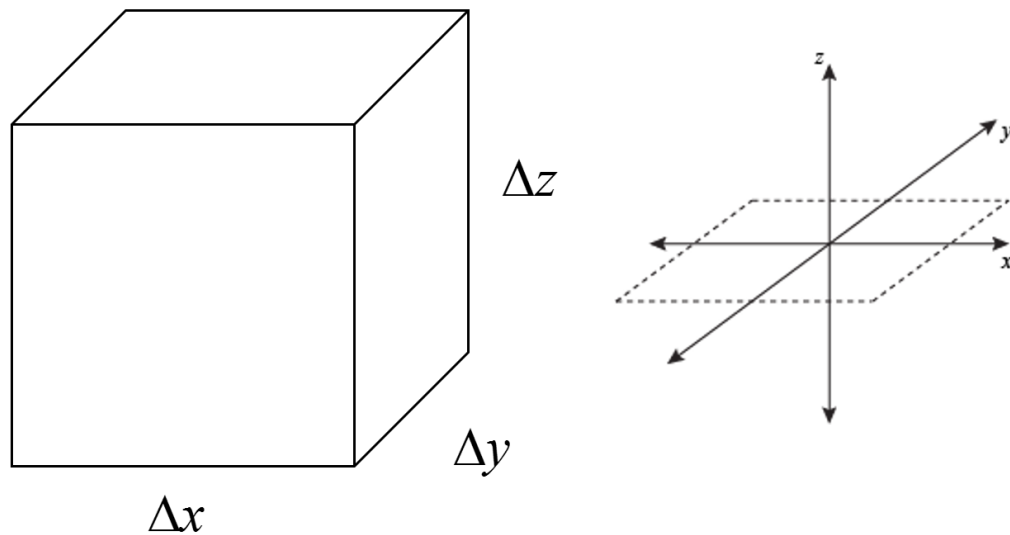


Figure A.1 The control volume of the acidizing model

Equation (A.1) shows the mass balance equation of the sandstone acid solution.

$$\text{Acid in} - \text{Acid out} + \text{Source} = \text{Accumulation} \quad (\text{A.1})$$

The mass of acid solution flowing into the control volume is described in Equation (A.2).

$$\Delta t \left((\rho u_x \Delta y \Delta z) \Big|_x + (\rho u_y \Delta x \Delta z) \Big|_y + (\rho u_z \Delta y \Delta x) \Big|_z \right) \quad (\text{A.2})$$

Where ρ is the density of the acid solution; and u_x , u_y and u_z are the average Darcy velocity in y-z plane, x-z plane and x-y plane respectively.

The mass of acid solution flowing out from the control volume is described in Equation (A.3).

$$\Delta t \left((\rho u_x \Delta y \Delta z) \Big|_{x+\Delta x} + (\rho u_y \Delta x \Delta z) \Big|_{y+\Delta y} + (\rho u_z \Delta y \Delta x) \Big|_{z+\Delta z} \right) \quad (\text{A.3})$$

Since the acid solution is assumed to be the only phase exist in the pore space of the sandstone core, the change in mass in the control volume over a period of time is defined in Equation (A.4).

$$\Delta x \Delta y \Delta z \left((\rho \phi)^{t+\Delta t} - (\rho \phi)^t \right) \quad (\text{A.4})$$

Assuming that during the acid injection, there is no source of acid solution in the core sample. Hence, the total acid solution flowing into the control volume equals to the accumulation of the acid solution. So, the expression of mass conservation of the acid solution is shown in Equation (A.5).

$$\begin{aligned} \Delta x \Delta y \Delta z \left((\rho \phi)^{t+\Delta t} - (\rho \phi)^t \right) = \Delta t \left((\rho u_x \Delta y \Delta z) \Big|_x + (\rho u_y \Delta x \Delta z) \Big|_y + (\rho u_z \Delta y \Delta x) \Big|_z \right) \\ - \Delta t \left((\rho u_x \Delta y \Delta z) \Big|_{x+\Delta x} + (\rho u_y \Delta x \Delta z) \Big|_{y+\Delta y} + (\rho u_z \Delta y \Delta x) \Big|_{z+\Delta z} \right) \end{aligned} \quad (\text{A.5})$$

Equation (A.5) is then divided by $\Delta x \Delta y \Delta z \Delta t$ to become Equation (A.6).

$$\frac{(\rho \phi)^{t+\Delta t} - (\rho \phi)^t}{\Delta t} = \frac{(\rho u_x)_x - (\rho u_x)_{x+\Delta x}}{\Delta x} + \frac{(\rho u_y)_y - (\rho u_y)_{y+\Delta y}}{\Delta y} + \frac{(\rho u_z)_z - (\rho u_z)_{z+\Delta z}}{\Delta z} \quad (\text{A.6})$$

The density of acid solution, ρ is set as constant due to the assumption that stated the acid solution is incompressible. The limits of x, y, z and t were taken as $\Delta x \rightarrow 0, \Delta y \rightarrow 0, \Delta z \rightarrow 0,$ and $\Delta t \rightarrow 0$. So, Equation (A.6) can then be expressed as Equation (A.7).

$$\frac{\partial \phi}{\partial t} = \frac{\partial u_x}{\partial x} + \frac{\partial u_y}{\partial y} + \frac{\partial u_z}{\partial z} \quad (\text{A.7})$$

In vector form, it can be defined as Equation (A.8).

$$\frac{\partial \phi}{\partial t} = \bar{\nabla} \cdot \bar{u} \quad (\text{A.8})$$

Where \bar{u} is the velocity vector $\{u_x, u_y, u_z\}$, defined as the Darcy velocity in Equation (A.9).

$$\bar{u} = -\frac{\bar{k}}{\alpha} \cdot (\bar{\nabla} P + \gamma \bar{\nabla} z) \quad (\text{A.9})$$

Where γ is the ratio of gravity. Since the gravitational effect is neglected, it can be expressed as Equation (A.10).

$$\bar{u} = -\frac{\bar{k}}{\alpha} \cdot \bar{\nabla} P \quad (\text{A.10})$$

Then, Equation (A.11) is obtained by substituting Equation (A.10) into Equation (A.8).

$$\frac{\partial \phi}{\partial t} = \bar{\nabla} \cdot \left(-\frac{\bar{k}}{\alpha} \cdot \bar{\nabla} P \right) = -\frac{1}{\alpha} \frac{\partial}{\partial x} \left(k_x \frac{\partial P}{\partial x} \right) - \frac{1}{\alpha} \frac{\partial}{\partial y} \left(k_y \frac{\partial P}{\partial y} \right) - \frac{1}{\alpha} \frac{\partial}{\partial z} \left(k_z \frac{\partial P}{\partial z} \right) \quad (\text{A.11})$$

When Equation (A.11) is solved during the simulation, the porosity in each time step is kept constant. So, it is then simplified to Equation (4.11).

$$\frac{1}{\alpha} \frac{\partial}{\partial x} \left(k_x \frac{\partial P}{\partial x} \right) + \frac{1}{\alpha} \frac{\partial}{\partial y} \left(k_y \frac{\partial P}{\partial y} \right) + \frac{1}{\alpha} \frac{\partial}{\partial z} \left(k_z \frac{\partial P}{\partial z} \right) = 0 \quad (4.11)$$

A.2 General Material Balance Equation

Generally, the material balance equation for the model can be described as Equation (A.12) – (A.14).

$$\frac{\partial W_i}{\partial t} + \bar{\nabla} \cdot \bar{N}_i = R_i \quad (A.12)$$

$$W_i = \phi \sum_{j=1}^{Np} \rho_j St_j \omega_{i,j} + (1 - \phi) \rho_s \omega_{i,s} \quad (A.13)$$

$$\bar{N}_i = \sum_{j=1}^{Np} u_j \rho_j \omega_{i,j} - \phi \sum St_j \rho_j \bar{k}_{i,j} \cdot \bar{\nabla} \omega_{i,j} \quad (A.14)$$

Where W_i = Overall mass of component i in the control volume;

$\omega_{i,j}$ = Mass fraction of component i in phase j ;

$\omega_{i,s}$ = Mass fraction of component i in solid phase;

ϕ = Porosity;

St_j = Saturation of phase j ;

ρ_j = Density of phase j ;

ρ_s = Density of solid;

N_i = Flux of component i ;

u_j = Darcy velocity of phase j ;

$K_{i,j}$ = Dispersion coefficient of component i in phase j ;

R_i = Source of component i ;

i = Component index;

j = Phase index

A.3 Mass Conservation Equation of Acid Components

Referring to Equation (A.13), the mass component of i in the liquid phase is represented

in the first term ($\phi \sum_{j=1}^{N_p} \rho_j S_{t,j} \omega_{i,j}$) on the right hand side whereas the mass component of i in

the solid phase is represented in the second term ($(1 - \phi) \rho_s \omega_{i,s}$) of the equation. Since the core flooding process is assumed as single phase flow, then the term N_p and S_t becomes 1 and the subscript j can be neglected. Secondly, the second term on the right hand side of Equation (A.13) can be cancelled out as no sorption on the solid phase is assumed during the acid treatment process. Finally, Equation (A.13) had been simplified as Equation (A.15).

$$W_i = \phi \rho \omega_i \quad (\text{A.15})$$

In the control volume of this simulation, the mass of acid i is considered in term of concentration, C_i . Therefore, the term $\rho \omega_i$ becomes C_i as shown in Equation (A.16).

$$W_i = \phi C_i \quad (\text{A.16})$$

Where C_i = Concentration of acid i ;

Referring to Equation (A.14), the convection flow of component i is represented by the first term ($\sum_{j=1}^{N_p} u_j \rho_j \omega_{i,j}$) on the right hand side while the dispersion flow of component i is represented by the second term ($-\phi \sum St_j \rho_j \bar{k}_{i,j} \cdot \bar{\nabla} \omega_{i,j}$) on the equation. In the model, the effect of dispersion can be neglected from the equation as the spread of acid front is dominantly controlled by the chemical reactions between the acids and the minerals. Hence, assuming no dispersion, the second term on the right hand side of Equation (A.14) can be cancelled thus simplifying the equation into Equation (A.17).

$$\bar{N}_i = \bar{u} \rho \omega_i \quad (\text{A.17})$$

Similarly, as Equation (A.15), the mass balance term of acid i is being replaced with the concentration term, C_i as shown in Equation (A.18).

$$\bar{N}_i = \bar{u} C_i \quad (\text{A.18})$$

Referring to Equation (A.12), the source term on the right hand side, R_i is known as the reaction rate of acid i . So, Equation (A.12) can be simplified by substituting Equation (A.16) and (A.18) into it and form a new expression for the mass conservation of the acid solution as shown in Equation (A.19).

$$\frac{\partial(C_i \phi)}{\partial t} + \bar{\nabla} \cdot (\bar{u} C_i) = R_i \quad (\text{A.19})$$

Where R_i = the rate of appearance of acid i in the solution;

So, the source term R_i in Equation (A.19) is specifically the reaction rate of acid i whereas R_i in Equation (A.12) represents the source in just a general way.

Generally, the definition of reaction rate is the speed at which a chemical reaction proceeds. In other words, it is the rate of appearance in the species solution at a specific period of time. This can be expressed in Equation (A.20).

$$R_i = r_i S_j \quad (\text{A.20})$$

Where r_i = the surface area – specific reaction rate of i ;

S_j = the surface area of mineral j in a unit of bulk volume;

Usually, R_i is dependent on the concentration of the reacting species. So, it is expressed as Equation (A.21).

$$-R_i = E_{f,i,j} C_i^\alpha S_j \quad (\text{A.21})$$

Where $E_{f,i,j}$ = the reaction rate constant between acid i and mineral j ;

During the core flooding treatment, the acid is consumed and the rate of acid consumption in the solution is shown in Equation (A.22).

$$R_i = -\sum_{j=1}^{N_m} E_{f,i,j} S_j^* V_j (1-\phi) C_i^\alpha \quad (\text{A.22})$$

Where N_m = the number of minerals reacting with acid i ;

S_j^* = the specific surface area per unit volume of solid;

V_j = the volume fraction for mineral j ;

Substituting Equation (A.22) into (A.19) to yield Equation (4.13).

$$\frac{\partial(C_i\phi)}{\partial t} + \bar{\nabla} \cdot (\bar{u}C_i) = -\sum_{j=1}^{N_m} E_{f,i,j} S_j^* V_j (1-\phi) C_i^\alpha \quad i = 1, 2 \quad (4.13)$$

A.4 Mass Conservation Equation of HF

HF is being used up by its reactions with three mineral groups. At the same time, it is continuously being produced as a result of HBF₄ hydrolysis. Hence the rate of HF generation equals to the rate of HBF₄ hydrolysis. So, the general material balance equation for HF ($i=1$) is written as Equation (A.23).

$$\frac{\partial(C_1\phi)}{\partial t} + \bar{\nabla} \cdot (\bar{u}C_1) = -\sum_{j=1}^{N_m} E_{f,1,j} S_j^* V_j (1-\phi) C_1^\alpha + r_h \quad (A.23)$$

Referring to Equation (A.23), the terms at the left hand side represents the total change in mass of HF per unit time and sub change in mass due to fluid transport whereas the terms at the right hand side is the sub change in mass due to HF chemical reactions and HBF₄ hydrolysis.

During the sandstone acidizing, HF is commonly known to react with three mineral lumped group exist in a sandstone matrix. So, $N_m = 3$. In an expanded form, it can be written as Equation (A.24).

$$\frac{\partial(C_1\phi)}{\partial t} + \bar{\nabla} \cdot (\bar{u}C_1) = -(E_{f,1,1} S_1^* V_1 (1-\phi) + E_{f,1,2} S_2^* V_2 (1-\phi) + E_{f,1,3} S_3^* V_3 (1-\phi)) C_1^\alpha + r_h \quad (A.24)$$

Assigning new term C_{D1} and t_D into the equation. Let $C_{D1} = \frac{C_1}{C_1^0}$ and $t_D = \frac{ut}{\phi L}$, where C_1^0

is the initial concentration of HF, ϕ is the initial porosity and u is the velocity of injected acid. During the simulation, the acid concentration equation is solved such that the porosity, ϕ is assumed to be constant throughout the process. The rate of injection, u is assumed to be constant too. Therefore, it is described as Equation (A.25).

$$\frac{\phi C_1^0 \partial C_{D1}}{\frac{\phi L}{u} \partial t_D} + \bar{\nabla} \cdot (\bar{u} C_{D1} C_1^0) = r_h - (E_{f,1,1} S_1^* V_1 (1-\phi) + E_{f,1,2} S_2^* V_2 (1-\phi) + E_{f,1,3} S_3^* V_3 (1-\phi)) C_1^\alpha \quad (\text{A.25})$$

Assuming α to be 1, it becomes Equation (A.26).

$$\frac{\partial C_{D1}}{\partial t_D} + \bar{\nabla} \cdot \left(\frac{\bar{u}}{u} L C_{D1} \right) = r_h - \left(E_{f,1,1} S_1^* V_1 + E_{f,1,2} S_2^* V_2 + E_{f,1,3} S_3^* V_1^0 \frac{V_3}{V_1^0} \right) C_{D1} \frac{L}{u} (1-\phi) \quad (\text{A.26})$$

Let $\bar{u}_D = \frac{\bar{u}}{u}$ and $\bar{\nabla}_D = L \cdot \bar{\nabla} = \frac{\partial}{\partial x_D} + \frac{\partial}{\partial y_D} + \frac{\partial}{\partial z_D}$, then it becomes Equation (A.27).

$$\begin{aligned} \frac{\partial C_{D1}}{\partial t_D} + \bar{\nabla}_D \cdot (\bar{u}_D C_{D1}) &= r_h \\ - \left(E_{f,1,1} S_1^* V_1^0 \frac{V_1}{V_1^0} + E_{f,1,2} S_2^* V_2^0 \frac{V_2}{V_2^0} + E_{f,1,3} S_3^* V_3^0 \frac{V_3}{V_3^0} \right) C_{D1} \frac{L}{u} (1-\phi) & \end{aligned} \quad (\text{A.27})$$

In the form of dimensionless equation, mass balance equation for HF is expressed as Equation (A.28).

$$\frac{\partial C_{D1}}{\partial t_D} + \bar{\nabla}_D \cdot (\bar{u}_D C_{D1}) = r_h - (N_{Da,1} \Lambda_1 + N_{Da,2} \Lambda_2 + N_{Da,3} \Lambda_3) C_{D1} \quad (\text{A.28})$$

The term N_{Da} is known as the Damkohler number. It is the ratio of the acid consumption rate to the acid convection rate. During the sandstone acid treatment, the specific surface area of the mineral is assumed constant. Hence, the Damkohler numbers of the reactions between HF and the three mineral groups are defined as Equations (A.29) to (A.31).

$$N_{Da,1} = \frac{E_{f,1,1} S_1^* V_1^0 (1-\phi) L}{u} \quad (\text{A.29})$$

$$N_{Da,2} = \frac{E_{f,1,2} S_2^* V_2^0 (1-\phi) L}{u} \quad (\text{A.30})$$

$$N_{Da,3} = \frac{E_{f,1,3} S_3^* V_3^0 (1-\phi) L}{u} \quad (\text{A.31})$$

The term Λ is called the dimensionless composition of mineral. The definition of the dimensionless volume fractions of the three groups of minerals are expressed in Equations (A.32) to (A.34).

$$\Lambda_1 = \frac{V_1}{V_1^0} \quad (\text{A.32})$$

$$\Lambda_2 = \frac{V_2}{V_2^0} \quad (\text{A.33})$$

$$\Lambda_3 = \frac{V_3}{V_3^0} \quad (\text{A.34})$$

A.5 Mass Conservation Equation of H_2SiF_6

In the acid solution, the in-situ product of the three chemical reactions between HF and the three reactive sandstone mineral groups, which is the fluorosilicic acid, H_2SiF_6 is also considered. Comparing to the HF, H_2SiF_6 also has a significant dissolving capacity. At the same time, H_2SiF_6 is the reactant of one reaction. It reacts with the fast reacting minerals to precipitate silica gel. Therefore, the mass balance equation of H_2SiF_6 ($i = 2$) is shown in Equation (A.35).

$$\begin{aligned} \frac{\partial(C_2\phi)}{\partial t} + \bar{\nabla} \cdot (\bar{u}C_2) = & -E_{f,2,1} S_1^* V_1 (1-\phi) C_2^\alpha \\ & + \left(\frac{v_5}{v_1} E_{f,1,1} S_1^* V_1 (1-\phi) + \frac{v_6}{v_2} E_{f,1,2} S_2^* V_2 (1-\phi) + \frac{v_7}{v_3} E_{f,1,3} S_3^* V_3 (1-\phi) \right) C_1^\alpha \end{aligned} \quad (\text{A.35})$$

The term ν_i are the stoichiometric coefficients described in the chemical reaction model. Their values are determined from the previously done experimental investigations.

Assigning new term C_{D2} and t_D into the equation. Let $C_{D2} = \frac{C_2}{C_1}$ and $t_D = \frac{ut}{\phi L}$, Equation (A.36) is being defined as follow.

$$\begin{aligned} \frac{\phi C_1^0 \partial C_{D2}}{\phi L \partial t_D} + \bar{\nabla} \cdot (\bar{u} C_{D2} C_1^0) = & -(E_{f,2,1} S_1^* V_1 (1-\phi)) C_2^\alpha \\ & + \left(\frac{\nu_5}{\nu_1} E_{f,1,1} S_1^* V_1 (1-\phi) + \frac{\nu_6}{\nu_2} E_{f,1,2} S_2^* V_2 (1-\phi) + \frac{\nu_7}{\nu_3} E_{f,1,3} S_3^* V_3 (1-\phi) \right) C_1^\alpha \end{aligned} \quad (A.36)$$

Assuming α to be 1, it becomes Equation (A.37).

$$\begin{aligned} \frac{\partial C_{D2}}{\partial t_D} + \bar{\nabla}_D \cdot \left(\frac{\bar{u}}{u} C_{D2} \right) = & -(E_{f,2,1} S_1^* V_1^0 (1-\phi)) C_{D2} \frac{V_1}{V_1^0} \frac{L}{u} \\ & + \left(\frac{\nu_5}{\nu_1} E_{f,1,1} S_1^* V_1^0 (1-\phi) \frac{V_1}{V_1^0} + \frac{\nu_6}{\nu_2} E_{f,1,2} S_2^* V_2^0 (1-\phi) \frac{V_2}{V_2^0} \right. \\ & \left. + \frac{\nu_7}{\nu_3} E_{f,1,3} S_3^* V_3^0 (1-\phi) \frac{V_3}{V_3^0} \right) C_{D1} \frac{L}{u} \end{aligned} \quad (A.37)$$

In the form of dimensionless equation, mass balance equation for H_2SiF_6 is expressed as Equation (A.38).

$$\frac{\partial C_{D2}}{\partial t_D} + \bar{\nabla}_D \cdot (\bar{u}_D C_{D2}) = -N_{Da,4} \Lambda_1 C_{D1} + \left(\frac{\nu_5}{\nu_1} N_{Da,1} \Lambda_1 + \frac{\nu_6}{\nu_2} N_{Da,2} \Lambda_2 + \frac{\nu_7}{\nu_3} N_{Da,3} \Lambda_3 \right) C_{D1} \quad (A.38)$$

The Damkohler number for the reaction between H_2SiF_6 and the fast reacting minerals, $N_{Da,4}$ is defined in Equation (A.39).

$$N_{Da,4} = \frac{E_{f,2,1} S_1^* V_1^0 (1-\phi) L}{u} \quad (A.39)$$

A.6 Mass Conservation Equation of Minerals

The term $(\phi \sum_{j=1}^{N_p} \rho_j S t_j \omega_{i,j})$ in Eq. (A.13) can be cancelled out and $(1-\phi)V_j$ corresponds to the amount of mineral j that appear in solid phase. Also, assuming that there is no flow of solid phase, the term $\bar{\nabla} \cdot \bar{N}_i$ is removed from Equation (A.12). The source term R_i in Equation (A.12) represents the rate of reaction of mineral j during the core flooding. It is determined by the rate of reaction and dissolving power of the acid. The dissolving power of acid is defined as the amount of mineral that is reacted and consumed by a specific amount of acid. In the basis of mass, it can be written as Equation (A.40).

$$\beta = \frac{V_{\text{mineral}} MW_{\text{mineral}}}{V_{\text{acid}} MW_{\text{acid}}} \quad (\text{A.40})$$

A.7 Mass Conservation Equation of Fast-Reacting Minerals

Based on the general material balance equation for minerals, the dimensionless form of material balance for all the three minerals have been developed. Firstly, the fast reacting mineral ($j = 1$) is being dissolved by both the acids, HF and H_2SiF_6 . So, the mass balance of fast reacting mineral is expressed as Equation (A.41).

$$\frac{\partial((1-\phi)V_1)}{\partial t} = - \frac{MW_{\text{HF}} S_1^* V_1 (1-\phi) \beta_{\text{HF},1} E_{f,\text{HF},1} C_{\text{HF}}}{\rho_1} - \frac{MW_{\text{H}_2\text{SiF}_6} S_1^* V_1 (1-\phi) \beta_{\text{H}_2\text{SiF}_6,1} E_{f,\text{H}_2\text{SiF}_6,1} C_{\text{H}_2\text{SiF}_6}}{\rho_1} \quad (\text{A.41})$$

Similarly, the porosity is considered as constant in the reaction process as shown in Equation (A.42).

$$\frac{\partial V_1}{\partial t} = - \left(MW_{\text{HF}} \beta_{\text{HF},1} E_{f,\text{HF},1} C_{\text{HF}} + MW_{\text{H}_2\text{SiF}_6} \beta_{\text{H}_2\text{SiF}_6,1} E_{f,\text{H}_2\text{SiF}_6,1} C_{\text{H}_2\text{SiF}_6} \right) \frac{S_1^* V_1}{\rho_1} \quad (\text{A.42})$$

Then, the dimensionless volume fraction of fast reacting mineral defined in Equation (A.32) and dimensionless time are substituted into the equation and written as Equation (A.43).

$$\begin{aligned} \frac{\partial \Lambda_1}{\partial t_D} &= - \left(MW_{HF} \beta_{HF,1} E_{f,HF,1} C_{HF} + MW_{H_2SiF_6} \beta_{H_2SiF_6,1} E_{f,H_2SiF_6,1} C_{H_2SiF_6} \right) \frac{S_1^* V_1 \phi L}{\rho_1 u V_1^0} \\ &= - \left[\frac{(1-\phi) V_1^0 E_{f,HF,1} S_1^* L}{u} \cdot \frac{1}{(1-\phi) V_1^0} \cdot \frac{\phi MW_{HF} C_{HF}^0 \beta_{HF,1} C_{HF}}{\rho_1 C_{HF}^0} \right. \\ &\quad \left. + \frac{(1-\phi) V_1^0 E_{f,H_2SiF_6,1} S_1^* L}{u} \cdot \frac{1}{(1-\phi) V_1^0} \cdot \frac{\phi MW_{HF} C_{HF}^0 \beta_{H_2SiF_6,1} C_{H_2SiF_6}}{\rho_1 C_{HF}^0} \right] \frac{V_1}{V_1^0} \end{aligned} \quad (A.43)$$

Considering the Damkohler numbers as shown in Equations (A.29) and (A.39), the equation is further simplified into Equation (A.44).

$$\frac{\partial \Lambda_1}{\partial t_D} = - (N_{Da,1} \cdot N_{Ac,1} \cdot C_{D1} + N_{Da,4} \cdot N_{Ac,4} \cdot C_{D2}) \cdot \Lambda_1 \quad (A.44)$$

The term N_{Ac} is a dimensionless number known as the acid capacity number. The definition of N_{Ac} is the ratio of the amount of mineral consumed by the acid in a volumetric pore space to the amount of mineral exist in the volumetric sandstone matrix. The acid capacity number for the reaction between HF and fast-reacting mineral; and between H_2SiF_6 and fast-reacting mineral are expressed in Equations (A.45) and (A.46) respectively.

$$N_{Ac,1} = \frac{\phi C_{HF}^0 MW_{HF} \beta_{HF,1}}{(1-\phi) V_1^0 \rho_1} \quad (A.45)$$

$$N_{Ac,4} = \frac{\phi C_{HF}^0 MW_{H_2SiF_6} \beta_{H_2SiF_6,1}}{(1-\phi) V_1^0 \rho_1} \quad (A.46)$$

A.8 Mass Conservation Equation of Slow-Reacting Minerals

As shown in the chemical reaction model, the slow-reacting mineral ($j = 2$) only reacts with HF. Thus, the material balance is written in the form of Equation (A.47).

$$\frac{\partial((1-\phi)V_2)}{\partial t} = -\frac{MW_{HF}S_2^*V_2(1-\phi)\beta_{HF,2}E_{f,HF,2}C_{HF}}{\rho_2} \quad (\text{A.47})$$

Taking the porosity as a constant in the reaction, it becomes Equation (A.48).

$$\frac{\partial V_2}{\partial t} = -\left(MW_{HF}\beta_{HF,2}E_{f,HF,2}C_{HF}\right)\frac{S_2^*V_2}{\rho_2} \quad (\text{A.48})$$

After that, the dimensionless volume fraction of slow reacting mineral defined in Equation (A.33) and dimensionless time are substituted into the equation, forming Equation (A.49).

$$\begin{aligned} \frac{\partial \Lambda_2}{\partial t_D} &= -\left(\frac{MW_{HF}S_2^*V_2\beta_{HF,2}E_{f,HF,2}C_{HF}}{\rho_2}\right)\frac{\phi L}{uV_2^0} \\ &= -\left(\frac{(1-\phi)V_2^0E_{f,HF,2}S_2^*L}{u} \cdot \frac{1}{(1-\phi)V_2^0} \cdot \frac{\phi MW_{HF}C_{HF}^0\beta_{HF,2}C_{HF}}{\rho_2}\right)\frac{V_2}{V_2^0} \end{aligned} \quad (\text{A.49})$$

Substituting the Damkohler numbers from Equation (A.30) into it, the simplified Equation (A.50) is formed.

$$\frac{\partial \Lambda_2}{\partial t_D} = N_{Da,2}N_{Ac,2}\Lambda_2C_{D1} \quad (\text{A.50})$$

Then, the acid capacity number for the reaction between HF and the slow-reacting mineral is formulated as Equation (A.51).

$$N_{Ac,2} = \frac{\phi C_{HF}^0 MW_{HF} \beta_{HF,2}}{(1-\phi) V_2^0 \rho_2} \quad (A.51)$$

A.9 Mass Conservation Equation of Silica Gel

The precipitated product, which is the silica gel is considered as mineral 3 in this model ($j = 3$). It is being reacted with HF during the acid injection but at the same time, it is being produced when H_2SiF_6 reacts with the fast-reacting minerals. The amount of silica gel being generated can be determined from the amount of fast-reacting minerals removed as well as the stoichiometry of the reaction.

$$\begin{aligned} \frac{\partial((1-\phi)V_3)}{\partial t} = & -\frac{MW_{HF} S_3^* V_3 (1-\phi) \beta_{HF,3} E_{f,HF,3} C_{HF}}{\rho_3} \\ & + \frac{MW_{H_2SiF_6} S_1^* V_1 (1-\phi) \beta_{H_2SiF_6,1} E_{f,H_2SiF_6,1} C_{H_2SiF_6}}{\rho_3} \frac{\nu_8 MW_3}{MW_1} \end{aligned} \quad (A.52)$$

Based on Equation (A.52), the term $S_1^* V_1 (1-\phi) E_{f,H_2SiF_6,1} C_{H_2SiF_6}$ is the number of moles of H_2SiF_6 being reacted or consumed. The term $MW_{H_2SiF_6} S_1^* V_1 (1-\phi) \beta_{H_2SiF_6,1} E_{f,H_2SiF_6,1} C_{H_2SiF_6}$ corresponds to the mass of removed or dissolved fast-reacting mineral by H_2SiF_6 per unit volume whereas the term $\frac{MW_{H_2SiF_6} S_1^* V_1 (1-\phi) \beta_{H_2SiF_6,1} E_{f,H_2SiF_6,1} C_{H_2SiF_6}}{\rho_3} \frac{\nu_8 MW_3}{MW_1}$ represents the volume of silica gel that is being precipitated during the reaction between H_2SiF_6 and the fast-reacting mineral.

Considering the porosity being constant in the reaction, Equation (A.53) is developed.

$$\begin{aligned} \frac{\partial V_3}{\partial t} = & -\left(MW_{HF} \beta_{HF,3} E_{f,HF,3} C_{HF} \right) \frac{S_3^* V_3}{\rho_3} \\ & + \left(MW_{H_2SiF_6} \beta_{H_2SiF_6,1} E_{f,H_2SiF_6,1} C_{H_2SiF_6} \right) \frac{\nu_8 MW_3}{MW_1} \frac{S_1^* V_1}{\rho_3} \end{aligned} \quad (A.53)$$

Substituting the dimensionless volume fraction of silica gel defined in Equations (A.32) and (A.34); and dimensionless time into the equation, Equation (A.54) is formed.

$$\begin{aligned} \frac{\partial \Lambda_3}{\partial t_D} &= - \left(\begin{array}{l} MW_{HF} \beta_{HF,3} E_{f,HF,3} C_{HF} \frac{S_3^* V_3}{\rho_3} \\ - MW_{H_2SiF_6} \beta_{H_2SiF_6,1} E_{f,H_2SiF_6,1} C_{H_2SiF_6} S_1^* V_1 \frac{\nu_8 MW_3}{MW_1 \rho_3} \end{array} \right) \frac{\phi L}{u V_1^0} \\ &= - \frac{(1-\phi) V_1^0 E_{f,HF,3} S_3^* L}{u} \cdot \frac{1}{(1-\phi) V_1^0} \cdot \frac{\phi MW_{HF} C_{HF}^0 \beta_{HF,3} C_{HF}}{\rho_3 C_{HF}^0} \cdot \frac{V_3}{V_1^0} \\ &+ \frac{(1-\phi) V_1^0 E_{f,H_2SiF_6,1} S_1^* L}{u} \cdot \frac{1}{(1-\phi) V_1^0} \cdot \frac{\phi MW_{H_2SiF_6} C_{HF}^0 \beta_{H_2SiF_6,1} C_{H_2SiF_6}}{\rho_1 C_{HF}^0} \cdot \frac{V_1}{V_1^0} \cdot \frac{\nu_8 MW_3}{MW_1} \cdot \frac{\rho_1}{\rho_3} \end{aligned} \quad (A.54)$$

Substituting the Damkohler numbers from Equation (A.31) and (A.39) into it, the equation is simplified to become Equation (A.55).

$$\frac{\partial \Lambda_3}{\partial t_D} = -N_{Da,3} \cdot N_{Ac,3} \cdot \Lambda_3 \cdot C_{D1} + N_{Da,4} \cdot N_{Ac,4} \cdot \Lambda_1 \cdot C_{D2} \frac{\nu_8 MW_3}{MW_1} \frac{\rho_1}{\rho_3} \quad (A.55)$$

The acid capacity number for the reaction between HF and the silica gel is expressed in Equation (A.56).

$$N_{Ac,3} = \frac{\phi C_{HF}^0 MW_{HF} \beta_{HF,3}}{(1-\phi) V_1^0 \rho_3} \quad (A.56)$$

A.10 Change in Porosity

In expanded form, the porosity equation can be written as Equation (A.57).

$$\begin{aligned}
 \frac{\partial \phi}{\partial t} = & - \frac{MW_{HF} S_1^* V_1 \beta_{HF,1} E_{f,HF,1} C_{HF}}{\rho_1} - \frac{MW_{H_2SiF_6} S_1^* V_1 \beta_{H_2SiF_6,1} E_{f,H_2SiF_6,1} C_{H_2SiF_6}}{\rho_1} \\
 & - \frac{MW_{HF} S_2^* V_2 \beta_{HF,2} E_{f,HF,2} C_{HF}}{\rho_2} - \frac{MW_{HF} S_3^* V_3 \beta_{HF,3} E_{f,HF,3} C_{HF}}{\rho_3} \\
 & + \frac{MW_{H_2SiF_6} S_1^* V_1 \beta_{H_2SiF_6,1} E_{f,H_2SiF_6,1} C_{H_2SiF_6}}{\rho_3} + \frac{\nu_8 MW_3}{MW_1}
 \end{aligned} \tag{A.57}$$

A.11 Initial Conditions

In dimensionless form, the initial conditions are written as Equation (A.58).

$$\left. \begin{aligned}
 C_{D,1} = C_{D,2} = 0 \\
 \Lambda_1 = \Lambda_2 = \Lambda_3 = 1 \\
 \phi = \phi^0
 \end{aligned} \right\} \text{ at } t_D = 0 \tag{A.58}$$

A.12 Boundary Conditions

In dimensionless form, the boundary conditions applied in the simulation are expressed as Equations (A.59) – (A.61).

$$\left. \begin{aligned}
 C_{D,1} = 1 \\
 Q = \text{Constant}
 \end{aligned} \right\} \text{ at } x_D = 0 \tag{A.59}$$

$$P = P_{out} \text{ at } x_D = 1 \tag{A.60}$$

$$\frac{\partial P}{\partial r} = 0 \text{ at } r = r_c \tag{A.61}$$